Short- and Long-term Model Simulations of the Evolution of Vatnajökull Ice Cap

Louise Steffensen Schmidt

Faculty of Earth Sciences
University of Iceland
2019

Short- and Long-term Model Simulations of the Evolution of Vatnajökull Ice Cap

Louise Steffensen Schmidt

Dissertation submitted in partial fulfillment of a
Philosophiae Doctor degree in Geophysics

Advisor
Guðfinna Aðalgeirsdóttir

PhD Committee
Finnur Pálsson
Sverrir Guðmundsson
Peter L. Langen
Helgi Björnsson

Opponents
Shawn Marshall
Xavier Fettweis

Faculty of Earth Sciences
School of Engineering and Natural Sciences
University of Iceland
Reykjavik, January 2019

Short- and Long-term Model Simulations of the Evolution of Vatnajökull Ice Cap
Short- and Long-term Simulations of Vatnajökull
Dissertation submitted in partial fulfillment of a *Philosophiae Doctor* degree in Geophysics

Faculty of Earth Sciences
School of Engineering and Natural Sciences
University of Iceland
Sturlugata 7
101, Reykjavik
Iceland

Telephone: 525-4000

Bibliographic information:
Louise Steffensen Schmidt, 2019, *Short- and Long-term Model Simulations of the Evolution of Vatnajökull Ice Cap*, PhD dissertation, Faculty of Earth Sciences, University of Iceland, 149 pp.

ISBN 978-9935-9300-6-4

Printing: Haskolaprent
Reykjavik, Iceland, January 2019

Abstract

This dissertation describes the research results from applying regional climate models (RCMs) to simulate the near-past and future evolution of Vatnajökull, the largest ice cap in Iceland, and investigate the sensitivity of ablation to albedo and spring snow cover.

The output of the RCM HIRHAM5 is first validated over Vatnajökull using available automatic weather station and mass balance observations, and the albedo parameterisation is improved by adding an ice albedo map based on MODIS observations. Although the ice albedo map improves the simulations, there is still an average overestimation of the albedo simulations over the ablation season due to an overestimation in the amount of snowfall and the lack of simulations of the effect of dust storms. As a result, the mean ablation over the melt season is generally underestimated compared to observations. However, the specific mass balance is well simulated by the model, which captures the trends in mass loss since the 1991-92 glaciological year.

The overestimation of the accumulation in HIRHAM5 was suspected to be partly due to the hydrostatic approximation used in the atmospheric model, and experiments forcing the well-validated snow pack model from HIRHAM5 with meteorological parameters from other climate models were therefore conducted. The snow pack model simulates the surface energy balance, the total melt, and subsurface processes like melt percolation and refreezing. The meteorological forcing from the non-hydrostatic (i.e. solves the vertical momentum equation) numerical weather prediction model (NWP) HARMONIE-AROME is shown to provide improved simulation over Vatnajökull, in particular due to improvements in the simulation of accumulation. The HARMONIE-AROME forced model is used to simulate the runoff from 1980-2015 and estimate the sensitivity of runoff to variations in spring snow thickness. It is found that the runoff is much more sensitive to changes in the summer weather overall, although the north-facing outlet glaciers Brúarjökull and Dyngjujökull show a large sensitivity to spring snow thickness. The effect of the ice albedo on the runoff from 1980-2015 is also investigated, with 14% of the runoff from Vatnajökull simulated to be derived from melting of exposed ice, and 27% of the runoff from Brúarjökull.

The future evolution of the ice cap is simulated by forcing the ice flow model PISM with simulated mass balance fields. The mass balance is simulated by the HIRHAM5 snow pack model, but with different meteorological forcing. For the reanalysis period (1980-2016), HARMONIE-AROME meteorological reanalysis forcing is used, and from 2017-2100 mass balance anomaly fields (1990-2010 reference period) from HIRHAM5 forced by EC-EARTH is used under the representative concentration pathway (RCP) 4.5 and 8.5 scenarios. From 2100-2300, the 2081-2100 climate is repeated. The simulations

show that the ice cap loses 45% of its volume and 25% of its area by 2300, under the RCP 4.5 scenario and 85% of its volume and 65% of its area in the RCP 8.5 scenario. Using available meteorological forcing from the Coordinated Regional Downscaling Experiment (CORDEX) simulations for the same period, a wide range of geometries are derived: 50-95% decrease in volume and 25-80% decrease in area.

Útdráttur

Í ritgerðinni er lýst niðurstöðum rannsókna á að nota svæðisbundin loftlagslíkön til að herma þróun Vatnajökuls, stærsta jökuls Íslands, nokkra undangengna ártugi og næstu framtíð. Einnig er rannsakað hve næm leysing jökulsins er fyrir breytilegu endurkasti sólarljóss frá yfirborði (endurkastsstuðli; en: albedo) og þykktar snjólags að vori.

Fyrst var metið hve vel svæðisbundna loftlagslíkanið HIRHAM5 lýsir aðstæðum á Vatnajökli með því að bera lýsingu þess við mæligögn frá sjálfvirkum veðurstöðvum og afkomumælingar. Endurkastsstuðull ísyfirborðs jökulsins (eftir að vetrarsnjó hefur leyst) í líkaninu er metinn eftir gögnum frá MODIS gervihnettinum. Jafnvel þótt niðurstöður líkansins verði á þennan hátt nær sanni, er ennþá að jafnaði of hár endurkastsstuðull á leysingatíma bæði vegna þess að snjóþykktin á sporðum er ofmetin í líkaninu og ekki er tekið tillit til loftborins ryks sem berst í yfirborðið og dekkir það. Vegna þessa er hermda leysingin heldur minni en sú mælda að jafnaði. Þrátt fyrir þessa annmarka hermir líkanið heildarafkomu jökulsins vel og sýnir samskonar sveiflur í massa tapi og hafa verið mældar síðan jökulárið 1991-92. Ofmat ákomu í HIRHAM5 er a.m.k. að hluta til vegna nálgunar sem gerð er í lofthjúpshluta líkansins (hydrostatic approximation) og því voru gerðar tilraunir með að keyra snjósöfnunarhluta líkansins, sem er vel staðfestur, með veðurfarsþáttum frá öðrum loftlagslíkönum. Með því að nota veðurþætti frá veðurspá líkaninu HARMONIE-AROME, sem ekki gerir þessa nálgun (non-hydrostatic model) fást betri niðurstöður fyrir afkomu Vatnajökuls, sérstaklega vegna bættrar úrkomu í líkaninu. HARMONIE-AROME var þess vegna notað til að herma leysingu Vatnajökuls jökulárin 1980 til 2015 og meta hversu næm leysingin er fyrir þykkt snjólags að vori. Niðurstöður sýna að leysing alls jökulsins ræðst að mestu leiti af sumarveðri, þótt að leysing norðurjöklanna; Brúarjökuls og Dyngjujökuls, sé einnig mjög háð þykkt snjólags að vori. Áhrif endurkastsstuðuls íssins á leysingu eru einnig metin á sama tímabili; 14% leysingar alls Vatnajökul er vegna bráðnunar íss sem kemur undan snjólagi vetrar en 27% leysingar Brúarjökuls.

Þróun Vatnajökuls í framtíðinni er hermd með ísflæðilíkaninu PISM og mati afkomu út frá loftlagslíkani sem byggir á spá um þróun loftlags. Afkoman er hermd með snjóhluta HIRHAM5 líkansins með mismunandi veðurþáttum. Fyrir tímabilið 1980-2016 eru notaðir veðurþættir frá endurgreiningu HARMONIE-AROME líkansins. Fyrir tímabilið 2017-2100 eru notuð metin frávik frá viðmiðunartímabili (1990-2010), reiknuð með HIRHAM5 með inngangstærðum frá EC-EARTH á jöðrunum og sviðsmyndunum RCP4.5 and RCP8.5 um þróun loftlags. Fyrir tímabilið 2100-2300 er ísflæðilíkanið keyrt áfram með endurteknu afkomumati áranna 2081-2100. Við lok reikninganna, hermt ár 2300, hefur Vatnajökull misst 45% af rúmmáli sínu og 25% af flatarmáli sínu,

ef miðað er við sviðsmynd RCP4.5, en misst 85% af rúmmáli og 65% af flatarmáli útfrá sviðsmynd RCP8.5. Sams konar keyrslur með tiltækum framtíðarspám fyrir akomu úr CORDEX verkefninu sýna að rýrnun ísrúmmáls getur orðið á bilinu 50-95% og minnkun flatarmáls jökla 25-80%.

Table of Contents

Abstract iii

Útdráttur v

Table of Contents vii

List of Figures ix

List of Tables xi

List of Original Papers xiii

Abbreviations xv

List of variables xvii

Acknowledgments xix

1 Introduction 1

1.1 Research objectives . . . 3

1.2 Thesis Outline . . . 3

2 Theoretical background 5

2.1 Surface energy balance . . . 5

2.2 Mass balance modelling . . . 7

2.2.1 Empirical and physical ablation models . . . 7

2.2.2 Global and Regional climate models . . . 8

2.2.3 Future direction of RCMs . . . 10

2.3 Modelling of ice flow . . . 11

2.4 Coupling of mass balance and ice flow . . . 14

3 Observations 17

3.1 Study area . . . 17

3.2 Ground-based observations . . . 19

3.2.1 Automatic weather stations . . . 19

3.2.2 Mass balance and velocity . . . 20

3.2.3 Discharge observations . . . 21

3.2.4 Bedrock topography . . . 22

3.3 Satellite observations . . . 23

3.3.1 MODIS albedo . . . 23

3.3.2 Surface topography . . . 24

3.4 Reanalysis . . . 24

4 Methods 27

4.1 HIRHAM5 . . . 27

4.1.1 Snow pack scheme . . . 28

4.1.2 Offline runs . . . 31

4.2 HARMONIE-AROME 32
4.3 CORDEX 32
4.4 PISM 33
5 Paper I: The importance of accurate albedo simulations 37
5.1 Summary 37
5.2 Main results 38
6 Paper II: Sensitivity of runoff to spring snow thickness 41
6.1 Summary 41
6.2 Main results 41
7 Paper III: Future projections under different climate scenarios 45
7.1 Summary 45
7.2 Main results 46
8 Conclusions and outlook 49
References 51
Paper I 65
Paper II 87
Paper III 113

List of Figures

2.1 SIA + SSA 13
2.2 Flowchart of model coupling 14
3.3 Geological map of Iceland 18
3.4 Observations overview map 20
3.5 Bedrock Topography 21
3.6 Bedrock Topography 22
4.7 HIRHAM5 domain 28
4.8 HIRHAM5 Iceland domain 31
4.9 EURO-CORDEX domain 33
5.10 Simulates SMB by HIRHAM5 38
5.11 HIRHAM5 simulated SMB with Öræfajökull correction 39
6.12 Comparison of HARMONIE-AROME and HIRHAM5 winter SMB . . . 42
6.13 Sensitivity to spring snow thickness 43
7.14 Change in area and volume using HIRHAM5-EC-EARTH forcing 46
7.15 Change in area and volume using CORDEX forcing 47

List of Tables

4.1 CORDEX simulations used in this study. 34

List of Original Papers

This thesis is based on the following three original, first-authored papers

I: **Schmidt LS**, Aðalgeirsdóttir G, Guðmundsson S, Langen PL, Pálsson F, Mottram R, Gascoin S, and Björnsson H (2017). The importance of accurate glacier albedo for estimates of surface mass balance on Vatnajökull: evaluating the surface energy budget in a regional climate model with automatic weather station observations, *The Cryosphere*, **11**, 1665-1684 (https://doi.org/10.5194/tc-11-1665-2017)

II: **Schmidt LS**, Langen PL, Aðalgeirsdóttir G, Pálsson F, Guðmundsson S, and Gunnarsson A (2018). Sensitivity of Glacier Runoff to Winter Snow Thickness Investigated for Vatnajökull Ice Cap, Iceland, Using Numerical Models and Observations, *Atmosphere*, **9**, 450 (doi:10.3390/atmos9110450)

III: **Schmidt LS**, Aðalgeirsdóttir G, Guðmundsson S, Langen PL, Pálsson F, and Björnsson H (2019). Dynamic simulations of Vatnajökull ice cap from 1980-2300, *To be submitted to The Cryosphere.*

In addition to the first authored papers that are the focus of this thesis, I contributed to two other co-authored papers which are related to this study

A1: Wittmann M, Zwaaftink CDG, **Schmidt LS**, Guðmundsson S, Pálsson F, Arnalds O, Björnsson H, Thorsteinsson T, and Stohl A (2017). Impact of dust deposition on the albedo of Vatnajökull ice cap, Iceland. *The Cryosphere*, **11**, 741-754 (https://doi.org/10.5194/tc-11-741-2017)

A2: Gascoin S, Guðmundsson S, Aðalgeirsdóttir G, Pálsson F, **Schmidt LS**, Berthier E, Björnsson H (2017). Evaluation of MODIS Albedo Product over Ice Caps in Iceland and Impact of Volcanic Eruptions on Their Albedo. *Remote Sensing*, **9**, 399 (doi:10.3390/rs9050399)

List of Abbreviations

Symbol	Description
AWS	Automatic Weather Station
CORDEX	Coordinated Regional Climate Downscaling Experiment
CMIP	Coupled Model Intercomparison Project
DMI	Danish Meteorological Office
ECMWF	European Centre for Medium-Range Weather Forecasts
GCM	Global Climate Model
GWC	Glacial Water Catchment
IMO	Icelandic Meteorological Office
ISMIP	Ice Sheet Model Intercomparison Project
ICRA	Iceland reanalysis project
MODIS	Moderate Resolution Imaging Spectroradiometer
NWP	Numerical Weather Prediction model
RCM	Regional Climate Model
RCP	Representative Concentration Pathway
RESM	Regional Earth System Model
SIA	Shallow Ice Approximation
SSA	Shallow Shelf Approximation
SMB	Surface Mass Balance
w. eq.	water equivalent
WRF	Weather Research and Forecast model

List of variables

Symbol	Description	Units
A	rate factor or flow parameter	$s^{-1}\,Pa^{-3}$
α	albedo	
α_{mx}	minimum snow albedo from ageing	
α_{snow}	snow albedo	
α_{ice}	ice albedo	
α_{max}	maximum albedo for fresh snow	
b	bedrock elevation	m a.s.l.
br	albedo refreshment rate	
β	positive degree day factor	mm w.eq. $^{\circ}$C day^{-1}
c_0	till cohesion	kPa
$c_{RO,1}$,$c_{RO,2}$,$c_{RO,3}$	timescale coefficients	days
C_c	compressibility coefficient	
d	snow depth	m w.eq.
d_s	characteristic snow depth	m w.eq.
$D_{i,j}$	strain rate tensor	s^1
δ	effective fraction overburden	
$\delta_{i,j}$	Kroenecker delta	
e_0	reference void ratio	
E	evaporation/sublimation	m w.eq.
f	weighing function between 0 and 1	
g	acceleration due to gravity	m s^{-2}
G	ground heat flux	Wm^{-2}
H	glacier or ice cap thickness, $H = z_s - z_b$	m
L_f	latent heat of fusion	J kg^{-1}
LW	short-wave radiation	Wm^{-2}
M	total ablation	m w.eq.
n	exponent in Glen's flow law	
N_0	reference effective pressure	kPa
N_{till}	effective pressure on the till	kPa
$\bar{\nu}$	vertically-integrated viscosity	m^2 s^{-1}
p_i	ice pressure	Pa
p_{liquex}	water above retention threshold	m w. eq.
P	precipitation	m w.eq.
P_0	ice overburden pressure	kPa

Symbol	Description	Units
ϕ	till friction angle	$^\circ$
q	pseudo-plastic exponent	
Q_0	energy flux towards glacier surface	Wm^{-2}
Q_H	sensible heat flux	Wm^{-2}
Q_L	latent heat flux	Wm^{-2}
Q_R	heat flux from rain	Wm^{-2}
R	net radiation	Wm^{-2}
RF	refreezing	m w.eq.
Rn	rainfall	m w.eq.
RO	runoff	m w.eq.
ρ_w,ρ_i	densities of water/ice	kg m^{-3}
S	surface slope	
S_0	critical amount of snowfall pr time step	m w.eq. day^{-1}
S_f	amount of snowfall pr time step	m w.eq. day^{-1}
Sn	snowfall	m w.eq.
SW	short-wave radiation	Wm^{-2}
t	time	s, day, a
t_{RO}	runoff timescale	days
T_{pdd}	sum of positive daily mean temperatures	$^\circ$C
$T_{i,j}$	vertically averaged stress tensor	N m^{-2}
τ	second invariant of the deviatoric stress	N m^{-2}
τ_b	bed parallel shear stress	kPa
τ_c	yield stress	kPa
τ_{ij}	deviatoric stress tensor	N m^{-2}
τ_x	albedo ageing timescale	s
u,v,w	components of the velocity vector $\mathbf{u}$	m s^{-1}
$\mathbf{u}$	velocity vector, $\mathbf{u} = (u,v,w)$	m s^{-1}
$\mathbf{u}_b$	basal velocity vector	m s^{-1}
$u_{threshold}$	threshold speed in psuedo-plastic power law	m s^{-1}
W_{till}	effective water thickness in the till	m
W_{max}	maximum water thickness in the till	m
x_1, x_2, z	space coordinates	m
$\mathbf{x}$	position vector, $\mathbf{x} = (x_1, x_2, z)$	m
z_b	bed elevation of the ice sheet	m
z_s	surface elevation of the ice sheet	m
ζ	the vertical integration variable in the SIA equation	

Acknowledgments

I would first and foremost like to thank my entire PhD committee - Guðfinna, Helgi, Finnur, Sverrir, and Peter - whom in different ways helped and supported my studies throughout the last four years. I would especially like to acknowledge my main supervisor, Guðfinna Aðalgeirsdóttir, who gave me invaluable guidance throughout the course of my PhD. Always helpful and ready with a constructive comment or friendly encouragement, she was an great supervisor.

In addition, I would like to thank Peter Langen and Ruth Mottram at DMI for invaluable help with the HIRHAM5 simulations and always quickly answering any question I had. Thanks to Bolli and Nick at the IMO for providing HARMONIE-AROME files and answering any inquiry I had about the model setup. Furthermore, the modelling work would have taken several additional years without the help of Máni, who helped me set up the various models in the super computing environment provided by the Icelandic High Performance Computing Centre at the University of Iceland.

I would also like to express my gratitude to the glaciology group at the University of Iceland - Finnur, Eyfi, Helgi, Mona, Sverrir, Alex, Bergur, Joaquin, Águst, Tollý, and Becca - for helpful and interesting discussions. A special thanks goes to Becca for numerous long discussions, which were always interesting although rarely helpful.

I am very thankful for the friends I have made in Iceland during the last four years. Thank you, for the movies, the beers, the walks, the ice cream breaks, and for letting me hang out with your dogs. My time in Iceland would have been a lot less enjoyable without you.

Tak til min familie, som, trods jokes om chokoladeis og en dum hund der ødelægger mine dyre høretelefoner, altid var rare at komme hjem til. Tak til mine venner i Danmark for ikke at glemme mig helt mens jeg er oppe i det kolde nord. Specielt tak til Sanndra, som altid var klar til en rejse hvis jeg havde behov for at komme lidt væk.

Last but not least, thanks to Tobi. Whether through long tea breaks in Iceland or via early morning texts from the other side of the world, you were always a great distraction.

This work was financially supported by the University of Iceland Research Fund, Landsvirkjun research fund, and the Icelandic Research Fund (RANNÍS, Grant no. 140920-051). Measurements from automatic weather stations and in situ mass balance surveys were provided from joint projects between the National Power Company of

Iceland and the Glaciology group at the Institute of Earth Sciences, University of Iceland. Discharge observations were kindly provided by Landsvirkjun and the Icelandic Meteorological office. In addition, I would like to acknowledge the World Climate Research Programme's Working Group on Regional Climate and the Working Group on Coupled Modelling for coordinating CORDEX and CMIP5. Thanks to the many climate modelling groups which produced and made available their model output within the CORDEX initiative.

1 Introduction

Glacial ice masses (including glaciers, ice caps, and ice sheets) play an important role in the Earth system and are a vital source of natural resources. They modify the local and global climate by altering the energy balance of the lower atmosphere and affecting large scale air circulation (e.g. Broccoli and Manabe, 1987; van den Broeke, 1997) as well as contributing to sea-level rise, the hydrology of rivers, and fresh water inflow to the oceans, which e.g. affects the ocean ecosystem (e.g. Kaser et al., 2010; Xu et al., 2012; Boberg et al., 2018). On regional scales, glaciers provide an important source of drinking water in e.g. south Asia and China (Immerzeel et al., 2010; Kraaijenbrink et al., 2017), and feed glacial rivers used for hydropower production and irrigation systems (e.g. Kaser et al., 2010). Glaciers also pose a natural hazard by e.g. releasing large amounts of meltwater in jökulhlaup events, possibly destroying roads and infrastructure (e.g. Russell, 1989; Björnsson, 2003).

Glaciers and ice caps are currently responding to a globally warming climate by melting at increasing rates and contributing to a global sea level rise. From 1993-2009, land ice outside of Greenland and Antarctica has contributed 0.76 (0.39 to 1.13) mm a^{-1} to the global sea level rise (Church et al., 2013). The Greenland and Antarctic Ice Sheets are also losing mass, contributing 0.33 (0.25 to 0.41) mm a^{-1} and 0.27 (0.16 to 0.38) mm a^{-1}, respectively, from 1993-2010 to sea level rise (Church et al., 2013). Although the amount of ice stored in glaciers and ice caps ($\sim$0.4 m sea level equivalent (Church et al., 2013)) is much smaller than for the Greenland and Antarctic ice sheets ($\sim$7 and $\sim$58 m sea level equivalent, respectively), their contribution to sea level rise has been significant over the last two decades (e.g. Church et al., 2013; Gardner et al., 2013; Björnsson et al., 2013; Bamber et al., 2018). On century timescales, they are expected to continue to provide a significant contribution to sea level change due to their large sensitivity to climate variations (e.g. Oerlemans, 2001).

High-resolution regional climate models (RCMs) which model the full surface energy balance are important tools for simulating the response of ice masses to a changing climate. However, they often have systematic biases in temperature and/or precipitation (e.g. Christensen et al., 2008; Hagemann et al., 2011), which need to be estimated and corrected in order to get the most accurate estimates of future runoff and sea level change. Since runoff is a nonlinear function of precipitation, model bias estimation is especially important for hydrological modelling (e.g. Hagemann et al., 2011; Muerth et al., 2013). In order to have confidence in future projections simulated by RCMs, it is therefore important to do a thorough evaluation of the simulations of the present climate (e.g. Rae et al., 2012). In addition to systematic biases in precipitation (e.g. Box and Rinke, 2003), one of the largest uncertainties in RCMs pertain to the seasonal and

annual variability of albedo and the amount of refreezing at the surface. The albedo is an important component of the energy balance and has a large influence on the glacial melt (e.g. Cuffey and Paterson, 2010) and Arctic amplification, the term for the faster increase in warming over the Arctic than the global mean, has been shown to be closely linked to albedo feedback (Arrhenius, 1896; Pithan and Mauritsen, 2014; Graversen et al., 2014). Accurate albedo simulations are therefore important for projections of the future climate.

Like most glaciers worldwide, Icelandic glaciers and ice caps are shrinking at an increasing rate (e.g. Gudmundsson et al., 2011; Pálsson et al., 2012; Jóhannesson et al., 2013; Björnsson et al., 2013). Although they are not large in total volume, only containing approximately 1 cm sea level equivalent (Björnsson and Pálsson, 2008), they are very sensitive to changes in climate and can provide important information about past and present climate change. Icelandic glaciers are very dynamic, with a high mass turnover and surge-type outlet glaciers (Björnsson and Pálsson, 2008). Several of the ice caps are in active volcanic areas, where geothermal or volcanic activity melts the ice at the base (e.g. Björnsson, 2003; Magnússon et al., 2005). This can e.g. lead to increased basal sliding, or the meltwater may accumulate in a subglacial lake which is later drained in a jökulhlaup event (e.g. Björnsson et al., 2001b; Björnsson and Pálsson, 2008). In addition, volcanic eruptions can melt their way through the glaciers (e.g. Gudmundsson et al., 1997; Magnússon et al., 2012) and/or deposit ash on the glacier surface which alters its spectral properties and either acts as a melt enhancer or insulator (e.g. Möller et al., 2014; Dragosics et al., 2016; Gascoin et al., 2017). Due to tephra layers within the glacier ice and frequent dust storms, there is a large spatial and temporal variability in the albedo (e.g. Larsen et al., 2016). Icelandic glaciers therefore provide an interesting and challenging area of study. In addition, the temperate outlet glaciers from Icelandic ice caps resemble many of the land-terminating outlet glaciers from the Southwest Greenland ice sheet, and may be viewed as an analogue for the warmer and wetter future of Arctic glaciers (Björnsson, 2017). This includes e.g. an increased contribution from turbulent fluxes and albedo to the future melt.

Since 1991, a long-term monitoring program has been active on Icelandic glaciers, including direct mass balance (Björnsson et al., 1998, 2002; Magnússon et al., 2005; Pálsson et al., 2012) and automatic weather station (AWS) observations on the largest ice caps (e.g. Oerlemans et al., 1999; de Ruyter de Wildt et al., 2003; Björnsson et al., 2006; Guðmundsson et al., 2006). Compared to e.g. Greenland and Antarctica, observations are recorded in a relatively small area, offering a good opportunity to evaluate the spatial and temporal variability of ablation models on a regional scale. In addition, since only minimal refreezing occurs for Icelandic glaciers and they have large spatial and temporal variations in albedo, they are ideal for studying the sensitivity of ablation and runoff to variations in the albedo.

However, while much work has gone into evaluating RCMs over Greenland and Antarctica (e.g. Fettweis et al., 2011; Rae et al., 2012; Agosta et al., 2015; Fettweis et al., 2017; Langen et al., 2017), energy balance simulations by a RCM have not previously been evaluated for Icelandic glaciers. The output from RCMs has been used in studies of the future evolution of Icelandic glaciers (e.g. Aðalgeirsdóttir et al., 2011), but only the temperature and precipitation fields were used as input for a positive degree day model which simulated the mass balance. Future projections of the evolution of ice caps

or glaciers in Iceland have been made by e.g. Jóhannesson et al. (1995), Björnsson et al. (2001a), Marshall et al. (2005), Flowers et al. (2005), Hubbard (2006), Guðmundsson et al. (2009a), and Aðalgeirsdóttir et al. (2011), but using empirical methods to estimate the mass balance. A numerical, physical model of the mass balance has therefore not previously been used for simulations of the future evolution of Icelandic ice caps.

1.1 Research objectives

The overall aim of this dissertation is to use the wealth of available in-situ observations to evaluate and improve the predictability of glacier ablation in RCMs for Vatnajökull, the largest ice cap in Iceland. A particular focus has been on albedo simulations and sensitivity studies. The improved model scheme is used to simulate the evolution of Vatnajökull for a range of different RCM scenarios at different model resolutions.

The thesis can be summed up with four main objectives:

1 To improve the simulations of the albedo for Vatnajökull ice cap in the RCM HIRHAM5 and evaluate the model simulations using available in-situ observations of the energy and mass balance components. This includes both simulations forced at the lateral boundaries by reanalysis, which aims at assimilating historical observational data over a period with numerical forecast models, and by a general circulation model (GCM) for future simulations.

2 Set up a framework for forcing the improved snow pack scheme from HIRHAM5 with meteorological input from other climate models and validate the new model output.

3 Estimate the sensitivity of ablation and runoff to changes in albedo, e.g. as a result of variations in the spring snow thickness.

4 Simulate the future evolution of Vatnajökull by using a one-way coupling between a range of RCMs and an ice flow model. This includes setting up and tuning the ice flow model, model initialization, and estimations of the effect of elevation feedback on the mass balance.

1.2 Thesis Outline

This doctoral thesis is based on the results presented in three original, first-author papers. The first paper was published in the peer-reviewed international journal *The Cryosphere* in 2017, and the second paper was published in the peer-reviewed international journal *Atmosphere* in 2018. The third paper is in preparation for *The Cryosphere*, to be submitted in 2019.

The structure of the thesis is as follows: Chapter 1 gives a general introduction to the thesis, and Chapter 2 gives a brief overview of the theoretical background behind surface energy balance, mass balance modelling, and ice flow models. Chapter 3 presents the

used observations, while Chapter 4 presents the used methods and models. Chapters 5-7 give a short summary of the main results of the three first-authored papers, and Chapter 8 presents the general conclusions found in this thesis.

Finally, the three papers are reproduced in their entirety at the end of the thesis. The three papers are

I: Schmidt LS, Aðalgeirsdóttir G, Guðmundsson S, Langen PL, Pálsson F, Mottram R, Gascoin S, and Björnsson H (2017). The importance of accurate glacier albedo for estimates of surface mass balance on Vatnajökull: evaluating the surface energy budget in a regional climate model with automatic weather station observations, *The Cryosphere*, **11**, 1665-1684.

II: Schmidt LS, Langen PL, Aðalgeirsdóttir G, Pálsson F, Guðmundsson S, and Gunnarsson A (2018) Sensitivity of Glacier Runoff to Winter Snow Thickness Investigated for Vatnajökull Ice Cap, Iceland, Using Numerical Models and Observations, *Atmosphere*, **9**, 450 (doi:10.3390/atmos9110450)

III: Schmidt LS, Aðalgeirsdóttir G, Guðmundsson S, Langen PL, Pálsson F, and Björnsson H (2019), Dynamic simulations of Vatnajökull ice cap from 1980-2300, *To be submitted to The Cryosphere.*

2 Theoretical background

The specific mass balance of a glacier is the total change in mass in a vertical column of glacier material. Snow fall is the dominant process causing accumulation, while the dominant ablation process generally is glacier melt followed by runoff of melt water. However, in Antarctica, the higher parts of Greenland and the drier parts of the tropics, sublimation is the dominant ablation process (Greuell and Genthon, 2004).

Surface melting of glaciers is determined by the energy balance, which is the balance of positive and negative fluxes to the glacier surface. Positive fluxes provide energy, thus either warming or melting the glacier surface, while negative energy fluxes remove energy, thus cooling the surface (e.g. Oerlemans, 2001). The energy balance is controlled both by meteorological parameters and the properties of the glacier surface. There is a complex interaction between the surface and the atmosphere due to feedback mechanisms between the atmosphere, energy balance, and surface properties. If the glacier surface is below 0°C, excess energy is used to warm the surface to the melting point, after which it is used for melting.

When simulating the mass balance of glaciers, it is important to also consider the flow of ice. Glacier flow transports ice from the accumulation zone to the lower elevation ablation zone, and therefore provide an important contribution to glacier melt. In addition, the changing geometry of glaciers also affects the mass balance due to strong elevation-mass balance feedbacks.

In this chapter, I present an overview of the components of the surface energy and mass balance and the different processes contributing to glacier mass balance. In addition, I introduce methods commonly used to model both glacier mass balance and ice flow.

2.1 Surface energy balance

The total energy flux from the atmosphere towards a glacier (Q_0) is

$$Q_0 = R + Q_H + Q_L + Q_R + G \tag{1}$$

where R is the net radiation, Q_H is the sensible heat flux, Q_L is the latent heat flux, Q_R is the heat flux from rain, and G is the ground heat flux. In most cases, Q_R and G can be considered negligible.

The net radiation is the balance between shortwave (SW) and longwave (LW) radiative fluxes:

$$R = LW\downarrow - LW\uparrow + SW\downarrow - SW\uparrow \tag{2}$$

The incoming longwave radiation depends on the temperature and vapour pressure of the atmosphere, clouds, and atmospheric composition. Clouds have a significant impact on the flux, which increases with cloud amount, cloud emissivity, and cloud base temperature (Greuell and Genthon, 2004). The outgoing longwave radiation is a function of the surface temperature.

The incoming shortwave radiation depends on the solar constant, zenith angle, topographic surface effects, clouds and the atmospheric transmissivity (Cuffey and Paterson, 2010). The outgoing shortwave radiation depends on the albedo α, which is the reflectivity of the glacier surface

$$SW\uparrow = SW\downarrow \alpha \tag{3}$$

The albedo depends on the material properties of the surface, like e.g. impurities, grain size, and liquid water content. Common albedo values for glacier surfaces span from 0.2 to 0.9, and the albedo is therefore a dominant component of the surface mass balance (e.g. Cuffey and Paterson, 2010).

Fresh snow typically has an albedo of 0.8-0.9, which then decreases as a function of time since last snowfall. Several processes contribute to the lowering of the albedo. As the age of the snow increases, snow metamorphism increases the grain size which in turn lowers the albedo as larger snow grains are more absorptive. Similarly, if the liquid water content in the snow pack increases during melting, the albedo decreases because the water replaces air between ice grains, thus effectively increasing the grain size (Warren, 1982). Ponding of meltwater or an increase in impurities darken the surface, thus lowering the albedo and increasing melt. However, once a critical thickness of sediments is reached on the surface, they will instead act as an insulator (e.g. Dragosics et al., 2016). The snow albedo also depends on the snow thickness, as when the snow pack becomes thin enough, the albedo is affected by the properties of the underlying surface. Generally the upper 10-20 cm of snow determine the albedo (Wiscombe et al., 1980).

Ice generally has a lower albedo than snow, but it has large spatial variations within the ablation area. Ponding of meltwater and impurities in the ice also affect the ice albedo, as do the crystal size and bubble content (Cuffey and Paterson, 2010). Debris in the ice can can be concentrated over many years, e.g. the spectral properties of ice in the ablation zone of Vatnajökull are controlled by tephra layers in the ice (e.g. Reijmer et al., 1999; Larsen et al., 2016). Very low ice albedo values, dropping below 0.03 in late summer, are therefore not unusual for the ablation zone of Vatnajökull.

Albedo also depends on the solar zenith angle, and it therefore changes both with the time of day and with the time of year. For example in Reykjavik, the solar zenith angle in winter is close to 90°, compared to almost 40° in the summer (Sasaki et al., 2003). The albedo also varies as a function of radiation wavelength, with the greatest reflection within the visible spectrum.

The sensible heat flux is the energy transfer of heat in the air, and depends on the temperature gradient through the atmosphere and the wind speed. The latent heat flux

is the energy released/consumed during a phase change and depends on the vapour pressure gradient and wind speed. Generally, the net radiation contributes the most energy to the surface, contributing up to >90% of the melt energy (Oerlemans et al., 1999). The turbulent heat fluxes are most important for maritime climates. For example on Bægisárjökull in the north of Iceland the average contribution of the turbulent fluxes to the melt energy was found to be 43-49% for observation periods in 1967-68 (Björnsson, 1972), on Brúarjökull (a northern outlet glacier of Vatnajökull) the average contribution of the turbulent fluxes to the energy melt energy is currently around 33% (e.g. Björnsson et al., 2006; Guðmundsson et al., 2006), and on Brewster glacier in New Zealand the contribution is generally ∼50% (Anderson et al., 2010). As the climate warms, the contribution of turbulent fluxes to the melt over e.g. Greenland is likely to increase (e.g. van den Broeke et al., 2008; Hartmann et al., 2013; Fausto et al., 2016).

If the energy balance is positive, the energy is used to either warm up the surface, if the glacier surface temperature is below the melting point, or as melt energy. The energy available for melt can be used to estimate the total ablation, M, in m water equivalent (m w.eq.) using

$$M = \begin{cases} \frac{Q_0}{\rho_w L_f}, & \text{if } Q_0 \geq 0 \\ 0, & \text{if } Q_0 < 0 \end{cases}$$

where ρ_w is the density of water and L_f is the latent heat of fusion.

2.2 Mass balance modelling

2.2.1 Empirical and physical ablation models

The ablation of glaciers can be estimated using either physical or empirical methods (e.g. Greuell and Genthon, 2004). Empirical models, e.g. positive degree-day models, describe the statistical relations between melt and temperature and possibly other weather parameters. Although the energy balance is what determines how much ice will melt, over timescales of weeks or months it has been shown that melting correlates well with air temperature. This is because many of the energy balance components depend on temperature in some fashion. Typically, positive degree day models are of the form

$$M = \beta T_{pdd} \tag{4}$$

where β is the positive degree-day factor and T_{pdd} is the sum of all positive daily mean temperature in °C over the observation period. β is a constant which must be determined from field data. The effect of *e.g.* irradiance, wind speed, humidity, and cloud amount are all lumped into β. It is quite common to use two different values of β, one for snow and a higher one for ice, reflecting the differences in albedo. Positive degree day models have been used in many studies of the surface mass balance of Icelandic glaciers (e.g. Jóhannesson et al., 1995; Flowers et al., 2005; Marshall et al., 2005; Guðmundsson et al., 2009b,a), as they are practical and can be used with only limited input.

A drawback of these models is that they are not based on physics but on simple statistics. As a result, studies have shown that degree-day factors can change substantially both on seasonal and decadal timescales due to varying feedbacks from energy balance components which are not determined by the temperature like e.g. albedo (Guðmundsson et al., 2006; Bougamont et al., 2007; Huss and Bauder, 2009; van den Broeke et al., 2010). Guðmundsson et al. (2006) estimated that the positive degree day factors used for Vatnajökull could provide reasonable predictions for a temperature increase of less than 3°C, but only if no substantial changes in albedo occur.

In addition, a problem occurs when the temperature is around melting point, as, depending on radiation balance, the threshold between melt and no-melt could be above or below 0°C. It is also impossible to compute sublimation of snow and ice by means of degree-day models.

Physical models, i.e. energy balance models, provide direct estimates of the energy balance which can be used to model the ablation. The energy balance of a temperate glacier can be calculated using observations of the net radiation, air temperature, humidity and wind speed at one or more levels, where the wind speed, temperature, and humidity are used to estimate the turbulent fluxes. Parameterisations are often used in order to estimate the radiation components, as direct observations of the radiation are often not available due to the expense and difficulty in obtaining the observations (Hock, 2005). Since more observations, which are often not available, are needed to calculate the full energy balance, this method is less practical than positive degree day models.

Simulations of the past or future evolution of the mass balance can be conducted using both positive degree-day and energy balance models. One option is to prescribe a temperature and precipitation change onto observed, present day fields of these variables and use a positive degree day model to simulate the evolution of the mass balance (e.g. Flowers et al., 2005). A more complex option is to deploy climate models which simulate the meteorological forcing needed to estimate the ablation, and investigate the simulated change in mass balance during different climatic conditions and emission scenarios. The simulated temperature and precipitation fields can then be used to model the mass balance using a positive degree-day approach (e.g. Aðalgeirsdóttir et al., 2011), or if the model includes a full surface energy and mass balance model for the ice cap, the total simulated energy balance can be used (e.g. Boberg et al., 2018). High-resolution climate models which include a multi-layer snow pack scheme can also account for internal accumulation.

In this dissertation, only physical models are used to estimate the mass balance of Vatnajökull.

2.2.2 Global and Regional climate models

Global Climate Models (GCMs) are numerical models that combine atmospheric and ground surface physics. A major characteristic of these models is that they explicitly solve the hydrodynamic equations of the atmosphere. These equations determine the transfer of moisture from source regions (e.g. Greuell and Genthon, 2004), and are therefore of vital importance for simulations of the mass balance of glaciers. GCMs

are used internationally to make past and future projections of the large-scale effects of a changing climate. The Coupled Model Intercomparison Project (CMIP) was created in 1995 to provide a framework for GCM validation, as well as provide publicly available simulations from a large range of models. Simulations from phase 5 of the project (Taylor et al., 2012) have provided simulations spanning until at least 2100, and the results have been used in studies of climate change worldwide, e.g. within the CORDEX (Coordinated Regional Downscaling Experiment) framework (Giorgi et al., 2009). Simulations from the next phase of the project (Eyring et al., 2016) started becoming available in 2018. However, due the large domain and therefore high computational cost of GCMs, they run with a coarse (100-200 km) resolution which does not resolve smaller glaciers nor take all significant surface processes into account. Regional downscaling through Regional Climate Models (RCMs) are therefore often used to provide additional complexity to simulations of the cryosphere.

RCMs are forced by a GCM or reanalysis at the boundaries of their domain. RCMs run on a smaller domain than GCMs, only focusing on a specific region, and can therefore be used at higher resolution and can include more complex models of the cryosphere. High-resolution RCMs, such as RACMO (Meijgaard et al., 2008), the Weather Research and Forecast model (WRF) (Skamarock et al., 2008), MAR (Gallée and Schayes, 1994), and HIRHAM5 (Christensen et al., 2006), are therefore valuable tools to estimate the mass balance of glaciers or ice sheets. Many RCMs are therefore well validated over Greenland (e.g. Box and Rinke, 2003; Langen et al., 2017) and Antarctica (e.g. Lenaerts and Van Den Broeke, 2012; Agosta et al., 2015).

RCMs are derived from Numerical Weather Prediction models (NWPs). NWPs use physical models of the atmosphere and oceans to predict the weather based on current weather conditions. Like RCMs, they are forced by a GCM or reanalysis at the boundaries of their domain. While RCMs project climate scenarios, NWPs are used to predict the weather. The major difference between the two types of models is therefore the scale of the simulations: NWPs generally operate over smaller domains and much smaller time scales (days as opposed to decades for RCMs). For this reason, NWPs are often run at a higher resolution than RCMs.

RCMs and NWPs are generally one-way nested within GGMs, with a lateral buffer zone at the domain boundaries and an inner domain. The GCM forcing is only applied in the buffer zone so that the RCM equations can be freely integrated within the model interior. The climatology of a RCM is heavily influenced by the driving GCM, and any systematic errors in the GCM forcing will likely be transmitted to the RCM. It is therefore important to analyze the GCM forcing before applying a regional downscaling (e.g. Radić et al., 2011). The influence of the driving GCM is highest near the domain boundary and lowest in the middle of a domain. Larger domains are therefore less influenced by the driving forcing than smaller domains (Giorgi and Gutowski, 2015).

Only few studies have been conducted with two-way nesting of a RCM within a GCM. These studies show that including RCM feedback may improve GCM simulations (Lorenz and Jacob, 2005), but the importance depends on the investigated region (Giorgi and Gutowski, 2015).

A source of error which can be substantial within RCMs is the internal variability,

which is caused by nonlinear and stochastic model processes. The internal variability depends e.g. on season, region, and domain size (Giorgi and Gutowski, 2015). In some cases, it can create a spatially coherent model response, for example in the form of a temperature increase, which can be confused with a response to the model forcing (Giorgi and Bi, 2000; Rinke and Dethloff, 2000). For RCM sensitivity studies, it is therefore important to consider the magnitude of the internal variation. The effect of internal variability is largest for short-term simulations (Giorgi and Bi, 2000).

In 2009, the international project CORDEX (Coordinated Regional Downscaling Experiment) was initiated (Giorgi et al., 2009). The aim of this initiative was to advance and evaluate models used for regional downscaling through international cooperation. A collection of historical and future simulations from many different RCMs has been made available through this project (CORDEX, 2018), which include different climate scenarios, driving GCMs, and initialization.

2.2.3 Future direction of RCMs

Currently, RCM development is moving in two primary directions: i) towards higher resolution (1-5 km) simulations and ii) towards coupling in regional Earth system models (RESMs).

Early work of very-high resolution modelling shows that one of the major improvements is in the representation of precipitation (e.g. Lucas-Picher et al., 2012). The models provide more accurate simulations of the diurnal cycle, and climate change signals could substantially change with higher resolution due to changes in simulated intensity and frequency of precipitation events (e.g. Kendon et al., 2012; Fosser et al., 2015).

However, a higher resolution will not improve simulations of the climate if the model dynamics and physics are not appropriate. When switching towards very high-resolution modelling, a major shift in both the dynamics and physics of lower resolution RCMs has to occur. Most RCMs have a hydrostatic core, but at resolutions smaller than 4 km, a shift to non-hydrostatic dynamics is necessary, as non-hydrostatic features like deep convection can be explicitly resolved (Weisman et al., 1997). In many regions, deep convection is a dominant source of precipitation, so the improved precipitation found for high resolution RCMs is in large part due the change in the dynamical core, but also due to the better resolved topography. Physical parameterizations of e.g. cloud microphysics, which often utilizes a prognostic precipitation scheme, would also need improvements at higher resolutions (Rockel, 2015).

At present, e.g. WRF (Skamarock et al., 2008) and COSMO-CLM (Rockel et al., 2008) have performed very high resolution climate simulations with non-hydrostatic dynamics. At the Swedish Meteorological and Hydrological Institute, the non-hydrostatic NWP HARMONIE-AROME is currently being developed into a climate model (HARMONIE-CLIMATE). Mottram et al. (2017b) showed that with some changes to the HARMONIE-AROME mass balance scheme, the NWP could provide improved estimations of the surface mass balance of the Greenland ice sheet.

Several factors control how much the resolution of a RCM can be increased. The resolution of the driving GCM is of some importance, as a ratio of 10 between RCM

and GCM resolutions is considered to be the upper limit to still obtain good downscaling ability (Antic et al., 2006). In addition, there is the issue of computing cost, as a doubling in resolution leads to a factor eight increase in computing time. Some models circumvent this issue by using variable resolutions within the model grid. This method has e.g. been used in Polar-WRF to simulate the climate over Svalbard glaciers. Claremar et al. (2012) used three nested domains with grid sizes of 24, 8, and 2.7 km to simulate the meteorological conditions over Svalbard glaciers, in addition to conducting a 900 m resolution run for a small domain. Aas et al. (2015, 2016) used nested domains of 9 and 3 km to estimate the mass balance of Svalbard glaciers from 2003-2013, in addition to a 1 km nested grid for a one-month only simulation.

The second main direction of climate models is coupling of the models into RESMs. Interactions between different components of the climate system occur on spatial scales smaller than those GCMs can resolve, and interactions can therefore be better captured at RCM resolutions (e.g. Giorgi, 1995). Due to great difficulty in creating a comprehensive, coupled RESM, e.g. due to varying temporal and spatial scales of the different Earth system components, inclusion of different aspects of the Earth system is done in slow, incremental steps. However, several models which include more than one part of the Earth system already exist, which couple RCMs with e.g. ocean models (e.g. Schrum, 2017), aerosol models (e.g. Nabat et al., 2015), or cryospheric models (e.g. Kotlarski et al., 2010).

One example of a developing coupled RESM is HIRHAM5-HYCOM-CICE-PISM-GIPL (Christensen et al., 2014) which is developed at the Danish Meteorological Institute to investigate climate interactions in the Arctic domain. It couples the RCM HIRHAM5 with an ocean model (HYCOM), a sea ice model (CICE), an ice flow model (PISM), and a permafrost model (GIPL). However, while HIRHAM5 is coupled to each of these elements, they do not all run simultaneously at the present time.

2.3 Modelling of ice flow

Glacier ice is described as a slow moving, incompressible fluid which deforms under its own weight. It therefore follows the equations that govern fluids mechanics, the Navier-Stokes equations (e.g. Paterson, 1983). The flow of a fluid is generally computed based on a balance between acceleration terms and body forces, but since glacier ice is a slow moving fluid the acceleration terms can be neglected. The Navier-Stokes equations can therefore be simplified as the Stokes equations, which can be expressed as

$$\nabla \cdot \mathbf{u} = 0 \qquad \text{(mass continuity)} \tag{5}$$

$$-\nabla p + \nabla \cdot \tau_{ij} + \rho g = 0 \qquad \text{(stress balance)} \tag{6}$$

where p is the ice pressure, $\mathbf{u}$ is the 3D ice velocity, τ_{ij} is the deviatoric stress tensor, ρ is the ice density, and g is the acceleration of gravity.

In order to estimate the velocity of an ice sheet, the material properties have to be defined. Experimental work has shown that ice flow follows a power law relationship known as Glen's flow law (Glen, 1955), which can be expressed as

$$D_{ij} = A\tau^{n-1}\tau_{ij} \qquad \text{(flow law)} \tag{7}$$

where D_{ij} is the strain rate tensor, given by $D_{ij} = \frac{1}{2}(u_{i,j} + u_{j,i})$, and τ is the second invariant of the deviatoric stress, given by $\tau = (\frac{1}{2}\tau_{ij}\tau_{ji})^{\frac{1}{2}}$. The flow exponent n is commonly assumed to be equal 3 (e.g. Cuffey and Paterson, 2010), but recent experimental work has indicated that higher values of n may be more appropriate (e.g. Goldsby and Kohlstedt, 2001). Nevertheless, the classical value of $n = 3$ is used in this study. The ice softness A is highly dependent on ice temperature, but is also affected by other parameters such as grain size, impurities, water content, and the flow exponent n (Cuffey and Paterson, 2010).

Complex flow models will solve the full Stokes equations to determine the full stress field and its evolution through time. However, due to the high computational costs of these simulations, most models approximate the stress field by solving a simplified version of the Stokes equation. One such example is the shallow-ice approximation (SIA) (Fowler and Larson, 1978; Hutter et al., 1981; Hutter, 1983).

The SIA assumes that since the thickness of an ice sheet is generally small in comparison to its horizontal dimensions, the horizontal changes in the vertical component of the stress are negligible. Under this assumption, the Stokes equations for the stress balance can be reduced to

$$\frac{\delta\tau}{\delta z} = -\nabla_x p \tag{8}$$

$$\frac{\delta p}{\delta z} = -\rho g \tag{9}$$

with the boundary conditions that p and τ are zero at the surface and $\nabla_x = (\delta/\delta x, \delta/\delta y)$ (Schoof and Hewitt, 2013). When combined with Glen's flow law, the deformation velocity $\mathbf{u}$ can be expressed as

$$\mathbf{u} = -2(\rho g)^n |\nabla z_s|^{n-1} \left[\int_{z_b}^{z_s} A(z_s - \zeta)^n d\zeta \right] \nabla h \tag{10}$$

where z_s is the surface elevation, and ζ represents the vertical integration variable from the base z_b to the glacier surface z_s. The SIA significantly reduces the computational cost of solving full Stokes. However, basal sliding is difficult to implement into the SIA model, and the accuracy of the simulations decreases as the contribution of basal sliding increase (Fowler, 2001; Pattyn, 2003). The model is therefore not appropriate for simulating e.g. ice streams, grounding lines, and ice shelves. However, sliding laws have been implemented into SIA models, with schemes that usually depend on the driving stress (e.g. Huybrechts et al., 1999; Payne et al., 2000; Marshall et al., 2002; Aðalgeirsdóttir et al., 2005). These schemes can cause discontinuities in the velocity field and do not represent a physical parameterisation for glacier sliding, as sliding should depend on the amount of water at the base and the strength of the glacier till (Bueler and Brown, 2009).

Bueler and Brown (2009) suggest that a more appropriate way to include sliding in SIA

models is to combine the SIA with the shallow shelf approximation (SSA) (Morland, 1987; Weis et al., 1999). As the name suggests, the SSA was developed to model ice shelves and fast-moving ice streams, which are generally dominated by longitudinal stresses. For the SSA solution, the flow law is described by

$$\tau_{ij} = A^{\frac{1}{n}} D^{\frac{1}{n}-1} D_{ij} \tag{11}$$

where $D = \sqrt{\frac{1}{2} D_{ij} D_{ij}}$ (Bueler and Brown, 2009). In the combined model, the SSA basically functions as a sliding law, where the sliding depends on the strength of the glacier till. By combining the simplified Stokes equations of the SSA with the described flow law, the velocity due to sliding can be calculated by solving (Bueler and Brown, 2009)

$$\frac{\delta T_{i,1}}{\delta x_1} + \frac{\delta T_{i,2}}{\delta x_2} + \tau_{b,i} = \rho g H \frac{\delta H}{\delta x_i} \qquad \text{for i=1,2} \tag{12}$$

where x_i is the horizontal coordinates, H=$z_s - z_b$ is the ice thickness and $T_{i,j}$ is the vertically averaged stress tensor. It is given by

$$T_{i,j} = 2\bar{\nu} H (D_{i,j} + (D_{11} + D_{22})\delta_{i,j}) \qquad \text{for i=1,2} \tag{13}$$

where $\bar{\nu}$ is the vertically-integrated viscosity and $\delta_{i,j}$ is the Kronecker delta. The proportion of the velocity calculated from SIA and SSA varies across the simulated ice sheet, from SIA-only in the ice sheet interior, to combined SIA and SSA for ice streams, and SSA-only for ice shelves (see Figure 2.1). This allows accurate simulation of ice in areas where most of the displacement is due to basal slip. This method has been successfully applied to glaciers in Greenland (e.g. Aschwanden et al., 2016) and Antarctica (e.g. Pollard and DeConto, 2009; Seroussi et al., 2012; Winkelmann et al., 2011).

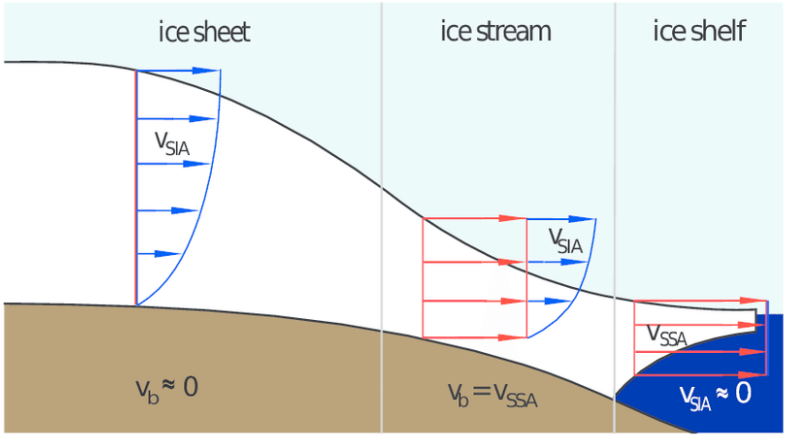

Figure 2.1. Illustration of combination of velocities in a coupled SSA + SIA approach. From Winkelmann et al. (2011).

Several studies have focused on the differences between SIA and full model simulations, to understand the difference in model simulations for different research topics. Leysinger-Vieli and Gudmundsson (2003) found that for the purpose of investigating glacier snout advance and retreat rates, similar results are obtained using SIA and full system models. However, modelled surface velocities are not necessarily the same between the two models due to the simplified stress balance used by SIA. Aðalgeirsdóttir et al. (2000) showed that for ice caps with spatial scales larger than 10 times the ice thickness, the approximation gives similar results to the full system model in terms of ice thickness. In addition, the uncertainties introduced in the ice cap evolution from e.g. mass balance biases are currently much greater than those introduced by the stress balance approximations (Goelzer et al., 2017).

2.4 Coupling of mass balance and ice flow

As mentioned in Section 2.3.3, regional climate models are moving towards more comprehensive Earth system models, which e.g. include dynamic glaciers. Several previous studies have worked on coupling both empirical and physical models of the mass balance with ice flow models, with varying complexities of the coupled simulations (e.g. Aðalgeirsdóttir, 2003; Gong et al., 2014; Schäfer et al., 2015; Gilbert et al., 2016).

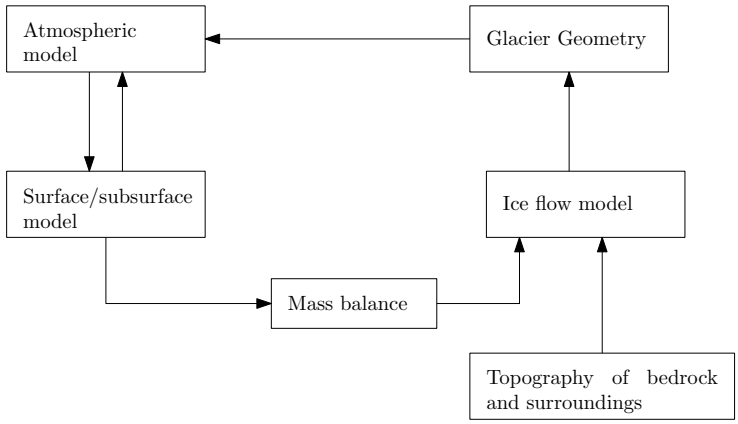

Figure 2.2. Flowchart showing the relationship between the changes in geometry of a glacier with the meteorological conditions.

The simplest coupling technique is to perform a one-way coupling between the mass balance model and the ice flow model (e.g. Aðalgeirsdóttir et al., 2011; Gong et al., 2014). In these simulations, the simulated mass balance is used to force the ice flow model, but changes in glacier geometry do not affect the simulations. However, due to the strong coupling between elevation and mass balance, ignoring elevation feedback on the mass balance can lead to significant errors. Edwards et al. (2014) showed that for a 2°C warming, the sea level change due to melting from Greenland was underestimated by 2-7% after 100 years. Similar results were found for coupled

simulations of Austfonna in Svalbard, where the underestimation was 10-20% after a century depending on the warming scenario (Schäfer et al., 2015).

Two-way coupled simulations have been conducted using empirical models (e.g. Aðalgeirsdóttir, 2003; Schäfer et al., 2015) as well as physical models (e.g. Edwards et al., 2014). However, for this overview I will mostly focus on the coupling of ice flow models to RCMs. Figure 2.2 shows a flowchart of two-way coupled RCM-ice flow simulations.

An issue when dynamically including ice flow models in RCMs is the differences in temporal and spatial scales between glacier processes and the RCM resolution. In order to properly resolve the ice flow, either parameterisation for sub-grid scale processes is needed or higher resolution models. Using variable resolutions within the model grid similar to the RCM simulations performed by POLAR-WRF by Claremar et al. (2012), could be the way forward for more accurate simulations of flow. Ice flow studies using varying grid resolution, so that fast-moving outlet glaciers are better resolved than the slower ice cap interior, have been conducted with finite element grids (e.g. Schlegel et al., 2015) and adaptive mesh grids which update during the run (e.g. Cornford et al., 2013; Lee et al., 2015).

Fully coupled RCM-ice flow models have been conducted over Greenland with e.g. the RCM MAR coupled to five ice flow models of different complexity (Edwards et al., 2014).

The Ice Sheet Model Intercomparison Project (ISMIP) (Nowicki et al., 2016) is currently working on coupling climate model output from CMIP6 to ice sheet models in order to produce projection of sea level change. Most of the projections are planned using a one-way coupling between GCMs and ice flow model, but a small number of fully coupled simulations are planned to address the feedbacks introduced by interactive ice sheets (Goelzer et al., 2018).

3 Observations

In this thesis, ground observations from AWSs, mass balance surveys, and river gauges are used to optimize and/or evaluate simulations of the energy and mass balance of Vatnajökull. In addition, MODIS observations of the albedo are used to create a background albedo map to improve the simulation of ablation. Finally, interpolated maps of the bedrock and the surface topography are used for initialization of the flow model PISM.

3.1 Study area

Iceland, 103000 km^2, is an island situated in the North Atlantic Ocean, just south of the Arctic circle. The North Atlantic and Irminger ocean currents give the island a mild maritime climate, with winter temperatures around 0°C and summer temperatures around 10-13°C at the southern coast. The Icelandic low, a persistent low pressure center between Iceland and Greenland, often brings heavy precipitation to Iceland.

Due to the temperate climate and high precipitation, approximately 11% of Iceland is glacierized (Björnsson and Pálsson, 2008). Most of the glaciers are located along the southern coast, due to the high orographic precipitation in this region. Mass balance observations have been conducted on many of the larger ice caps since the beginning of the 1990s, and AWSs are operated during the summer on several of the glaciers.

The focus of this thesis is Vatnajökull ice cap, with an area of 7800 km^2 and a volume of $\sim$3100 km^2 (Björnsson, 2017), is the largest ice cap in Europe. It has a surface elevation spanning from 0–2110 m above sea level (a.s.l.). The ice cap is located close to the southeastern coast of Iceland (Figure 3.3), and average temperatures on the ice cap are close to or below freezing. The summer balance is normally negative for the entire ice cap, but the central area occasionally turns slightly positive during repeated cold spells. At the highest areas of the glacier, days with melting only occur 10-20 days of the year, while at lower levels the ablation season generally lasts 3-4 months (Björnsson and Pálsson, 2008). For outlets that lie at a very low elevation (<100 m a.s.l.), even the winter balance is negative. Above 1300 m a.s.l. on the southern flanks of Vatnajökull, precipitation can exceed 4-5 m w.eq. per year (Crochet et al., 2007), while the northern lee side of the ice cap is in a dry region which receives precipitation in the order of 0.4-0.7 m w.eq. (Björnsson and Pálsson, 2008).

Vatnajökull lies partly within the active volcanic zone (Figure 3.3), and covers several of Iceland's largest volcanoes where eruptions are frequent (e.g. Gudmundsson et al., 2012). Western Vatnajökull mainly lies on porous lava beds, while eastern

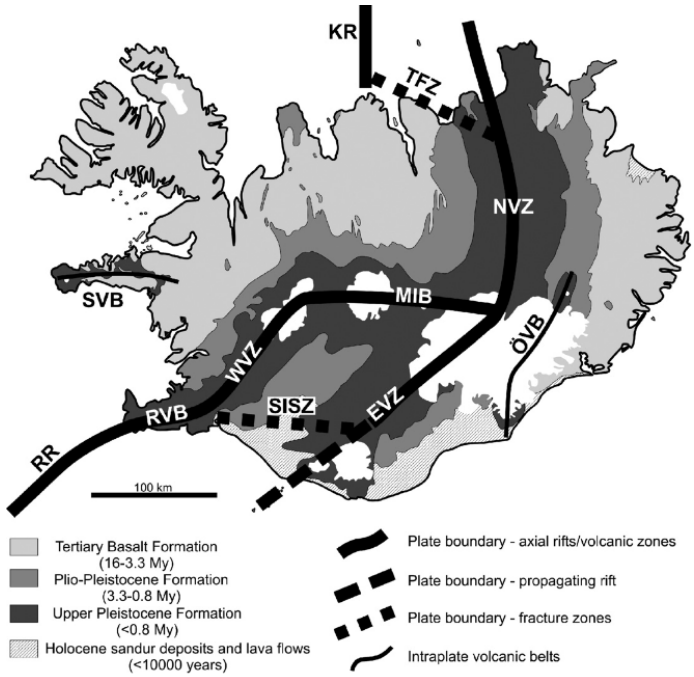

Figure 3.3. Geological map of Iceland, including the main fault structures. From Thordarson and Larsen (2007).

Vatnajökull lies on impermeable unconsolidated till (e.g. Björnsson, 1988). Tephra layers in the glacier ice dominate its spectral properties and volcanic ash therefore has a large effect on the melt in the ablation zone, as the albedo can drop below 0.1. Frequent dust storms also occur over the ice cap, darkening the surface and increasing melt (e.g. Dragosics et al., 2016). Geothermal activity at the bed provides a small contribution to the total melt (Björnsson and Pálsson, 2008), with constant melting occurring above areas with a high geothermal heat flux, like the Grímsvötn volcano (Björnsson et al., 1998) and the two Skaftá cauldrons (Björnsson, 1977, 1988; Einarsson et al., 2017). Here, water collects in sub-glacial lakes above the geothermal areas, which regularly is released in jökullhlaup events (e.g. Björnsson, 1977).

All the major glacial outlets of Vatnajökull are surge-type, and about 75% of the ice cap area can be affected by surges (Björnsson et al., 2003). Recorded surge histories suggest that some glaciers surge at regular intervals, with e.g. north-facing Brúarjökull surging at 80-100 years intervals. Other outlets surge at very varying intervals, with e.g. south-east facing Breiðamerkurjökull surging at between 6 and 38 year intervals. In the 1990s, approximately 25% of the ice surplus in the accumulation area of Vatnajökull was transported to the ablation area by surges (Björnsson et al., 2003).

3.2 Ground-based observations

3.2.1 Automatic weather stations

AWSs have been operated on Vatnajökull since 1994, with 1-13 stations measuring on the ice cap during the summer months (e.g. Oerlemans et al., 1999; Guðmundsson et al., 2006). The program is a collaboration between the National Power Company of Iceland and the Institute of Earth Sciences at the University if Iceland. The 2 m temperature, 2 m relative humidity, 4 m wind speed, and the 4 m wind direction have been measured since 1994, while the radiation components have been measured since 1996. Most of the AWSs on the ice cap are operating approximately from May until October, with a few select stations operating year round. A sonic echo sounder is placed a few meters from the AWSs, which measures the daily surface changes both due to ablation and snow accumulation. Based on measurements of the seasonal evolution of the density conducted in the summer of 1996, a density profile was created which can be used to calculate the corresponding ablation (Guðmundsson et al., 2006). The instruments were calibrated each year in Reykjavík in April and the AWSs were visited in July/August each year until 2009 to ensure that they were working properly and to lower the sonic echo sounder (Björnsson et al., 1996, 1997a,b; Guðmundsson et al., 1999, 2000, 2001, 2002). Measurements from both the AWS and sonic sounder are currently conducted at 10 min intervals, but before 2006 the sonic sounder was operated at 30 min intervals. The daily albedo is estimated from the observed incoming and outgoing short wave radiation. It is calculated as the average of the observations obtained between 13 and 14 UTC, as the solar zenith angle is smallest during this period (Guðmundsson et al., 2006).

The uncertainties of the AWS observations vary depending on the sensor. The temperature and humidity sensors have an accuracy of 0.2°C and 2% for temperature and humidity, respectively, while the accuracy of the wind speed is 0.2 m s^{-1} (Guðmundsson et al., 2009b). The radiative fluxes were measured using either Kipp and Zonen CM14, CNR1 or CNR4 sensors that have a maximum manufacturer-reported uncertainty of $\pm 10\%$ for daily averages (Kipp and Zonen, 2002). However, the uncertainty has independently been evaluated to be only 3–5 % when used in an ice sheet environment (van den Broeke et al., 2004; Guðmundsson et al., 2009b).

The turbulent fluxes are not measured by the AWSs, but are estimated from observations of temperature, humidity and wind speed using a one-level eddy flux model, which is described in detail by Guðmundsson et al. (2009b). The model utilizes Monin–Obukhov similarity theory (Monin and Obukhov, 1954; Björnsson, 1972) and implements different roughness lengths for the vertical profiles of temperature, wind and water vapour (Andreas, 1987). Uncertainties of this model for example pertain to the aerodynamic roughness length for momentum z_0, as it is assumed to have a constant value of 1 mm. This assumption is an oversimplification, as the roughness may vary significantly over the ablation season (e.g. Grainger and Lister, 1966), but measurements of z_0 are generally not available over the entire measuring period. However, the roughness profile can be derived from observations of the wind profile (Björnsson, 1972).

In this thesis, I have mainly focused on the observations from five AWSs, three on

Brúarjökull and two on Tungnaárjökull. These stations were chosen since they have been operated at approximately the same location since at least 2001, with two stations in the accumulation zone, one near the equilibrium line, and two in the ablation zone. The locations of the stations are shown in Figure 3.4.

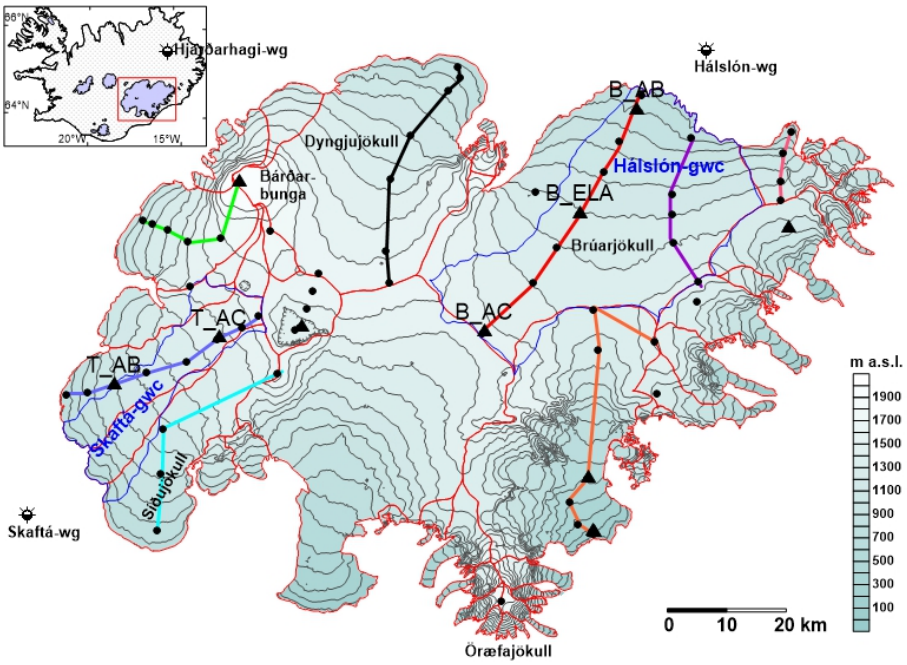

Figure 3.4. Overview of available observations used in this thesis. Triangles show AWS locations, black circles show mass balance survey points, colored lines connecting the survey points show flowlines along which velocity observations are used, and symbols outside the ice cap show the locations of the used water gauges. Hálslón and and Skaftá glacial water catchments are marked with blue, while ice divides are marked with red.

3.2.2 Mass balance and velocity

In situ mass balance and surface velocity measurements have been carried out twice a year every glaciological year since 1991-92 (Björnsson et al., 1998), with an average of 60 measured locations every year (Figure 3.4). In April or May of each year, winter mass balance cores are drilled through the winter layer, and the snow/firn density is measured along the core. The summer mass balance is measured in September or October by measuring stakes or wires which were drilled into the surface during the winter measurements in the spring. The uncertainty in the mass balance measurements has been estimated to be ± 0.3 m w.eq. (Björnsson et al., 1995, 2013). The results from the mass balance surveys are extrapolated into distributed mass balance maps of the surface using the kriging interpolation technique. Observations on e.g. Öræfajökull and Skeiðarárjökull are rarely conducted, and the mass balance is therefore generally

extrapolated by considering the mass balance of the other glacier outlets. These maps are used to compute the specific summer, winter, and net mass balance for all of Vatnajökull, see Figure 3.5. The mass balance observations and maps are used in this thesis to validate the simulations from the RCM HIRHAM5 and the NWP HARMONIE-AROME.

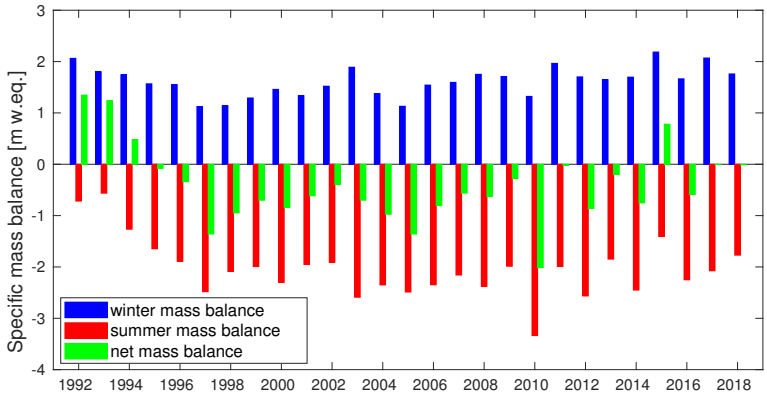

Figure 3.5. Observed summer (red), winter (blue), and net (green) surface mass balance of Vatnajökull. From e.g Pálsson et al. (2017), expanded to 2017-18.

The GPS locations of the mass balance stakes or wires are measured both in spring and autumn of every year, which can be used to compute average surface velocities between survey times. The velocities along eight flowlines are used in this study to evaluate the surface velocities simulated by the flow model: Eastern and Western Brúarjökull, Eyjabakkajökull, Breiðamerkurjökull, Síðujökull, Tungnaárjökull, Köldukvíslarjökull, and Dyngjujökull. The flow lines are marked with colors in Figure 3.4. The length of the measurement time series along the flowlines varies, but all used points have been observed for several years. The velocity time series for Tungnáarjökull and Dynjujökull include years with surge velocities. These years are discarded in the model comparison.

3.2.3 Discharge observations

Measurements of the discharge into two glacial rivers, Skaftá and Jökulsá á Dal, are used in this thesis (Figure 3.4). The closest hydrometric station to the ice cap along Skaftá is at Sveinstindur (V299), 25 km down-river from the glacier margin. It has been operated since 1986 (Icelandic Meteorological Office Database, 2017). The Sveinstindur station has a catchment area of 714 km^2 (Harðardóttir and Snorrason, 2003), where approximately 400 km^2 is glacierized. The glacial part of the catchment contains Skaftárjökull and parts of Tungnáarjökull, and it spans from approximately 700-1600 m a.s.l.

The runoff data comes with a quality flag for each daily datapoint. Only data that are of full quality were used while data that required corrections due to ice interference on the runoff or other issues have been discarded.

Until 2007, the closest hydrometric station to the ice cap along Jökulsá á Dal river was at Hjarðarhagi (VHM110) (Landsvirkjun, 2017). The size of the Hjarðarhagi catchment area is $\sim$3300 km^2 (Snorrason et al., 1998), where approximately 1200 km^2 is covered by the ice cap. The glacial component of the catchment includes approximately 80% of Brúarjökull, and spans from $\sim 750 - 1600$ m a.s.l.

In autumn 2007, the Hálslón reservoir started operations on the uppermost former path of the Jökulsá á Dal river, near the edge of Brúarjökull. The water level has been monitored since the impoundment of the dam (Landsvirkjun, 2017). The runoff to the reservoir is estimated based on a relationship between reservoir water level and storage in a time series of daily averaged inflow. The size of the Hálslón catchment area is about 1800 km^2, where approximately 1200 km^2 is covered by the ice cap. The glacial component is the same as for the Hjarðarhagi catchment.

In order to get a time series of the discharge into Jökulsá á Dal that spans the entire simulated period (1980-present day), observations from Hjarðarhagi are used from 1980-2007, after which the observations from Hálslón reservoir are used. However, due to the larger area of the Hjarðarhagi catchment, the contribution of melt from non-glacierized areas is significantly larger than for Hálslón.

3.2.4 Bedrock topography

Since 1977, radio-echo soundings of the ice thicknesses of Vatnajökull have been performed by the Institute of Earth Sciences at University of Iceland in cooperation with Landsvirkjun, the National Power Company of Iceland (Björnsson, 1986, 1988).

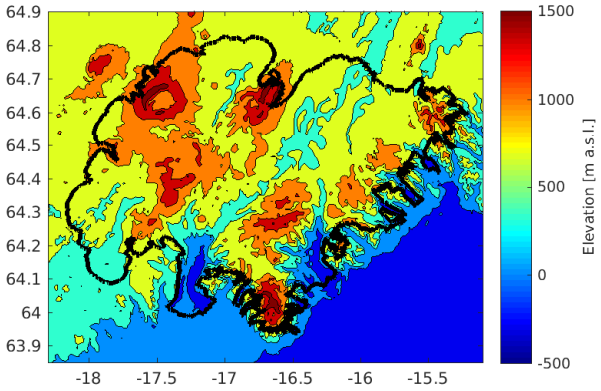

Figure 3.6. Map of the interpolated bed topography of Vatnajökull. Outline of the present day ice cap is shown in black.

Pulses with a duration of 0.2 μs are transmitted into a 30 m dipole antenna with a repetition rate of 1 kHz. The reflected signal is received by an identical antenna and fed to a receiver with a bandwidth of 1-5 MHz (Björnsson, 1986, 2000). Each pulse from the transmitter illuminates an approximate disc with a radius of 100-200 m, so the received echo is composed of energy from that disc. An attempt to trace the energy to point

sources at the bed is made using migration along the profile; the process is described in detail in e.g. Magnússon et al. (2016). The sounding lines were typically conducted 1 km apart and then interpolated onto a map using manual interpolation. The uncertainty of the ice thickness along each sounding line is estimated to be approximately ± 15 m (Björnsson, 2000), but due to uncertainty in the interpolation, the error in the bedrock topography map is estimated to be 20-50 m. In this study a map with a 500 m resolution is used (Figure 3.6). This map is used in the simulations of the flow of Vatnajökull.

3.3 Satellite observations

3.3.1 MODIS albedo

Observations of the broadband albedo in the shortwave spectrum (0.3–5.0 m) from the MODerate Resolution Imaging Spectroradiometer (MODIS) are used to create a background map of the ice albedo at all glacier grid points in HIRHAM5. In December 1999, the first MODIS instrument was launched into Earth's orbit on board the NASA Terra Satellite, and with it a new capability for deriving moderate resolution estimates of broadband albedo was initiated (Schaaf et al., 2002). In 2002 a second instrument was launched on board the Aqua Satellite. The MODIS instruments are well suited for albedo monitoring, as they image the snow covered areas of mid-to-high latitude regions with a high spatial resolution. In addition, they can continuously measure spatial variations for long periods, except in cases where the ground is obscured by clouds. The instruments take images of the entire Earth every 1-2 days, retrieving data in 36 spectral bands ranging in wavelength from 0.4 μm to 14.4 μm.

MODIS (Aqua/Terra combined) albedo product MCD43A3 v006 (Schaaf and Wang, 2015), tile h17v02, was used in this study as it covers all of Vatnajökull. Before the 2nd of July 2002, when the instrument was only on board Terra, the acquisition time was at approximately 10:30 GMT. When the instrument launched on Aqua, the new acquisition time was approximately 13:30 GMT.

For this study, the MODIS broadband albedo in the shortwave domain (0.3-5.0μm) is used, which is calculated using the first seven visible and near-infrared MODIS bands (Klein and Stroeve, 2002). The data was extracted in geographical coordinates at a resolution of 0.005°, which is close to the original MODIS resolution of 500 m. This was done using the MODIS reprojection tool with the bilinear resampling method. These MODIS data were then resampled to match the rotated HIRHAM5 lon-lat grid coordinates by bilinear interpolation using MATLAB's interpn function (MATLAB, 2015). No gap filling was used for the missing values. In order to maximize the number of observations, data with a low quality flag were not removed. However, periods with a high solar zenith angle were discarded due to the lowered resolution of the albedo observations (Stroeve et al., 2005; Schaaf et al., 2011; Schaaf and Wang, 2015).

Several studies have shown that MODIS agrees reasonably well with in situ observations from weather stations on the Greenland ice sheet, especially in regards to seasonal albedo cycles and mean seasonal values when only small variability occur (e.g. Stroeve et al., 2005, 2006; Box et al., 2012). However, the albedo of Icelandic glaciers is more

variable both temporally and spatially than the albedo of the Greenland ice sheet. The albedo data from the MODIS retrievals were therefore compared to those observed by AWSs on Vatnajökull and Langjökull by Gascoin et al. (2017), to asses if the MODIS product is able to capture the large variability in the albedo of Icelandic glaciers. The authors found that there is a good agreement between the ground observations and the MODIS albedo, with root mean square errors between 0.08-0.21 for the 11 investigated AWS sites.

The MODIS albedo is compared to albedo observations from AWSs calculated between 13:00 and 14:00 in this study. Using the albedo at highest radiation, as opposed to the daily albedo value, should be directly comparable to the MODIS observations, which for most of the time series have an acquisition time of 13:30. However, the average difference between the daily and high radiation AWS albedo is on average <1%, so the choice in albedo should not have much effect on the comparison.

The MODIS observations include more of the near-infrared spectrum (0.3-5.0μm) than the AWS observations (0.3-3.0μm), but given the low solar radiation in the infrared spectrum this difference in wavelength should not matter for the results.

3.3.2 Surface topography

A map of the surface topography of the ice cap in 2010 is used for initialization of the flow model and for evaluation of the simulated initial state. The map is based on images from the SPOT5 satellite (Berthier and Toutin, 2008) from June and September 2010 with a 5 m resolution. The uncertainty on the acquisition day is approximately 1-2 m. However, due to differences in the surface elevation between acquisition days due to glacier melt, the uncertainty may be higher ($\sim$5 m).

3.4 Reanalysis

Reanalysis is a method for developing comprehensive data sets for climate research. It is created using a data assimilation scheme, which combines all available observations within a 6-12 hour time period with a numerical forecast model.

For this thesis, ERA-Interim reanalysis (Dee et al., 2011) is used as boundary forcing for RCM and NWP simulations. ERA-Interim is a global atmospheric reanalysis produced by the ECMWF which covers the period from 1 January 1979 until present day. It has a horizontal resolution of 0.75°x0.75° Available data products include 3-hourly surface parameters, describing weather, ocean, and land-surface conditions, and 6-hourly parameters covering the troposphere and stratosphere (Dee et al., 2011). Observations include both ground-based observations, upper-air observations from e.g. weather balloons, and satellite observations, with the majority of the observations provided by satellites. The wealth of available observations have grown exponentially from 1979 until present day, and currently approximately 7-9 million observations are included in each time step (Dee et al., 2014).

Although reanalysis is based on a wealth of observations, there can still be significant

biases in the available meteorological fields. The changing number of observations can produce artificial variability over the time series, and the simulations will in general depend on the amount of observations within the investigated region. In areas with sparse observations, like e.g. the Arctic, the reanalysis is more dependant on the physics in the used forecast model than in regions with a wealth of observations. The difference between different reanalysis products is therefore largest in data-sparse regions. Lindsay et al. (2014) investigated seven reanalysis data sets over the Arctic domain from 1981–2010, and found that ERA-Interim compared favourably with the other reanalysis products, obtaining the most consistently good correlation with observations.

4 Methods

4.1 HIRHAM5

The RCM HIRHAM5, which was originally developed in a collaboration between the Danish Meteorological Institute, the Royal Netherlands Meteorological Institute and the Max Planck Institute, is the main tool used in this thesis. It is a hydrostatic RCM which combines the dynamical core of the HIRLAM7 (High Resolution Limited Area Model) numerical forecasting model (Unden et al., 2002; Eerola, 2006) and physics schemes from the ECHAM5 general atmospheric circulation model (Roeckner et al., 2003).

The primary objective of HIRLAM7 is to provide an operational system which can be used for short-range weather forecasts. It is used for this purpose in a number of meteorological institutes in e.g. the Scandinavian countries (Unden et al., 2002). Only a subset of the full HIRLAM7 system is used in HIRHAM5. The physics scheme of HIRLAM7 is replaced by ECHAM5 physics, and thus only the time integration module for prediction of the key meteorological variables (for example horizontal wind components, temperature, specific humidity, and turbulent kinetic energy) is included in HIRHAM5. ECHAM5 is developed by the Max Planck Institute, and has provided global predictions of the past and present climate for e.g. the 5th and 6th phase of the CMIP project (e.g. Taylor et al., 2012). The physics in both models is applied in vertical columns, with no connection between neighbouring grid points in the horizontal direction.

HIRHAM5 is one-way driven by different global data sets, either from global re-analysis or from a GCM, at the lateral and lower boundaries of its domain. The model is forced by temperature, wind, relative humidity and surface pressure at the lateral boundary, and sea surface temperature and sea ice fraction at the lower boundary at 6 hour intervals

For simulations of the mass balance from 1980-2014, simulations forced by the ERA-Interim reanalysis dataset (Dee et al., 2011) are used in this thesis. HIRHAM5 model simulations using ERA-Interim forcing have been successfully validated over Greenland (e.g. Box and Rinke, 2003; Stendel et al., 2008; Lucas-Picher et al., 2012; Rae et al., 2012; Langen et al., 2015, 2017) using AWS and ice core data.

For future projections, simulations forced by the GCM EC-EARTH (Hazeleger et al., 2012) are used. EC-EARTH is based on the operational seasonal forecast system of the European Centre for Medium-Range Weather Forecasts (ECMWF). It has a 2°C cold bias over the Arctic (Koenigk et al., 2013), which leads to an overestimation in the sea ice extent, but it performs well in simulating dynamic variables when compared to other coupled models with similar complexity (Hazeleger et al., 2012). HIRHAM5

model simulations using EC-EARTH forcing have been validated over Greenland by Boberg et al. (2018) using AWS data. Projections are available under the Representative Concentration Pathways (RCP) 4.5 and 8.5 scenarios. The RCP 4.5 scenario (Thomson et al., 2011) represents a more moderate emission scenario, leading to a worldwide temperature increase of 2.4 °C by 2100, while the RCP 8.5 scenario (Riahi et al., 2011) represents a high emission scenario which leads to an average worldwide temperature increase of 4.7°C.

The HIRHAM5 simulations used in this thesis were conducted for a domain containing both Iceland and Greenland (Figure 4.7), with a horizontal resolution of 0.05° x 0.05° on a rotated-pole grid. This corresponds to $\sim$ 5.5 km resolution over Iceland. The whole domain contains 402 x 602 grid cells. The atmosphere has 31 irregularly spaced vertical levels, from the surface to 10 hPa, and a time step of 90 s.

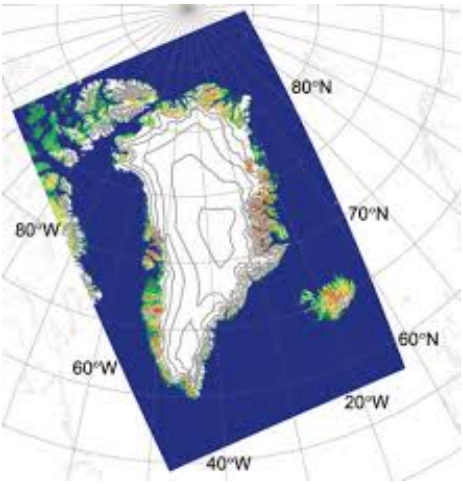

Figure 4.7. HIRHAM5 domain and topography. From Mottram et al. (2017a)

4.1.1 Snow pack scheme

In this thesis, the snow pack scheme developed for HIRHAM5 is applied. While the original HIRHAM5 used unchanged ECHAM5 physic, an updated model version was developed by Langen et al. (2015) which e.g. includes an improved dynamic surface/subsurface scheme, which describes the energy and mass transfer in the uppermost part of the glacier.

The snow pack model prescribes a 60 m w.eq. glacier on all gridpoints with permanent ice cover. The glacier is divided into 25 layers with time-constant water equivalent thicknesses. The thicknesses of the layers increase exponentially with depth in order to increase the resolution near the surface, and each layer consists of a liquid water fraction, a snow fraction, and an ice fraction. Mass is conserved between the layers by calculating the mass flux to the surface and from the bottom of the model. The

changes in each layer are first calculated based on the added mass (snowfall, rainfall, condensation) at the top of the model column. If mass is added, the scheme advects mass downward through the column in order to ensure a constant water equivalent thickness of each layer. When mass is removed from the column through runoff, sublimation or evaporation, mass is shifted up in a similar fashion from an infinite pure ice reservoir beneath the lowest model layer. The movement of mass through the layers is accompanied by a vertical transfer of sensible heat, snow density, grain size and water/snow/ice fractions. Falling snow is assumed to have the temperature of the surface, while rain is assumed to have a temperature of 0°C. Possible energy fluxes from rain warmer than melting point is therefore not accounted for in the model (Langen et al., 2017).

The changes in each layer due to melting or percolation of water is calculated after the layer shift due to accumulation. Melt occurs at the top layer based on the ice surface temperature. The ice temperature is updated in each time step, accounting for both the surface energy balance as well as diffusive and advective heat exchange between subsurface layers. If available energy exceeds that needed to bring the surface to the melting point, the excess heat is used for melting of the surface layer. During melting, mass is changed from the snow and ice fractions to the liquid water fraction, with snow always melting before ice.

If the liquid water in a layer exceed the retention threshold, set to 4% of the snow mass in the layer, water percolates down through the lower layers until it reaches an impermeable layer. A layer is considered impermeable if the density exceed 810 kg or it is already at the retention threshold. When the water reaches an impermeable layer, it either becomes runoff or refreezes.

In order for water to run off, the layer temperature must be at the melting point and the layer must be at the retention threshold. The runoff RO per time step Δt is determined by

$$RO = p_{liquex} \frac{\Delta t}{\tau_{RO}} \tag{14}$$

where p_{liquex} is the amount of water above the retention threshold and τ_{RO} is a characteristic runoff timescale. It is given by

$$\tau_{RO} = c_{RO,1} + c_{RO,2} e^{-c_{RO,3} S} \tag{15}$$

where S is the surface slope and $c_{RO,1} = 0.33$ day, $c_{RO,2} = 25$ days, and $c_{RO,3} = 140$ are timescale coefficients (Langen et al., 2017). Water exceeding the retention threshold may therefore linger in a layer until it forms superimposed ice, refreezes or runs off. There is no routing of melt water in the present model, so all water prescribed as runoff exits the model. All runoff is compensated by an upward flux of ice and snow to preserve mass conservation in the layer.

Refreezing depends on the cold content, i.e. the energy required to warm the snow pack to the melting point, of each layer. The cold content is used to freeze liquid water, which releases latent heat and therefore increases the temperature of the layer. Refreezing occurs instantaneously until no liquid water is present in the layer or the cold content is depleted.

The updated model also features an updated snow albedo scheme (Nielsen-Englyst, 2015), which depends both on the age of the snow and the surface temperature. The scheme is similar to that used by Oerlemans and Knap (1998), which assumes that the albedo decays exponentially as it ages, but with an added temperature component. If snow is present at the surface, the change in snow albedo from one time step to the next depends on whether the surface is in a cold (<-2 °C) or wet regime (≥ -2 °C). No melting occurs in the cold regime, whereas in the warm regime temperatures are high enough for melting to occur. The snow albedo changes over each timestep as

$$\alpha_{snow}^{t} = (\alpha_{snow}^{t-1} - \alpha_{mx}) \cdot e^{-\delta t/\tau_x} + \alpha_{mx} \tag{16}$$

where α_{mx} is the minimum snow albedo value that can be reached from ageing of the snow and τ_x is a timescale which determines how fast the albedo reaches its minimum value. These two variables take on different values depending on whether the snow is in the dry (x=d) or wet (x=w) regime.

Refreshment of the albedo to the fresh snow value only occurs if snowfall constitutes more than 95 % of the total precipitation. A partial refreshment is possible, as the albedo is only refreshed to the maximum value if the amount of snowfall on that day (S_0) is higher than a threshold value. The rate of refreshment br is given by

$$br = min\left[1, \frac{S_f}{S_0}\right] \tag{17}$$

where S_f is the amount of snowfall during the model time step in m w. eq. Using this rate, the albedo is then refreshed using

$$\alpha_{snow}^{t+1} = \alpha_{snow}^{t} + br \cdot (\alpha_{max} - \alpha_{snow}^{t}) \tag{18}$$

where α_{max} is the maximum albedo for freshly fallen snow.

In the case of small snow depths, the surface albedo will be affected by the albedo of the underlying ice. A smooth transition between the snow and bare ice albedo is therefore implemented, and the final albedo is thus expressed as

$$\alpha^{t+1} = \alpha_{snow}^{t+1} + (\alpha_{ice} - \alpha_{snow}^{t+1}) \cdot exp(\frac{-d^{n+1}}{d_s}) \tag{19}$$

where d is the snow depth, and d_s is a characteristic scale for snow depth. Following Oerlemans and Knap (1998), the characteristic scale is set to 3.2 cm snow depth. If no snow is present, the albedo is set to the bare ice albedo.

The surface mass balance is calculated from the simulated precipitation P, evaporation/sublimation E, and liquid water runoff RO. The precipitation is the sum of rain Rn and snowfall Sn, and the runoff is the melt M and rainfall R which ran off without refreezing RF. The surface mass balance is thus calculated as (Langen et al., 2015)

$$SMB = P - E - RO = (Sn + Rn) - E - (M + Rn - RF) = (Sn - E) - M + RF \tag{20}$$

4.1.2 Offline runs

The snow pack scheme described in the previous section is run offline in this study, following e.g. Langen et al. (2015). This is done by forcing the scheme with 6-hour surface energy (incoming shortwave and longwave radiation and turbulent fluxes) and mass fluxes (snow, rain, evaporation, and sublimation) from a previous HIRHAM5 experiment. While a fully coupled, high-resolution HIRHAM5 run is computationally very expensive, this offline model offers a quicker alternative to test new model implementations and perform quick model spin-ups. One disadvantage of this approach is that changes in feedbacks between surface conditions, like e.g. the albedo and surface temperature, and the atmosphere are ignored. However, the albedo parameterisation is the only alteration from the online HIRHAM5 simulations used to force the snow pack scheme in this work. Since surface temperatures on Vatnajökull are generally around melting points during the summer, changes in the albedo simulations should not affect the upward longwave radiation and turbulent fluxes. The error due to neglected feedbacks is therefore expected to be small for simulations of Vatnajökull.

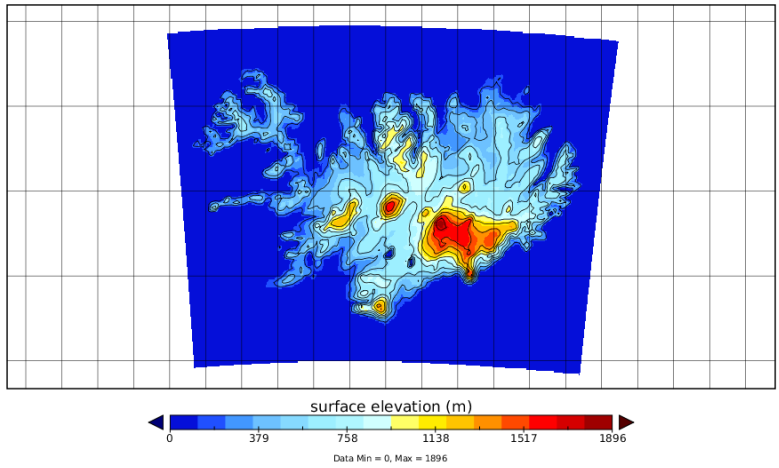

Figure 4.8. HIRHAM5 Iceland domain and topography used in the offline runs. The resolution is ∼5.5 x 5.5 km.

For offline simulations, the HIRHAM5 grid was reduced to a 100x80 gridpoints by isolating the Iceland domain (Figure 4.8).

The snow pack scheme can also be forced by output from other RCMs or NWPs. In this thesis, the snow pack scheme is also forced by HARMONIE-AROME reanalysis simulations, and future projections from CORDEX.

4.2 HARMONIE-AROME

HARMONIE-AROME is a non-hydrostatic convection-permitting NWP model which was developed in a cooperation between HIRLAM, ALADIN and Meteo-France (Bengtsson et al., 2017). The original forecast model was based on the AROME-France model (e.g. Seity et al., 2011), but it now differs from the original model in various aspects (Bengtsson et al., 2017). Since HARMONIE-AROME is non-hydrostatic and calculates precipitation diagnostically, it should provide a better representation of the accumulation in areas with high orographic forcing than HIRHAM5.

In autumn 2015, the Icelandic Meteorological Office (IMO) started a reanalysis project for Iceland (ICRA) using HARMONIE-AROME (Nawri et al., 2017). ICRA currently spans from September 1st, 1979, until December 31st, 2017. It is run over a domain containing only Iceland at a horizontal resolution of 0.025° x 0.025°, corresponding to $\sim$ 2.5 km. The domain contains 289 x 229 gridpoints. The atmosphere has 65 vertical levels, from the surface to 10 hPa, with a model timestep of 60 s. The HARMONIE-AROME ICRA runs are forced by ERA-Interim reanalysis data at the lateral boundaries at 6 hour intervals, and the output is given at 1 hour intervals.

The simulations use the upper-air physics from AROME to determine radiation, turbulence, convection, clouds and precipitation, while surface and soil processes are described by SURFEX version 7.2 (Masson et al., 2013). SURFEX uses the model terrain and input from the lowest atmospheric level to calculate e.g. the outgoing radiation and turbulent heat fluxes.

In order to prevent unrealistic snow accumulation in the simulations, the model was only run continuously for one hydrological year at a time, which was defined to start on September 1st. A 10-day spin-up period was started on August 20th, with all snow outside of the glaciers removed and 10 m w.eq. of snow added onto all glacier points. This ensures that the glaciers can melt and have realistic radiative properties.

So that the reanalysis is comparable with operational runs from the IMO (Nawri, 2014), the reanalysis simulations were conducted in weather prediction mode rather than climate mode. This means the ICRA reanalysis time series is a combination of many 12 hour forecast runs. Due to spin-up effects in the model during the first 6 hours of forecasts (Nawri, 2014), only hours 6-12 of each run were used to create a longer time series, with new runs operated every 6 hours.

4.3 CORDEX

In this thesis, available simulations within the CORDEX project are also considered. Iceland is represented both in the Europe and Arctic domain, but the highest resolution simulation (12 km) can be found in the Europe domain. The whole EURO-CORDEX domain is shown in Figure 4.9.

Two emission scenarios are considered: RCP 4.5 (Thomson et al., 2011) and RCP 8.5 (Riahi et al., 2011). Simulations were only used if i) they had an appropriate snow/ice mask over Vatnajökull, ii) they provided the meteorological parameters needed

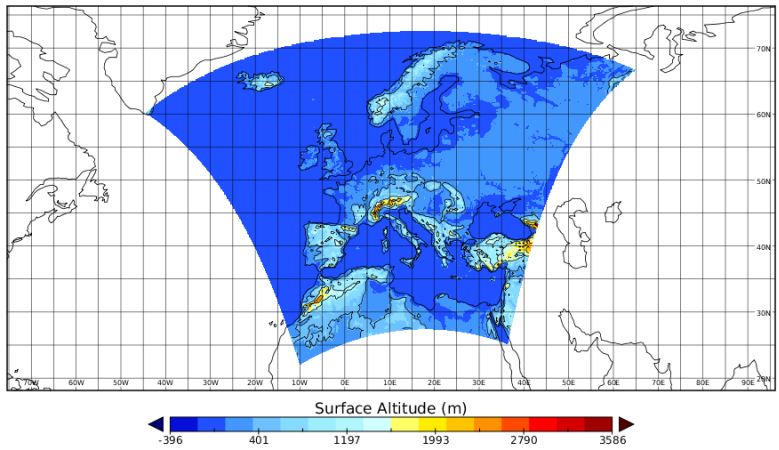

Figure 4.9. EURO-CORDEX domain and topography.

to force the HIRHAM5 snow pack scheme, and iii) they provided the variables with at least a daily temporal resolution.

For the RCP 8.5 scenario, a total of 30 simulations are available at a 12 km resolution, but only 15 simulations provided the output parameters needed for this study. 5 different RCMs, 8 GCMs, and 3 ensembles with different initial states are represented by these simulations.

Fewer simulations are available for the RCP 4.5 scenario, as only 19 simulations are available at a 12 km resolution. Of these, 11 simulations provided the output parameters needed for this study. 4 different RCMs, 6 GCMs, and 3 ensembles are represented by these simulations. A list of the simulations used in this study are shown in Table 4.1.

4.4 PISM

The Parallel Ice Sheet Model (PISM) (Bueler and Brown, 2009) is an open-source, 3-D, thermo-mechanically coupled ice-sheet model which has been applied in various studies of the Greenland and Antarctic ice sheets (e.g. Winkelmann et al., 2011; Aschwanden et al., 2013; Aðalgeirsdóttir et al., 2014). The model allows users to select the preferred approximation applied to the Stokes equation. The options include both the zero order approximations SIA and SSA, a hybrid model, and the higher order Blatter-Pattyn approximation (The PISM authors, 2018).

In this thesis, the hybrid SSA and SIA model described by Bueler and Brown (2009) is used. The model numerically solves the equations for the SIA (Equation 10) and SSA (Equation 12) in each time step (Bueler and Brown, 2009). Under this scheme, PISM

RCM	GCM	Ensemble	Reference
HIRHAM5	EC-EARTH	r3i1p1	Christensen et al. (2006)
	HadGEM	r1i1p1	
	NorESM	r1i1p1	
CCLM4-8-1	CanESM	r1i1p1	Rockel et al. (2008)
	MIROC	r1i1p1	
RACMO22E	EC-EARTH	r12i1p1	Van Meijgaard et al. (2008)
	EC-EARTH	r1i1p1	
	HadGEM	r1i1p1	
RCA4	EC-EARTH	r12i1p1	Samuelsson et al. (2011)
	CNRM-CM5	r1i1p1	
	CM5A-MR	r1i1p1	
	HadGEM	r1i1p1	
	MPI-ESM	r1i1p1	
	NorESM	r1i1p1	
WRF331F	CM5A-MR	r1i1p1	Hines et al. (2008)

Table 4.1. CORDEX simulations used in this study.

solves the SIA in parallel with the SSA; the SIA is solved with a non-sliding base and the SSA is used as a sliding law.

The model can determines the ice rheology using a hierarchy of flow models with different complexities. The enthalpy-based Glen-Paterson-Budd-Lliboutry-Duval law (Lliboutry and Duval, 1985), where the ice softness depends on both the temperature and liquid water fraction, is the PISM default and the most complex option. The other options are only temperature dependent, and include e.g. isothermal Glen's flow law (Glen, 1955), where the ice softness is fixed for the entire run but can be changed manually, Hooke flow law (LeB. Hooke, 1981), and the Paterson Budd flow law (Paterson and Budd, 1982). The enthalpy based scheme is the default as it should do a better job at simulating polythermal ice than the purely temperature dependent schemes, since the latent heat of liquid water within the ice is taken into account (Aschwanden et al., 2012), and energy conservation is therefore better simulated.

In general, the model parameters within PISM are highly customizable. Previous studies have determined what the optimal parameters are for e.g. Greenland (e.g. Aschwanden et al., 2013) and Antactica (e.g. Winkelmann et al., 2011).

To simulate sliding, it is necessary to use a sliding law that determines where sliding can occur given the membrane driving stresses. Basal sliding can be determined using a fully plastic or pseudo-plastic law (The PISM authors, 2018). In the case of a pseudo-plastic power law, it relates bed-parallel shear stress, τ_b, to the basal velocity $\mathbf{u}_b$

$$\tau_{\mathbf{b}} = -\tau_c \frac{\mathbf{u}_b}{u_{threshold}^q |\mathbf{u}_b|^{1-q}} \tag{21}$$

where τ_c is the yield stress, which represents the strength of the glacier till, $\mathbf{u}_{threshold}$ is a threshold speed, and q is the pseudo-plastic exponent. Setting $q = 0$ gives the fully

plastic case. The yield stress can either be considered constant or calculated dynamically by relating the till material properties, expressed by the till friction angle ϕ and the till cohesion c_0, with the effective pressure on the till, N_{till}, using the Mohr-Coulomb criterion:

$$\tau_c = c_0 + tan\phi \cdot N_{till} \tag{22}$$

The effective pressure on the till is given by

$$N_{till} = min\left\{ P_o, N_0 \left(\frac{\delta P_o}{N_0} \right)^{W_{till}/W_{till}^{max}} 10^{(e_0/C_c)(1-W_{till}/W_{till}^{max})} \right\} \tag{23}$$

where P_o is the ice overburden pressure, determined entirely by the ice thickness, density and the gravitational acceleration, and W_{till} is the effective thickness of water in the till computed in each time step. The remaining variables are constants which describe the till mechanics: $N_0 = 1000$ kPa is the reference effective pressure of the till, δ is the effective fraction overburden, $e_0 = 0.69$ is the reference void ratio, $C_c = 0.12$ is the compressibility coefficient, and $W_{till}^{max} = 2$m is the maximum water thickness allowed in the till (Tulaczyk et al., 2000; Bueler and van Pelt, 2015).

The till friction angle is a measure of the ability of the till to withstand a shear stress and can either be set as a constant or determined as a linear function of the bedrock elevation. The elevation dependence is expressed as follows

$$\phi(x,y) = \begin{cases} \phi_{min}, & \text{if } b(x,y) \leq b_{min} \\ \phi_{min} + (b(x,y) - b_{min}\frac{\phi_{max}-\phi_{min}}{b_{max}-bmin}), & \text{if } b_{min} < b(x,y) < b_{max} \\ \phi_{max}, & \text{if } b(x,y) \geq b_{max} \end{cases}$$

where b_{min}, b_{max}, ϕ_{min}, and ϕ_{max} are chosen constraints on the bed elevation and till friction angle, respectively. The reasoning for using the elevation-based till friction angle for Greenland is that low-lying bedrock with a marine history is expected to be weaker than high-elevation bedrock.

Since the hybrid model is using SSA as a sliding law, it is necessary to combine the SSA and SIA velocities. The horizontal velocity (u,v) is calculated using

$$(u,v) = f(|\mathbf{u}_b|)\mathbf{u}_{sia} + (1 - f(|\mathbf{u}_b|))\mathbf{u}_b \tag{24}$$

where $|\mathbf{u}_b| = \sqrt{u_{b,1}^2 + u_{b,2}^2}$ and f is a weighting function between 0 and 1 given by

$$f(|\mathbf{u}_b|) = 1 - \frac{2}{\pi} arctan\left(\frac{|\mathbf{u}_b|^2}{u_{threshold}^2} \right) \tag{25}$$

The SSA velocities are the basal velocities, u_b, and the SIA velocities are denoted by u_{sia}. Using the weighting function guarantees a velocity field that is mathematically continuous, ensuring a smooth velocity distribution along the ice cap (Bueler and Brown, 2009).

5 Paper I: The importance of accurate albedo simulations

5.1 Summary

RCMs are important tools for the reconstruction of the climate system, both expanding the time series further back than available observational records and projecting the future climate. However, in order to have confidence in RCM projections, it is important to validate how well the present climate is simulated by a RCM.

In this study, the RCM HIRHAM5, which has been well-validated over the Greenland ice sheet (e.g, Langen et al., 2017), is used to simulate the energy and mass balance of Vatnajökull ice cap, Iceland. The model is forced by ERA-Interim reanalysis at the lateral boundaries. The model was developed for the Greenland ice sheet, which has a higher reflectivity than Icelandic glaciers. Due to tephra layers within the ice and the effect of dust storms, the albedo of Vatnajökull is highly variable both temporally and spatially. Observations from AWSs show that the albedo can range from 0.95 after a fresh snowfall to 0.01 in the ablation zone. Any simulations of melt are therefore highly dependent on accurate estimations of the albedo.

In order to improve the albedo scheme within HIRHAM5, the ageing of snow is tuned to fit the conditions observed on Vatnajökull, and an ice albedo map based on available MODIS observations at the end of the ablation season is added to reflect the high spatial variability within the ablation zone.

The updated model is used to simulate the energy and mass balance of Vatnajökull from 1980-2014. Results from the model simulations are thoroughly validated using available observations of the energy balance components from five AWSs operated on the ice cap since at least 2001 and mass balance observations conducted from the 1991-1992 glaciological year until 2014-2015. A good correlation is found between the observed and modelled parameters, albeit with a large overestimation of accumulation in areas of high orographic forcing. An overestimation of accumulation in parts of the ablation zone is also found, which affects the albedo simulations. Overall, the model captures the variation in mass balance well, giving confidence in the RCM's ability to perform future projections, depending on the skills of the driving GCM.

5.2 Main results

- The HIRHAM5 snow pack scheme is improved for simulations over Vatnajökull by tuning the albedo parameterisation and adding a spatially variable ice albedo into the model. We find that the model simulates the surface energy balance and surface mass balance well, albeit with general underestimations of the incoming radiation components and the albedo. The average total underestimation of the available energy for five used AWSs is -47.5 Wm^{-2} during the summer.

- Although the albedo simulations have been improved with the MODIS based ice albedo map, the simulated albedo is generally overestimated during the summer in the ablation zone and does not reach the lowest yearly value as early in the year as the measured albedo. This is partly attributed to the fact that point observations are compared to the modelled mean of a 5.5 x 5.5 km^2 area, which e.g. means that an overestimation of the ice albedo map is observed when compared with AWS observations, even though higher-resolution MODIS (500 m) observations show a good correlation with the point observations (Gascoin et al., 2017). In addition, an overestimation of the snow thickness in the ablation zone and the fact that the model does not account for the temporal effect of volcanic dust deposition during eruptions and dust events on the albedo contributes to the underestimation of the simulated ablation.

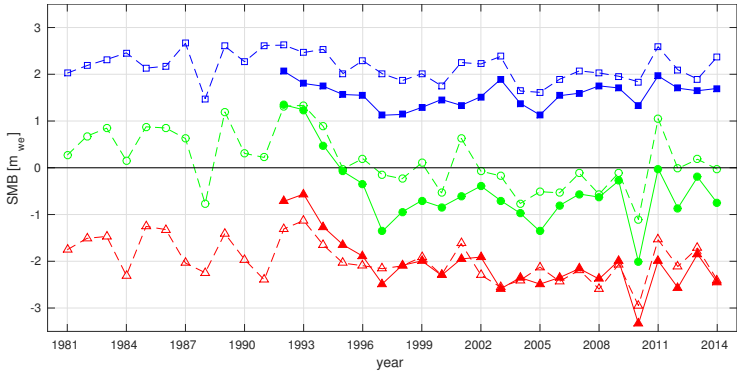

Figure 5.10. Average specific summer (red), winter (blue) and net (green) surface mass balance of Vatnajökull. The solid lines show the mass balance of Vatnajökull based on mass balance measurements and manual interpolation (Pálsson et al., 2015), while the dashed lines show the mass balance as simulated by HIRHAM5

- The mean specific summer, winter and net mass balances are reconstructed for all of Vatnajökull from the 1980-81 glaciological year until 2014-15 and estimates of the specific SMB based on in situ SMB measurements are compared to the reconstructed specific SMB for the period 1995-2014 (Figure 5.10).The summer ablation is underestimated by -0.06 m w.eq. on average, with too much ablation in 1995 and too little ablation in years with, or following, volcanic eruptions. The low errors of the specific summer mass balance is attributed to biases in

different parts of the ice cap cancelling each other out, with e.g. the AWS sites having a general overestimation of the mass balance and the low-lying Skeiðarárjökull having an underestimation of the mass balance. The winter balance is overestimated by 0.5 m w.eq., mostly due to a large overestimation at the high elevation plateau of Öræfajökull. If the overestimation at these points is corrected, the simulated winter balance for the whole ice cap fits well with observations as the overestimation drops to around 0.1 m w.eq. (Figure 5.11).

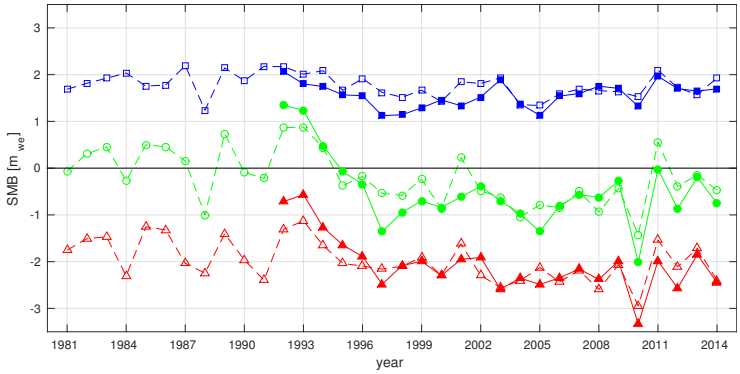

Figure 5.11. Same as Fig. 5.10 but with corrected winter precipitation over the Öræfajökull area by reducing the HIRHAM5 simulated winter balance with 50%.

- The simulations capture the shift in mass balance observed in the mid-1990s. This and the high correlation for the whole time series, gives confidence that the model estimates the specific mass balance of Vatnajökull well over the entire period from 1980-2014. HIRHAM5 has therefore proven to be a useful tool to expand the time series of the specific SMB beyond the measurement years, if a good GCM is used.

6 Paper II: Sensitivity of runoff to spring snow thickness

6.1 Summary

In this study, the runoff from Vatnajökull from 1980-2015 is simulated and the sensitivity of runoff to spring snow thickness is evaluated. Due to the overestimation of the winter balance in HIRHAM5 found in paper I, we attempted to improve the simulations by forcing the HIRHAM5 snow pack model with meteorological input from the NWP HARMONIE-AROME. This model was chosen due to its complex atmospheric model which uses non-hydrostatic physics and prognostic precipitation. Comparison with available observations shows that the model simulates the incoming energy and mass fluxes better than the atmospheric model in HIRHAM5. The combined model is used to simulate runoff from Vatnajökull, which is evaluated against available discharge observations from Skaftá glacial water catchment (GWC) and Hálslón GWC.

The sensitivity of runoff to the spring snow thickness is evaluated by running a set of sensitivity runs, using all the spring conditions from 1980-2015 as a starting point for runs over all the summers in the same period. Since the runoff from the accumulation zone is not as dependent on the variations in snow thickness and the runoff from the ablation zone, we mostly focus on the effect on the ablation zone. We find that the variability in summer weather has a larger effect on the runoff than the variability in spring snow thickness, although especially the north-facing outlets have a high sensitivity to variations in spring snow thickness. An additional simulation was conducted using thick enough snow so that the underlying ice surface is never exposed. This run was used to evaluate how much of the runoff from 1980-2015 was due to exposed dirty ice.

6.2 Main results

- the non-hydrostatic model HARMONIE-AROME provides a more accurate simulation of the winter mass balance than HIRHAM5 (Figure 6.12). The simulations are especially improved in areas with high orographic forcing like e.g. Öræfajökull. Using the HARMONIE-AROME model as a forcing for the snow pack model provides a better estimate of the energy and mass balance, but significant biases are still found in the precipitation (as shown in Figure 6.12a) which needs to be corrected.

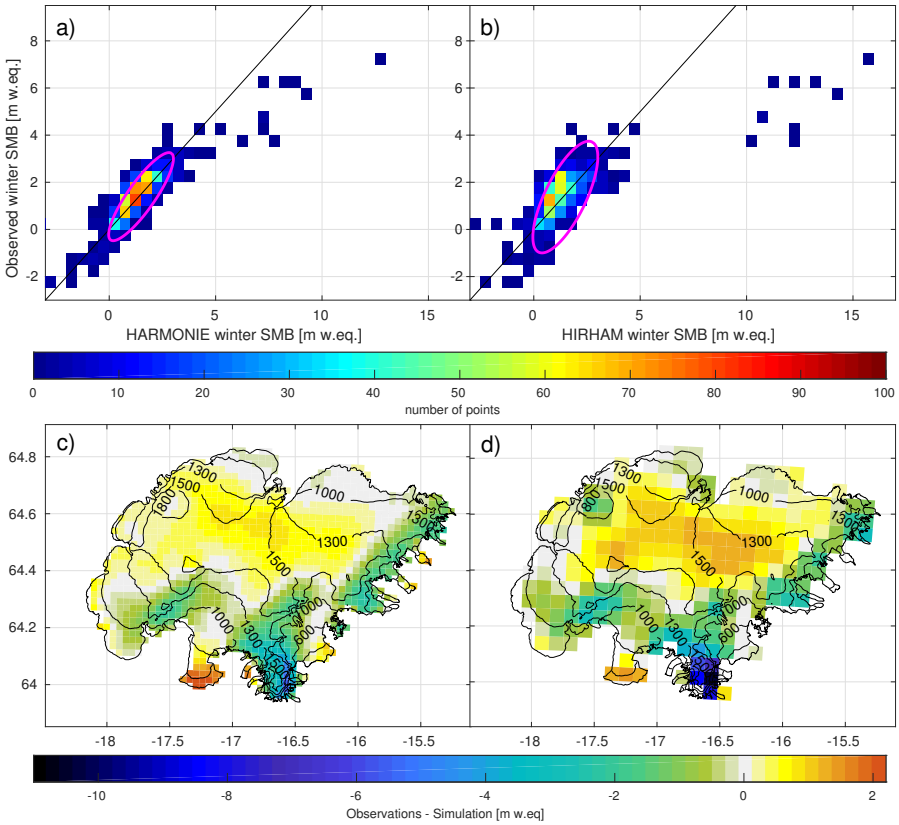

Figure 6.12. a) HARMONIE and b) HIRHAM5 winter mass balance compared to measurements from 1992-2014. Colour bar shows how many points are in the same spot and purple ellipsis outlines 68% of the points. Interpolated observed mean winter mass balance maps from 1992-2014 compared to c) HARMONIE and d) HIRHAM5 winter mass balance.

- The total runoff is well simulated by the model as comparison with discharge observations from two rivers with a large glacial component confirms. The correlation is found to be 0.78 for Skaftá GWC and 0.89 for Hálslón. The average difference between the measured and modelled summer runoff is 16% and 29% for Skaftá GWC and Hálslón GWC, respectively. Improved estimates of the runoff from ice-free zones would improve the comparison.

- The sensitivity of the total summer runoff to the spring snow cover is evaluated by setting up a set of model runs using the simulated state of the subsurface on April 1st from 1980-2015 as initialization for simulations of all the summer over the same time period. 1296 summers are simulated for the evaluation.

- We find that in general the runoff is controlled more by variations in summer

weather than by variations in spring snow thickness (Figure 6.13). The average variation in runoff due to changes in snow cover equal 31% of the variation due to summer weather for the whole ice cap. However, the spring snow thickness is still an important factor, especially for the north-facing outlets, as e.g. Brúarjökull has an average variation in runoff due to changes in snow cover equal to 51% of the variation due to summer weather.

- We estimate that there was approximately a 14% increase in runoff from Vatnajökull due to the exposure of dirty ice from 1980-2015 and a 27% increase from Brúarjökull. A maximum of 31% of the runoff from Vatnajökull was found to be due to the exposure of dirty, while a maximum of 77% was simulated for Brúarjökull.

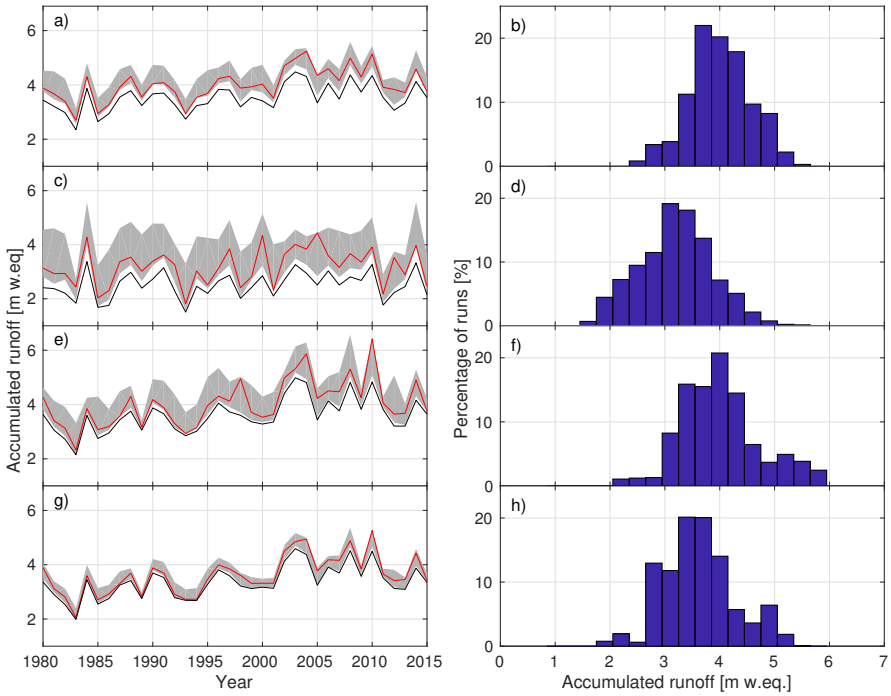

Figure 6.13. Time series of accumulated runoff for April-October from (a) Vatnajökull, (c) Brúarjökull, (e) Síðujökull, (g) Skaftá GWC for different spring conditions. The red line is the original run where the spring conditions of the specific year are used, the grey area shows the range in runoff when the spring conditions are changed, and the black line shows how much melt would occur if the underlying ice is never exposed. Probability distributions for the runoff created using the results of the sensitivity runs are shown for (b) Vatnajökull, (d) Brúarjökull, (f) Síðujökull, (h) Skaftá GWC

7 Paper III: Future projections under different climate scenarios

7.1 Summary

For the third paper, the models discussed in Papers I and II are used to simulate the evolution of Vatnajökull from 1980-2300 by using the RCM output as a forcing for the ice flow model PISM (The PISM authors, 2018). The flow model is first tuned by comparing simulated surface velocities for the current glacier geometry to available velocity measurements and the optimal flow parameters are determined for simulations of the flow of Vatnajökull.

The ice flow model is forced by the 2.5 km resolution climatic mass balance simulated by HARMONIE-HIRHAM5, forced by ERA-Interim reanalysis at the lateral boundaries, from 1980-2016, which was used and evaluated in Paper II. For the future climate we use 5.5 km resolution simulations by HIRHAM5 forced by EC-EARTH at the model boundaries, as well as available CORDEX simulations at a 12 km resolution. The RCP 4.5 and 8.5 scenarios are investigated, and all future simulations provide forcing until 2100. The 5.5 km forcing is only available in time slices (1990-2010, 2030-2050 and 2080-2100), while continous forcing is available for the CORDEX simulations. Due to high biases in the GCM forced mass balance simulations, anomaly maps are used to force the ice flow model after 2017.

To initialize the coupled simulations, a steady state ice cap in balance with the applied forcing was achieved by repeating the model climate from 1980-1999. The evolution of the ice cap geometry is simulated by using the mass balance forcing until 2100, and the time series is expanded by continuing the run until 2300 by recycling the 2081-2100 forcing for 200 years.

These simulations are performed with a one way coupling of the RCM outputs with PISM, and therefore do not include elevation feedback on the climatic mass balance. To determine the effect of elevation changes on the mass balance, a precipitation and temperature lapse rate is included in some of the simulations. An experiment was conducted to determine if the ice cap would be able to rebuild if the climate was brought back to that of 1980-1999, and it was found that $\sim$80% of the area and $\sim$60% of the volume of the reference ice cap would grow back but it would take about 1500 years to reach a steady state. Low-elevation, south-facing Skeiðarárjökull and Breiðamerkurjökull and north-facing Brúarjökull and Dyngjujökull are not restored due to the high mass balance-elevation feedback.

7.2 Main results

- The ice flow model PISM is evaluated for simulations of the flow of Vatnajökull. By comparing observed surface velocities with simulated velocities, the PISM model parameters which provide the best comparison with observations are found. A combined SIA+SSA sliding scheme is used, with a till-friction angle that linearly depends on the bed elevation.
- 5.5 km HIRHAM5 simulations forced by EC-EARTH at the lateral boundaries are evaluated from 1991-2010 using available SMB and temperature observations. A -1.9°C temperature bias is found over Vatnajökull, and an average overestimation of the annual mass balance of 1.9 m w.eq. is found. Only mass balance anomaly maps are therefore used to force the ice flow model into the future.
- The evolution of the ice cap geometry was simulated under the RCP 4.5 and RCP 8.5 scenarios by forcing PISM with the simulated mass balance fields (Figure 7.14). By 2300, the ice cap has lost 44% of its volume and 23% of its area under the RCP 4.5 scenario, equivalent to a ∼3.0°C warming over Iceland. In the RCP 8.5 scenario, equivalent to an approximately 4.7°C warming over Iceland, the ice cap has lost 85% of its volume and 65% of its area by 2300.

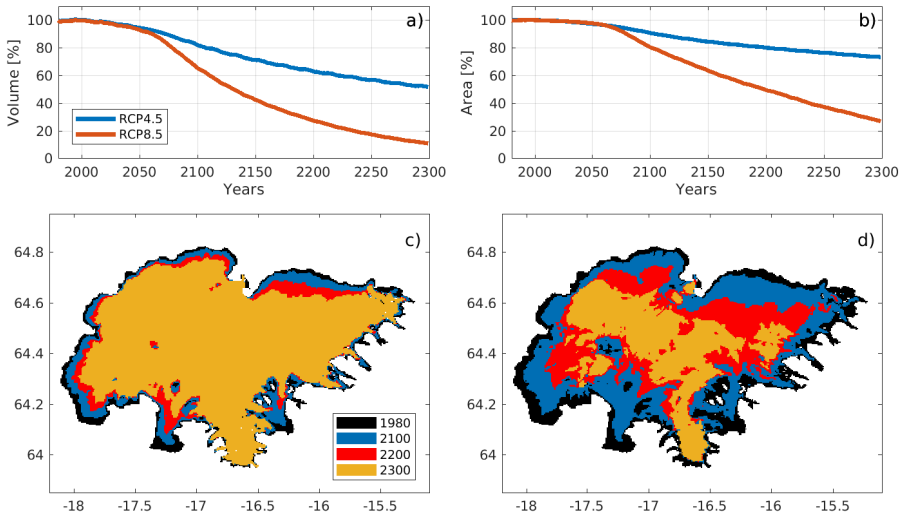

Figure 7.14. a-b) Changes in glacier volume and area with HIRHAM5-EC-EARTH 5.5 km forcing from 1980-2100 for RCP 4.5 and RCP 8.5 scenarios, and continued until 2300 using repeated 2081-2100 forcing. c-d) The areal extent of the ice cap at 100 year time intervals for c) RCP 4.5 and d) RCP 8.5 scenarios.

- To determine the effect of elevation changes on the mass balance, additional runs are conducted where a precipitation and temperature lapse rate is included in the simulations. By 2300, the glacier area is 9-20% smaller than in the runs

with no feedback, and the volume is 9-14% smaller. Especially Brúarjökull and Dyngjujökull are found to be sensitive to changes in precipitation, in agreement with the findings from paper II.

- Equilibrium experiments for response times of ice cap growth and decay are conducted using a precipitation and temperature lapse rate to estimate the elevation feedback. Three scenarios are used, all from the HIRHAM5-EC-EARTH simulations: RCP 4.5 2031-2050 climate (ΔT=1.5°C), RCP 4.5 2081-2100 climate (ΔT=3.0°C), and RCP 8.5 2081-2100 climate (ΔT=4.7°C). After a steady state is reached, the climate is brought back to the simulated 1980-2000 climate. We find that the ice cap rebuilds much slower than it shrinks for the highest forcing scenarios and reaches a steady state with an area and volume that are 80% and 55%, respectively, of the reference ice cap. The response time of the ice cap (i.e. the time it takes the ice cap to adjust all but 1/e from one steady state to another steady state) to a 4.7°C climate forcing is 150 years, and the rebuilding response time to the 1980-2000 climate is 520 years. The response times for the 3.0°C climate forcing is 340 years (warming) and 540 years (rebuilding), while for the 1.5°C climate forcing the response time is 690 years (warming) and 500 years (rebuilding).

- Using available CORDEX simulations as model forcing, a wide range of temperature increases and possible future ice cap geometries are found (Figure 7.15). Volume losses between 31 and 64 % and area losses between 13 and 37% are found for the RCP 4.5 scenario in 2300. For the RCP 8.5 scenario, volume losses between 51% and 94% and area losses between 24% and 80% are simulated by 2300. The large span in model results shows the importance of investigating several different models and initialization for future projections.

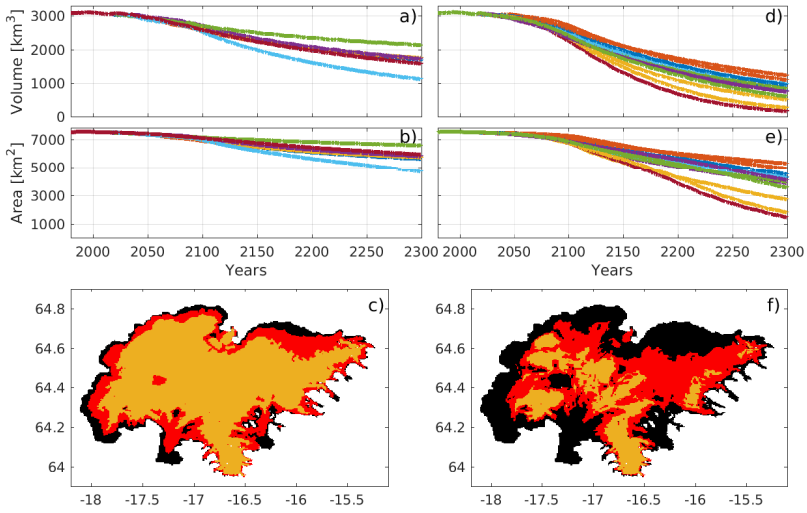

Figure 7.15. Results of CORDEX forced PISM runs for RCP 4.5 (a-c) and RCP 8.5 (d-f). a+d) volume change, b+e) area change, and c+f) the reference area (black), the largest simulated 2300 area (red) and the smallest simulated 2300 area (yellow)

8 Conclusions and outlook

The global climate is changing as a result of antropogenic climate change. The evolution of the future climate is uncertain and depends on the future emission of greenhouse gasses. The relative contribution of components that govern the melt of glaciers, the radiation components and turbulent fluxes, may change during a warming climate, as a result of increased albedo feedback and larger turbulent fluxes. Models based on empirical relationships may therefore not be applicable for future climate scenarios, and it is important to conduct projections with models that adequately capture the physics behind the processes. In this dissertation, physically based models were succesfully used to simulate the mass balance of the recent past past (1980-2016) and the future (until 2300) of Vatnajökull ice cap, Iceland.

Although the future climate may change substantially from the present day, it is important that models simulate the present climate well. Thorough validation of the model physics against observations is therefore an important process in order to have confidence in model projections. In this dissertation, RCMs were used to simulate the physical processes in the atmosphere, on the glacier surface, and within the glacier itself. Through improved albedo simulations and validation of the hydrostatic RCM HIRHAM5, forced by ERA-Interim reanalysis at the lateral boundaries, the model was successfully used to create realistic simulations of the specific mass balance of Vatnajökull from 1980-2014. However, one major cause of bias in the simulated mass balance is found to be due to an overestimation in the precipitation. This e.g. affects the albedo simulations and therefore leads to an underestimation of the ablation. By employing the non-hydrostatic, higher resolution model HARMONIE-AROME, the precipitation biases were significantly reduced especially in areas of high orographic forcings, although significant errors still remain. As RCMs develop towards very high resolution models with a non-hydrostatic core and prognostic precipitation schemes, the representation of precipitation will continue to improve.

The sensitivity of the simulated runoff to changes in winter precipitation was estimated using a precipitation-corrected HARMONIE-AROME forcing and the snow pack scheme from HIRHAM5. The runoff was found to be more sensitive to variations in summer weather than to variations in spring snow thickness over the investigated period. However, variation in spring snow thickness still has an important effect on the melt, especially on the north-facing Brúarjökull and Tungnaárjökull which show a large sensitivity to changes in winter precipitation.

From simulations with and without exposed ice, it was estimated that exposed ice accounted for approximately 14% of the runoff from Vatnajökull from 1980-2015 and 27% of the runoff from Brúarjökull. As the climate warms and the ablation season becomes longer, the effect of the ice albedo on the total melt is expected to increase.

Accurate simulations of the future ablation therefore require accurate estimates of the ice albedo and accumulation.

Future projections were conducted by forcing the ice flow model PISM with simulated mass balance fields from a range of climate models. The simulated change in glacier geometry for the same emission scenario is very variable between the models. For example under the RCP 8.5 scenario, the volume loss is between 51% and 94 % and the area loss is between 24% and 80% by 2300. The large span in model results shows the importance of investigating several different models and initializations for future projections.

Important feedbacks between elevation and mass balance are not included in these simulations. To estimate the effect of elevation changes on the surface mass balance, simulations with a precipitation and temperature lapse rate were conducted and showed that the feedback contributed to a significant increase in the simulated ablation. As RCMs develop towards more comprehensive RESMs, fully coupled simulations of the ice dynamics can more accurately determine the effect of the elevation feedbacks.

Although a solid physical foundation is preferable and necessary for future simulations, this is currently not always possible nor practical. In this thesis, the SIA and SSA stress balance approximations are used to model the ice flow in order to avoid high computing costs, and e.g. some components of the sliding parameterisation are not based on the physical properties of the till but are instead tuned to give the most accurate velocity simulations. Representing physical processes more feasibly in numerical models could improve future projections by e.g. including surge dynamics. However, for simulations on century time scales the changes in the mass balance and runoff will be mostly controlled by the climatic forcing. Until the representation of the climate forcing is improved, the error due to flow approximations can be considered small.

References

Aas, K. S., Berntsen, T. K., Boike, J., Etzelmüller, B., Kristjánsson, J. E., Maturilli, M., Schuler, T. V., Stordal, F., Westermann, S., Aas, K. S., Berntsen, T. K., Boike, J., Etzelmüller, B., Kristjánsson, J. E., Maturilli, M., Schuler, T. V., Stordal, F., and Westermann, S. (2015). A Comparison between Simulated and Observed Surface Energy Balance at the Svalbard Archipelago. *Journal of Applied Meteorology and Climatology*, 54(5):1102–1119.

Aas, K. S., Dunse, T., Collier, E., Schuler, T. V., Berntsen, T. K., Kohler, J., and Luks, B. (2016). The climatic mass balance of Svalbard glaciers: a 10-year simulation with a coupled atmosphere–glacier mass balance model. *The Cryosphere*, 10(3):1089–1104.

Agosta, C., Fettweis, X., and Datta, R. (2015). Evaluation of the CMIP5 models in the aim of regional modelling of the Antarctic surface mass balance. *The Cryosphere*, 9(6):2311–2321.

Anderson, B., Mackintosh, A., Stumm, D., George, L., Kerr, T., Winter-Billington, A., and Fitzsimons, S. (2010). Climate sensitivity of a high-precipitation glacier in New Zealand. *Journal of Glaciology*, 56(195):114–128.

Andreas, E. L. (1987). A theory for the scalar roughness and the scalar transfer coefficients over snow and sea ice. *Boundary-Layer Meteorology*, 38(1-2):159–184.

Antic, S., Laprise, R., Denis, B., and de Elía, R. (2006). Testing the downscaling ability of a one-way nested regional climate model in regions of complex topography. *Climate Dynamics*, 26(2-3):305–325.

Arrhenius, S. (1896). On the influence of carbonic acid in the air upon the temperature of the ground. *The London, Edinburgh, and Dublin Philosophical Magazine and Journal of Science*, 41(251):237–276.

Aschwanden, A., Aðalgeirsdóttir, G., and Khroulev, C. (2013). Hindcasting to measure ice sheet model sensitivity to initial states. *The Cryosphere*, 7(4):1083–1093.

Aschwanden, A., Bueler, E., Khroulev, C., and Blatter, H. (2012). An enthalpy formulation for glaciers and ice sheets. *Journal of Glaciology*, 58(209):441–457.

Aschwanden, A., Fahnestock, M. A., and Truffer, M. (2016). Complex Greenland outlet glacier flow captured. *Nature Communications*, 7(1):10524.

Aðalgeirsdóttir, G. (2003). *Flow dynamics of Vatnajökull ice cap, Iceland*. PhD thesis, ETH Zürich.

Aðalgeirsdóttir, G., Aschwanden, A., Khroulev, C., Boberg, F., Mottram, R., Lucas-Picher, P., and Christensen, J. (2014). Role of model initialization for projections of 21st-century Greenland ice sheet mass loss. *Journal of Glaciology*, 60(222):782–794.

Aðalgeirsdóttir, G., Gudmundsson, G. H., and Björnsson, H. (2000). The response of a glacier to a surface disturbance: a case study on Vatnajökull ice cap, Iceland. *Annals of Glaciology*, 31:104–110.

Aðalgeirsdóttir, G., Gudmundsson, G. H., and Björnsson, H. (2005). Volume sensitivity of Vatnajökull Ice Cap, Iceland, to perturbations in equilibrium line altitude. *Journal of Geophysical Research: Earth Surface*, 110(F4):n/a–n/a.

Aðalgeirsdóttir, G., Guðmundsson, S., Björnsson, H., Pálsson, F., Jóhannesson, T., Hannesdóttir, H., Sigurðsson, S. T., and Berthier, E. (2011). Modelling the 20th and 21st century evolution of Hoffellsjökull glacier, SE-Vatnajökull, Iceland. *The Cryosphere*, 5(4):961–975.

Bamber, J. L., Westaway, R. M., Marzeion, B., and Wouters, B. (2018). The land ice contribution to sea level during the satellite era. *Environmental Research Letters*, 13(6):063008.

Bengtsson, L., Andrae, U., Aspelien, T., Batrak, Y., Calvo, J., de Rooy, W., Gleeson, E., Hansen-Sass, B., Homleid, M., Hortal, M., Ivarsson, K.-I., Lenderink, G., Niemelä, S., Nielsen, K. P., Onvlee, J., Rontu, L., Samuelsson, P., Muñoz, D. S., Subias, A., Tijm, S., Toll, V., Yang, X., and Køltzow, M. Ø. (2017). The HARMONIE–AROME Model Configuration in the ALADIN–HIRLAM NWP System. *Monthly Weather Review*, 145(5):1919–1935.

Berthier, E. and Toutin, T. (2008). SPOT5-HRS digital elevation models and the monitoring of glacier elevation changes in North-West Canada and South-East Alaska. *Remote Sensing of Environment*, 112(5):2443–2454.

Björnsson, H. (1972). Bægisárjökull, North Iceland. result of glaciological investigations 1967-1968. Part II. The energy balance. *Jökull*, 22:44–61.

Björnsson, H. (1977). The cause of jökulhlaups in the Skaftá-river, Vatnajökull. *Jökull*, 27:71–78.

Björnsson, H. (1986). Surface and Bedrock Topography of Ice Caps in Iceland, Mapped by Radio Echo-Sounding. *Annals of Glaciology*, 8:11–18.

Björnsson, H. (1988). *Hydrology of Ice Caps in Volcanic Regions*. Visindafelag Íslendiga, rit 45, 139 s, 21 maps. Reykjavik.

Björnsson, H. (2000). Surface and bedrock topography of the Mýrdalsjökull ice cap Iceland: The Katla caldera, eruption sites and routes of jökulhlaups. *Jökull*, 49:29–46.

Björnsson, H. (2003). Subglacial lakes and jökulhlaups in Iceland. *Global and Planetary Change*, 35(3-4):255–271.

Björnsson, H. (2017). *The glaciers of Iceland : a historical, cultural and scientific overview*. Advances in Quarternary Science. Atlantis Press. ISBN: 978-94-6239-206-9.

Björnsson, H., Guðmundsson, S., Haraldssson, H. H., and Pálsson, F. (1996). Veðurathuganir og jökulleysing á Vatnajökli sumarið 1995 og samanburður við veðurstöðvar utan jökuls. Technical report, RH-18-96.

Björnsson, H., Guðmundsson, S., and Pálsson, F. (2006). Glacier winds on Vatnajökull ice cap, Iceland, and their relation to temperatures of its lowland environs. *Annals of Glaciology*, 42:291–296.

Björnsson, H., Guðmundsson, S., Pálsson, F., and Haraldsson, H. H. (1997a). Veðurathuganir og jökulleysing á Vatnajökli sumarið 1996. Technical report, RH-10-97.

Björnsson, H., Guðmundsson, S., Pálsson, F., and Haraldsson, H. H. (1997b). Veðurathuganir og jökulleysing á Vatnajökli sumarið 1997. Technical report, RH-5-98.

Björnsson, H. and Pálsson, F. (2008). Icelandic glaciers. *Jökull*, 58:365–386.

Björnsson, H., Pálsson, F., and Gudmundsson, S. (2001a). Jökulsárlón at Breidamerkur-

sandur, Vatnajökull, Iceland: 20th century changes and future outlook. *Jökull*, 50:1–18.

Björnsson, H., Pálsson, F., and Guðmundsson, M. T. (1995). Afkoma, hreyfing og afrennsli á vestan- og norðanverðum Vatnajokli jökulárin 1992–1993 og 1993 (Mass balance, movement and runoff on western and northern Vatnajökull hydrological years 1992–1993 and 1993–1994). Technical report, University of Iceland, Reykjavik.

Björnsson, H., Pálsson, F., Guðmundsson, M. T., and Haraldsson, H. H. (1998). Mass balance of western and northern Vatnajökull, Iceland, 1991-1995. *Jökull*, 45(45):35–58.

Björnsson, H., Pálsson, F., Guðmundsson, S., Magnússon, E., Aðalgeirsdõttir, G., Jóhannesson, T., Berthier, E., Sigurdsson, O., and Thorsteinsson, T. (2013). Contribution of Icelandic ice caps to sea level rise: Trends and variability since the Little Ice Age. *Geophysical Research Letters*, 40(8):1546–1550.

Björnsson, H., Pálsson, F., and Haraldsson, H. H. (2002). Mass balance of Vatnajökull (1991-2001) and Langjökull (1996-2001), Iceland. *Jökull*, 51:75–78.

Björnsson, H., Pálsson, F., Sigurðsson, O., and Flowers, G. E. (2003). Surges of glaciers in Iceland. *Annals of Glaciology*, 36:82–90.

Björnsson, H., Rott, H., Gudmundsson, S., Fischer, A., Siegel, A., and Gudmundsson, M. T. (2001b). Glacier–volcano interactions deduced by SAR interferometry. *Journal of Glaciology*, 47(156):58–70.

Boberg, F., Langen, P. L., Mottram, R. H., Christensen, J. H., and Olesen, M. (2018). 21st-century climate change around Kangerlussuaq, west Greenland: From the ice sheet to the shores of Davis Strait. *Arctic, Antarctic, and Alpine Research*, 50(1):S100006.

Bougamont, M., Bamber, J. L., Ridley, J. K., Gladstone, R. M., Greuell, W., Hanna, E., Payne, A. J., and Rutt, I. (2007). Impact of model physics on estimating the surface mass balance of the Greenland ice sheet. *Geophysical Research Letters*, 34(17):L17501.

Box, J. E., Fettweis, X., Stroeve, J. C., Tedesco, M., Hall, D. K., and Steffen, K. (2012). Greenland ice sheet albedo feedback: thermodynamics and atmospheric drivers. *The Cryosphere*, 6(4):821–839.

Box, J. E. and Rinke, A. (2003). Evaluation of Greenland Ice Sheet Surface Climate in the HIRHAM Regional Climate Model Using Automatic Weather Station Data. *Journal of Climate*, 16:1302–1319.

Broccoli, A. J. and Manabe, S. (1987). The influence of continental ice, atmospheric CO2, and land albedo on the climate of the last glacial maximum. *Climate Dynamics*, 1(2):87–99.

Bueler, E. and Brown, J. (2009). Shallow shelf approximation as a "sliding law" in a thermomechanically coupled ice sheet model. *Journal of Geophysical Research: Solid Earth*, 114(3).

Bueler, E. and van Pelt, W. (2015). Mass-conserving subglacial hydrology in the Parallel Ice Sheet Model version 0.6. *Geoscientific Model Development*, 8(6):1613–1635.

Christensen, J. H., Boberg, F., Christensen, O. B., and Lucas-Picher, P. (2008). On the need for bias correction of regional climate change projections of temperature and precipitation. *Geophysical Research Letters*, 35(20):L20709.

Christensen, J. H., Mottram, R. H., Langen, P. L., Madsen, K. S., Stendel, M., Rode-

hacke, C., Romanocsky, V. E., and Marchenko, S. S. (2014). A Regional Coupled Model System to Examine Ocean-Atmosphere-Sea Ice, Ice Sheet and Permafrost Interactions in the Arctic: HIRHAM5 – HYCOM – CICE – PISM – GIPL. In *American Geophysical Union 2014 Abstract*, San Francisco.

Christensen, O. B., Drews, M., Christensen, J. H., Dethloff, K., Ketelsen, K., Hebestadt, I., and Rinke, A. (2006). The HIRHAM Regional Climate model Version 5. Technical report, Danish Meteorological institute.

Church, J., Clark, P., Cazenave, A., Gregory, J., Jevrejeva, S., Levermann, A., Merrifield, M., Milne, G., Nerem, R., Nunn, P., Payne, A., Pfeffer, W., Stammer, D., and Unnikrishnan, A. (2013). Sea Level Change. In Stocker, T., Qin, D., Plattner, G.-K., Tignor, M., Allen, S., Boschung, J., Nauels, A., Xia, Y., Bex, V., and Midgley, P., editors, *limate Change 2013: The Physical Science Basis. Contribution of Working Group I to the Fifth Assessment Report of the Intergovernmental Panel on Climate Change*. Cambridge University Press, Cambridge, United Kingdom and New York, NY, USA.

Claremar, B., Obleitner, F., Reijmer, C., Pohjola, V., Waxegård, A., Karner, F., and Rutgersson, A. (2012). Applying a Mesoscale Atmospheric Model to Svalbard Glaciers. *Advances in Meteorology*, 2012:1–22.

CORDEX (2018). http://www.cordex.org/.

Cornford, S. L., Martin, D. F., Graves, D. T., Ranken, D. F., Le Brocq, A. M., Gladstone, R. M., Payne, A. J., Ng, E. G., and Lipscomb, W. H. (2013). Adaptive mesh, finite volume modeling of marine ice sheets. *Journal of Computational Physics*, 232(1):529–549.

Crochet, P., Jóhannesson, T., Jónsson, T., Sigurðsson, O., Björnsson, H., Pálsson, F., Barstad, I., Crochet, P., Jóhannesson, T., Jónsson, T., Sigurðsson, O., Björnsson, H., Pálsson, F., and Barstad, I. (2007). Estimating the Spatial Distribution of Precipitation in Iceland Using a Linear Model of Orographic Precipitation. *Journal of Hydrometeorology*, 8(6):1285–1306.

Cuffey, K. M. and Paterson, W. S. B. (2010). *The Physics of Glaciers*. Elsevier.

de Ruyter de Wildt, M. S., Klok, E. J., and Oerlemans, J. (2003). Reconstruction of the mean specific mass balance of vatnajökull (iceland) with a seasonal sensitivity characteristic. *Geografiska Annaler: Series A, Physical Geography*, 85(1):57–72.

Dee, D. P., Balmaseda, M., Balsamo, G., Engelen, R., Simmons, A. J., Thépaut, J.-N., Dee, D. P., Balmaseda, M., Balsamo, G., Engelen, R., Simmons, A. J., and Thépaut, J.-N. (2014). Toward a Consistent Reanalysis of the Climate System. *Bulletin of the American Meteorological Society*, 95(8):1235–1248.

Dee, D. P., Uppala, S. M., Simmons, A. J., Berrisford, P., Poli, P., Kobayashi, S., Andrae, U., Balmaseda, M. A., Balsamo, G., Bauer, P., Bechtold, P., Beljaars, A. C. M., Bidlot, J., Bormann, N., Delsol, C., Dragani, R., Fuentes, M., Geer, A. J., Isaksen, L., Haimberger, L., Healy, S. B., Hersbach, H., Matricardi, M., Mcnally, A. P., Peubey, C., Rosnay, P. D., Tavolato, C., and Vitart, F. (2011). The ERA-Interim reanalysis: configuration and performance of the data assimilation system. *Quarterly Journal of the Royal Meteorological Society*, 137(April):553–597.

Dragosics, M., Meinander, O., Jónsdóttír, T., Dürig, T., De Leeuw, G., Pálsson, F., Dagsson-Waldhauserová, P., and Thorsteinsson, T. (2016). Insulation effects of Icelandic dust and volcanic ash on snow and ice. *Arabian Journal of Geosciences*,

9(2):126.

Edwards, T. L., Fettweis, X., Gagliardini, O., Gillet-Chaulet, F., Goelzer, H., Gregory, J. M., Hoffman, M., Huybrechts, P., Payne, A. J., Perego, M., Price, S., Quiquet, A., and Ritz, C. (2014). Effect of uncertainty in surface mass balance–elevation feedback on projections of the future sea level contribution of the Greenland ice sheet. *The Cryosphere*, 8(1):195–208.

Eerola, K. (2006). About the performance of HIRLAM version 7.0. *HIRLAM Newsletter*, 51:93–102.

Einarsson, B., Jóhannesson, T., Thorsteinsson, T., Gaidos, E., and Zwinger, T. (2017). Subglacial flood path development during a rapidly rising jökulhlaup from the western Skaftá cauldron, Vatnajökull, Iceland. *Journal of Glaciology*, 63(240):670–682.

Eyring, V., Bony, S., Meehl, G. A., Senior, C. A., Stevens, B., Stouffer, R. J., and Taylor, K. E. (2016). Overview of the Coupled Model Intercomparison Project Phase 6 (CMIP6) experimental design and organization. *Geoscientific Model Development*, 9(5):1937–1958.

Fausto, R. S., van As, D., Box, J. E., Colgan, W., Langen, P. L., and Mottram, R. H. (2016). The implication of nonradiative energy fluxes dominating Greenland ice sheet exceptional ablation area surface melt in 2012.

Fettweis, X., Box, J. E., Agosta, C., Amory, C., Kittel, C., Lang, C., van As, D., Machguth, H., and Gallée, H. (2017). Reconstructions of the 1900–2015 Greenland ice sheet surface mass balance using the regional climate MAR model. *The Cryosphere*, 11(2):1015–1033.

Fettweis, X., Tedesco, M., Van Den Broeke, M., and Ettema, J. (2011). Melting trends over the Greenland ice sheet (1958-2009) from spaceborne microwave data and regional climate models. *Cryosphere*, 5(2):359–375.

Flowers, G. E., Marshall, S. J., Björnsson, H., and Clarke, G. K. C. (2005). Sensitivity of Vatnajökull ice cap hydrology and dynamics to climate warming over the next 2 centuries. *Journal of Geophysical Research*, 110(F2):F02011.

Fosser, G., Khodayar, S., and Berg, P. (2015). Benefit of convection permitting climate model simulations in the representation of convective precipitation. *Climate Dynamics*, 44(1-2):45–60.

Fowler, A. C. (2001). Modelling the Flow of Glaciers and Ice Sheets. In *Continuum Mechanics and Applications in Geophysics and the Environment*, pages 201–221. Springer Berlin Heidelberg, Berlin, Heidelberg.

Fowler, A. C. and Larson, D. A. (1978). On the Flow of Polythermal Glaciers. I. Model and Preliminary Analysis. *Proceedings of the Royal Society A: Mathematical, Physical and Engineering Sciences*, 363(1713):217–242.

Gallée, H. and Schayes, G. (1994). Development of a Three-Dimensional Meso-γ Primitive Equation Model: Katabatic Winds Simulation in the Area of Terra Nova Bay, Antarctica.

Gardner, A. S., Moholdt, G., Cogley, J. G., Wouters, B., Arendt, A. A., Wahr, J., Berthier, E., Hock, R., Pfeffer, W. T., Kaser, G., Ligtenberg, S. R. M., Bolch, T., Sharp, M. J., Hagen, J. O., van den Broeke, M. R., and Paul, F. (2013). A reconciled estimate of glacier contributions to sea level rise: 2003 to 2009. *Science*, 340(6134):852–7.

Gascoin, S., Guðmundsson, S., Aðalgeirsdóttir, G., Pálsson, F., Schmidt, L., Berthier, E., and Björnsson, H. (2017). Evaluation of MODIS Albedo Product over Ice Caps

in Iceland and Impact of Volcanic Eruptions on Their Albedo. *Remote Sensing*, 9(5):399.

Gilbert, A., Flowers, G. E., Miller, G. H., Rabus, B. T., Van Wychen, W., Gardner, A. S., and Copland, L. (2016). Sensitivity of Barnes Ice Cap, Baffin Island, Canada, to climate state and internal dynamics. *Journal of Geophysical Research: Earth Surface*, 121(8):1516–1539.

Giorgi, F. (1995). Perspectives for regional earth system modeling. *Global and Planetary Change*, 10(1-4):23–42.

Giorgi, F. and Bi, X. (2000). A study of internal variability of a regional climate model. *J. Geophys. Res.*, 105(D24):29503–29522.

Giorgi, F. and Gutowski, W. J. (2015). Regional Dynamical Downscaling and the CORDEX Initiative. *Annual Review of Environment and Resources*, 40(1):467–490.

Giorgi, F., Jones, C., and Asrar, G. R. (2009). Addressing climate information needs at the regional level: The CORDEX framework. *World Meteorological Organization Bulletin*.

Glen, J. W. (1955). The Creep of Polycrystalline Ice. *Proceedings of the Royal Society of London A: Mathematical, Physical and Engineering Sciences*, 228(1175):519–538.

Goelzer, H., Nowicki, S., Edwards, T., Beckley, M., Abe-Ouchi, A., Aschwanden, A., Calov, R., Gagliardini, O., Gillet-Chaulet, F., Golledge, N. R., Gregory, J., Greve, R., Humbert, A., Huybrechts, P., Kennedy, J. H., Larour, E., Lipscomb, W. H., Le clec'h, S., Lee, V., Morlighem, M., Pattyn, F., Payne, A. J., Rodehacke, C., Rückamp, M., Saito, F., Schlegel, N., Seroussi, H., Shepherd, A., Sun, S., van de Wal, R., and Ziemen, F. A. (2018). Design and results of the ice sheet model initialisation experiments initMIP-Greenland: an ISMIP6 intercomparison. *The Cryosphere*, 12(4):1433–1460.

Goelzer, H., Robinson, A., Seroussi, H., and van de Wal, R. S. (2017). Recent Progress in Greenland Ice Sheet Modelling. *Current Climate Change Reports*, 3(4):291–302.

Goldsby, D. L. and Kohlstedt, D. L. (2001). Superplastic Deformation of ice: Experimental Observations. *Journal of Geophysical Research*, 106(B6):11017–11030.

Gong, Y., Cornford, S. L., and Payne, A. J. (2014). Modelling the response of the Lambert Glacier–Amery Ice Shelf system, East Antarctica, to uncertain climate forcing over the 21st and 22nd centuries. *The Cryosphere*, 8(3):1057–1068.

Grainger, M. E. and Lister, H. (1966). Wind speed, stability and eddy viscosity over melting ice surfaces. *J. Glaciol.*, 6(43):101–127.

Graversen, R. G., Langen, P. L., Mauritsen, T., Graversen, R. G., Langen, P. L., and Mauritsen, T. (2014). Polar Amplification in CCSM4: Contributions from the Lapse Rate and Surface Albedo Feedbacks. *Journal of Climate*, 27(12):4433–4450.

Greuell, W. and Genthon, C. (2004). Modelling land-ice surface mass balance. In Bamber, J. L. and Payne, A. J., editors, *Mass Balance of the Cryosphere*, pages 117–168. Cambridge University Press.

Gudmundsson, M. T., Sigmundsson, F., and Björnsson, H. (1997). Ice–volcano interaction of the 1996 Gjálp subglacial eruption, Vatnajökull, Iceland. *Nature*, 389(6654):954–957.

Gudmundsson, M. T., Thordarson, T., Höskuldsson, , Larsen, G., Björnsson, H., Prata, F. J., Oddsson, B., Magnússon, E., Högnadóttir, T., Petersen, G. N., Hayward, C. L., Stevenson, J. a., and Jónsdóttir, I. (2012). Ash generation and distribution from the

April-May 2010 eruption of Eyjafjallajökull, Iceland. *Scientific Reports*, 2:1–12.

Gudmundsson, S., Björnsson, H., Magnússon, E., Berthier, E., Pálsson, F., Gudmundsson, M. T., Högnadóttir, T., and Dall, J. (2011). Response of Eyjafjallajökull, Torfajökull and Tindfjallajökull ice caps in Iceland to regional warming, deduced by remote sensing. *Polar Research*, 30(1):7282.

Guðmundsson, S., Björnsson, H., Haraldsson, H. H., and Pálsson, F. (1999). Veðurathuganir og jökulleysing á Vatnajökli og Langjökli sumarið 1998. Technical report, RH-13-99.

Guðmundsson, S., Björnsson, H., Haraldsson, H. H., and Pálsson, F. (2000). Veðurathuganir og jökulleysing á Vatnajökli og Langjökli sumarið 1999. Technical report, RH-16-00.

Guðmundsson, S., Björnsson, H., Haraldsson, H. H., and Pálsson, F. (2001). Veðurathuganir og jökulleysing á Vatnajökli og Langjökli sumarið 2000. Technical report, RH-17-2001.

Guðmundsson, S., Björnsson, H., Haraldsson, H. H., and Pálsson, F. (2002). Veðurathuganir og jökulleysing á Vatnajökli og Langjökli sumarið 2001. Technical report, RH-17-2002.

Guðmundsson, S., Björnsson, H., Jóhannesson, T., Aðalgeirsdóttir, G., Pálsson, F., and Sigurðsson, O. (2009a). Similarities and differences in the response to climate warming of two ice caps in Iceland. *Hydrology Research*, 40(5):495–502.

Guðmundsson, S., Björnsson, H., Pálsson, F., and Haraldsson, H. H. (2006). Energy balance of Brúarjökull and circumstances leading to the August 2004 floods in the river Jökla, N-Vatnajökull. *Jökull*, 55:121–138.

Guðmundsson, S., Björnsson, H., Pálsson, F., and Haraldsson, H. H. (2009b). Comparison of energy balance and degree-day models of summer ablation on the Langjökull ice cap, SW-Iceland. *Jökull*, 59(59):1–18.

Hagemann, S., Chen, C., Haerter, J. O., Heinke, J., Gerten, D., Piani, C., Hagemann, S., Chen, C., Haerter, J. O., Heinke, J., Gerten, D., and Piani, C. (2011). Impact of a Statistical Bias Correction on the Projected Hydrological Changes Obtained from Three GCMs and Two Hydrology Models. *Journal of Hydrometeorology*, 12(4):556–578.

Hartmann, D. L., Tank, A. M. G. K., Rusticucci, M., Alexander, L. V., Brönnimann, S., Charabi, Y. A. R., Dentener, F. J., Dlugokencky, E. J., Easterling, D. R., Kaplan, A., Soden, B. J., Thorne, P. W., Wild, M., and Zhai, P. (2013). Observations: Atmosphere and Surface. In Intergovernmental Panel on Climate Change, editor, *Climate Change 2013 - The Physical Science Basis*, pages 159–254. Cambridge University Press, Cambridge.

Harðardóttir, J. and Snorrason, A. (2003). Sediment monitoring of glacial rivers in Iceland: new data on bed load transport. *Hydrological Sciences Journal/Journal des Sciences Hydrologiques*, 283:154–163.

Hazeleger, W., Wang, X., Severijns, C., Ştefănescu, S., Bintanja, R., Sterl, A., Wyser, K., Semmler, T., Yang, S., van den Hurk, B., van Noije, T., van der Linden, E., and van der Wiel, K. (2012). EC-Earth V2.2: description and validation of a new seamless earth system prediction model. *Climate Dynamics*, 39(11):2611–2629.

Hines, K. M., Bromwich, D. H., Hines, K. M., and Bromwich, D. H. (2008). Development and Testing of Polar Weather Research and Forecasting (WRF) Model. Part I:

Greenland Ice Sheet Meteorology*. *Monthly Weather Review*, 136(6):1971–1989.
Hock, R. (2005). Glacier melt: a review of processes and their modelling. *Progress in Physical Geography*, 29(3):362–391.
Hubbard, A. (2006). The validation and sensitivity of a model of the Icelandic ice sheet. *Quaternary Science Reviews*, 25(17-18):2297–2313.
Huss, M. and Bauder, A. (2009). 20th-century climate change inferred from four long-term point observations of seasonal mass balance. *Annals of Glaciology*, 50(50):207–214.
Hutter, K. (1983). *Theoretical Glaciology Material Science of Ice and the Mechanics of Glaciers and Ice Sheets*. Springer Netherlands.
Hutter, K., Legerer, F., and Spring, U. (1981). First-order stresses and deformations in glaciers and ice sheets. *Journal of Glaciology*, 27(96):227–270.
Huybrechts, P., de Wolde, J., Huybrechts, P., and Wolde, J. d. (1999). The Dynamic Response of the Greenland and Antarctic Ice Sheets to Multiple-Century Climatic Warming. *Journal of Climate*, 12(8):2169–2188.
Icelandic Meteorological Office Database (2017). discharge data 1986-2016.
Immerzeel, W. W., van Beek, L. P. H., and Bierkens, M. F. P. (2010). Climate change will affect the Asian water towers. *Science (New York, N.Y.)*, 328(5984):1382–5.
Jóhannesson, T., Björnsson, H., Magnússon, E., Guðmundsson, S., Pálsson, F., Sigurðsson, O., Thorsteinsson, T., and Berthier, E. (2013). Ice-volume changes, bias estimation of mass-balance measurements and changes in subglacial lakes derived by lidar mapping of the surface of Icelandic glaciers. *Annals of Glaciology*, 54(63):63–74.
Jóhannesson, T., Sigurdsson, O., Laumann, T., and Kennett, M. (1995). Degree-day glacier mass-balance modelling with applications to glaciers in Iceland, Norway and Greenland. *Journal of Glaciology*, 41(138):345–358.
Kaser, G., Grosshauser, M., and Marzeion, B. (2010). Contribution potential of glaciers to water availability in different climate regimes. *Proceedings of the National Academy of Sciences of the United States of America*, 107(47):20223–7.
Kendon, E. J., Roberts, N. M., Senior, C. A., and Roberts, M. J. (2012). Realism of Rainfall in a Very High-Resolution Regional Climate Model. *Journal of Climate*, 25(17):5791–5806.
Kipp and Zonen (2002). CNR1 Net Radiometer Instruction Manual.
Klein, A. G. and Stroeve, J. (2002). Development and validation of a snow albedo algorithm for the MODIS instrument. *Annals of Glaciology*, 34:45–52.
Koenigk, T., Brodeau, L., Graversen, R. G., Karlsson, J., Svensson, G., Tjernström, M., Willén, U., and Wyser, K. (2013). Arctic climate change in 21st century CMIP5 simulations with EC-Earth. *Climate Dynamics*, 40(11-12):2719–2743.
Kotlarski, S., Jacob, D., Podzun, R., and Paul, F. (2010). Representing glaciers in a regional climate model. *Climate Dynamics*, 34(1):27–46.
Kraaijenbrink, P. D. A., Bierkens, M. F. P., Lutz, A. F., and Immerzeel, W. W. (2017). Impact of a global temperature rise of 1.5 degrees Celsius on Asia's glaciers. *Nature*, 549(7671):257–260.
Landsvirkjun (2017). Wiski database 28.11.2017 - M00328.
Langen, P. L., Fausto, R. S., Vandecrux, B., Mottram, R. H., and Box, J. E. (2017). Liquid Water Flow and Retention on the Greenland Ice Sheet in the Regional Climate

Model HIRHAM5: Local and Large-Scale Impacts. *Frontiers in Earth Science*, 4.

Langen, P. L., Mottram, R. H., Christensen, J. H., Boberg, F., Rodehacke, C. B., Stendel, M., van As, D., Ahlstrøm, A. P., Mortensen, J., Rysgaard, S., Petersen, D., Svendsen, K. H., Aðalgeirsdóttir, G., and Cappelen, J. (2015). Quantifying energy and mass fluxes controlling godthåbsfjord freshwater input in a 5-km simulation (1991-2012). *J. Climate*, 28(202):3694–3713.

Larsen, K. M. H., Gonzalez-Pola, C., Fratantoni, P., Beszczynska-Möller, A., and Hughes, S. L. (2016). ICES Report On Ocean Climate 2015. *ICES Cooperative Research Report*, 331:79.

LeB. Hooke, R. (1981). Flow law for polycrystalline ice in glaciers: Comparison of theoretical predictions, laboratory data, and field measurements. *Reviews of Geophysics*, 19(4):664.

Lee, V., Cornford, S. L., and Payne, A. J. (2015). Initialization of an ice-sheet model for present-day Greenland. *Annals of Glaciology*, 56(70):129–140.

Lenaerts, J. T. M. and Van Den Broeke, M. R. (2012). Modeling drifting snow in Antarctica with a regional climate model: 2. Results. *Journal of Geophysical Research Atmospheres*, 117(5).

Leysinger-Vieli, G. J. M. C. and Gudmundsson, G. H. (2003). Evolution of rock glaciers and alpine glaciers: A model-model approach. *Permafrost, Vols 1 and 2*, 0(1):673–677.

Lindsay, R., Wensnahan, M., Schweiger, A., Zhang, J., Lindsay, R., Wensnahan, M., Schweiger, A., and Zhang, J. (2014). Evaluation of Seven Different Atmospheric Reanalysis Products in the Arctic*. *Journal of Climate*, 27(7):2588–2606.

Lliboutry, L. and Duval, P. (1985). Various isotropic and anisotropic ices found in glaciers and polar ice caps and their corresponding rheologies. *Annales Geophysicae*, 3(2):207–224.

Lorenz, P. and Jacob, D. (2005). Influence of regional scale information on the global circulation: A two-way nesting climate simulation. *Geophysical Research Letters*, 32(18):n/a–n/a.

Lucas-Picher, P., Wulff-Nielsen, M., Christensen, J. H., Aðalgeirsdóttir, G., Mottram, R. H., and Simonsen, S. B. (2012). Very high resolution regional climate model simulations over Greenland: Identifying added value. *Journal of Geophysical Research*, 117:2108.

Magnússon, E., Björnsson, H., Dall, J., and Pálsson, F. (2005). Volume changes of Vatnajökull ice cap, Iceland, due to surface mass balance, ice flow, and subglacial melting at geothermal areas. *Geophysical Research Letters*, 32(5):L05504.

Magnússon, E., Gudmundsson, M. T., Roberts, M. J., Sigurðsson, G., Höskuldsson, F., and Oddsson, B. (2012). Ice-volcano interactions during the 2010 Eyjafjallajökull eruption, as revealed by airborne imaging radar. *Journal of Geophysical Research: Solid Earth*, 117(B7):n/a–n/a.

Magnússon, E., Muñoz-Cobo Belart, J., Pálsson, F., S. Anderson, L., Th. Gunnlaugsson, A., Berthier, E., Agustsson, H., and Geirsdóttir, (2016). The subglacial topography of Drangajokull ice cap, NW-Iceland, deduced from dense RES-profiling. *Jokull*, 66:1–26.

Marshall, S. J., Björnsson, H., Flowers, G. E., and Clarke, G. K. C. (2005). Simulation of Vatnajökull ice cap dynamics. *Journal of Geophysical Research*, 110(F3):F03009.

Marshall, S. J., James, T. S., and Clarke, G. K. (2002). North American Ice Sheet reconstructions at the Last Glacial Maximum. *Quaternary Science Reviews*, 21(1-3):175–192.

Masson, V., Le Moigne, P., Martin, E., Faroux, S., Alias, A., Alkama, R., Belamari, S., Barbu, A., Boone, A., Bouyssel, F., Brousseau, P., Brun, E., Calvet, J.-C., Carrer, D., Decharme, B., Delire, C., Donier, S., Essaouini, K., Gibelin, A.-L., Giordani, H., Habets, F., Jidane, M., Kerdraon, G., Kourzeneva, E., Lafaysse, M., Lafont, S., Lebeaupin Brossier, C., Lemonsu, A., Mahfouf, J.-F., Marguinaud, P., Mokhtari, M., Morin, S., Pigeon, G., Salgado, R., Seity, Y., Taillefer, F., Tanguy, G., Tulet, P., Vincendon, B., Vionnet, V., and Voldoire, A. (2013). The SURFEXv7.2 land and ocean surface platform for coupled or offline simulation of earth surface variables and fluxes. *Geoscientific Model Development*, 6(4):929–960.

MATLAB (2015). *version 8.5.0 (R2015a)*. The MathWorks Inc.

Meijgaard, E. V., Ulft, L. H. V., Bosveld, F. C., Lenderink, G., and Siebesma, a. P. (2008). The KNMI regional atmospheric climate model RACMO version 2.1. *Technical report; TR - 302*, page 43.

Möller, R., Möller, M., Björnsson, H., Guðmundsson, S., Pálsson, F., Oddsson, B., Kukla, P. A., and Schneider, C. (2014). MODIS-derived albedo changes of Vatnajökull (Iceland) due to tephra deposition from the 2004 Grímsvötn eruption. *International Journal of Applied Earth Observation and Geoinformation*, 26:256–269.

Monin, A. S. and Obukhov, A. M. (1954). Basic laws of turbulent mixing in the surface layer of the atmosphere. *Contrib. Geophys. Inst. Acad. Sci. USSR*, 24(151):163–187.

Morland, L. W. (1987). Unconfined Ice-Shelf Flow. pages 99–116. Springer, Dordrecht.

Mottram, R., Boberg, F., Langen, P. L., Yang, S., Rodehacke, C., Christensen, J. H., and Madsen, M. S. (2017a). Surface mass balance of the Greenland ice sheet in the regional climate model HIRHAM5: Present state and future prospects. *Low Temperature Science*, 75:105–115.

Mottram, R., Nielsen, K. P., Gleeson, E., and Yang, X. (2017b). Modelling Glaciers in the HARMONIE-AROME NWP model. *Advances in Science and Research*, 14:323–334.

Muerth, M. J., Gauvin St-Denis, B., Ricard, S., Velázquez, J. A., Schmid, J., Minville, M., Caya, D., Chaumont, D., Ludwig, R., and Turcotte, R. (2013). On the need for bias correction in regional climate scenarios to assess climate change impacts on river runoff. *Hydrology and Earth System Sciences*, 17(3):1189–1204.

Nabat, P., Somot, S., Mallet, M., Sevault, F., Chiacchio, M., and Wild, M. (2015). Direct and semi-direct aerosol radiative effect on the Mediterranean climate variability using a coupled regional climate system model. *Climate Dynamics*, 44(3-4):1127–1155.

Nawri, N. (2014). Evaluation of HARMONIE reanalyses of surface air temperature and wind speed over Iceland. Technical report, Veðurstofa Íslands.

Nawri, N., Pálmason, B., Petersen, N. G., Björnsson, H., and Þorsteinsson, S. (2017). The ICRA atmospheric reanalysis project for Iceland. Technical report.

Nielsen-Englyst, P. (2015). *Impact of albedo parameterizations on surface mass balance and melt extent on the Greenland Ice Sheet*. Master's thesis. Danish Meterorological Institute and Copenhagen University.

Nowicki, S. M. J., Payne, T., Larour, E., Seroussi, H., Goelzer, H., Lipscomb, W., Gregory, J., Abe-Ouchi, A., and Shepherd, A. (2016). Ice Sheet Model Intercom-

parison Project (ISMIP6) contribution to CMIP6. *Geoscientific model development*, 9(12):4521–4545.

Oerlemans, J., Björnsson, H., Kuhn, M., Obleitner, F., Palsson, F., Smeets, C., Vugts, H. F., and Wolde, J. D. (1999). Glacio-Meteorological Investigations On Vatnajökull, Iceland, Summer 1996: An Overview. *Boundary-Layer Meteorology*, 92(1):3–24.

Oerlemans, J. and Knap, W. H. (1998). A 1-year record of global radiation and albedo in the ablation zone of Marteratschgletscher, Switzerland. *Journal of Glaciology*, 44(147):231–238.

Oerlemans, J. J. (2001). *Glaciers and climate change*. A.A. Balkema Publishers.

Pálsson, F., Gunnarsson, A., Gunnlaugsson, , Jónsson, G., Pálsson, H. S., Steinþórsson, S., and Jónsson, (2017). VATNAJÖKULL: Mass balance, meltwater drainage and surface velocity of the glacial year 2016_17. Technical report, Institute of Earth Sciences University of Iceland and National Power Company, RH-07-2017.

Pálsson, F., Gunnarsson, A., Jónsson, Þ., Steinþórsson, S., and Pálsson, H. S. (2015). Vatnajökull: Mass balance, meltwater drainage and surface velocity of the glacial year 2014_15. Technical report, Institute of Earth Sciences, University of Iceland and National Power Company, RH-06-2015.

Pálsson, F., Guðmundsson, S., Björnsson, H., Berthier, E., Magnússon, E., Guðmundsson, S., and Haraldsson, H. H. (2012). Mass and volume changes of Langjökull ice cap , Iceland , 1890 to 2009 , deduced from old maps , satellite images and in situ mass balance measurements. *Jökull*, 62:81–96.

Paterson, A. R. A. R. (1983). *A first course in fluid dynamics*. Cambridge University Press.

Paterson, W. and Budd, W. (1982). Flow parameters for ice sheet modeling. *Cold Regions Science and Technology*, 6(2):175–177.

Pattyn, F. (2003). A new three-dimensional higher-order thermomechanical ice sheet model: Basic sensitivity, ice stream development, and ice flow across subglacial lakes. *Journal of Geophysical Research*, 108(B8):2382.

Payne, A. J., Huybrechts, P., Abe-Ouchi, A., Calov, R., Fastook, J. L., Greve, R., Marshall, S. J., Marsiat, I., Ritz, C., Tarasov, L., and Thomassen, M. P. A. (2000). Results from the EISMINT model intercomparison: the effects of thermomechanical coupling. *Journal of Glaciology*, 46(153):227–238.

Pithan, F. and Mauritsen, T. (2014). Arctic amplification dominated by temperature feedbacks in contemporary climate models. *Nature Geoscience*, 7(3):181–184.

Pollard, D. and DeConto, R. M. (2009). Modelling West Antarctic ice sheet growth and collapse through the past five million years. *Nature*, 458(7236):329–332.

Radić, V., Clarke, G. K. C., Radić, V., and Clarke, G. K. C. (2011). Evaluation of IPCC Models' Performance in Simulating Late-Twentieth-Century Climatologies and Weather Patterns over North America. *Journal of Climate*, 24(20):5257–5274.

Rae, J. G. L., Aðalgeirsdóttir, G., Edwards, T. L., Fettweis, X., Gregory, J. M., Hewitt, H. T., Lowe, J. A., Lucas-Picher, b., Mottram, R. H., Payne, A. J., Ridley, J. K., Shannon, S. R., van de Berg, W. J., van de Wal, R. S. W., and van den Broeke, M. R. (2012). Greenland ice sheet surface mass balance: evaluating simulations and making projections with regional climate models. *The Cryosphere*, 6(6):1275–1294.

Reijmer, C. H., Knap, W. H., and Oerlemans, J. (1999). The Surface Albedo Of The Vatnajökull Ice Cap, Iceland: A Comparison Between Satellite-Derived And

Ground-Based Measurements. *Boundary-Layer Meteorology*, 92(1):123–143.

Riahi, K., Rao, S., Krey, V., Cho, C., Chirkov, V., Fischer, G., Kindermann, G., Nakicenovic, N., and Rafaj, P. (2011). RCP 8.5-A scenario of comparatively high greenhouse gas emissions. *Climatic Change*, 109(1):33–57.

Rinke, A. and Dethloff, K. (2000). On the sensitivity of a regional Arctic climate model to initial and boundary conditions. *Climate Research - CLIMATE RES*, 14:101–113.

Rockel, B. (2015). The Regional Downscaling Approach: a Brief History and Recent Advances. *Current Climate Change Reports*, 1(1):22–29.

Rockel, B., Will, A., and Hense, A. (2008). The Regional Climate Model COSMO-CLM (CCLM). *Meteorologische Zeitschrift*, 17(4):347–348.

Roeckner, E., Bäuml, G., Bonaventura, L., Brokopf, R., Esch, M., Giorgetta, M., Hagemann, S., Kirchner, I., Kornblueh, L., Manzini, E., Rhodin, A., Schlese, U., Schulzweida, U., and Tompkins, A. (2003). The atmospheric general circulation model ECHAM 5 PART I: Model description. Technical Report 349, Report / MPI für Meteorologie.

Russell, A. J. (1989). A Comparison of two Recent Jökulhlaups from An Ice-dammed Lake, Søndre Strømfjord, West Greenland. *Journal of Glaciology*, 35(120):157–162.

Samuelsson, P., Jones, C. G., Will´En, U., Ullerstig, A., Gollvik, S., Hansson, U., Jansson, E., Kjellstro¨M, C., Nikulin, G., and Wyser, K. (2011). The Rossby Centre Regional Climate model RCA3: model description and performance. *Tellus A: Dynamic Meteorology and Oceanography*, 63(1):4–23.

Sasaki, H., Kawakami, Y., Ono, M., Jonasson, F., Shui, Y. B., Cheng, H.-M., Robman, L., McCarty, C., Chew, S. J., and Sasaki, K. (2003). Localization of Cortical Cataract in Subjects of Diverse Races and Latitude. *Investigative Opthalmology & Visual Science*, 44(10):4210.

Schaaf, C. and Wang, Z. (2015). MCD43A3 MODIS/Terra+Aqua BRDF/Albedo Daily L3 Global—500 m V006. *NASA EOSDIS Land Processes DAAC*.

Schaaf, C. B., Gao, F., Strahler, A. H., Lucht, W., Li, X., Tsang, T., Strugnell, N. C., Zhang, X., Jin, Y., Muller, J.-P., Lewis, P., Barnsley, M., Hobson, P., Disney, M., Roberts, G., Dunderdale, M., Doll, C., d'Entremont, R. P., Hu, B., Liang, S., Privette, J. L., and Roy, D. (2002). First operational BRDF, albedo nadir reflectance products from MODIS. *Remote Sensing of Environment*, 83(1-2):135–148.

Schaaf, C. B., Wang, Z., and Strahler, A. H. (2011). Commentary on Wang and Zender—MODIS snow albedo bias at high solar zenith angles relative to theory and to in situ observations in Greenland. *Remote Sensing of Environment*, 115(5):1296–1300.

Schäfer, M., Möller, M., Zwinger, T., and Moore, J. (2015). Dynamic modelling of future glacier changes: mass-balance/elevation feedback in projections for the Vestfonna ice cap, Nordaustlandet, Svalbard. *Journal of Glaciology*, 61(230):1121–1136.

Schlegel, N.-J., Larour, E., Seroussi, H., Morlighem, M., and Box, J. E. (2015). Ice discharge uncertainties in Northeast Greenland from boundary conditions and climate forcing of an ice flow model. *Journal of Geophysical Research: Earth Surface J. Geophys. Res. Earth Surf*, 120:29–54.

Schoof, C. and Hewitt, I. (2013). Ice-sheet dynamics. *Annual Review of Fluid Mechanics*, 45:217–239.

Schrum, C. (2017). *Regional Climate Modeling and Air-Sea Coupling*, volume 1.

Oxford University Press.

Seity, Y., Brousseau, P., Malardel, S., Hello, G., Bénard, P., Bouttier, F., Lac, C., Masson, V., Seity, Y., Brousseau, P., Malardel, S., Hello, G., Bénard, P., Bouttier, F., Lac, C., and Masson, V. (2011). The AROME-France Convective-Scale Operational Model. *Monthly Weather Review*, 139(3):976–991.

Seroussi, H., Ben Dhia, H., Morlighem, M., Larour, E., Rignot, E., and Aubry, D. (2012). Coupling ice flow models of varying orders of complexity with the Tiling method. *Journal of Glaciology*, 58(210):776–786.

Skamarock, W. C., Skamarock, W. C., Klemp, J. B., Dudhia, J., Gill, D. O., Barker, D. M., Wang, W., and Powers, J. G. (2008). A description of the Advanced Research WRF version 3. NCAR Technical note -475+STR.

Snorrason, A., Gunnarsson, A., Jónsson, P., Einarsson, K., and Sigurðsson, O. (1998). Summary of available hydrological information in the Jökulsá á Deal and Jökulsá í Fljótsdal basins, Iceland. Technical report, Orkustofnun, Reykjavik.

Stendel, M., Christensen, J. H., and Petersen, D. (2008). *High-Arctic Ecosystem Dynamics in a Changing Climate*, volume 40 of *Advances in Ecological Research*. Elsevier.

Stroeve, J., Box, J. E., Gao, F., Liang, S., Nolin, A., and Schaaf, C. (2005). Accuracy assessment of the MODIS 16-day albedo product for snow: comparisons with Greenland in situ measurements. *Remote Sensing of Environment*, 94(1):46–60.

Stroeve, J. C., Box, J. E., and Haran, T. (2006). Evaluation of the MODIS (MOD10A1) daily snow albedo product over the Greenland ice sheet. *Remote Sensing of Environment*, 105(2):155–171.

Taylor, K. E., Stouffer, R. J., and Meehl, G. A. (2012). An overview of CMIP5 and the experiment design. *Bulletin of the American Meteorological Society*, 93(4):485–498.

The PISM authors (2018). PISM, a Parallel Ice Sheet Model. Technical report.

Thomson, A. M., Calvin, K. V., Smith, S. J., Kyle, G. P., Volke, A., Patel, P., Delgado-Arias, S., Bond-Lamberty, B., Wise, M. A., Clarke, L. E., and Edmonds, J. A. (2011). RCP4.5: A pathway for stabilization of radiative forcing by 2100. *Climatic Change*, 109(1):77–94.

Thordarson, T. and Larsen, G. (2007). Volcanism in Iceland in historical time: Volcano types, eruption styles and eruptive history. *Journal of Geodynamics*, 43(1):118–152.

Tulaczyk, S., Kamb, W. B., and Engelhardt, H. F. (2000). Basal mechanics of Ice Stream B, west Antarctica: 1. Till mechanics. *Journal of Geophysical Research: Solid Earth*, 105(B1):463–481.

Unden, P., Rontu, L., Järvinen, H., Lynch, P., Calvo, J., Cats, G., Cuxart, J., Eerola, K., Fortelius, C., Garcia-Moya, J. A., Jones, C., Geert, Lenderlink, G., Mcdonald, A., Mcgrath, R., Navascues, B., Nielsen, N. W., Degaard, V., Rodriguez, E., Rummukainen, M., Sattler, K., Sass, B. H., Savijarvi, H., Schreur, B. W., Sigg, R., and The, H. (2002). HIRLAM-5 Scientific Documentation.

van den Broeke, M., Bus, C., Ettema, J., and Smeets, P. (2010). Temperature thresholds for degree-day modelling of Greenland ice sheet melt rates. *Geophysical Research Letters*, 37(18):n/a–n/a.

van den Broeke, M., Smeets, P., Ettema, J., van der Veen, C., van de Wal, R., and Oerlemans, J. (2008). Partitioning of melt energy and meltwater fluxes in the ablation zone of the west Greenland ice sheet. *The Cryosphere*, 2(2):179–189.

van den Broeke, M., van As, D., Reijmer, C., and van de Wal, R. (2004). Assessing and improving the quality of unattended radiation observations in Antarctica. *Journal of Atmospheric and Oceanic Technology*, 21(9):1417–1431.

van den Broeke, M. R. (1997). Momentum, Heat, and Moisture Budgets of the Katabatic Wind Layer over a Midlatitude Glacier in Summer. *Journal of Applied Meteorology*, 36(6):763–774.

Van Meijgaard, E., Van Ulft, L. H., de Berg, W. J., Bosveld, F. C., den Hurk, B., Lenderink, G., and Siebesma, A. P. (2008). The KNMI regional atmospheric climate model RACMO version 2.1. *Koninklijk Nederlands Meteorologisch Instituut*, 43.

Warren, S. G. (1982). Optical properties of snow. *Reviews of Geophysics*, 20(1):67.

Weis, M., Greve, R., and Hutter, K. (1999). Theory of shallow ice shelves. *Continuum Mechanics and Thermodynamics*, 11(1):15–50.

Weisman, M. L., Skamarock, W. C., and Klemp, J. B. (1997). The Resolution Dependence of Explicitly Modeled Convective Systems. *Monthly Weather Review*, 125(4):527–548.

Winkelmann, R., Martin, M. A., Haseloff, M., Albrecht, T., Bueler, E., Khroulev, C., and Levermann, A. (2011). The Potsdam Parallel Ice Sheet Model (PISM-PIK) – Part 1: Model description. *The Cryosphere*, 5(3):715–726.

Wiscombe, W. J., Warren, S. G., Wiscombe, W. J., and Warren, S. G. (1980). A Model for the Spectral Albedo of Snow. I: Pure Snow. *Journal of the Atmospheric Sciences*, 37(12):2712–2733.

Xu, M., Yan, M., Kang, J., and Ren, J. (2012). Comparative studies of glacier mass balance and their climatic implications in Svalbard, Northern Scandinavia, and Southern Norway. *Environmental Earth Sciences*, 67(5):1407–1414.

Paper I

The importance of accurate glacier albedo for estimates of surface mass balance on Vatnajökull: evaluating the surface energy budget in a regional climate model with automatic weather station observations

Louise Steffensen Schmidt, Guðfinna Aðalgeirsdóttir, Sverrir Guðmundsson, Peter L. Langen, Finnur Pálsson, Ruth Mottram, Simon Gascoin, and Helgi Björnsson

The Cryosphere, 11, 1665-1684, https://doi.org/10.5194/tc-11-1665-2017, 2017

The Cryosphere, 11, 1665–1684, 2017
https://doi.org/10.5194/tc-11-1665-2017

The Cryosphere Open Access EGU

The importance of accurate glacier albedo for estimates of surface mass balance on Vatnajökull: evaluating the surface energy budget in a regional climate model with automatic weather station observations

Louise Steffensen Schmidt[1], Guðfinna Aðalgeirsdóttir[1], Sverrir Guðmundsson[1,2], Peter L. Langen[3], Finnur Pálsson[1], Ruth Mottram[3], Simon Gascoin[4], and Helgi Björnsson[1]

[1]University of Iceland, Institute of Earth Sciences, Reykjavik, Iceland
[2]Keilir Institute of Technology, Reykjanesbær, Iceland
[3]Danish Meteorological Institute, Copenhagen, Denmark
[4]Centre d'Etudes Spatiales de la Biosphère, Université de Toulouse, CNES/CNRS/IRD/UPS, Toulouse, France

Correspondence to: Louise Steffensen Schmidt (lss7@hi.is)

Received: 3 February 2017 – Discussion started: 24 February 2017
Revised: 24 May 2017 – Accepted: 5 June 2017 – Published: 14 July 2017

Abstract. A simulation of the surface climate of Vatnajökull ice cap, Iceland, carried out with the regional climate model HIRHAM5 for the period 1980–2014, is used to estimate the evolution of the glacier surface mass balance (SMB). This simulation uses a new snow albedo parameterization that allows albedo to exponentially decay with time and is surface temperature dependent. The albedo scheme utilizes a new background map of the ice albedo created from observed MODIS data. The simulation is evaluated against observed daily values of weather parameters from five automatic weather stations (AWSs) from the period 2001–2014, as well as in situ SMB measurements from the period 1995–2014. The model agrees well with observations at the AWS sites, albeit with a general underestimation of the net radiation. This is due to an underestimation of the incoming radiation and a general overestimation of the albedo. The average modelled albedo is overestimated in the ablation zone, which we attribute to an overestimation of the thickness of the snow layer and not taking the surface darkening from dirt and volcanic ash deposition during dust storms and volcanic eruptions into account. A comparison with the specific summer, winter, and net mass balance for the whole of Vatnajökull (1995–2014) shows a good overall fit during the summer, with a small mass balance underestimation of 0.04 m w.e. on average, whereas the winter mass balance is overestimated by on average 0.5 m w.e. due to too large precipitation at the highest areas of the ice cap. A simple correction of the accumulation at the highest points of the glacier reduces this to 0.15 m w.e. Here, we use HIRHAM5 to simulate the evolution of the SMB of Vatnajökull for the period 1981–2014 and show that the model provides a reasonable representation of the SMB for this period. However, a major source of uncertainty in the representation of the SMB is the representation of the albedo, and processes currently not accounted for in RCMs, such as dust storms, are an important source of uncertainty in estimates of snow melt rate.

1 Introduction

Worldwide, glaciers and ice caps are losing mass at increasing rates as a response to climate change (e.g. Vaughan et al., 2013). Major changes in the dimensions of glaciers are expected to affect the sea level and climate throughout the world, and it is therefore important to describe and understand the glacier climate. Glacier retreat and mass loss at significantly increasing rates are also observed for Icelandic glaciers (Björnsson et al., 2013), which could potentially contribute to the rise in sea level by 1 cm (Björnsson and Pálsson, 2008; Björnsson et al., 2013). The runoff from Vatnajökull ice cap is economically important to hy-

Published by Copernicus Publications on behalf of the European Geosciences Union.

dropower production in Iceland and the present and future mass balance is thus of keen interest. Numerical high-resolution regional climate models (RCMs), such as MAR (Gallée and Schayes, 1994), RACMO2 (Meijgaard et al., 2008), or HIRHAM5 (Christensen et al., 2006), are valuable tools for estimating the meteorological parameters and mass balance variability at the surface of glaciers. However, to carry out reliable future projections, or reconstruct the past climate, it is important to evaluate how well models simulate the present climate

Evaluation of RCMs is important, not only because it reveals possible biases in the model but also because it could yield recommendations for model improvements. Much work has gone into evaluating RCMs over Greenland (e.g. Box and Rinke, 2003; Noël et al., 2015; Rae et al., 2012; Langen et al., 2017; Fettweis et al., 2017) and Antarctica (e.g. Lenaerts and Van Den Broeke, 2012; Agosta et al., 2015), but less effort has gone into evaluating them over Iceland (e.g. Ágústsson et al., 2013; Nawri, 2014).

However, a long-term meteorological monitoring programme has been conducted on Icelandic glaciers since the 1991–1992 glaciological year (e.g. Björnsson et al., 1998). Therefore, Icelandic glaciers are excellent candidates for evaluating modelled meteorological and SMB components. Compared to Greenland, observations are recorded in a relatively small area, offering a good opportunity to evaluate the spatial and temporal variability of the HIRHAM5 model on a regional scale. As albedo in Iceland is significantly different from that of Greenland or Antarctica, e.g. due to frequent dust storms and occasional volcanic eruptions, model evaluations over Iceland provides important insight into the effect of albedo changes on the glacier energy balance.

Due to the large spatial and temporal variation in albedo of Icelandic glaciers (spanning from less than 0.1 for dirty ice in the ablation zone to 0.9–0.95 for new snow), and the large sensitivity of melt to variations in albedo, it is crucial to have correct estimates of the albedo when modelling the surface mass balance. However, accurate modelling of the albedo can be challenging. For example, volcanic eruptions and dust storms can significantly lower the glacier albedo, and thus increase the amount of melt (e.g. Conway et al., 1996; Gascoin et al., 2017; Wittmann et al., 2017), but are difficult to include in albedo models. Accurate simulations of the ice albedo is also problematic, as for some glaciers it varies with elevation (e.g. Knap et al., 1999) but not for others (e.g. Greuell et al., 1997). In addition, the ice albedo may decrease with time (e.g. Reijmer et al., 1999), increase with time (e.g. Oerlemans and Knap, 1998), or remain constant (e.g. Greuell et al., 1997) depending on the glacier.

Here we present a 1981–2014 SMB data set of Vatnajökull ice cap modelled by HIRHAM5 at 5.5 km resolution. HIRHAM5 is a state-of-the-art, high-resolution RCM that has been well validated over Greenland (e.g. Box and Rinke, 2003; Lucas-Picher et al., 2012; Rae et al., 2012; Langen et al., 2017). In this study, HIRHAM5 incorporates an updated albedo scheme, using a background MODIS ice albedo field, in the aim of capturing the effect of dust and tephra on ice albedo in the ablation zone. This method of determining the ice albedo has previously been used by, for example, van Angelen et al. (2012). Model simulation results are compared to observations from automatic weather stations (AWSs) and in situ mass balance observations, in an effort to improve the performance of the model. The possible physical reasons for any model biases are discussed, and recommendations for corrections are made where possible.

2 Model description

2.1 HIRHAM5

In this study we employed the RCM HIRHAM5 (Christensen et al., 2006), which was developed at the Danish Meteorological Institute. It is a hydrostatic RCM which combines the dynamical core of the HIRLAM7 numerical forecasting model (Eerola, 2006) and physics schemes from the ECHAM5 general circulation model (Roeckner et al., 2003). Model simulations have been successfully validated over Greenland using AWS and ice core data (e.g. Box and Rinke, 2003; Stendel et al., 2008; Lucas-Picher et al., 2012; Langen et al., 2015; Rae et al., 2012; Langen et al., 2017).

While the original HIRHAM5, as described in Christensen et al. (2006), used unchanged ECHAM physics, an updated model version, which includes a dynamic surface scheme that explicitly calculates the surface mass budget on the surface of glaciers and ice sheets, is used in this study. This new scheme takes melting of snow and bare ice into account and resolves the retention and refreezing of liquid water in the snow pack (Langen et al., 2015, 2017). In addition, the five-layer surface scheme in ECHAM has been expanded to 25 layers.

2.1.1 New albedo parametrization

The updated model also features a more sophisticated snow albedo scheme (Nielsen-Englyst, 2015) than that used in the original HIRHAM5; whereas the previous scheme was purely temperature dependent, the new scheme depends both on the age of the snow and the surface temperature. The scheme is similar to that used in Oerlemans and Knap (1998), which assumes that the albedo decays exponentially as it ages, but in this study an additional temperature component is applied. If there is snow on the surface, the change in the snow albedo from one time step to the next depends on whether the surface is in a dry (< 271 K) or wet regime (≥ 271 K). In the dry regime, the surface temperature is too low for any melting to occur, while in the wet regime the temperature in the surface layer is high enough for the surface to be melting. The snow albedo changes over a time step, δt, as

$$\alpha^{t}_{\mathrm{snow}} = (\alpha^{t-1}_{\mathrm{snow}} - \alpha_{\mathrm{mx}}) \cdot e^{-\delta t/\tau_x} + \alpha_{\mathrm{mx}}, \quad (1)$$

where α_{mx} is the minimum snow albedo value that can be reached from ageing of the snow and τ_x is a timescale which determines how fast the albedo reaches its minimum value. These two variables take on different values depending on whether the snow is in the dry (d) or wet (w) regime.

Observations from the AC and ELA stations were used to determine α_{mx} and τ_x. The optimal variables were found by minimizing the weighted mean RMSE between the modelled and measured albedo by varying the values of α_{mx} and τ_x. The best-fit values were found to be $\alpha_{md} = 0.65$, α_{mw}=0.41, $\tau_{md} = 5$ days, and $\tau_{mw} = 10$ days.

Albedo is only refreshed to the maximum value if snowfall constitutes more than 95 % of the total precipitation. A partial refreshment is possible as the albedo is only reset to the maximum allowed value if the amount of snowfall on that day (S_0) is higher than 0.03 m w.e. This threshold was chosen to provide the best fit with the AWS observations. The rate of refreshment b is given by

$$b = \min\left[1, \frac{S_f}{S_0}\right], \tag{2}$$

where S_f is the amount of snowfall during the model time step in m w.e. and S_0 is the critical amount of snowfall in m w.e. per model time step needed to completely refresh the albedo. Using this rate, the albedo is then refreshed using

$$\alpha_{snow}^{t+1} = \alpha_{snow}^{t} + b \cdot (\alpha_{max} - \alpha_{snow}^{t}), \tag{3}$$

where α_{max} is the maximum albedo for freshly fallen snow, set equal to 0.85 as this provides the best average fit with the observations.

In the case of shallow snow cover, the surface albedo will be affected by the albedo of the underlying ice. A smooth transition between the snow and bare ice albedo is therefore implemented, and the final albedo is thus expressed as

$$\alpha^{t+1} = \alpha_{snow}^{t+1} + (\alpha_{ice} - \alpha_{snow}^{t+1}) \cdot \exp\left(\frac{-d^{t+1}}{d_s}\right), \tag{4}$$

where d is the snow depth, and d_s is a characteristic scale for snow depth. Following Oerlemans and Knap (1998), the characteristic scale is set to 3.2 cm snow depth. If no snow is present, the albedo is set to the bare ice albedo. The bare ice albedo is determined from a background ice albedo map which was created using MODIS observations from the period 2001–2012. How this map was created is described in Sect. 3.

The extent to which this bare ice MODIS albedo map improves the simulations will be estimated by comparing the results with those from a model simulation using a constant ice albedo in Sect. 4.8.

2.1.2 Experimental design

In this study, HIRHAM5 is run at a resolution of 0.05° (equivalent to ∼ 5.5 km) on a rotated pole grid for the period 1980–2014. The model uses 31 irregularly spaced vertical atmospheric levels from the surface to 10 hPa with a model time step of 90 s in the dynamical scheme. The model is configured for a domain containing all of Greenland and Iceland. The model is forced at the lateral and lower boundaries by the ECMWF ERA-Interim reanalysis data set (Dee et al., 2011), which uses observations from satellites, weather balloons, and ground stations to create a comprehensive reanalysis of the atmosphere. The model is forced by temperature, wind, relative humidity, and surface pressure at the lateral boundary, and sea surface temperature and sea ice fraction at the lower boundary at 6 h intervals.

The new snow/ice surface scheme discussed above is run offline in this study, meaning that the subsurface scheme is run separately from the atmospheric code. This is done by forcing the subsurface scheme every 6 h by radiative and turbulent surface fluxes, as well as snow, rain, evaporation, and sublimation data from a HIRHAM5 experiment (Mottram et al., 2016) with a previous version of the albedo and refreezing schemes (e.g. Langen et al., 2017). While a full, high-resolution HIRHAM5 run is computationally very expensive, the offline model offers a fast and flexible option to test new model implementations and allows for a quick and thorough spin-up of the subsurface. The offline model was initialized with values from a previous offline model run with a different albedo scheme and then a model spin-up was performed by integrating the model for 150 years repeating the forcing from 1980. The largest adjustments occurred during the first 75 years of the spin-up, after which the variation was much smaller than the interannual variability. At the end of the run, the solar radiation, surface mass balance, runoff, snow depth, and refreezing had all converged, as had the temperature, liquid and snow content in all 25 subsurface layers. The final state of the spin-up was then used as the initial condition for the 1980–2014 model simulation. The reported values of albedo, upward longwave and shortwave radiation, and surface mass balance in the following are all from the offline run.

A disadvantage of this method is that it neglects feedbacks between the atmospheric circulation and the surface conditions like the albedo and temperature. However, since the surface temperature of Vatnajökull is typically near the melting point during the summer, both in reality and in the model, changes in the albedo should not have a large effect on upward longwave radiation and the turbulent fluxes. Thus, while the updated surface scheme is important for the mass balance components, the error due to the neglected feedbacks is likely small in the model calculations.

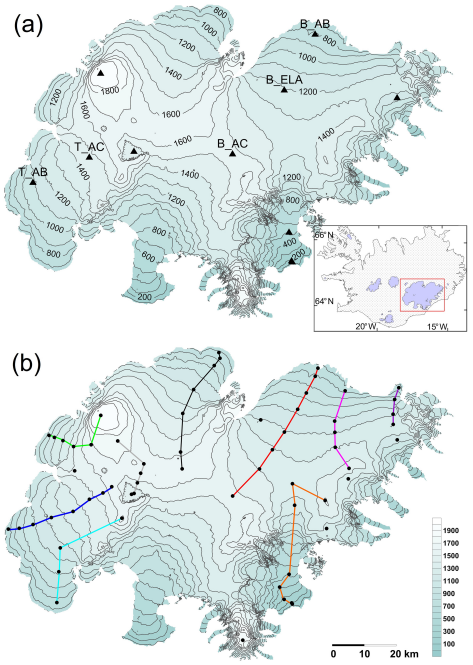

Figure 1. (a) The average location of the AWS sites. Only the labelled sites were used in this study. **(b)** The average location of the mass balance sites from 1995 to 2014. The coloured lines connect mass balance sites along a transect. Not all mass balance sites were measured every year.

2.1.3 Model uncertainty

Due to nonlinearities in the HIRHAM5's model dynamics and physics, it has an implicit uncertainty due to internal model variability originating from nonlinear processes (e.g. Giorgi and Bi, 2000; de Elía et al., 2002). This variability is caused by numerical sensitivity, uncertainty in the boundary and initial conditions, and errors due to model parametrizations (e.g. Box and Rinke, 2003), including, for example, the albedo parameterization, the vertical gradients in the boundary layer, or cloud radiative effects. In addition, using a constant value of z_0 for both snow and bare ice could lead to large errors in the turbulent fluxes (e.g. Brock et al., 2000).

3 Observational data

The primary observational data set used in this study was collected by AWSs at selected locations on Vatnajökull. Since 1994, 1–13 stations have been operated on the ice cap during the summer months (e.g. Oerlemans et al., 1999; Guðmundsson et al., 2006). The temperature, relative humidity, wind speed, and wind direction at 2 m above the surface have been measured during the entire period (1992–present), while the radiation components have been measured since 1996. For this study, data from five AWSs were considered – three on Brúarjökull (B) and two on Tungnaárjökull (T) (see Fig. 1). Both Brúarjökull and Tungnaárjökull are outlet glaciers of Vatnajökull ice cap. Two stations are situated in the ablation zone (henceforth referred to as the AB stations), one station is situated near the equilibrium line altitude (ELA station), and two stations are in the accumulation zone (AC stations). The average elevation of each station is shown in Table 1. All five stations have been operated on the glacier every year during the period 2001–2014. Observations of 2 m temperature, humidity, wind speed, and radiative fluxes were used to validate HIRHAM5 over Vatnajökull.

Table 1. Average measured elevation and average bias of the interpolated HIRHAM5 elevation at each station for 2001–2014.

Station	Average elevation (m)	Average model elevation bias (m)
B_{AB}	839	22
T_{AB}	1089	47
B_{ELA}	1205	31
B_{AC}	1526	17
T_{AC}	1457	13

The uncertainties of the AWS observations vary depending on the sensor. The temperature and humidity sensors have an accuracy of 0.2 K and 2 % for temperature and humidity, respectively, while the accuracy of the wind speed is 0.2 m s^{-1} (Guðmundsson et al., 2009). The radiative fluxes were measured using either Kipp and Zonen CM14, CNR1 or CNR4 sensors that have a maximum manufacturer-reported uncertainty of ±10 % for daily totals (e.g. Kipp and Zonen, 2002). However, the uncertainty has independently been evaluated to be lower (3–5 %) when used in an ice sheet environment (van den Broeke et al., 2004; Guðmundsson et al., 2009). The turbulent fluxes, combining sensible and latent heat fluxes, and surface pressure were not measured at the stations, but were estimated using the methods described in Sect. 3.1.

In addition to AWS data, in situ mass balance measurements were used to evaluate the simulated surface mass balance (SMB) at several sites on Vatnajökull. Conventional in situ mass balance measurements have been carried out every glaciological year since 1991–1992, with 60 stations measured each year on average. The measurement sites are shown in Fig. 1. The uncertainty of the mass balance measurements has been estimated to be ±0.3 m w.e.

The SMB measurements are conducted at the beginning and end of the accumulation season in order to measure both

the winter and summer balance. The winter balance is measured in the beginning of the melt season by drilling down to the previous summer layer and weighting the snow column. The summer surface is used as the reference level even if some snow accumulation had occurred by the time the summer balance measurements were conducted. The snow thickness on top of the summer surface at the time of the autumn survey has been measured since 1995. This is needed when comparing with the simulation of snow accumulation.

Observations of the broadband albedo in the shortwave spectrum (0.3–5.0 µm) from the MODerate Resolution Imaging Spectroradiometer (MODIS) were used to create a background map of the ice albedo at all glacier grid points in HIRHAM5, which was used in the implemented HIRHAM5 albedo scheme. MODIS product MCD43A3 v006 was used for the background map (Schaaf, 2015). The MODIS estimates of the albedo on Vatnajökull are in good agreement with AWS data (Gascoin et al., 2017). The MODIS data were extracted in geographical coordinates (long–lat) at a resolution of 0.005°, i.e. close to the original MODIS resolution of 500 m. This was done using the MODIS reprojection tool with the bilinear interpolation method. These MODIS data in latitude-longitude coordinates were then resampled to match the rotated HIRHAM5 long–lat grid coordinates by bilinear interpolation using MATLAB's interpn function (MATLAB, 2015).

In order to determine the bare ice albedo at each grid point, daily MODIS data over Iceland from the period 2001–2012 were used. Years with volcanic eruptions were discarded, as the volcanic ash lowered the albedo values far below the average. The minimum autumn albedo value was then determined in each grid point using values from July–September and that value used to create a bare ice albedo map of the glaciers. The final albedo map had ice albedo values in the range 0.03–0.3 for Vatnajökull. The spectral properties of ice in the ablation zone are controlled by tephra layers in the ice, which are exposed as the glacier melts (Larsen et al., 1996). Additional tephra or dust deposition will therefore only have a small effect on the spectral properties of the ice, as the ice surface is already covered in dark bands. In addition, field observations suggest that the new particles are generally washed off from year to year. Applying one background map for the entire period should therefore provide the same results as applying a map created for each year. In addition, it allows us to run the model for years where no MODIS observations are available or where the amount of observations over the ice cap are sparse due to, for example, clouds.

3.1 AWS point models

The turbulent energy fluxes were calculated from AWS measurements using a one-level eddy flux model (Björnsson, 1972; Guðmundsson et al., 2009) which uses Monin–Obukhov similarity theory (Monin and Obukhov, 1954) and implements different roughness lengths for the vertical profiles of wind, temperature, and water vapour (Andreas, 1987). The model is described in detail in Guðmundsson et al. (2009). Uncertainties of this model for example pertain to the aerodynamic roughness length for momentum z_0. The majority of z_0 values recorded over melting glacier surfaces vary over 2 orders of magnitude (between 1 and 10 mm), but over fresh snow or smooth ice surfaces the roughness length is generally around 0.1 mm (Brock et al., 2006). An order of magnitude increase in z_0 can more than double the estimated turbulent fluxes (Brock et al., 2000), so the chosen roughness length parametrization can greatly affect the performance of the model. Generally, a constant value of z_0 is prescribed for snow and/or ice surfaces (Brock et al., 2006), which is an oversimplification as the roughness may vary significantly over the ablation season (e.g. Grainger and Lister, 1966).

However, since measurements of the evolution of z_0 over the entire measurement period are not available, a constant roughness length of 1 mm was chosen in the calculation of the non-radiative fluxes. Sensitivity tests were conducted to estimate how large an error this choice of roughness length could lead to at the used AWS sites. A roughness length of 0.1 mm would decrease the calculated turbulent fluxes by 16–22 %, while using a roughness length of 10 mm would increase the calculated fluxes by 10–19 %, depending on the station. Since the contribution of the turbulent fluxes to the total energy balance is generally low, this translates into an increase or a decrease in the total energy balance at the stations by a maximum of 7 %.

The surface air pressure at the station is also needed to calculate the turbulent fluxes, but it is not measured at the AWS sites. Instead it is estimated at the relevant elevation h using synoptic observations from meteorological stations operated by the Icelandic Met Office and the following relationship:

$$P(h) = P(h_0)\left(1 - \frac{0.0065(h - h_0)}{T(h_0)}\right)^{5.25}, \quad (5)$$

where $P(h_0)$ and $T(h_0)$ are the air pressure and air temperature, respectively, observed at an elevation h_0 (e.g Wallace et al., 2006). This method has previously been applied successfully at various locations on Vatnajökull and Langjökull (e.g. Guðmundsson et al., 2006, 2009).

3.2 Validation method

AWS data from the period 2001–2014 for three Brúarjökull stations and two Tungnaárjökull stations are considered, as well as SMB point measurements from 1995 to 2014. All stations were operated during the summer months, but since 2006 the lowest Brúarjökull station has been operated year round. Comparisons are made between daily averages from the HIRHAM5 model and the in situ observations collected at the AWSs. HIRHAM5 daily means are calculated from 6-hourly outputs, while the AWS daily means are calculated from observations at 10 min intervals.

Comparisons between station values and model values are made by bilinearly interpolating the model output to the measurement position using the four closest model grid points and using only glacier-surface type grid cells.

In order to remove the effect of seasonally varying magnitudes of the energy balance components, the percentage errors listed in Tables 2–4 are calculated as the root mean square error (RMSE) divided by the observations.

HIRHAM5 uses an elevation model over Iceland which has been interpolated onto the 5.5 km model grid. Since errors in the elevation of the glacier surface can introduce significant biases in temperature and pressure which are not caused by physical model errors (Box and Rinke, 2003), any elevation bias in the model has to be taken into account before validating the results. The elevation bias was calculated as the difference between the model elevation and GPS observations at each site (Table 1).

The temperature was corrected for the elevation bias in order to compare the model results to the AWS measurements at AWS locations. This was done using a constant lapse rate of $6.5\,\mathrm{K\,km^{-1}}$, which resulted in temperature corrections on the order of 0.1–0.3 K. Pressure is corrected using Eq. (5) decreasing the bias down to 0.1 to 0.5 hPa. Thus, although the HIRHAM5 elevation is consistently overestimated, the resulting differences are not large enough to introduce significant biases in temperature and surface pressure.

4 Results and discussion

4.1 Meteorological variables

As the sensible and latent heat fluxes are computed using the surface pressure p_{sl}, air temperature at 2 m, $T_{2\,\mathrm{m}}$, relative humidity $r_{2\,\mathrm{m}}$, and wind speed u, these model variables were evaluated at all five stations at the measurement height. How well these variables are simulated should indicate the model's ability to simulate the turbulent fluxes.

The comparison of modelled and observed mean daily values during the summer months from the period 2001–2014 is shown in Fig. 2 and Table 2. The surface pressure, p_{sl}, which was not observed at the stations but estimated using Eq. (5), is generally forecast with only a small error. At each station there is a high positive correlation ($r > 0.9$) between modelled and estimated pressure (Eq. 5), for the entire time series and for each individual year.

The model also captures the 2 m temperatures, $T_{2\,\mathrm{m}}$, satisfactorily. The largest deviation from the observations is found at the $\mathrm{B_{AB}}$ station, which underestimates the temperature by 0.8 K on average. The temperature is also underestimated at the four other stations, but by at most 0.6 K. The model simulates the variation in temperature well; for example, it captures the temperature dampening over a melting glacier surface. This is expressed in the high correlation values for all five stations ($r \sim 0.9$).

The measured relative humidity, $r_{2\,\mathrm{m}}$, at all five stations is generally high, with only 1–3 % of the data points at each station falling below 70 %, and the minimum daily value between 42 and 58 %. The model simulates a lower mean humidity than the measured at all five stations, with 8–20 % of the points at each stations having values lower than 70 % and minimum daily values between 18 and 30 %. Since the exchange coefficient for moisture is a function of the atmospheric temperature profile, the underestimation of the relative humidity could be due to a too low temperature gradient between the atmosphere and the surface. This is consistent with the underestimation found in the 2 m temperature. The correlation of between 0.68 and 0.7 indicates that the model simulates the humidity fluctuations satisfactorily.

The lowest wind speed level in HIRHAM5 is at 10 m and the AWS wind speeds are measured at between 2 and 4 m, depending on the year, the HIRHAM5 wind speed is extrapolated to the measurement height using a logarithmic profile with a roughness length of 1 mm. At all five locations, HIRHAM5 simulates winds that are too weak on average. This could be due to the uncertainty arising from the interpolation of the model winds from second-lowest level (30 m) to the lowest level (10 m) under stable conditions, as the wind speed can change significantly over the 20 m interval.

4.2 Longwave radiation

As shown above, HIRHAM5 underestimates the temperature at all five stations, with the largest underestimation at the $\mathrm{B_{AB}}$ station. As a result, a similar underestimation of incoming longwave radiation is obtained at all five stations, with the largest difference occurring at the $\mathrm{B_{AB}}$ station 3. The average percentage difference is approximately 8 % for all five locations (see Table 3), and falls well within the 10 % uncertainty of the AWS observations. However, Fig. 3a also shows that 25–30 % of the simulated days have errors larger than 10 %.

The incoming LW radiation is mainly emitted from clouds and atmospheric greenhouse gases, and therefore a source of the underestimation could be that the model underrates cloud formation and/or simulates clouds that are too optically thin in the LW region of the spectrum. An underestimation of the temperature in the atmosphere could also be causing the underestimation.

Figure 3b shows the comparison of the modelled and measured outgoing LW radiation. There is a small overestimation at the $\mathrm{T_{AC}}$ station, and a small underestimation of the other four stations, but in general the model reproduces the daily values well ($r \sim 0.76$). The average percentage deviation between the modelled and measured values is only around 3 %, combined with between 0.5 and 2 % of the HIRHAM5 data points having deviations larger than 10 %.

Due to an underestimation of the incoming LW radiation, and only small negative or positive biases in the outgoing

Table 2. Comparison of the surface pressure p_{sl}, air temperature at 2 m, $T_{2\,m}$, relative humidity $r_{2\,m}$, and wind speed u, from HIRHAM5 simulations and AWS measurements during the summer months (April–October) for the period 2001–2014. The HIRHAM5 bias (HIRHAM5-AWS), the root-mean-square error (RMSE), the percentage error, and the correlation (r) are shown.

Parameter	Station	AWS value	HIRHAM5 bias	RMSE	% error	r
p_{sl} (hPa)	B_{AB}	911.9	−0.2	2.8	0.3	0.96
	T_{AB}	884.2	−0.4	3.0	0.3	0.95
	B_{ELA}	872.1	−0.6	2.9	0.3	0.95
	B_{AC}	837.0	0.1	2.2	0.3	0.97
	T_{AC}	845.1	−0.9	2.7	0.3	0.96
$T_{2\,m}$ (K)	B_{AB}	274.1	−0.8	1.5	0.6	0.94
	T_{AB}	274.0	−0.6	1.3	0.5	0.89
	B_{ELA}	272.9	−0.1	1.1	0.4	0.91
	B_{AC}	271.6	−0.1	1.4	0.5	0.90
	T_{AC}	272.1	0.0	1.2	0.5	0.91
$r_{2\,m}$	B_{AB}	87.9	−6.2	12.2	13.9	0.68
	T_{AB}	89.6	−6.1	11.5	12.9	0.76
	B_{ELA}	91.8	−3.8	9.8	10.7	0.73
	B_{AC}	93.9	−3.5	9.6	10.2	0.68
	T_{AC}	90.0	−2.6	9.7	10.7	0.72
u (m s^{-1})	B_{AB}	5.1	−1.2	2.0	39.0	0.80
	T_{AB}	5.3	−0.3	1.8	33.0	0.87
	B_{ELA}	4.4	−0.1	1.8	41.1	0.82
	B_{AC}	5.9	−0.7	1.8	30.8	0.86
	T_{AC}	5.2	−0.1	2.0	38.9	0.82

LW, the net LW (incoming–outgoing) radiation has a mean negative bias at all AWS locations ($-7.9\,W\,m^{-2}$).

4.3 Shortwave radiation and albedo

Figure 4 and Table 3 show the comparisons of the modelled and measured components of the shortwave (SW) radiation as well as the surface albedo. On average, the incoming SW radiation is underestimated at all five stations. This underestimation is also present in the means at all five stations for most years, except in 2002, 2004, 2005, and 2014 at the B_{AB} station. This suggests that there are errors in either the modelling of the clouds, e.g. due to an overestimation of the cloud fraction, the amount of cloud formation, or the optical thickness of the clouds in the shortwave region, and/or because of errors in the clear-sky fluxes.

The albedo comparison is shown in Fig. 4b. The modelled albedo at the two AB stations has the largest deviation from the observations; this is partly due to the modelled snow cover, which either does not completely disappear or disappears later in the year than the AWS data show. At the B_{AB} station, the ice layer is generally exposed in the model (except in 2001 and 2011–2013), although the snow cover always persists longer than in reality. One exception occurs in 2001, where the modelled albedo never drops down to the ice value, whereas observations show albedo values as low as 0.03. This one year therefore highly contributes to the average overestimation of the albedo. This very low albedo value could be due to a layer of dust or tephra beneath the station, so it may not represent the ice albedo. However, very low ice albedo values down to 0.05 are not uncommon in the ablation zone of Vatnajökull (e.g. Gascoin et al., 2017). Comparisons with the mass balance measurements (discussed in Sect. 4.6.1) show that the winter balance is overestimated during approximately half of the measured years, which contributes to delay the albedo drop in the model.

At the T_{AB} station, a too-thick modelled snow cover in winter is also the cause of some of the discrepancy. Comparisons with mass balance measurements (Sect. 4.6.1) show that the winter balance is always overestimated at this station. An overestimation of the snow thickness at the beginning of summer, combined with an underestimation in the radiation and turbulent fluxes, leads to persistent snow cover at the end of summer. As a result, the ice surface is never exposed in the model during any of the modelled years, and the albedo never drops much below 0.4 (the minimum snow albedo), even though the AWS data shows that the ice surface was exposed during all but two years, i.e. 2008 and 2010. During these two years, the simulated albedo fits well with observations.

Another issue which affects both stations is that the MODIS albedo at these points is not as low as the measured albedo. The MODIS ice albedo at these stations is 0.10 (B_{AB}) and 0.16 (T_{AB}), whereas the observations show the albedo

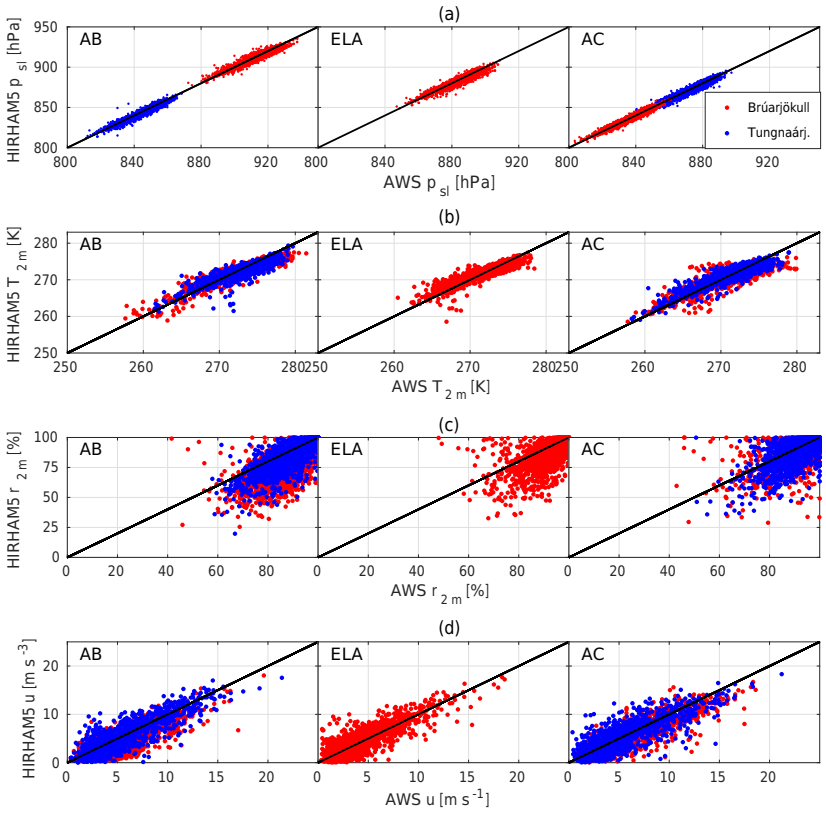

Figure 2. Scatter plots of the measured **(a)** surface pressure, **(b)**, air temperature at 2 m, **(c)** relative humidity at 2 m, and **(d)** wind speed at 2 m, by stations on Bruarjökull (red) and Tungnaárjökull (blue) versus the same components simulated by HIRHAM5 at the same locations.

can drop as low as 0.01 at both stations. The albedo drops below the MODIS value every year at the B_{AB}, and during 2001–2005 and 2011 at the T_{AB} stations. This is presumably due to the heterogeneity of the albedo in the ablation zone, which means that a low in situ albedo value at a point cannot be captured at the current HIRHAM5 resolution.

At the ELA station, the mean albedo value is underestimated (Table 3). Close to the equilibrium line, the albedo is highly variable both temporally and spatially; for example, there is a large difference in albedo depending on whether the previous year's summer surface was exposed or not. In general, the model overestimates the albedo during years where the summer surface was exposed, and underestimates the albedo during years where it was not. In addition, the winter mass balance at this station is always underestimated (Sect. 4.6.1), meaning that the thickness of snow layer in spring is underestimated and the effect of the underlying ice layer will therefore be overestimated, leading to the underestimation in albedo.

The smallest difference between modelled and observed albedo is found at the two AC stations. The B_{AC} station generally provides the best fit with the observations, while the model tends to underestimate the albedo at the T_{AC} station. An exception to this is found in 2010 and 2011, where the albedo was overestimated by the model at both stations due to ash deposition from the Eyjafjallajökull and Grímsvötn eruptions (e.g. Gudmundsson et al., 2012).

A general reason for the model overestimating the albedo is that it does not take the albedo changes due to dust storms or volcanic dust deposition into account. For instance, the

Table 3. Comparison of incoming and outgoing long- and shortwave radiation, albedo (α), turbulent fluxes (H_{s+l}), and total energy (E) from HIRHAM5 simulations and AWS measurements during summer months (April–October) from the period 2001–2014. The HIRHAM5 bias (HIRHAM5-AWS), the root-mean-square error (RMSE), the percentage error, and the correlation (r) are shown.

Parameter	Station	AWS value	HIRHAM5 bias	RMSE	% error	r
LW↓ ($W m^{-2}$)	B_{AB}	290.6	−16.9	26.3	9.1	0.79
	T_{AB}	287.3	−7.0	20.9	7.3	0.80
	B_{ELA}	283.9	−9.0	21.7	7.7	0.79
	B_{AC}	280.9	−8.5	24.4	8.7	0.79
	T_{AC}	274.1	−3.8	20.4	7.4	0.83
LW↑ ($W m^{-2}$)	B_{AB}	309.2	−1.9	7.3	2.4	0.87
	T_{AB}	311.9	−2.5	7.4	2.4	0.78
	B_{ELA}	309.9	−3.3	10.5	3.4	0.70
	B_{AC}	299.9	−1.5	12.9	4.3	0.76
	T_{AC}	301.4	2.6	11.6	3.9	0.68
SW↓ ($W m^{-2}$)	B_{AB}	189.1	−4.0	55.5	29.3	0.81
	T_{AB}	220.8	−35.2	72.2	32.7	0.79
	B_{ELA}	229.3	−36.2	64.6	28.1	0.83
	B_{AC}	236.8	−43.7	69.9	29.5	0.82
	T_{AC}	247.2	−41.9	72.5	29.2	0.79
SW↑ ($W m^{-2}$)	B_{AB}	86.6	18.1	61.0	70.4	0.64
	T_{AB}	112.5	−6.9	54.7	48.7	0.73
	B_{ELA}	146.1	−29.9	59.2	40.5	0.75
	B_{AC}	173.2.9	−31.3	56.4	32.6	0.79
	T_{AC}	173.5	−33.4	65.6	37.8	0.68
α (%)	B_{AB}	34.6	12.7	23.6	68.2	0.75
	T_{AB}	44.5	9.96	21.0	47.2	0.68
	B_{ELA}	60.7	−2.9	18.4	30.2	0.57
	B_{AC}	72.2	0.8	10.5	14.5	0.62
	T_{AC}	70.1	−2.2	16.1	22.9	0.47
H_{s+l} ($W m^{-2}$)	B_{AB}	34.7	−5.0	28.6	116	0.71
	T_{AB}	36.2	−3.8	25.2	69.6	0.79
	B_{ELA}	24.5	−2.0	26.2	107	0.71
	B_{AC}	20.7	−12.3	28.2	136	0.31
	T_{AC}	20.8	−6.3	23.0	110	0.49
E ($W m^{-2}$)	B_{AB}	131.6	−44.4	82.8	62.9	0.67
	T_{AB}	120.1	−36.7	98.0	72.3	0.58
	B_{ELA}	84.4	−13.4	49.6	58.8	0.68
	B_{AC}	64.8	−28.6	50.3	77.5	0.53
	T_{AC}	67.7	−21.2	78.6	89.7	0.43

very low albedo values obtained at the T_{AC} station (Fig. 4b) are due to tephra deposition on the glacier during the 2010 eruption of Eyjafjallajökull (e.g. Gudmundsson et al., 2012; Gascoin et al., 2017). Even though dust events do not cause as large changes in albedo as a volcanic eruption, they can still significantly lower the albedo (e.g. Painter et al., 2007; Wittmann et al., 2017) . As previously mentioned, the albedo in HIRHAM5 often reaches its yearly minimum value later in the summer than the observed. Such discrepancy could be explained by dust events, advancing or delaying the drop in surface albedo. Wittmann et al. (2017) investigated 10 dust events which occurred at the B_{ELA} station in 2012, and found a lowering in the albedo during all events and showed that the dust storms have a significant effect on the resulting energy balance.

The error in the outgoing shortwave radiation is caused by errors in the albedo and the incoming SW. At the B_{AB} station, the incoming radiation is slightly underestimated but the albedo is overestimated; hence, the outgoing SW is overestimated. The values at the four other stations are all underestimated, due to larger underestimations of the incoming SW radiation and lower albedo errors.

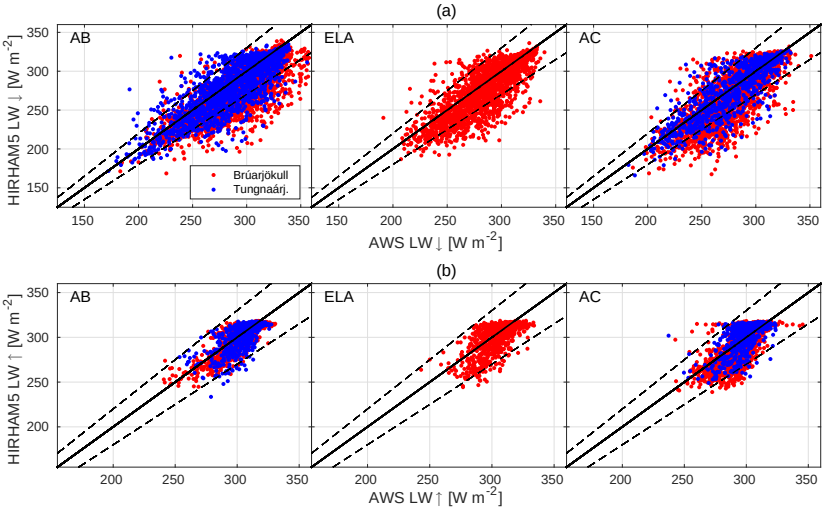

Figure 3. Scatter plots of the measured longwave radiation components, LW↓ and LW↑, by stations on Brúarjökull (red) and Tungnaárjökull (blue) versus the LW radiation components simulated by HIRHAM5 at the same locations. The dashed line corresponds to ±10 %, i.e. the manufacturer-reported uncertainty of the AWS measurements.

As both the incoming and outgoing SW radiation are underestimated at most stations, the net SW shows a negative bias of ~ -6 to $-12\,\mathrm{W\,m^{-2}}$ at the AC and ELA stations, and of -22 and $-28\,\mathrm{W\,m^{-2}}$ at the two AB stations. The resulting average model error at all five stations is $-15.5\,\mathrm{W\,m^{-2}}$.

4.4 Turbulent fluxes

As HIRHAM5 underestimates meteorological variables at all stations, similar underestimation is obtained for the turbulent fluxes (Table 3 and Fig. 5). The two AC stations have the largest differences and also the lowest correlation (0.45 and 0.49) between the AWS estimate and the HIRHAM simulation. The other three stations also have significantly lower values in the HIRHAM5 model than in the AWS model, but with higher correlation coefficients (0.69–0.73).

It is important to bear in mind that this comparison is a model–model comparison, so while the eddy flux model may give a good estimate of the turbulent fluxes, model errors still affect the results, e.g. due to the use of a constant roughness length.

4.5 Total energy balance

After the simulated components of the energy balance were evaluated against AWS observations, the total energy balance was estimated (see Table 3). The energy balance (E) is found using

$$E = \mathrm{LW_{net}} + \mathrm{SW_{net}} + H_{s+l}, \quad (6)$$

where $\mathrm{LW_{net}}$ is the net LW radiation, $\mathrm{SW_{net}}$ is the net SW radiation, and H_{s+l} are the turbulent fluxes. Overall, the melt energy is underestimated, owing to all elements of the energy balance generally being underestimated. This is in large part due to the underestimation of the modelled incoming radiation. We attribute this to an error in the modelling of the clouds, but since both the incoming SW and LW radiation are underestimated, inaccurate cloud representation cannot be the the only source of the error. Errors in the interaction of clouds and radiation, e.g. error in the optical thickness of the clouds, or in the clear-sky fluxes, could partly explain these discrepancies. The underestimation of the incoming LW radiation could also be due to errors in the vertical atmospheric temperature gradient.

Since the simulated outgoing LW radiation generally only has a small negative bias, the deviation in net LW radiation is governed by the incoming radiation. Errors in the simulated albedo mean that both the in- and outgoing SW radiation greatly contribute to the deviation in net SW radiation. These errors can be partly attributed to ash and dust deposition during volcanic eruptions and dust storms, which are not taken into account in HIRHAM5. In addition, errors in the simulated albedo also stem from snow cover that disappears too slowly compared to AWS records in the ablation

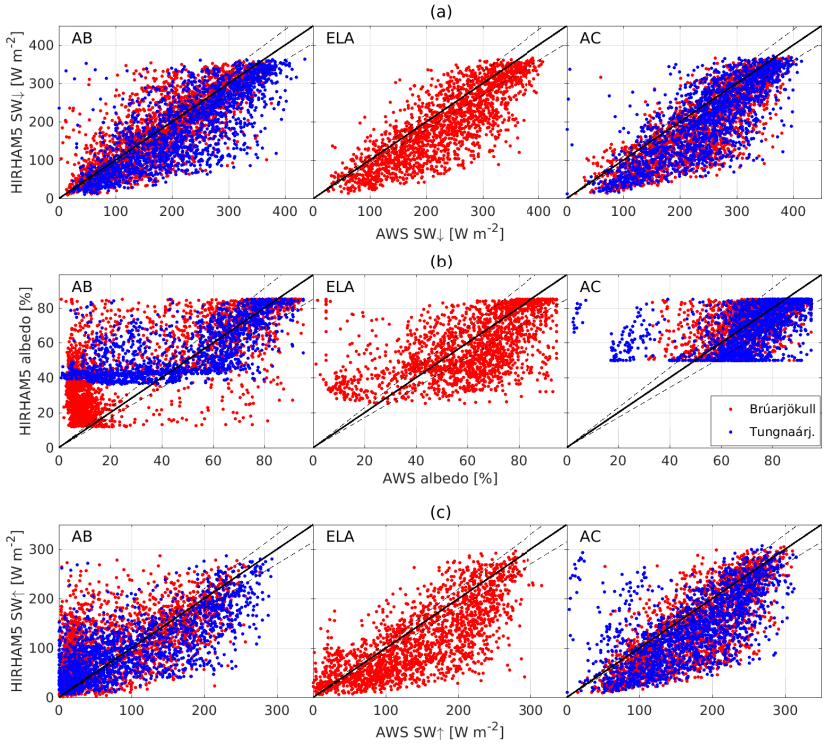

Figure 4. Scatter plots of the measured shortwave radiation components, **(a)** SW↓, **(b)** albedo, and **(c)** SW↑, by stations on Bruarjökull (red) and Tungnaárjökull (blue) versus the shortwave radiation components simulated by HIRHAM5 at the same locations. The dashed line corresponds to the uncertainty of the measured AWS components.

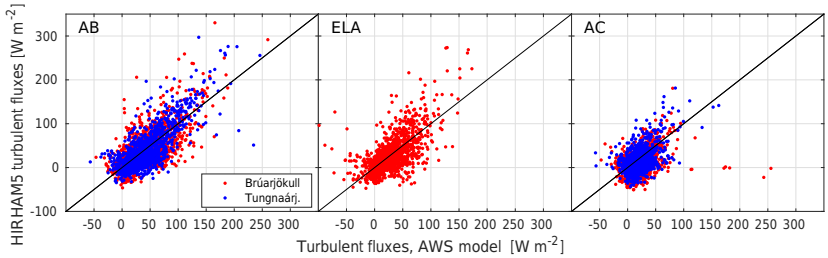

Figure 5. The total turbulent fluxes calculated from AWS stations using the one-level flux model versus the HIRHAM5 simulated values.

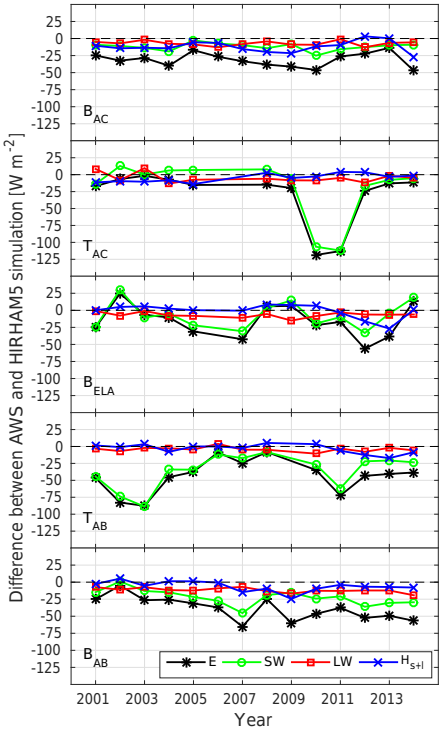

Figure 6. The average summer (April–October) bias of each energy balance component for the measurement period at each AWS site. The large deviation in the SW radiation at the Tunaárjökull sites in 2010–2011 is due to deposition of ash on the glacier during the 2010 Eyjafjallajökull and 2011 Grímsvötn eruptions.

zone. As a result, modelled albedo drops too slowly compared to the measured albedo. The underestimation of the net SW and LW radiation and the turbulent fluxes leads to underestimated melt energy. This contributes to the overestimation of the modelled snow thickness.

In order to estimate how much the different components contribute to the energy difference on a year-to-year basis, the mean difference between modelled and observed energy components during each summer (April–October) is shown for each station (Fig. 6).

At the B_{AC} station, the contribution of the long- and shortwave radiation and turbulent fluxes to the energy difference is consistent for the entire period, with the error of each component being almost equal, varying between -25 and $0\,\mathrm{W\,m^{-2}}$. At the T_{AC} station, the error due to the three components is also of the same order of magnitude, except in 2010 and 2011 where the error in the net SW radiation is much larger than that in the other components. This is due to a large drop in the albedo as a result of the Eyjafjallajökull (2010) and Grímsvötn (2011) eruptions. The mean difference between observations and the simulations of the SW radiation for non-eruption years is $-3\,\mathrm{W\,m^{-2}}$, whereas the radiation difference in 2010 is $-106\,\mathrm{W\,m^{-2}}$. Assuming the larger deviation from the mean in 2010 is only due to the volcanic eruption, the increase in available energy due to the eruption is $103\,\mathrm{W\,m^{-2}}$. If it is further assumed that the surface was always at melting point, the increase in melt due to the 2010 Eyjafjallajökull eruption over the 128-day measuring period would be ~ 3.1 m w.e. at this station.

At the ELA site, the contribution from the modelled turbulent fluxes to the energy balance deviation generally varies between $\pm 10\,\mathrm{W\,m^{-2}}$, except in 2013 where the bias is around $-25\,\mathrm{W\,m^{-2}}$. Modelled longwave radiation is consistently underestimated by $-10\,\mathrm{W\,m^{-2}}$. The deviation in the shortwave radiation is more variable, as expected from the results of the albedo comparison. Depending on whether bare ice was exposed or not, the albedo is generally either over- or underestimated. For example, at B_{ELA}, the ice surface was reached in, for example, 2007 and 2012, resulting in an overestimation of the albedo. In, for example, 2002 and 2009, however, the albedo was high the entire summer as no ice was exposed, resulting in an underestimation of the predicted albedo.

At the T_{AB} station, both the net LW radiation and the turbulent fluxes agree well with observations for the entire period. The net SW radiation, however, is always underestimated, especially in the period 2001–2003 and 2011. These years, the measured albedo at the station goes below 0.1, while the HIRHAM5 albedo stays around 0.4. As previously discussed, this albedo bias, and hence underestimated net SW radiation, occurs because of an overestimation of the snow cover at the station due to an overestimation of the winter accumulation and possibly also the proximity of the equilibrium line. An underestimation of the incoming SW radiation, which we attribute to an error in cloud cover amount of clear-sky fluxes, also contributes to this error.

At the B_{AB} station, the longwave radiation bias is relatively constant with values close to $0\,\mathrm{W\,m^{-2}}$ for much of the measurement period. The absolute deviation due to the turbulent fluxes is less than $10\,\mathrm{W\,m^{-2}}$ for most of the period, although with slightly larger deviations from the period 2007–2010. The SW radiation is always underestimated at this station, mostly due to the previously discussed overestimation of the albedo.

4.6 Surface mass balance

4.6.1 At AWS sites

Scatter plots of measured and HIRHAM5 simulated SMB are shown in Fig. 7 and the average deviations are shown in Table 4.

The winter mass balance comparison allows to evaluate of the winter precipitation in HIRHAM5. The simulated mass balance at the B_{ELA} and B_{AC} are always underestimated, while the T_{AC} stations is underestimated during all years but one (2012). The simulated value at the T_{AB} station is overestimated over the whole period. The modelled mass balance at the B_{AB} station has an almost equal amount of years which are over- and underestimated. Apparently the model either carries too much precipitation when the clouds reach the glacier, resulting in too much precipitation at the ice sheet margin, or more melting occurs at the ablation area stations during the winter months than the model estimates.

The summer SMB results are in good agreement with the results of the energy balance calculations. The summer SMB is generally overestimated, although it is underestimated occasionally at all stations except T_{AB}. The ELA station has the largest amount of underestimated points, which is consistent with the findings from the energy balance calculations. Besides the errors introduced due to the underestimation of the energy balance, possible over- or underestimations of the modelled summer accumulation contribute to these errors as well.

Due to the difference in the summer and winter balance, the net balance at the B_{AC}, T_{AC}, and B_{ELA} stations is generally underestimated in HIRHAM5, while the balance at the two AB stations is generally overestimated. This is due to a general overestimation of the winter balance in the ablation area, due to either an underestimation of the winter melt or an overestimation of precipitation, as discussed above.

4.6.2 At all measurement sites

SMB is also measured at 25–120 non-AWS sites, depending on the year (Fig. 1). In order to estimate how well the model represents the SMB at non-AWS sites, the data from all the sites between 1995 and 2014 were compared with the HIRHAM5 simulation (Fig. 8; Table 4).

The winter balance at all measured points is slightly overestimated by HIRHAM5 on average. However, this is mostly due to a large difference between measured and simulated SMB at the ice-covered, high-elevation, central volcano Öræfajökull (the white dots in Fig. 8). Only one site has been measured on this glacier for a few years only (Guðmundsson, 2000), in a spot that always receives a large amount of precipitation. However, since HIRHAM5 consistently overestimates the accumulation by 100–200 %, this one point has a large effect on the mean error. This is a well-known issue with hydrostatic models like HIRHAM5, as they characteristically overestimate the precipitation on the upslope and peaks in complex terrain. The reason for this is that the precipitation is calculated as a diagnostic variable – i.e. it is not governed by an equation that is a derivative of time, meaning that when the required conditions for precipitation are met in the local atmosphere, the precipitation appears instantaneously on the surface. Thus, the scheme does not allow horizontal advection of snow and rain by atmospheric winds, which is a key process in complex terrain, as it can force the precipitation downslope (e.g. Forbes et al., 2011). Without this effect, precipitation is generally overestimated at high peaks like Öræfajökull. Removing this location from the comparison, the total difference drops to one-third the difference with respect to the AWS sites only (-0.09 m w.e.). The reason the difference is smaller than for the AWS sites only is that more sites close to the edge of the ice cap are included. The winter balance at the measurement points at the outer parts of the icecap generally is overestimated in the model, and therefore these points partly offset the underestimation in the middle of the ice cap.

On average, the summer ablation is underestimated, which is consistent with the findings from the AWS stations that there is an average underestimation of the energy available for melt. The mean error and RMSE is only slightly larger than at the AWS sites.

The mean net balance is overestimated by approximately the same amount as the summer balance, partly due to the low mean deviation in the winter SMB. Due to the large deviation at Öræfajökull in the winter SMB, the Öræfajökull points clearly have the largest bias. If these points are excluded, a RMSE closer to that for the AWS locations is found (1.1 m).

4.7 Reconstructing the SMB of Vatnajökull

Spatial maps of the (uncorrected) average winter, summer, and net SMB from the 1980–1981 glaciological year until 2013–2014 are shown in Fig. 9. The approximate location of the average ELA is marked in the figure. The model captures the position of the ELA fairly well, but at, for example, Brúarjökull, where the average ELA is at 1200 m, the position of the average ELA is at a too high elevation. The average deviation between observation and model over the observation period at each measurement location is also shown in Fig. 9, in order to give an indication of the average error of the model at different parts of the ice cap. The winter balance (Fig. 9e) is generally overestimated at low elevations and underestimated at high elevations, except for at Öræfajökull, where there is a large overestimation of the winter balance, as discussed in the previous section. As can be seen in Fig. 9e, there is generally a low SMB bias at high elevations and a high SMB bias at low elevations during the summer. This is consistent with the comparisons with AWS stations, as we found that the bias in the energy available for melt was smaller at high elevation than at low elevation (see Table 3).

Table 4. Comparison of HIRHAM5 and mass balance measurements, both at AWS sites and for all measuring sites on Vatnajökull.

	Season	AWS value	HIRHAM5 bias	RMSE	% error
AWS locations	Winter	1.37	−0.26	0.71	51.6
	Summer	−2.34	0.48	0.81	−34.6
	Total	−0.98	0.23	1.15	−118
All locations	Winter	1.46	0.04	1.21	82.9
	Summer	−2.28	0.52	0.94	−41.1
	Total	−0.83	0.56	1.56	−186

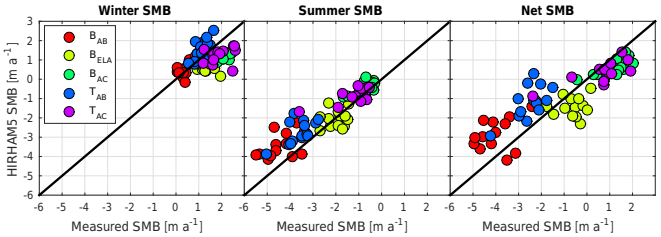

Figure 7. Comparison of the winter, summer, and net mass balance from the period 1995–2014 between the mass balance measurements at the five AWS sites and the HIRHAM5 simulation.

This was partly due to a larger albedo bias for stations in the ablation zone than for stations in the accumulation zone.

In addition to the spatial maps, the winter, summer, and net mass balances of Vatnajökull were calculated for the entire simulation period, and the results were compared with an estimate of the specific balance from 1995 to 2014, created by interpolation of the mass balance measurements (e.g. Pálsson et al., 2015); see Fig. 10. The model prediction of the mean specific summer mass balance generally fits well with the interpolated observations, with an overall difference of only 0.06 m w.e. The largest deviations are obtained in 1995, where ablation is overestimated in the simulation, and in 1997, 2005, and 2010–2012, where ablation is underestimated, most likely due to ash depositions on the glacier following the 1996 Gjálp eruption, the 2004 and 2011 Grímsvötn eruptions or the 2010 Eyjafjallajökull eruption, which are not taken into account in the model.

Excluding the years where the albedo was affected by volcanic eruptions, the average difference becomes smaller but the model also predicts slightly too much ablation, as the difference becomes −0.02 m w.e.

There is a shift in the summer and annual mass balance calculated by the model and the in situ MB measurements around 1996, with a generally more negative mass balance after 1996 than before. This is consistent with the increase of the annual mean temperature of Iceland in the mid-1990s, which resulted in a mean annual temperature ~ 1 K higher in the decade after than the decade prior to 1995. This is likely linked with atmospheric and ocean circulation changes around Iceland, as there was a rapid increase in ocean temperatures off the southern coast in 1996 (Björnsson et al., 2013).

The specific winter mass balance is overestimated in HIRHAM5 for the entire measurement period with an average of 0.54 m w.e. Due to this difference, and only the small negative mean difference in summer mass balance, the annual mass balance of Vatnajökull is overestimated every year with an average difference of 0.50 m w.e.

However, this is mostly due to the large overestimation of the winter accumulation on Öræfajökull; comparison with the mass balance measurements showed that the model overestimated the winter accumulation by 100–200 % compared with the observations. In an attempt to estimate how much this error affects the results, a simple correction was added to the Öræfajökull points by reducing the simulated winter SMB by 50 %. The correction was added to four model grid points around Öræfajökull, due to the high (> 10 m yr^{-1}) annual specific mass balance in these points (see Fig. 9a). The resulting modelled winter and annual specific balance are shown in Fig. 11. The winter balance is still overestimated, but the difference between modelled and interpolated values has been reduced to only 0.1 m w.e. In addition, the average difference between the HIRHAM5 and interpolated annual SMB drops to only 0.08 m w.e.

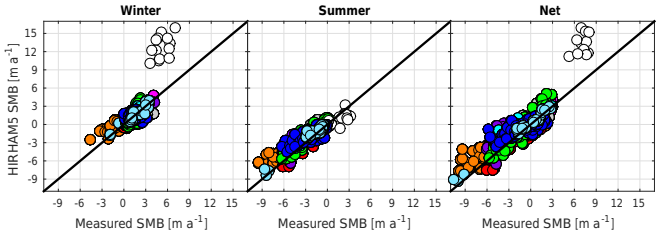

Figure 8. Comparison of SMB measurements from Vatnajökull ice cap from 1995 to 2014 and HIRHAM5 simulated values. Different colours represent different outlet glaciers; see Fig. 1b. The white dots are from a point on Öræfajökull.

4.8 Comparison with constant ice albedo simulation

In order to quantify the changes in the model performance resulting from the new albedo scheme used in this study, which utilizes an albedo map based on MODIS data (Gascoin et al., 2017), the results are compared to those of a previous run using a constant ice albedo of 0.3. The average difference in albedo and mass balance over the period 2001–2014 in each grid point are shown in Fig. 12, as well as the position of the AWS stations.

There is little to no difference between the two runs in the accumulation zone, due to the year-round snow cover. In the ablation zone, however, using the MODIS ice albedo map has a large effect on the simulated albedo. The largest differences are found on the southern outlet glacier Skeiðarárjökull, which is unfortunately a glacier where no mass balance or AWS measurements have been conducted. The B_{AB} and B_{ELA} stations are located in areas that are affected by the ice albedo, either because ice is exposed (B_{AB}) or because the underlying surface contributes to the albedo (B_{ELA}). The T_{AB} station is located in the ablation area, but the ice surface is never exposed in the model due to an overestimation of the winter accumulation. The albedo estimate at this station was therefore not improved by using the MODIS albedo.

When the model is run with the constant ice albedo of 0.3, the amount of ablation will be lower and thus the specific summer balance will be higher. Compared to the simulation using the MODIS map (Fig. 11), the constant ice albedo simulation results in an increase in the specific summer SMB by an average of 0.37 m w.e., or 18 %, per year for the period 1995–2014. The increase in the summer SMB ranges from 14 cm (in 2014) to 85 cm (in 2001) and the percentage increase varies between 8 % (in 2011) and 39 % (in 1995). As the winter balance is not dependant on the ice albedo, there are no changes in the specific winter SMB between the two simulations.

5 Conclusions

The comparison of a HIRHAM5 simulation with data from five AWSs on Vatnajökull ice cap allows us to evaluate the model performance. By comparing observations from April to October with model output, it was found that the model simulates the surface energy balance components and surface mass balance well, albeit with general underestimations of the energy balance components. Even though the energy balance was generally underestimated, the model simulated the near-surface temperature well. The reason for this is that the comparisons only use observations from the summer months, where the glacier surface is generally at the melting point, and thus the energy is used for melting and not for raising the temperature of the surface.

The modelled incoming radiation is underestimated on average in both the shortwave and longwave spectrum, which we suggest is due to biases in the modelling of the cloud cover combined with errors in the optical thickness in the short- or longwave spectrum, or errors in the clear-sky fluxes.

Whereas the modelled outgoing LW radiation component is within the uncertainty of the LW observations at the five stations, which is consistent with the ability of the model to capture surface temperatures, there was a larger difference between the modelled and measured outgoing SW radiation. This is partly due to the underestimation of the incoming SW radiation and partly due to inaccuracies in the simulated albedo. The albedo was simulated using an iterative, temperature-based albedo scheme (Nielsen-Englyst, 2015) with a bare ice albedo determined from MODIS data (Gascoin et al., 2017). The simulated albedo was generally overestimated during the summer and did not reach the lowest yearly value as early in the year as the measured albedo, particularly in the ablation zone. This was attributed to an overestimation of the snow cover in the ablation zone, an overestimation in the MODIS ice albedo compared with AWS observations, and the fact that the model does not account for the effect of volcanic dust deposition during eruptions and dust events on the albedo. A possible means of capturing dust storms or eruptions into the model is to implement a stochas-

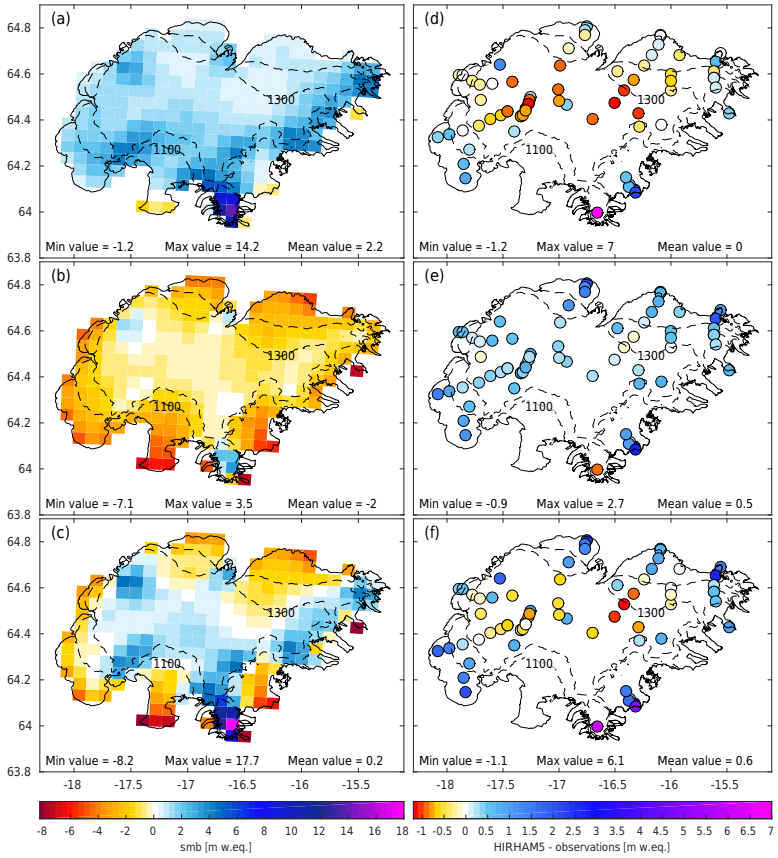

Figure 9. The average **(a)** winter, **(b)** summer, and **(c)** net SMB simulated by HIRHAM5 from the 1980–1981 glaciological year to 2013–2014. The contour lines marks the approximate location of the ELA, which generally lies between approximately 1100 and 1300 m elevation. Panels **(d)**–**(f)** show the average deviation between model and observations over the observation period (1992–2014) for each measurement location for the **(d)** winter, **(e)** summer, and **(f)** whole glaciological year.

tic ashes or dust generator, which distributes dust onto the glacier. Including simulations of dust depositions and concentrations from a dust mobilization model could also be an option, as Wittmann et al. (2017), for example, used the model FLEXDUST to simulate dust events on Vatnajökull in 2012, and found that the modelled dust events correspond well with albedo drops at two AWSs on Brúarjökull.

Due to the general underestimation of the energy balance components, the ablation during the summer months is underestimated on average. Comparison with mass balance measurements from the AWS sites and from sites scattered across Vatnajökull shows an overall overestimation of the summer balance by about 0.5 m w.e. The overestimation is largest in the ablation zone. The winter balance is on average underestimated at the survey sites, albeit with the highest measuring site (on Öræfajökull) having a large overestimation of the winter balance.

The mean specific summer, winter, and net mass balances are reconstructed for all of Vatnajökull from the period 1981–2014, and estimates of the specific SMB based on in situ SMB measurements are compared to the reconstructed specific SMB for the period 1995–2014. The summer balance is

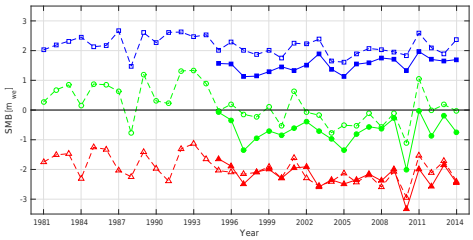

Figure 10. Average summer (red lines), winter (blue lines), and net (green lines) specific surface mass balance for the whole of Vatnajökull. The solid lines are the mass balance of Vatnajökull based on mass balance measurements and manual interpolation, while the dashed lines are the mass balance as simulated by HIRHAM5.

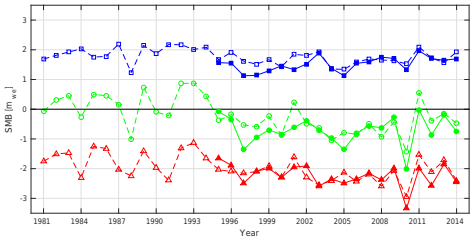

Figure 11. Same as Fig. 10, but corrected at the Öræfajökull area by reducing the HIRHAM5 simulated winter balance with 50 %.

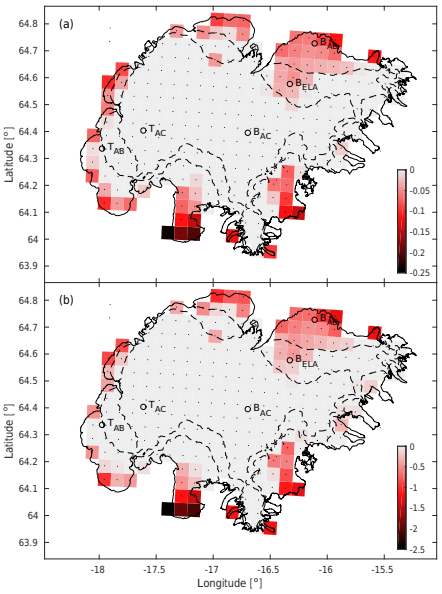

Figure 12. Difference in **(a)** mean albedo and **(b)** mean SMB in m w.e. for the period 2001–2014 between two runs with HIRHAM5, one using a MODIS bare ice albedo map and the other with a constant ice albedo. The locations of the AWS stations used in this study are shown with black circles.

overestimated by 0.06 m w.e. on average – i.e. there is generally too little ablation in the summer, with too much ablation in 1995, and too little ablation in years with, or following, volcanic eruptions. The winter balance is overestimated by 0.5 m w.e., mostly due to a large overestimation at the high elevation glacier Öræfajökull. This overestimation of accumulation at high elevation is characteristic for hydrostatic RCMs (Forbes et al., 2011). If the overestimation at these points is corrected, we estimate that the simulated winter balance would fit well with the observations, as the overestimation of the balance would drop to around 0.1 m w.e.

That the model catches the changes in the specific mass balance well over the mass balance measurement period, and also captures the shift in mass balance in the mid-1990s, gives us confidence that the model estimates the specific mass balance of Vatnajökull well over the entire simulated period from 1980 to 2014. HIRHAM5 is therefore a useful tool to expand the time series of the specific SMB beyond the measurement years. However, as ERA-Interim reanalysis data only go back to 1979, the model would need to be forced at the lateral, for example, by output of a general circulation model. However, using other reanalysis data probably leads to different errors; this needs further investigation. The model could also be a useful tool to estimate the future evolution of the SMB of the ice cap, but this would also require a different forcing at the lateral boundary like general circulation model output. This would most likely introduce larger biases than the ones found using ERA-Interim, and the magnitude of these biases would need to be estimated and corrected before using the model for future projections.

Data availability. HIRHAM5 output is freely accessible from http://prudence.dmi.dk/data/temp/RUM/HIRHAM/GL2/, as are MODIS data from https://modis.gsfc.nasa.gov/data/. Measurements from automatic weather stations and from in situ mass balance surveys are partially owned by the National Power Company of Iceland and are therefore not publicly available at this time.

Competing interests. The authors declare that they have no conflict of interest.

Acknowledgements. This work is supported by project SAMAR, funded by the Icelandic Research Fund (RANNIS, Grant no. 140920-051), as well as the National Power Company of Iceland (Landsvirkjun). Measurements from automatic weather stations and in situ mass balance surveys are from joint projects of the National Power Company and the Glaciology group at the Institute of Earth Sciences, University of Iceland.

Edited by: Xavier Fettweis
Reviewed by: two anonymous referees

References

Agosta, C., Fettweis, X., and Datta, R.: Evaluation of the CMIP5 models in the aim of regional modelling of the Antarctic surface mass balance, The Cryosphere, 9, 2311–2321, https://doi.org/10.5194/tc-9-2311-2015, 2015.

Ágústsson, H., Hannesdóttir, H., Thorsteinsson, T., Pálsson, F., and Oddsson, B.: Mass balance of Mýrdalsjökull ice cap accumulation area and comparison of observed winter balance with simulated precipitation, JÖKULL, 63, 91–104, 2013.

Andreas, E. L.: A theory for the scalar roughness and the scalar transfer coefficients over snow and sea ice, Bound.-Lay. Meteorol., 38, 159–184, https://doi.org/10.1007/BF00121562, 1987.

Björnsson, H.: Bægisárjökull, North Iceland. result of glaciological investigations 1967-1968. Part II. The energy balance, Jökull, 22, 44–61, 1972.

Björnsson, H. and Pálsson, F.: Icelandic glaciers, Jökull, 58, 365–386, 2008.

Björnsson, H., Pálsson, F., Guðmundsson, M. T., and Haraldsson, H. H.: Mass balance of western and northern Vatnajökull, Iceland, 1991–1995, Jökull, 45, 35–58, 1998.

Björnsson, H., Pálsson, F., Guðmundsson, S., Magnússon, E., Aðalgeirsdõttir, G., Jõhannesson, T., Berthier, E., Sigurdsson, O., and Thorsteinsson, T.: Contribution of Icelandic ice caps to sea level rise: Trends and variability since the Little Ice Age, Geophys. Res. Lett., 40, 1546–1550, https://doi.org/10.1002/grl.50278, 2013.

Box, J. and Rinke, A.: Evaluation of Greenland Ice Sheet Surface Climate in the HIRHAM Regional Climate Model Using Automatic Weather Station Data., J. Climate, 16, 1302–1319, 2003.

Brock, B. W., Willis, I. C., Sharp, M. J., and Arnold, N. S.: Modelling seasonal and spatial variations in the surface energy balance of Haut Glacier d'Arolla, Switzerland, Ann. Glaciol., 31, 53–62, 2000.

Brock, B. W., Willis, I. C., and Sharp, M.: Measurement and parametrisation of surface roughness variations at Haut Glacier d'Arolla, J. Glaciol., 52, 281–297, 2006.

Christensen, O. B., Drews, M., Christensen, J. H., Dethloff, K., Ketelsen, K., Hebestadt, I., and Rinke, A.: The HIRHAM Regional Climate model Version 5., Tech. rep., Danish Meteorological institute, 2006.

Conway, H., Gades, A., and Raymond, C. F.: Albedo of dirty snow during conditions of melt, Water Resour. Res., 32, 1713–1718, https://doi.org/10.1029/96WR00712, 1996.

Dee, D. P., Uppala, S. M., Simmons, A. J., Berrisford, P., Poli, P., Kobayashi, S., Andrae, U., Balmaseda, M. A., Balsamo, G., Bauer, P., Bechtold, P., Beljaars, A. C. M., Bidlot, J., Bormann, N., Delsol, C., Dragani, R., Fuentes, M., Geer, A. J., Isaksen, L., Haimberger, L., Healy, S. B., Hersbach, H., Matricardi, M., Mcnally, A. P., Peubey, C., Rosnay, P. D., Tavolato, C., and Vitart, F.: The ERA-Interim reanalysis: configuration and performance of the data assimilation system, Q. J. Roy. Meteor. Soc., 137, 553–597, 2011.

de Elía, R., Laprise, R., and Denis, B.: Forecasting Skill Limits of Nested, Limited-Area Models: A Perfect-Model Approach, Mon. Weather Rev., 130, 2006–2023, https://doi.org/10.1175/1520-0493(2002)130<2006:FSLONL>2.0.CO;2, 2002.

Eerola, K.: About the performance of HIRLAM version 7.0, HIRLAM Newsletter, 51, 93–102, 2006.

Fettweis, X., Box, J. E., Agosta, C., Amory, C., Kittel, C., Lang, C., van As, D., Machguth, H., and Gallée, H.: Reconstructions of the 1900–2015 Greenland ice sheet surface mass balance using the regional climate MAR model, The Cryosphere, 11, 1015–1033, https://doi.org/10.5194/tc-11-1015-2017, 2017.

Forbes, R., Tompkins, A. M., and Untch, A.: A new prognostic bulk microphysics scheme for the IFS, ECMWF Technical Memoranda, available at: https://www.ecmwf.int/sites/default/files/elibrary/2011/9441-new-prognostic-bulk-microphysics-scheme-ifs.pdf, 2011.

Gallée, H. and Schayes, G.: Development of a Three-Dimensional Meso-γ Primitive Equation Model: Katabatic Winds Simulation in the Area of Terra Nova Bay, Antarctica, Mon. Weather Rev., 122, 671, https://doi.org/10.1175/1520-0493(1994)122<0671:DOATDM>2.0.CO;2, 1994.

Gascoin, S., Guðmundsson, S., Aðalgeirsdóttir, G., Pálsson, F., Schmidt, L. S., and Berthier, E.: Evaluation of MODIS albedo product over ice caps in Iceland and impact of volcanic eruptions on albedo, Remote Sens., 9, 399, https://doi.org/10.3390/rs9050399, 2017.

Giorgi, F. and Bi, X.: A study of internal variability of a regional climate model, J. Geophys. Res., 105, 29503–29522, https://doi.org/10.1029/2000JD900269, 2000.

Grainger, M. E. and Lister, H.: Wind speed, stability and eddy viscosity over melting ice surfaces, J. Glaciol., 6, 101–127, 1966.

Greuell, W., Knap, W. H., and Smeets, P. C.: Elevational changes in meteorological variables along a midlatitude glacier during summer, J. Geophys. Res., 102, 25941, https://doi.org/10.1029/97JD02083, 1997.

Guðmundsson, M. T.: Mass balance and precipitation on the summit plateau of Öræfajökull, SE-Iceland, Jökull, 48, 49–54, 2000.

Guðmundsson, S., Björnsson, H., Pálsson, F., and Haraldsson, H. H.: Energy balance of Brúarjökull and circumstances leading to the August 2004 floods in the river Jökla, N-Vatnajökull, Jökull, 55, 121–138, 2006.

Guðmundsson, S., Björnsson, H., Pálsson, F., and Haraldsson, H. H.: Comparison of energy balance and degree-day models of summer ablation on the Langjökull ice cap, SW-Iceland, Jökull, 59, 1–18, 2009.

Gudmundsson, M. T., Thordarson, T., Höskuldsson, Á., Larsen, G., Björnsson, H., Prata, F. J., Oddsson, B., Magnússon, E., Högnadóttir, T., Petersen, G. N., Hayward, C. L., Stevenson, J. a., and Jónsdóttir, I.: Ash generation and distribution from the April-May 2010 eruption of Eyjafjallajökull, Iceland, Scientific Reports, 2, 1–12, https://doi.org/10.1038/srep00572, 2012.

Kipp and Zonen: CNR1 Net Radiometer Instruction Manual, available at: http://www.kippzonen.com/Download/87/CNR-1-Net-Radiometer-Brochure (last access: 3 July 2017), 2002.

Knap, W. H., Brock, B. W., Oerlemans, J., and Willis, I. C.: Comparison of Landsat TM-derived and ground-based albedos of Haut Glacier d'Arolla, Switzerland, Int. J. Remote Sens., 20, 3293–3310, https://doi.org/10.1080/014311699211345, 1999.

Langen, P. L., Mottram, R. H., Christensen, J. H., Boberg, F., Rodehacke, C. B., Stendel, M., van As, D., Ahlstrøm, A. P., Mortensen, J., Rysgaard, S., Petersen, D., Svendsen, K. H., Aðalgeirsdóttir, G., and Cappelen, J.: Quantifying energy and mass fluxes controlling godthåbsfjord freshwater input in a 5-km simulation (1991–2012), J. Climate, 28, 3694–3713, 2015.

Langen, P. L., Fausto, R. S., Vandecrux, B., Mottram, R. H., and Box, J. E.: Liquid Water Flow and Retention on the Greenland Ice Sheet in the Regional Climate Model HIRHAM5: Local and Large-Scale Impacts, Front. Earth Sci., 4, 10, https://doi.org/10.3389/feart.2016.00110, 2017.

Larsen, G., Guðmundsson, M. T., and Björnsson, H.: Tephrastratigraphy of Ablation Areas of Vatnajökull Ice Cap, Iceland, Glaciers, Ice Sheets and Volcanoes: A Tribute to Mark F. Meier, p. 75, 1996.

Lenaerts, J. T. M. and Van Den Broeke, M. R.: Modeling drifting snow in Antarctica with a regional climate model: 2. Results, J. Geophys. Res. Atmos., 117, D5, https://doi.org/10.1029/2010JD015419, 2012.

Lucas-Picher, P., Wulff-Nielsen, M., Christensen, J. H., Aðalgeirsdóttir, G., Mottram, R. H., and Simonsen, S. B.: Very high resolution regional climate model simulations over Greenland: Identifying added value, J. Geophys. Res., 117, 2108, https://doi.org/10.1029/2011JD016267, 2012.

MATLAB: version 8.5.0 (R2015a), The MathWorks Inc., 2015.

Meijgaard, E. V., Ulft, L. H. V., Bosveld, F. C., Lenderink, G., and Siebesma, A. P.: The KNMI regional atmospheric climate model RACMO version 2.1, Technical report; TR – 302, p. 43, 2008.

Monin, A. S. and Obukhov, A. M.: Basic laws of turbulent mixing in the surface layer of the atmosphere, Contrib. Geophys. Inst. Acad. Sci. USSR, 24, 163–187, 1954.

Mottram, R., Boberg, F., and Langen, P.: HIRHAM5 GL2 simulation dataset, available at: http://prudence.dmi.dk/data/temp/RUM/HIRHAM/GL2, 2016.

Nawri, N.: Evaluation of HARMONIE reanalyses of surface air temperature and wind speed over Iceland, Tech. rep., Veðurstofa Íslands, available at: http://www.vedur.is/media/vedurstofan/utgafa/skyrslur/2014/VI_2014_005.pdf (last access: 3 July 2017), 2014.

Nielsen-Englyst, P.: Impact of albedo parameterizations on surface mass balance and melt extent on the Greenland Ice Sheet, Master's thesis, 2015.

Noël, B., van de Berg, W. J., van Meijgaard, E., Kuipers Munneke, P., van de Wal, R. S. W., and van den Broeke, M. R.: Evaluation of the updated regional climate model RACMO2.3: summer snowfall impact on the Greenland Ice Sheet, The Cryosphere, 9, 1831–1844, https://doi.org/10.5194/tc-9-1831-2015, 2015.

Oerlemans, J. and Knap, W. H.: A 1-year record of global radiation and albedo in the ablation zone of Marteratschgletscher, Switzerland, J. Glaciol., 44, 231–238, 1998.

Oerlemans, J., Björnsson, H., Kuhn, M., Obleitner, F., Palsson, F., Smeets, C., Vugts, H. F., and Wolde, J. D.: Glacio-Meteorological Investigations On Vatnajökull, Iceland, Summer 1996: An Overview, Bound.-Lay. Meteorol., 92, 3–24, https://doi.org/10.1023/A:1001856114941, 1999.

Painter, T. H., Barrett, A. P., Landry, C. C., Neff, J. C., Cassidy, M. P., Lawrence, C. R., McBride, K. E., and Farmer, G. L.: Impact of disturbed desert soils on duration of mountain snow cover, Geophys. Res. Lett., 34, 12, https://doi.org/10.1029/2007GL030284, 2007.

Pálsson, F., Gunnarsson, A., Jónsson, Þ., Steinþórsson, S., and Pálsson, H. S.: Vatnajökull: Mass balance, meltwater drainage and surface velocity of the glacial year 2014_15, Tech. rep., Institute of Earth Sciences, University of Iceland and National Power Company, RH-06-2015, 2015.

Rae, J. G. L., Aðalgeirsdóttir, G., Edwards, T. L., Fettweis, X., Gregory, J. M., Hewitt, H. T., Lowe, J. A., Lucas-Picher, P., Mottram, R. H., Payne, A. J., Ridley, J. K., Shannon, S. R., van de Berg, W. J., van de Wal, R. S. W., and van den Broeke, M. R.: Greenland ice sheet surface mass balance: evaluating simulations and making projections with regional climate models, The Cryosphere, 6, 1275–1294, https://doi.org/10.5194/tc-6-1275-2012, 2012.

Reijmer, C. H., Knap, W. H., and Oerlemans, J.: The Surface Albedo Of The Vatnajökull Ice Cap, Iceland: A Comparison Between Satellite-Derived And Ground-Based Measurements, Bound.-Lay. Meteorol., 92, 123–143, https://doi.org/10.1023/A:1001816014650, 1999.

Roeckner, E., Bäuml, G., Bonaventura, L., Brokopf, R., Esch, M., Giorgetta, M., Hagemann, S., Kirchner, I., Kornblueh, L., Manzini, E., Rhodin, A., Schlese, U., Schulzweida, U., and Tompkins, A.: The atmospheric general circulation model ECHAM 5 PART I: Model description, Tech. Rep. 349, Report/MPI für Meteorologie, 2003.

Schaaf, Z. W.: MCD43A3 MODIS/Terra+Aqua BRDF/Albedo Daily L3 Global – 500m V006. NASA EOSDIS Land Processes DAAC., https://doi.org/10.5067/modis/mcd43a3.006, 2015.

Stendel, M., Christensen, J. H., and Petersen, D.: High-Arctic Ecosystem Dynamics in a Changing Climate, vol. 40 of Advances in Ecological Research, Elsevier, https://doi.org/10.1016/S0065-2504(07)00002-5, 2008.

van Angelen, J. H., Lenaerts, J. T. M., Lhermitte, S., Fettweis, X., Kuipers Munneke, P., van den Broeke, M. R., van Meijgaard, E., and Smeets, C. J. P. P.: Sensitivity of Greenland Ice Sheet surface mass balance to surface albedo parameterization: a study with a regional climate model, The Cryosphere, 6, 1175–1186, https://doi.org/10.5194/tc-6-1175-2012, 2012.

van den Broeke, M., van As, D., Reijmer, C., and van de Wal, R.: Assessing and improving the quality of unattended radiation observations in Antarctica, J. Atmos. Ocean. Tech., 21, 1417–1431, 2004.

Vaughan, D. G., Comiso, J. C., Allison, I., Carrasco, J., Kaser, G., Kwok, R., Mote, P., Murray, T., Paul, F., Ren, J., Rignot, E., Solomina, O., Steffen, K., and Zhang, T.: Observations: Cryosphere, in: Climate Change 2013: The Physical Science Basis. Contribution of Working Group I to the Fifth Assessment Report of the Intergovernmental Panel on Climate Change, edited by: Stocker, T. F., Qin, D., Plattner, G.-K., Tignor, M., Allen, S. K., Boschung, J., Nauels, A., Xia, Y., Bex, V., and Midgley,

P. M., Cambridge University Press, Cambridge, United Kingdom and New York, NY, USA, Cambridge, 2013.
Wallace, J. M., Hobbs, P. V., Wallace, J. M., and Hobbs, P. V.: 3. Atmospheric Thermodynamics, in: Atmospheric Science, Elsevier, 2nd Edn., 63–111, 2006.
Wittmann, M., Groot Zwaaftink, C. D., Steffensen Schmidt, L., Guðmundsson, S., Pálsson, F., Arnalds, O., Björnsson, H., Thorsteinsson, T., and Stohl, A.: Impact of dust deposition on the albedo of Vatnajökull ice cap, Iceland, The Cryosphere, 11, 741–754, https://doi.org/10.5194/tc-11-741-2017, 2017.

Paper II

Sensitivity of Glacier Runoff to Winter Snow Thickness Investigated for Vatnajökull Ice Cap, Iceland, Using Numerical Models and Observations

Louise Steffensen Schmidt, Peter L. Langen, Guðfinna Aðalgeirsdóttir, Finnur Pálsson, Sverrir Guðmundsson, and Andri Gunnarsson

Atmosphere,9, 450, doi:10.3390/atmos9110450,2018

atmosphere

MDPI

Article

Sensitivity of Glacier Runoff to Winter Snow Thickness Investigated for Vatnajökull Ice Cap, Iceland, Using Numerical Models and Observations

Louise Steffensen Schmidt [1,*], Peter L. Langen [2], Guðfinna Aðalgeirsdóttir [1], Finnur Pálsson [1], Sverrir Guðmundsson [1,3] and Andri Gunnarsson [4,5]

1 Institute of Earth Sciences, University of Iceland, 101 Reykjavik, Iceland; gua@hi.is (G.A.); fp@hi.is (F.P.); sg@hi.is (S.G.)
2 Climate and Arctic Research, Danish Meteorological Institute, 2100 Copenhagen, Denmark; pla@dmi.dk
3 Tækniþróun Veitna, Veitur Utilities, 110 Reykjavik, Iceland
4 Faculty of Civil and Environmental Engineering, University of Iceland, 101 Reykjavik, Iceland; Andri.Gunnarsson@landsvirkjun.is
5 Landsvirkjun, National Power Company of Iceland, 108 Reykjavik, Iceland
* Correspondence: lss7@hi.is

Received: 12 September 2018; Accepted: 12 November 2018; Published: 15 November 2018

Abstract: Several simulations of the surface climate and energy balance of Vatnajökull ice cap, Iceland, are used to estimate the glacier runoff for the period 1980–2015 and the sensitivity of runoff to the spring conditions (e.g., snow thickness). The simulations are calculated using the snow pack scheme from the regional climate model HIRHAM5, forced with incoming mass and energy fluxes from the numerical weather prediction model HARMONIE-AROME. The modeled runoff is compared to available observations from two outlet glaciers to assess the quality of the simulations. To test the sensitivity of the runoff to spring conditions, simulations are repeated for the spring conditions of each of the years 1980–2015, followed by the weather of all summers in the same period. We find that for the whole ice cap, the variability in runoff as a function of varying spring conditions was on average 31% of the variability due to changing summer weather. However, some outlet glaciers are very sensitive to the amount of snow in the spring, as e.g., the variation in runoff from Brúarjökull due to changing spring conditions was on average 50% of the variability due to varying summer weather.

Keywords: regional climate models; glaciers; snowfall; snow-albedo feedback; runoff sensitivity

1. Introduction

Glacier mass loss is a key contributor to sea-level change (e.g., [1]) as well as changes in river volume and seasonality (e.g., [2,3]). Worldwide, melt water from glaciers e.g., affect sediment transport, the availability of freshwater, and hydropower production (e.g., [4]). As the climate warms, the amount of runoff from glaciated areas will initially increase until a peak runoff is reached [5], following which the amount of runoff will decrease (e.g., [3,5,6]). On seasonal timescales, glacier mass loss affects the river flow by storing winter precipitation and releasing the most water during the summer months. A warming climate will change the timing of this seasonality, e.g., due to an earlier onset of glacier melt (e.g., [2]).

Like many other glaciers and ice caps worldwide (e.g., [7]), Icelandic glaciers are currently losing mass and retreating because of a warming climate [8]. Icelandic glaciers currently store the water equivalent of ∼20 years of precipitation [9], which is released over a range of timescales [2]. Due to the large discharge from Icelandic glaciers, glacial runoff is an important component of Icelandic hydrology, and many of the main Icelandic rivers have a significant glacial component. Since hydropower stations

produce over 80% of the electricity in Iceland, knowledge of the amount of runoff from glaciers is not only important due to the effect on sea level, but also for harnessing of hydropower.

The surface energy balance of a glacier, and therefore the runoff, has a large sensitivity to changes in albedo. Icelandic glaciers have a large spatial and temporal variation in albedo, spanning from less than 0.1 for dirty ice in the ablation zone to 0.9–0.95 for new snow. The low ice albedo is due to layers of volcanic ash, which dominate the spectral properties of the ice (e.g., [10,11]). How much glacier ice is exposed during the summer and the timing of when the winter snow melts away is therefore expected to have a large effect on the runoff over the ablation season. Due to climate change, the amount of solid precipitation is expected to change (e.g., [6,7,12]) and it is, therefore, important to investigate the sensitivity of ablation to snow thickness changes.

The ablation of glaciers can be estimated using either physical or empirical methods (e.g., [13]). While physical models, i.e., energy balance models, can provide direct estimates of the energy balance, a lack of observations and the many input parameters can make them impractical. Empirical models, i.e., degree-day models, describe the statistical relations between melt and temperature or other weather parameters. These models can be more practical but need to be tuned for every location and provide less information about the surface climate. Neither of these models can estimate the accumulation, and therefore a physically based atmospheric model is needed to simulate the mass balance.

Global Climate Models (GCMs) and Regional Climate Models (RCMs) combine atmospheric and surface physics. They are characterized by the explicit solution of the hydrodynamic equations of the atmosphere, which is of vital importance to the mass balance of glaciers as it e.g., determines the transfer of moisture from the source regions (e.g., [13]). RCMs are forced by a GCM or reanalysis at the boundaries of their domain, and by downscaling the GCM they provide added value to the simulations of the cryosphere. Since they are running on a smaller domain, they can run at higher resolution and include more complex models of the cryosphere. Numerical high-resolution RCMs, such as RACMO [14], WRF [15], MAR [16], and HIRHAM5 [17], are therefore valuable tools to estimate mass balance at the surface of glaciers, and much work has gone into evaluating these models over Greenland (e.g., [18,19]) and Antarctica (e.g., [20,21]). To advance and evaluate models used for regional downscaling through international cooperation, the Coordinated Regional Downscaling Experiment (CORDEX) was started in 2009 [22]. Through this project, a collection of historical and future simulations from many different RCMs were made publicly available.

Another type of models used for regional downscaling is Numerical Weather Prediction (NWP) models. These models use physical models of the atmosphere and oceans to predict the weather based on current weather conditions. RCMs are generally derived by NWPs, but the two categories of models serve different functions: NWPs predict the weather while RCMS project climate scenarios. The major difference between the two types of models is therefore the scale of the simulations. NWPs generally operate over smaller domains and much smaller time scales (days as opposed to decades for RCMs). For this reason, NWPs are often run at a higher resolution than RCMs, even if currently a big challenge is the execution of climate simulations at 1 km resolution (convection-permitting simulations), for example in the frame of CORDEX-CORE.

However, projects to use NWPs as a tool for climate reanalysis have been established. Over the Iceland domain, the NWP HARMONIE-AROME has been used for the ICRA reanalysis project [23] to estimate the climate from 1980 to 2016. The project has e.g., been focusing on adding an improved surface scheme for Icelandic glaciers, to achieve more accurate mass balance estimates. Overall, the reanalysis showed a good correlation with available Automatic Weather Station (AWS) observations over Iceland [23].

Although RCMs and NWPs are important tools for climate and weather predictions, they often have systematic biases in temperature and/or precipitation (e.g., [24,25]), which need to be corrected to get the most accurate estimates of changes in mass balance and runoff. Since runoff is a nonlinear function of precipitation, model bias correction is especially important for hydrological modeling (e.g., [25,26]). Numerous bias correction methods have been developed to remove these model

errors (e.g., [27,28]), for example by adjusting the modeled mean of the corrected variables to match observations more closely. Often a time-invariant method is used, where the error correction found over the evaluation period is assumed to be applicable to any time period. However, this method works best for short-term modeling, as the bias correction cannot be expected to be constant over longer timescales (e.g., [28]).

In this study, the RCM HIRHAM5 [17] and the NWP HARMONIE-AROME [29] are used to simulate the runoff from Vatnajökull and to quantify the impact of the snow thickness in spring on the runoff the following summer. The precipitation biases in both HIRHAM5 and HARMONIE-AROME are evaluated, and a simple bias correction is applied to the model precipitation. The impact of the spring conditions is then tested by setting up a model experiment which uses the simulated spring conditions at the end of the 31st of March for all years in the period 1980–2015 as a starting point for model runs forced by summer weather of all years in the same time period. Distributions of the likely runoff from Vatnajökull are created based on those 36 years, and we investigate to what extent spring snow thickness affects summer melt. While several studies have investigated the effect on increasing accumulation on the runoff (e.g., [30–32]), this is the first attempt to quantify the effect of spring snow cover on glacier melt.

2. Study Site and Observations

2.1. Study Site

Vatnajökull ice cap is the largest temperate ice cap in Europe, with an area of 8100 km^2. It is located close to the southeastern coast of Iceland, and covers active volcanic areas where eruptions are frequent (e.g., [33]). The surface elevation spans from 0 to 2110 m above sea level (a.s.l.). Most of its precipitation falls as snow, as the average temperatures on the ice cap is close to or below freezing. The summer balance is normally negative for the entire ice cap, but the central portions might turn slightly positive during repeated cold spells. At the highest areas of the glacier, days with melting only occur 10–20 days of the year, while at lower levels the ablation season generally lasts 3–4 months [9]. Vatnajökull is affected by frequent dust storms and tephra from volcanic eruptions. Tephra layers in the glaciers ice dominate its spectral properties [10], but the effect of tephra on the accumulation zone is generally small. In addition to surface melting, geothermal activity at the bed provides an on average small contribution to the total melt [9].

Surface and bedrock maps of Vatnajökull have been produced using interpolated profiles of radio-echo sounding and precision altimetry [9]. These have been used in conjunction to delineate the locations of glacial water catchments which feed glacial rivers.

2.2. Energy and Mass Balance

AWSs have been operated on Vatnajökull since 1994, with 1–13 stations measuring on the ice cap during the summer months (e.g., [34,35]). The 2 m temperature, 2 m relative humidity, 4 m wind speed, and the 4 m wind direction have been measured for the entire period, while the radiation components have been measured since 1996. Observations from five AWSs, three on Brúarjökull and two on Tungnaárjökull that have been operated at approximately the same location since 2001 are used to evaluate the simulated incoming radiative fluxes in HIRHAM5 and HARMONIE. In addition, estimations of the albedo at the stations in the ablation zone are used to evaluate how well the model captures the timing of the albedo drop from snow to ice values. The average locations of the stations are shown in Figure 1. The observations are conducted at 10 min intervals, but daily averages are used for the comparisons.

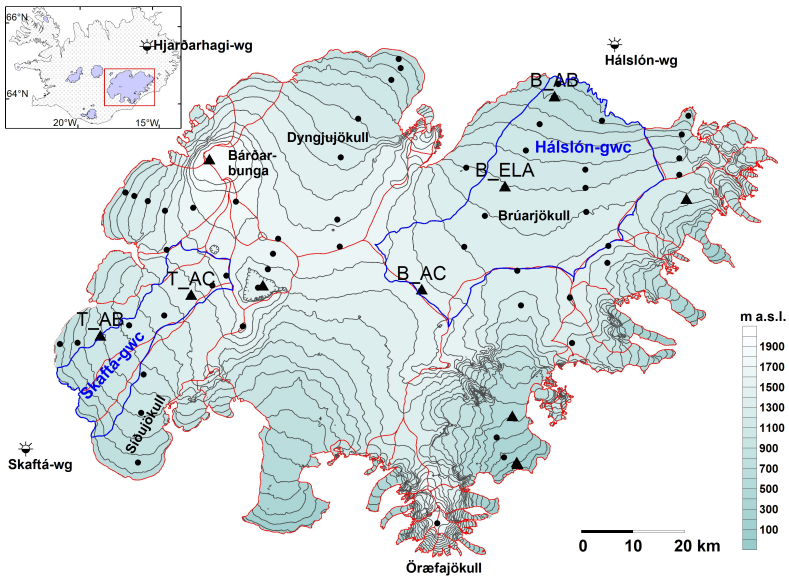

Figure 1. Location of AWS stations (black triangles) and surface mass balance sites (black dots) used in this study. The red lines show the outlines of the ice divides, while the bluelines show the outlines of the Skaftá (west) and Hálslón (east) glacial water catchments. The symbols outside the ice cap show the water gauges (wg).

To evaluate the modeled snow thickness in spring, the modeled winter balance was compared to in situ winter mass balance measurement at several sites on Vatnajökull. In situ mass balance measurements have been carried out twice a year every glaciological year since 1991–1992, with an average of 60 measured locations every year. The uncertainty in the measurements has been estimated to be ±0.3 m water equivalent (w.eq.) [8,36]. There are no precipitation observations for Vatnajökull, but it is generally assumed that the winter mass balance is equal to the winter precipitation (e.g., [10]). Almost all winter precipitation on Vatnajökull is snowfall and there is only little melt in the summer besides in the lowest part of the ablation zone. The winter balance is therefore considered a good measure of the winter precipitation and will therefore in this study be used to evaluate the simulated precipitation in the two models.

2.3. River Runoff

Substantial hydrological measurements have been conducted in glacial rivers in Iceland mainly due to their importance for hydropower production. Therefore, time series spanning over decades are available for several glacial rivers. In this study, the runoff into two rivers, Jökulsá á Dal and Skaftá, is used to evaluate the model runoff; both have a large glacial component. The outlines of the glacial water catchments (GWCs) that contribute to these rivers are shown in Figure 1.

About 80% of the runoff from Brúarjökull, a northern Vatnajökull outlet, flows into Hálslón reservoir, which lies on the uppermost former path of the Jökulsá á Dal river. Hálslón reservoir water level has been monitored since the impoundment of the dam in autumn 2007 [37]. The runoff to the reservoir is estimated based on a relationship between reservoir water level and storage in a time series of daily averaged inflow. Before Hálslón reservoir was created, the runoff from Brúarjökull was e.g., measured further down the Jökulsá á Dal river at Hjarðarhagi (VHM110) [37]. To expand the time series for Brúarjökull, the Hjarðarhagi observations are used from 1980 to 2007, after which the runoff was routed into Hálslón reservoir from 2007 to present. The size of the Hjarðarhagi catchment area is ~3300 km^2 [38] and the size of the Hálslón catchment area is about 1800 km^2, where approximately

1200 km^2 is covered with Brúarjökull. The glacial component of the catchment spans from ∼750 to 1600 m a.s.l. Runoff from non-glaciated areas has not been estimated for the Jökulsá á Dal sites, which adds further uncertainty to the results. About 80% of the catchment area of Hálslón is covered by Brúarjökull while the rest is non-glaciated land with a seasonal snow pack. It can very tricky to distinguish between glacier melt and seasonal snow pack melt from only an inflow time series. However, the range of snow pack storage has been observed since 1956, which can give a rough estimation of the contribution. Since 1956, the average seasonal spring snow pack has been estimated to store $\sim 0.19 \pm 0.08$ km^3 of water [37]. Since 2007, the yearly runoff into Hálslón has been observed to be between 3.0 and 4.5 km^3, and we therefore expect the runoff from non-glaciated areas in spring to contribute less than 10% to the yearly observed runoff. However, since the snow pack generally melts between April and middle of July, it can have a large contribution during the spring months. In 2013 there was an unusually high amount of seasonal snow in the catchment corresponding to approximately 0.25 km^3 of stored water. In the runoff time series, 0.58 km^3 water was observed between April and June, meaning the off glacier seasonal snow contributed about 40% to the spring runoff in 2013.

In addition, fall precipitation can also have a large contribution on the runoff time series. This was e.g., observed in autumns of 2015 and 2016.

Skaftá river receives runoff from the Skaftá GWC, which includes the outlet glacier Skaftárjökull and part of the outlet Tungnaárjökull. The closest hydrometric station to the glacier is at Sveinstindur (V299), 25 km down-river from the glacier margin, and has been operated since 1986 [39]. The Sveinstindur station has a catchment area of 714 km^2 [40], where approximately 400 km^2 is glacierized. The glacial area spans from approximately 700–1600 m a.s.l. The runoff data comes with a quality flag for each daily datapoint. Only data that are of full quality have been used for this evaluation, while data that have needed corrections due to ice interference on the runoff or other problems have been discarded. To isolate the glacial runoff in the river runoff record, the runoff originating from ice-free areas is estimated using the hydrological model WaSiM [41]. WaSiM is a physically based distributed model, which offer methods of varying complexity to simulate different elements of the hydrological cycle depending on available observations. It has in recent years been used for hydrological modeling of Iceland and includes interaction between glaciers and ice-free areas such as e.g., interflow. A detailed description of the setup for Iceland is given in Jónsdóttir [42] and Einarsson [43]. The WaSiM model was run with four equally good parameterizations by the Icelandic Meteorological Office [39] and the four outputs were used to assess the uncertainty of the model estimation. The difference between the four outputs is small overall, as the deviation from the mean of the four model outputs is on average $\pm 0.6\%$. However, it can deviate by up to $\pm 44.0\%$ on specific days. For the comparison presented here, a mean of all four WaSiM runs was used as an estimate for the non-glacial runoff.

There is a substantial uncertainty in the WaSiM simulations, which leads to a negative runoff from the glacier during years with a low runoff during early spring or late autumn. Discarding these negative values means that the total accumulated runoff might be overestimated. However, the days with negative values are removed in both simulated and observed time series, and therefore this should not be an issue for the comparison.

Jökulhlaups from the Skaftár cauldrons (e.g., [44,45]), two subglacial lakes at geothermal areas that collect water and release in jökulhlaup events, provide another complication in the runoff time series. The two cauldrons are located just north of the Skaftá GWC and drain every 2–3 years [44]. Since jökulhlaups are not simulated in the model, runoff on days when jökulhlaups are in progress are removed from the time series. The cauldrons do not contribute to the runoff into Skaftá when no jökullhlaup event is in progress, as the water gathers in the subglacial lakes. The cauldrons are in a different water catchment, and not a part of the Skaftá GWC, and therefore jökullhlaups do not affect the water balance of this catchment except on event days.

3. Model Description and Experimental Design

3.1. HIRHAM5 and HARMONIE-AROME

In this study, we apply the RCM HIRHAM5 [17] and the NWP HARMONIE-AROME [29]. HIRHAM5 is a hydrostatic RCM which combines the dynamical core of the HIRLAM7 numerical forecasting model [46] and physics schemes from the ECHAM5 general circulation model [47]. A detailed description of the model configuration can be found in Christensen et al. [17]. It is run over a domain containing Greenland and Iceland, with a horizontal resolution of $0.05^\circ \times 0.05^\circ$ on a rotated-pole grid. This corresponds to ∼5.5 km resolution. The atmosphere has 31 vertical levels, from the surface to 10 hPa. The time step is set equal to 90 s. The model is forced by ERA-Interim reanalysis data [48], which is a global atmospheric reanalysis by ECMWF spanning back to 1979, at the lateral boundaries at 6 h intervals. ERA-Interim sea surface temperatures and sea ice fraction are imposed in ocean points. The model output is at 6 h intervals. HIRHAM5 model simulations have been successfully validated over Greenland (e.g., [18,19,49–52]) and Iceland [10] using AWS and ice core data. While evaluating the incoming energy and mass balance fluxes over Vatnajökull in HIRHAM5, Schmidt et al. [10] found a generally good agreement between observations and simulations in the incoming energy fluxes. However, one important drawback with the simulation from HIRHAM5 was an overestimation of the winter accumulation in the ablation zone of several outlet glaciers, e.g., Brúarjökull, Dyngjujökull and Tungnaárjökull, as well as in areas with high orographic forcing. This was partly attributed to the model using hydrostatic physics and not allowing horizontal advection of snow.

HARMONIE-AROME is a non-hydrostatic convection-permitting NWP model and is developed in a cooperation between HIRLAM, ALADIN and Meteo-France [29]. The forecast model was based on the AROME-France model (e.g., [53]), but now differs from the original model in various aspects [29]. Details on the model configuration are described in Bengtsson et al. [29]. In autumn 2015, the Icelandic Meteorological Office started a reanalysis project for Iceland (ICRA) using the HARMONIE-AROME model [23]. Details on the reanalysis setup over Iceland can be found in Nawri et al. [23]. ICRA currently spans from 1 September 1979, until 31 December 2016. It is run over a domain containing only Iceland at a horizontal resolution of $0.025^\circ \times 0.025^\circ$, corresponding to ∼2.5 km. The atmosphere has 65 vertical levels, from the surface to 10 hPa. The time step is set equal to 60 s. Like HIRHAM5, HARMONIE-AROME is forced by ERA-Interim reanalysis data at the lateral boundaries at 6 h intervals. The output is given at 1 h intervals. Since HARMONIE-AROME is non-hydrostatic and calculates precipitation diagnostically, it provides a better representation of the accumulation in areas with high orographic forcing than HIRHAM5 (more details in Section 4.1).

Snow Pack Scheme

While the original HIRHAM5 [17] used unchanged ECHAM physics, an updated model version is used in this study which expands the 5-layer surface scheme in ECHAM to 25 layers. In addition, it includes a dynamic surface scheme that explicitly calculates the surface mass budget, takes melting of snow and bare ice into account, and resolves the retention and refreezing of liquid water in the snow pack [19,51].

This updated surface scheme in HIRHAM5 has previously been adopted to and evaluated for Vatnajökull by Schmidt et al. [10]. An updated snow-albedo scheme was tested in this study, depending both on the age of the snow and the surface temperature, and the snow aging parameters were tuned to better fit with observations from AWSs operated on Vatnajökull. The ice albedo, emerging as snow melts away in the ablation zone, was improved by using a map of the ice albedo based on MODIS observations [10,11]. HIRHAM5 does not have a scheme for routing of runoff. The only delay taken into account is a runoff timescale based on the surface slope of the glacier.

The snow pack scheme was created for HIRHAM5, and any new implementations to the scheme are first implemented into the offline version of the model [19]. The offline version of HIRHAM5 only

contains the HIRHAM5 glacier model, which is run offline forced by 6-h surface energy (incoming shortwave (SW↓) and longwave (LW↓) radiation and turbulent fluxes) and mass fluxes (snow, rain, evaporation, and sublimation) from a previous HIRHAM5 experiment. While a fully coupled, high-resolution HIRHAM5 run is computationally very expensive, this offline model offers a quicker alternative to test new model implementations. In this study, we are using this offline model, which we refer to as the HIRHAM5 snow pack scheme. This model can be forced by incoming energy and mass components from another climate model, although it will no longer be a fully coupled system and missing feedback must be taken into considerations.

The ICRA HARMONIE-AROME runs have a less advanced snow pack scheme, which e.g., does not track the thickness of the snow layers, making the HARMONIE-AROME snow pack scheme less suited for this study. In addition, since the HIRHAM5 snow pack model is computationally cheaper than running the online HARMONIE-AROME model, it is more applicable for the many model runs required in this study.

3.2. Experiment Design

To use the validated offline snow pack model from HIRHAM5 but also make use of the improved incoming mass flux and higher resolution of the HARMONIE-AROME meteorological forcing, a combination of the two models is used in this study. This is implemented by running the snow pack scheme from HIRHAM5, in the same way as described in Schmidt et al. [10], but forcing the snow pack model with the meteorological forcing from HARMONIE-AROME. The snow pack scheme is forced every 6 h by surface energy (incoming radiation and turbulent fluxes) and mass fluxes (snow, rain, and evaporation) from HARMONIE-AROME. To initialize the snow pack model, a 100-year spin-up was performed by repeating the forcing from 1980. At the end of the spin-up, all variables had converged in all model layers. The final state of the spin-up was then used for a 1980–2015 simulation, forced by 6 h HARMONIE-AROME input. A schematic diagram showing the coupling is shown in Figure 2.

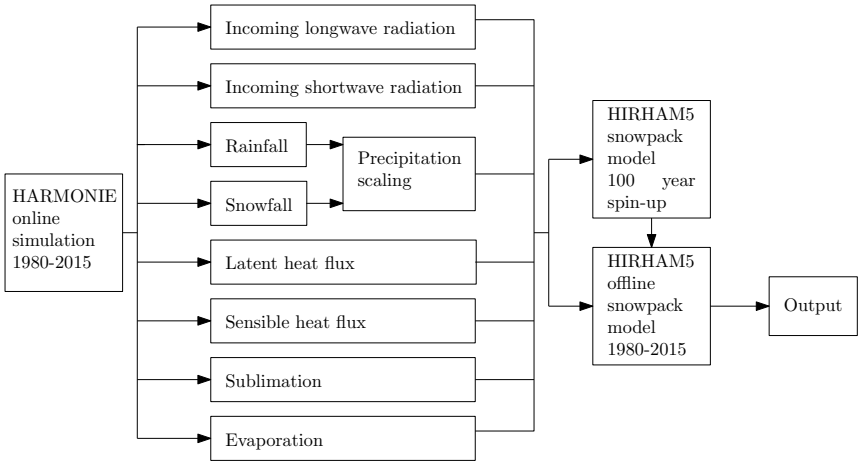

Figure 2. A schematic diagram of the coupling of HARMONIE-AROME and HIRHAM5. The precipitation scaling is discussed in Section 4.2.

To estimate the effect of the spring conditions on the summer runoff, sensitivity runs are conducted by repeating the modeled spring conditions of each year from 1980 to 2015, followed by the weather of all summers in the same period. Firstly, the HIRHAM5 snow pack scheme is run from 1980 to 2015 over all glacier points using HARMONIE-AROME incoming mass and energy fluxes, saving the state of the snow pack (snow thickness, temperature, albedo etc.) every year at the end of 31 March. Snow

ablation generally starts between late April and May, so this date was chosen to include the entire ablation season. The state of the surface on 31 March of each year is then used to initialize a model run using the atmospheric forcing (i.e., incoming energy and mass fluxes) for each of the 36 model years starting on 1 April. By the end of the model run, 36 × 36 = 1296 summers have been simulated. In addition, to create a case with only snow melt, the model is also initialized with a thick enough snow layer on the surface, so the underlying ice is never exposed. This is done to estimate how much the melt is affected by the change in albedo when the ice is exposed when compared to only snow melt.

4. Results

4.1. Evaluation of Model Precipitation

As mentioned above, the energy and mass balance in HIRHAM5 has previously been evaluated over Vatnajökull by Schmidt et al. [10], and an ice albedo map using MODIS data [54] was implemented in the model which improved the albedo simulations. Offline model simulations with HIRHAM5 showed that it overestimates the winter balance in the ablation zone as well as in areas with high orographic forcing. HARMONIE, on the other hand, appears to simulate the distribution of precipitation over the glacier more satisfactorily, overall. Scatter plots of the measured winter balance and model results, which have been interpolated onto the measurement locations using bilinear interpolation, are shown in Figure 3a,b and Table 1. The HARMONIE results are clearly closer to the one-to-one line than HIRHAM5, which is also evident from the lower root mean square error (RMSE) (0.6 m w.eq. for HARMONIE vs. 1.2 m w.eq. for HIRHAM5). The larger outliers, which correspond to the measuring site on Öræfajökull, which is the highest area within Vatnajökull, are also closer to the observations in HARMONIE than in HIRHAM5. Only a few observations are available for this location, as the summit has only been surveyed in the period 1993–1998 [55]. However, comparisons with geodetic mass balance from 1982 to 2010 [56] show that the simulated mass balance overestimation in both models occurs for the entire investigated period.

To assess the spatial distribution of the errors, mean difference maps were created by comparing the model simulations to interpolated mass balance maps based on measurements (Figure 3c,d). The distribution of the differences is similar in both models, with the steep, high-elevation areas in the south and south-east generally being too wet in the models and the middle of the ice cap generally being too dry. However, in areas with high orographic forcing, HARMONIE simulates the observations better than HIRHAM5. The difference on Öræfajökull is smaller in HARMONIE than in HIRHAM5, and the high-elevation area around Bárðarbunga is significantly better represented in HARMONIE. The precipitation in the center of the ice cap is also less underestimated in HARMONIE.

The other fluxes needed to force the snow pack model, i.e., the incoming radiative and turbulent fluxes, have also been evaluated in both models using observations from five AWSs from 2001 to 2014. The mean differences are shown in Table 1. It is important to note that the turbulent fluxes are not compared to observations but to a one-level eddy flux model [57] which uses the AWS observations of temperature, humidity, and wind speed at 2 m to estimate the turbulent fluxes.

Table 1. Evaluation of the simulated mass balance and energy flux components used to force the snow pack model, i.e., winter mass balance (a measure for precipitation), incoming short- and longwave radiation and turbulent fluxes, in HIRHAM5 and HARMONIE. The mean values of the average difference (model-observations), RMSE, and correlation (r) are given. The turbulent fluxes are a model-model comparison.

Components	Observed Value	HIR Diff	HAR Diff	HIR RMSE	HAR RMSE	HIR r	HAR r
Winter SMB (m w.eq.)	1.5	0.04	−0.07	1.2	0.6	0.82	0.87
SW↓ (W m^{-2})	224.7	−32.0	2.4	67.2	49.9	0.80	0.87
LW↓ (W m^{-2})	283.2	−9.0	−12.8	22.7	22.1	0.80	0.87
Turbulent fluxes (W m^{-2})	27.6	−6.5	−8.9	32	28.8	0.43	0.46

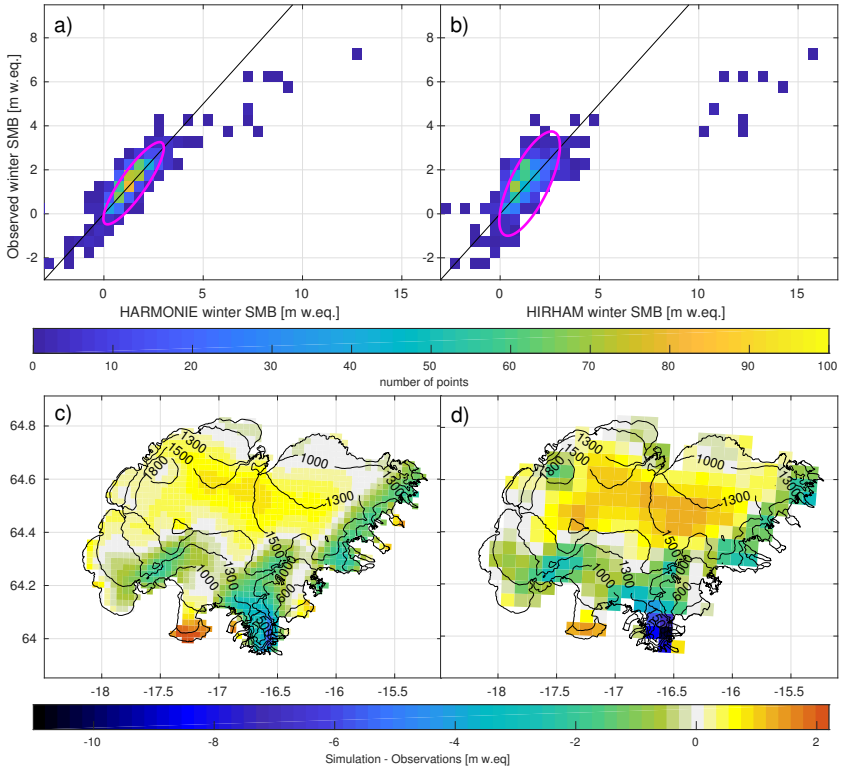

Figure 3. (**a**) HARMONIE and (**b**) HIRHAM5 winter mass balance compared to measurements from 1992 to 2014. Color bar shows how many points are in the same spot and purple ellipsis outlines 68% of the points. Statistics on the regression lines are given in Table 1. Interpolated observed mean winter mass balance maps from 1992 to 2014 compared to (**c**) HARMONIE and (**d**) HIRHAM5 winter mass balance.

The incoming solar radiation is better represented in HARMONIE, with both a smaller model difference and RMSE, as well as a higher correlation. The average difference is slightly smaller in HIRHAM5 for both the incoming longwave radiation and the turbulent fluxes, but the RMSE and correlation are better for both in HARMONIE. Overall, the incoming radiative flux seems to be better simulated by HARMONIE than HIRHAM5, at least at the five AWS locations.

Based on these comparisons, HARMONIE simulates the incoming mass and energy fluxes for the current Icelandic climate conditions better than HIRHAM5. The reason is the more complex model physics in HARMONIE than in HIRHAM5. Due to the higher-resolution and non-hydrostatic physics used in HARMONIE, the model can resolve non-hydrostatic features in the atmosphere not captured by the lower-resolution, hydrostatic HIRHAM5 model. The higher resolution also means that the topography is better resolves, which is especially important for simulations over the steep slopes of Öræfajökull. Another important distinction between the models is the treatment of precipitation. In HIRHAM5, precipitation is treated as a diagnostic variable. When the right conditions for precipitation are met, it immediately appears on the surface, and thus no horizontal advection of rain and snow occurs. In HARMONIE-AROME, the precipitation is treated as a prognostic variable and it therefore allows horizontal advection of snow and rain. This is a very important process in areas with high orographic forcing such as e.g., Öræfajökull.

Since HARMONIE-AROME has a higher resolution and a more complex representation of the atmosphere, which lead to a more accurate simulations of the meteorological variables, incoming mass and energy balance fluxes from HARMONIE were chosen to force the HIRHAM5 snow pack model in order to get the best representation of the incoming mass and energy fluxes for realistic runoff simulations. Using NWP models to force a snow pack scheme has previously been successfully done in studies by e.g., Bellaire and Jamieson [58] and Vionnet et al. [59].

4.2. Accumulation Scaling

Although the accumulation of precipitation in HARMONIE is an improvement over the HIRHAM5 results, there are still substantial biases in the winter balance compared to observations. Accurate estimation of the winter accumulation is especially important in the ablation zone, as too much modeled winter snow will delay the timing of the exposure of the underlying low albedo ice surface and thus cause underestimation of the amount of runoff. To get the most accurate representation of the snow thickness, a scaling is applied to each model year. The scaling is based on the average winter balance difference map from 1992 to 2015, as shown in Figure 3c. The same absolute scaling is used for every model year and is applied to each snow fall event. The scaling matrix is shown in Figure 4a.

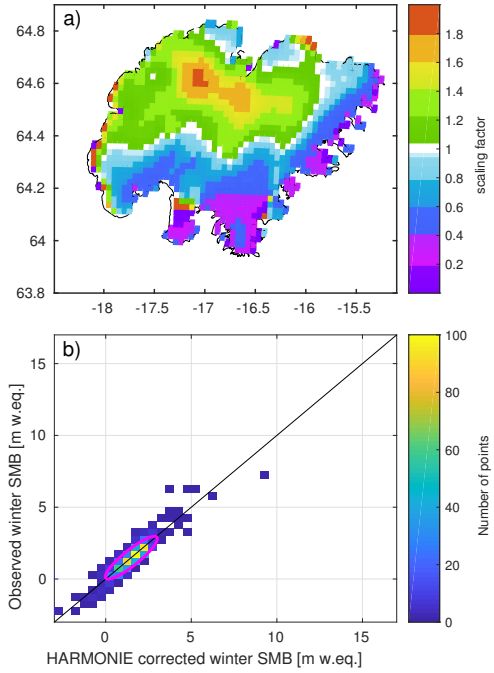

Figure 4. (**a**) The scaling matrix used for correction of each winter snowfall; (**b**) comparison between winter mass balance observations and the modeled corrected winter mass balance for 1992–2015. The RMSE is 0.4 m w.eq. and the correlation r = 0.89. Color bar shows how many points are in the same spot and purple ellipsis outlines 68% of the points.

A new spin-up of the subsurface was performed by integrating the model for 100 years repeating the corrected forcing from 1980. Only the incoming precipitation was corrected, all other incoming fluxes were unchanged HARMONIE forcing. A new model run for 1980–2015 was then conducted. A comparison of the winter mass balance observations with the winter mass balance simulated with the

corrected forcing is shown in Figure 4b. The largest difference from the uncorrected model comparison is that the Öræfajökull points are now much closer to the one-to-one line and the RMSE has now decreased to 0.37 m w.eq. This is almost within the error of the observations which is estimated to be 0.3 m w.eq.

Before the correction, the too high winter accumulation in the ablation zone resulted in a delay of the timing of the albedo drop from snow to ice in the model, and in some instances the ice surface was not exposed at all (not shown).

4.3. Comparison to Runoff Measurements

Model comparisons with runoff observations from Skaftá GWC into Skaftá river and from Brúarjökull into Jökulsá á Dal river at Hjarðarhagi (1980–2007) and Hálslón reservoir (2007–2015) are shown in Figure 5 and Table 2. In Skaftá, the average deviation in total summer runoff over the time period is -0.07 km^3, which is within the uncertainty of the compared time series. The correlation between model and data is also high at 0.78 for the whole period.

For the runoff from Brúarjökull, the deviation in total runoff between observations and model is at -0.6 km^3. This higher deviation is expected, both because no correction has been added to account for non-glacierized areas and because the runoff is estimated from the water level in the Hálslón reservoir for part of the time series, where the uncertainty is expected to be larger than for the conventional gauging from Skaftá or Hjarðarhagi. The correlation between model and data is still high at 0.89 for the whole period, which suggests that the variability is well captured.

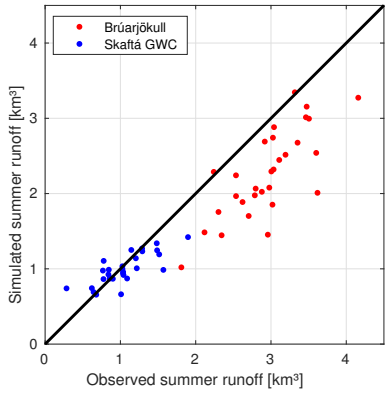

Figure 5. Total summer runoff (April–October) from Skaftá GWC (blue points) into Skaftá river and Brúarjökull (red points) into Jökulsá á Dal river at Hjarðarhagi (1980–2007) and Hálslón reservoir (2007–2015) compared to the modeled value.

Table 2. Comparison statistics of the average summer runoff (April–October) from Skaftá GWC into Skaftá river and from Brúarjökull into Jökulsá á Dal river at Hjarðarhagi (1980–2007) and Hálslón reservoir (2007–2015) according to observations and the simulation. The mean difference, RMSE, and correlation are given.

Glacial Catchment	Period	Mean Observed Summer Runoff (km^3)	Model-Obs (km^3)	RMSE	r
Skaftá GWC	1986–2015	1.06	−0.07	0.22	0.78
Bruárjökull	1980–2015	2.9	−0.6	0.74	0.89

For this study, the focus is generally on the runoff over the entire melt season. The snow pack model used here does not include any hydrological routing of runoff, and therefore a daily comparison of has larger deviations than a seasonal comparison.

4.4. Snow Thickness on 1 April

The conditions of the ice cap in spring will affect the summer runoff. Although the temperature in the winter snow is of importance, by far the most important variable is the thickness of accumulated snow on the ice in the ablation zone. This is because the snow thickness in the ablation zone determines the timing of the exposure of the underlying low albedo ice. To investigate snow thickness variability in 1980–2015, time series and histograms of the modeled average snow thickness in the ablation zone on April 1st for the whole ice cap as well as for selected outlet glaciers are shown in Figure 6. For the whole glacier, the modeled snow thickness (for ablation zone points below 1300 m) is found to have an average value of 1.2 m w.eq., with a 1.3 m w.eq. difference between the minimum and maximum value. However, since there might be a large variation in snow thickness for the different outlet glaciers, we focus on three outlet glaciers: the north-facing Brúarjökull with an average of 1.4 m w.eq., the south-west facing Skaftá GWC with an average of 1.2 m w.eq. and the south-facing Síðujökull with an average snow thickness of 1.1 m w.eq. The variation over the time series is 1.5–2.1 m w.eq. depending on the outlet.

All four histograms have a two-peaked distribution, which is especially apparent in the histogram for Brúarjökull. This is due to a shift in snow thickness in the mid-1990s. Around 1995, there was a rapid increase in ocean temperatures off the southern coast of Iceland which was likely due to atmospheric and ocean circulation changes around Iceland [60]. This resulted in an increase of the mean annual temperature of ∼1 °C after 2000 compared to the mid-1990s (e.g., [8,61]), and observations of the annual surface mass balance show a clear shift from positive to negative values in this period. From the time series of the snow thickness, it is clear that the model catches this shift.

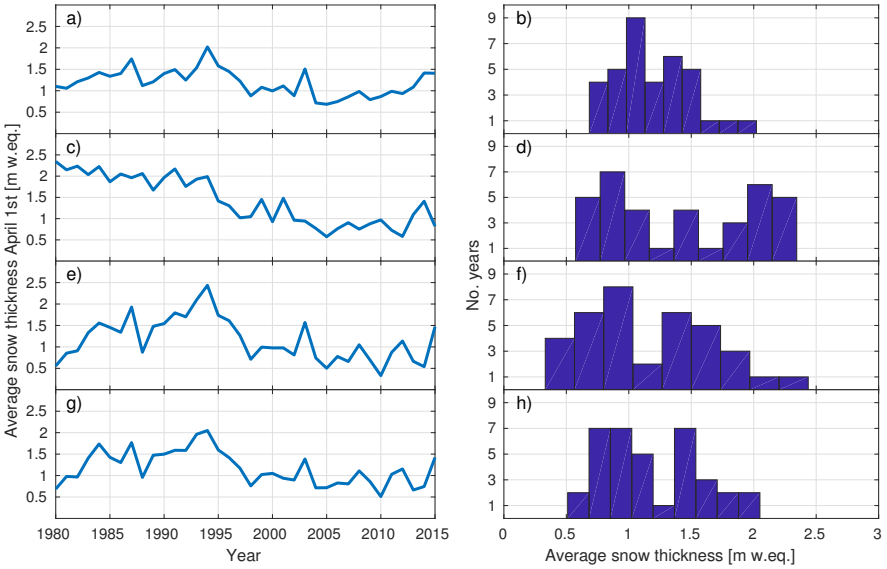

Figure 6. Time series and histograms of the mean modeled snow thickness on 1 April below 1300 m for (**a**,**b**) Vatnajökull; (**c**,**d**) Brúarjökull; (**e**,**f**) Síðujökull; and (**g**,**h**) Skaftá GWC. Brúarjökull terminates at 600 m a.s.l., Síðujökull at 650 m a.s.l. and Skaftá GWC at 740 m a.s.l.

4.5. Sensitivity Runs

The HIRHAM5 snow pack model was run to create 36 different simulated spring conditions, i.e., accumulated winter snow, each followed by 36 different summer conditions to assess the sensitivity of

the runoff to the thickness of the spring snow. Maps of the results from the sensitivity runs are shown in Figure 7, and time series and histograms of the results for the whole icecap and for selected outlet glaciers are shown in Figure 8. Only the ablation zone is shown in all figures as the different spring conditions are mostly going to affect the runoff from the ablation zone. The equilibrium line altitude (ELA), and therefore the ablation zone, varies both with location and between years, but has not been observed higher than 1300 m for the years under consideration. We have therefore defined the ablation zone as everything below 1300 m.

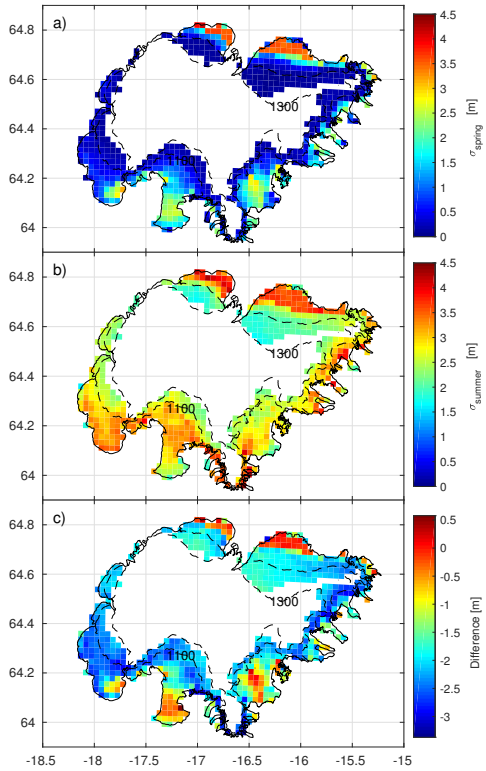

Figure 7. Maps showing the effect of the summer weather and spring conditions on runoff from the ablation area (here set as below 1300 m). (**a**) the average varying spring conditions std (σ_{spring}); (**b**) the varying summer weather std (σ_{summer}); (**c**) the difference between the maps (**a**,**b**).

For evaluation of the sensitivity run results, we introduce two terms: "variation in runoff for varying spring conditions std" σ_{spring} and "variation in runoff for varying summer weather std" σ_{summer}. Imagine a matrix of all 36 $\times$ 36 model combinations, where the rows are the 36 summers and the columns are the 36 spring conditions. Each point in the matrix is the total runoff over a summer from April to October. For σ_{spring}, a standard deviation across each row is calculated. Since the summer weather is constant within each row while the spring conditions varies, this parameter is used to determine the changes in runoff due to changing spring conditions. σ_{summer} is similar, but this time a standard deviation across each column is calculated. In this case, the runoff variations due to changes in the summer weather can be assessed.

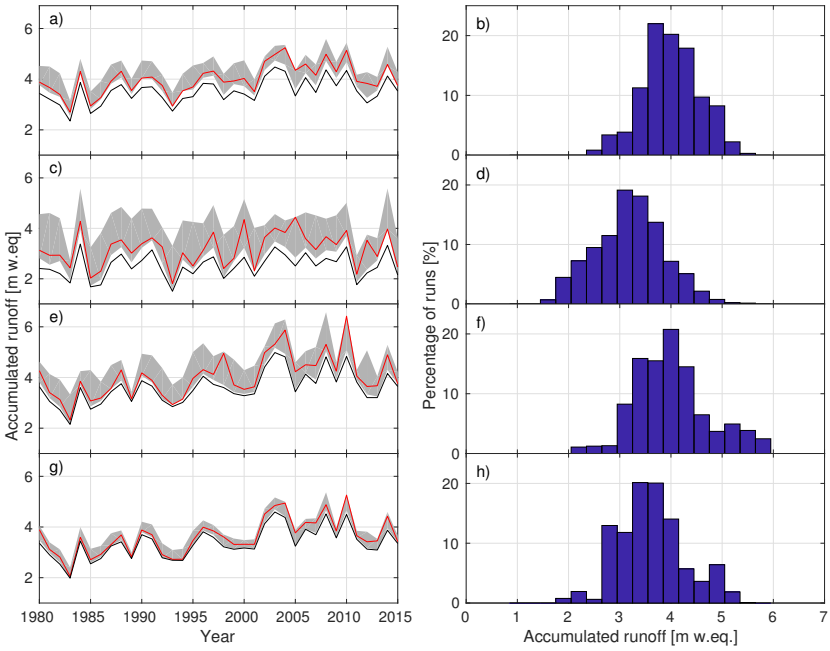

Figure 8. Time series of accumulated runoff for April–October from (**a**) Vatnajökull; (**c**) Brúarjökull; (**e**) Síðujökull; (**g**) Skaftá GWC for different spring conditions. The red line is the original run where the spring conditions of the specific year are used, the grey area shows the range in runoff when the spring conditions are changed, and the black line shows how much melt would occur if the underlying ice is never exposed. Probability distributions for the runoff created using the results of the sensitivity runs are shown for (**b**) Vatnajökull; (**d**) Brúarjökull; (**f**) Síðujökull; (**h**) Skaftá GWC.

Figure 7a shows the mean of σ_{spring}. The largest sensitivity to spring snow thickness is found in the lower parts of the north-facing glaciers Brúarjökull and Dyngjujökull. The south and east facing glaciers generally have a smaller but still significant sensitivity to changes in snow thickness, while the west facing glaciers only appear to have a small sensitivity to the spring conditions.

Figure 7b shows the mean of σ_{summer}. In many parts of the ablation zone, the summer weather clearly has a larger influence on the runoff variability than the spring snow thickness. There are several controlling factors for the variations in the summer weather. In addition to the amount of incoming solar radiation, an important factor for the summer melt on Vatnajökull is the amount of summer snow. This is an especially important factor for Brúarjökull, which is more likely to receive precipitation from cold northern winds and has a high-elevation ablation zone. This high dependence on summer snow could contribute to the high variability due to summer weather found in the simulations over the ablation zone of Brúarjökull. Figure 7c shows the difference between the two different maps (a,b). Except for parts of the north-facing glacier outlets, where the runoff variation due to changes in spring conditions and summer weather is approximately equal, and in a few points on two south-facing outlets, the runoff variability is much more affected by variations in summer weather than variations in spring snow thickness. For the whole ice cap, changing the spring snow thickness amounts to a maximum of 22% change between the minimum and maximum runoff over a summer. Individual outlet glaciers have a larger sensitivity to the spring snow thickness, and e.g., the runoff from Brúarjökull increases with a maximum of 72% compared to the minimum runoff.

On average, σ_{spring} for the whole ice cap is equal to 31% of σ_{summer}, with a maximum of 46%. The variability in runoff due to changes in summer weather is therefore much higher than the variability

due to changing spring conditions. For some individual outlet glaciers, the contribution of changing spring conditions is larger. For Brúarjökull, the average σ_{spring} is 50% of the σ_{summer}, with a maximum of 79%.

These results are also illustrated in Figure 8, which shows the time series for the whole glacier and for selected outlet glaciers for all model runs. Relevant statistical values for this figure are given in Table 3. The grey area shows the span of the runoff between the different runs and the red line shows runoff when the spring conditions of the specific year are used. Three outlet glaciers are shown, Brúarjökull, due to its high sensitivity to spring conditions, Síðujökull, which has a slightly smaller sensitivity, and Skaftá GWC, which has a low sensitivity. To get a range on the effect of the spring conditions over the entire time series, the best conditions for runoff are chosen for every year, i.e., the years with the least spring snow, and the worst conditions for runoff are chosen for every year, i.e., the years with the most spring snow. For Vatnajökull, the total runoff when the best conditions are chosen is ∼19% higher than the runoff when the worst conditions are chosen. For Brúarjökull this difference is ∼53%, for Síðujökull it is ∼27%, and for Skaftá GWC only ∼14%.

Table 3. The mean runoff of all the sensitivity runs (SR), the mean runoff when the maximum and minimum runoff is chosen for the whole time series and the percentage increase in runoff between the maximum and the minimum. σ_{spring} is the mean standard deviation in runoff when the spring conditions are varied and σ_{summer} is the mean standard deviation in runoff when the summer weather is varied. The mean runoff of the thick snow (TS) run, and the difference in runoff between the original simulation and the thick snow simulation are also given.

	Mean SR (m w.eq.)	Min SR (m w.eq.)	Max SR (m w.eq.)	SR Diff (%)	σ_{spring}	σ_{summer}	Mean TS (m w.eq.)	TS Diff (%)
Vatnajökull	4.0	3.8	4.5	19.4	0.17	0.54	3.5	13.6
Bruárjökull	3.2	2.8	4.3	53.3	0.31	0.61	2.5	27.2
Siðujökull	4.0	3.7	4.7	26.8	0.23	0.70	3.6	11.8
Skaftá GWC	3.6	3.4	3.9	13.6	0.12	0.64	3.4	7.4

The black lines in Figure 8 show the simulated amount of runoff for each year if there is a thick snow thickness that does not disappear during the summer. Comparing the thick snow run with the original runoff simulations (1980–2015 with accurate spring snow thickness), there is a 14% increase in runoff from Vatnajökull averaged over the entire period since 1980 when exposed ice is allowed, with a maximum amount of 31% in 2005. Individual outlet glaciers have a larger sensitivity to the spring conditions, as for Brúarjökull the simulations estimate that the runoff is increased with an average 27% over the entire period when ice is exposed compared to the thick snow run, with a maximum amount of 77% in 2005.

In addition to the sensitivity studies, the results of the experiment can be used as a statistical method to estimate the most likely runoff from the modeled outlet glaciers. Since snow thickness and summer weather from the last 36 years have been used, all these runs can provide an estimate of the most likely values of runoff based on present climate. Probability distributions for the whole ice cap and the three chosen outlet glaciers are shown in Figure 8b,d,f,h. These show the most likely runoff from the glaciers based on the present climate, as well as the lowest and highest expected values. However, it is important to note that the effect of volcanic eruptions and dust in the surface from sources outside the glacier [62,63], as well as glacial runoff in the form of jökulhlaups, are not considered with this evaluation. In these instances, the runoff can be much higher than the modeled distributions. This method therefore works best for an estimation of the lowest runoff from a glacier based on the current climate.

Another important aspect of hydrological monitoring is the timing and onset of melt. Figure 9 shows the percentage of the glacier area which is experiencing melt for the whole ice cap and the same three outlets discussed previously. As an example, the earliest and latest date that 20% of the area has experienced melt onset, defined as having experienced more than 0.1 mm w.eq. of melt over five

consecutive days, is shown with a stippled black line. Figure 9a,c,e,g show the melt area when the spring conditions are held constant using the simulated conditions from 2000, where the colored lines are the results using 1980–2015 summer forcing. The difference between when 20% of the area has experienced melt onset is 56–62 days depending on the outlet, and the difference in melt area between the different summers can be up to 80–98% of the area, depending on the outlet.

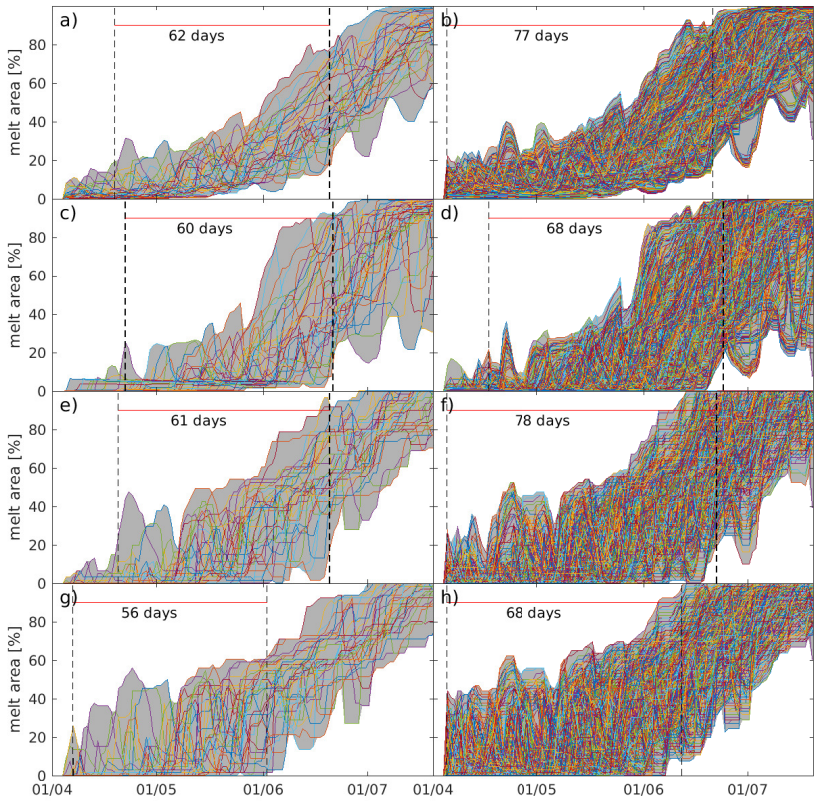

Figure 9. Time series of melt area for (**a**,**b**) Vatnajökull; (**c**,**d**) Brúarjökul; (**e**,**f**) Skaftá GWC; (**g**,**h**) Síðujökull. The four left figures show the melt area when the spring conditions are held constant, using the conditions from April 2000. The right figures show all the simulated runs. The colored lines are different summers from 1980 to 2015. The stippled lines show the earliest and latest day that 20% of the area has had an onset in melt.

Figure 9b,d,f,h show the melt area of all the runs, i.e., with both changing summer forcing and spring conditions. The changing spring conditions shift the dates when 20% melt onset occurs, but once again the effect is not as large as that of changing summer forcing. The difference between when 20% of the area has experienced melt onset is increased with 7–17 days, depending on the outlet.

To validate if the area of the ablation zone is accurate in the model and the variation in ELA between the SR, we investigate how often each model point becomes snow-free. Figure 10 shows the fraction of the 1296 runs in each grid point which becomes snow-free at some time over the summer. The location of the ablation is realistic. The ablation zone points always become snow-free, while around the equilibrium line it depends on the weather and initial conditions. The location of the

equilibrium line is generally consistent with observations. This can e.g., be seen for Brúarjökull, where the equilibrium line has been at approximately 1200 m since 1996 on the western part of the glacier, whereas on the eastern part it has been at approximately 1100 m in the same period. The simulations of the eastern part of Brúarjökull are consistent with this, while for about 60% of the model runs the ELA is slightly lower than observed on the western part.

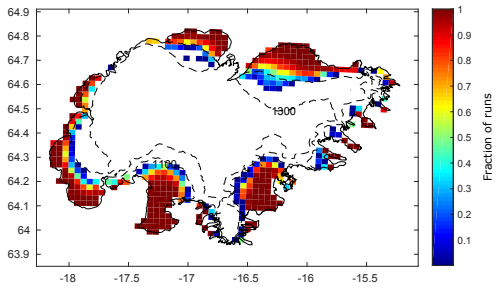

Figure 10. The fraction of the 1295 model runs where the grid points have exposed ice at some time during the summer.

Having determined that the location of the snow-free area is realistic, we also investigate how much the varying spring conditions advanced or delayed the timing of exposure of ice in each grid point. Figure 11 shows the mean spread (max-min) in the day when the ice surface is exposed when the summer weather is held constant while the spring conditions are varied. The largest spread is found in the lower part of Brúarjökull and Dyngjujökull, as well as the middle of Skeiðarárjökull. These areas all become snow-free every year and have a large dependency on the spring snow thickness. There is a fairly large average deviation between the first ice-free day when the spring conditions are varied, as most points have an average spread of 1–3 months between the first day the surface becomes snow-free.

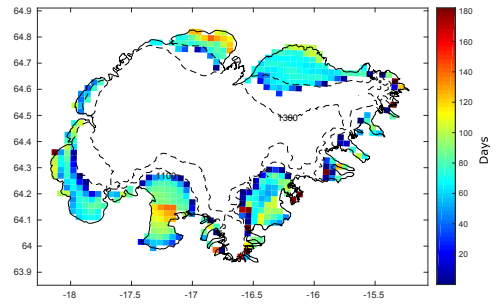

Figure 11. The average spread (max-min) in DOY when each ice point becomes snow-free when the summer weather is kept constant and the spring conditions are altered.

5. Discussion

5.1. Modelling of Runoff

While the simulated runoff from Skaftá GWC and Brúarjökull was captured well by the HIRHAM5 snow pack model in combination with HARMONIE-AROME meteorological forcing, with correlations of 0.78 and 0.89 and RMSEs of 0.2 km^3 and 0.7 km^3 (Table 2), comparisons to observations on a daily time scale yield larger deviations. The HIRHAM5 snow pack model is not a hydrological model,

and therefore does not have any scheme for routing of runoff. The only delay taken into account by the model is a runoff time scale based on the surface slope of the glacier. The structure of the path of the melt water determines how efficiently the water is expelled from the glacier. There are many processes which control the path, and the efficiency of water transport is very variable over the runoff season. For example, water flow through snow is significantly slower than flow over bare ice, and a thick snow pack therefore contributes to runoff delay (e.g., [64,65]). The presence and number of moulins and crevasses to transport water to the glacier bed (e.g., [65,66]) and the timing and shape of subglacial channels (e.g., [67]) also affect the timing of runoff to the rivers.

Since the runoff delay is not considered in the simulations, the daily runoff is more variable in the simulation than in the observations. Figure 12a shows an example from 2012 of the daily modeled and observed runoff. Compared to the seasonal means given in Table 2, the daily runoff has a much higher RMSE compared to the mean and a lower correlation (Table 4). To investigate the runoff delay, a 1-day shift in the observations was added to account for a runoff delay in the order of 12 h. This improved both the correlation, RMSE and NSE for both glacial rivers. Smoothing the time series but using a 7-day mean is another way to account for the delay. As shown in Figure 12b, a 7-day average improves the fit between observations and simulations. The Nash–Sutcliffe model efficiency coefficient (NSE) is also improved. The better fit for the 7-day average is also clearly showcased in the boxplot of the prediction error showed in Figure 12c. The 7-day average smoothes the time series which results in fewer outliers from the distribution. The quantiles and the median are also closer to zero in the weekly plot than in the daily.

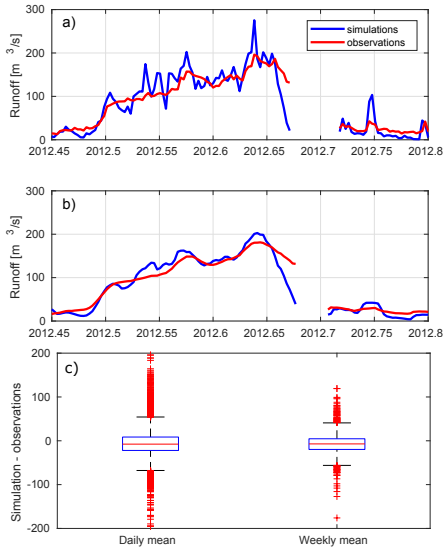

Figure 12. (**a**) Daily and (**b**) weekly mean observed and simulated runoff from Skaftá GWC; (**c**) Box plots of the prediction error for daily and weekly comparisons for the entire time series.

Table 4. Comparison statistics of the runoff (April–October) from Skaftá GWC into Skaftá river and from Brúarjökull into Jökulsá á Dal river at Hjarðarhagi (1980–2007) and Hálslón reservoir (2007–2015) according to observations and the simulation. The mean difference, RMSE, correlation, and Nash–Sutcliffe model efficiency coefficient are given. The RMSE, correlation, and NSE are calculated both for daily means, daily means with a model shift of one day, and weekly means.

Glacial Catchment	Period	Timescale	Mean Obs Runoff (m^3/s)	Model-Obs (m^3/s)	RMSE (m^3/s)	r	NSE
Skaftá GWC	1986–2015	Daily	58.0	−4.1	41.1	0.75	0.44
		1-day shift			38.9	0.78	0.50
		Weekly			32.0	0.82	0.66
Brúarjökull	1980–2015	Daily	183.9	−83.4	144.9	0.73	0.42
		1-day shift			137.6	0.77	0.51
		Weekly			121.7	0.84	0.59

5.2. Sensitivity of Runoff to Winter Snow Cover

One of the aims of this study was to quantify the sensitivity of runoff to the spring snow thickness for Vatnajökull and investigate whether the summer runoff could be inferred from the spring snow thickness. As shown in Figures 7 and 8, the summer runoff does not have a high dependency on the spring snow thickness, with the magnitude of the effect varying greatly between outlets. Although a large snow thickness will of course lead to less runoff than a small snow thickness, the weather conditions during the summer have a much larger effect on the runoff, as the effect of changing spring snow thickness is on average 31% of the variation due to changing weather conditions during the summer.

While the larger effect of changes in summer weather is not surprising, the advantage of the method used in this study is that we can quantify the importance of the spring snow thickness, and how much of the variability in runoff over the last 36 years is due to changes in summer conditions and how much is due to changes in winter accumulation. A study like this using over a thousand potential summer variations has not previously been done and provides a sound statistical background for assessing the sensitivity. For the entire glacier, we could estimate the amount of runoff due to the exposed dark ice (on average 14% for Vatnajökull since 1980) and how much of the runoff variability is due to changes in summer climate and how much due to changes in winter accumulation. The model runs also provide an estimate for individual outlet glaciers, as e.g., Brúarjökull has a large sensitivity to changes in spring snow thickness. According to the simulations, an estimated average of 27% of the runoff since 1980 is due to exposed dirty ice on Brúarjökull. In addition, the variation in runoff for Brúarjökull due to changing spring conditions is 50% of that due to changing summer weather.

5.3. Error Sources

HARMONIE-AROME meteorological forcing was chosen to drive the HIRHAM5 snow pack model to reduce the errors, but comparison with available AWS observations showed clear model biases. The incoming shortwave radiation still has an average overestimation of 2.4 W m^{-2} when compared to AWS observations, while the incoming longwave radiation and turbulent fluxes have an average underestimation of −13 W m^{-2} and −8.9 W m^{-2}, respectively. The outgoing longwave simulated by the snow pack scheme has an average underestimation of −1.3 W m^{-2}, while the outgoing shortwave is overestimated by 10 W m^{-2}. The deviation in outgoing shortwave radiation is partly due to an overestimation of incoming shortwave and precipitation, and partly due to the albedo scheme used in the snow pack model. The total deviation in energy available for melt is therefore approximately −28 W m^{-2} when compared to available AWS observations from May to September. This is equal to an underestimation in melt of approximately 0.7 cm/day. The meteorological input contributes a larger error than the snow pack simulations.

This general underestimation occurs even though the snow pack model and input data have been tuned to try to best fit available observations, as they are introduced into the simulations e.g., due to uncertainties in model structure, chosen parameters, and input data. One way we tried to correct the input data was by precipitation scaling by assume that the precipitation bias is time-invariant, and the scaling therefore can be applied to the entire time period. However, this assumption is only valid for short-term simulations, and the correction should therefore not be used for model runs of longer time scales. It is only applied to get the best possible simulation of the winter balance for the present day, so that the simulated spring conditions are as realistic as possible. In the mid-1990s there was a shift in the specific mass balance of Vatnajökull from positive to negative due to a rapid increase in the ocean temperature south of Iceland [8]. Few measurements of the mass balance before 1996 are available, and therefore the correction might not be applicable for the period before the shift. Nevertheless, the runoff from Skaftá GWC shows an equally good fit between model and measurements for the 1984–1996 period as for the 1996–present period.

Another error source is in the model setup. While running the snow pack scheme offline is a computationally cheap, fast, and flexible option, using this method ignores the feedbacks between the glacier conditions and the atmospheric circulation, such as e.g., the albedo and temperature. When forcing the snow pack scheme with HIRHAM5 incoming fluxes, the error due to neglected feedbacks is expected to be small. This is because only the refreezing [51] and the albedo [10] schemes have been altered from the online run, and changes in feedbacks due to these alterations should be small. On the other hand, running the snow pack scheme with a completely different model could lead to larger errors due to neglected feedbacks. For example, neither sublimation nor evaporation are calculated by the snow pack scheme, which affect the total water balance. However, since Vatnajökull is a temperate ice cap, sublimation and evaporation are generally assumed negligible.

6. Conclusions

In this study, we show that we can provide realistic estimates of the surface mass balance and runoff from Vatnajökull by combining the snow pack scheme from HIRHAM5 with the meteorological forcing from HARMONIE-AROME. HARMONIE-AROME was chosen as the forcing due to its complex atmospheric model using hydrostatic physics and prognostic precipitation, which simulate the incoming energy and mass fluxes needed to force the HIRHAM5 snow pack scheme better than atmospheric model in HIRHAM5.

The combined model can be used to simulate runoff on seasonal timescales, with high correlation (0.78 and 0.89) and small difference (16% and 29%) when compared to runoff observations from two rivers with a large glacial component. For this study, we were mostly interested in the total runoff from the glacier over the melt season and therefore not the routing of runoff. Coupling the snow pack scheme to a hydrological model which includes routing of runoff would be the next step to improve the comparison on short timescales. Additional work is also needed to simulate the runoff from ice-free zones, which would also improve the comparison.

The sensitivity of runoff to the spring snow thickness is evaluated by running a set of SR, using all the spring conditions from 1980 to 2015 as a starting point for runs over all the summers in the same period. We find that the variability in summer weather has a larger effect on the runoff than the variability in spring snow thickness, with an average variation in runoff due to changes in snow cover equal to only 31% of the variation due to summer weather for the whole ice cap. However, the spring snow thickness is still an important factor, especially for north-facing outlets, as e.g., Brúarjökull has an average variation in runoff due to changes in snow cover equal to 51% of the variation due to summer weather.

The range in values when the most extreme spring conditions are chosen are a good estimation of the importance of the spring conditions. The total runoff from Vatnajökull when the thinnest snow is chosen is ∼19% higher than the runoff when the thickest snow is chosen. For north-facing Brúarjökull this difference is ∼53%, for south-facing Síðujökull it is ∼27%, and for south-facing Skaftá GWC only

∼14%. Once again, we can conclude that while the spring snow cover is important for Brúarjökull, it is a less important factor for the south-facing outlets.

An additional simulation was conducted using thick enough snow so that the underlying ice surface is never exposed. This run was used to evaluate how much of the runoff from 1980 to 2015 was due to exposed dirty ice. We estimate that there was approximately a 14% increase in runoff from Vatnajökull due to the exposure of dirty ice from 1980 to 2015, a 27% increase from Brúarjökull, a 12% increase from Síðujökull, and a 7% increase from Skaftá GWC. As the climate warms and the dirty ice in the ablation zone is exposed earlier in the melt season, the amount of melt due to exposed ice is expected to increase. In these experiments, using only conditions simulated for the present climate, a maximum of 31% increase in runoff from Vatnajökull due to the exposure of dirty ice was found, while a maximum increase of 77% was simulated for Brúarjökull. The timing and duration of exposure of dirty ice can therefore have a large contribution to the amount of melt, and further investigations are needed to estimate the effect on the future mass balance. This could e.g., be done by using output from CORDEX simulations of the future climate to force the snow pack scheme. However, forcing the snow pack scheme with different models at lower resolution and not forced by reanalysis data will lead to new and larger biases that will need to be investigated and corrected before the model can be confidently applied.

Author Contributions: Conceptualization, L.S.S., P.L.L., G.A., F.P., S.G. and A.G.; Data curation, L.S.S.; Formal analysis, L.S.S.; Funding acquisition, L.S.S. and G.A.; Investigation, L.S.S.; Methodology, L.S.S., P.L.L., G.A. and F.P.; Software, L.S.S. and P.L.L.; Visualization, L.S.S.; Writing—original draft, L.S.S., P.L.L., G.A., F.P., S.G. and A.G.

Funding: This research was funded by the Icelandic Research Fund (RANNIS, Grant no. 140920-051), as well as the National Power Company of Iceland (Landsvirkjun) and Eimskip University fund.

Acknowledgments: This work is supported by project SAMAR, funded by the Icelandic Research Fund (RANNIS, Grant no. 140920-051), as well as the National Power Company of Iceland (Landsvirkjun) and Eimskip University fund. The simulations were performed on resources provided by the Icelandic High Performance Computing Centre at the University of Iceland. We would like to thank our editors Ivana Mae and Xue Liang, as well as three anonymous reviewers whose constructive feedback significanly improved this manuscript.

Conflicts of Interest: The authors declare that they have no conflict of interest.

References

1. Gregory, J.M.; White, N.J.; Church, J.A.; Bierkens, M.F.P.; Box, J.E.; van den Broeke, M.R.; Cogley, J.G.; Fettweis, X.; Hanna, E.; Huybrechts, P.; et al. Twentieth-Century Global-Mean Sea Level Rise: Is the Whole Greater than the Sum of the Parts? *J. Clim.* **2013**, *26*, 4476–4499. [CrossRef]
2. Jansson, P.; Hock, R.; Schneider, T. The concept of glacier storage: A review. *J. Hydrol.* **2003**, *282*, 116–129. [CrossRef]
3. Huss, M. Present and future contribution of glacier storage change to runoff from macroscale drainage basins in Europe. *Water Resour. Res.* **2011**, *47*. [CrossRef]
4. Kaser, G.; Grosshauser, M.; Marzeion, B. Contribution potential of glaciers to water availability in different climate regimes. *Proc. Natl. Acad. Sci. USA* **2010**, *107*, 20223–20227. [CrossRef] [PubMed]
5. Huss, M.; Hock, R. Global-scale hydrological response to future glacier mass loss. *Nat. Clim. Chang.* **2018**, *8*, 135–140. [CrossRef]
6. Aðalgeirsdóttir, G.; Guðmundsson, S.; Björnsson, H.; Pálsson, F.; Jóhannesson, T.; Hannesdóttir, H.; Sigurðsson, S.T.; Berthier, E. Modelling the 20th and 21st century evolution of Hoffellsjökull glacier, SE-Vatnajökull, Iceland. *Cryosphere* **2011**, *5*, 961–975. [CrossRef]
7. Vaughan, D.G.; Comiso, J.C.; Allison, I.; Carrasco, J.; Kaser, G.; Kwok, R.; Mote, P.; Murray, T.; Paul, F.; Ren, J.; et al. Observations: Cryosphere. In *Climate Change 2013: The Physical Science Basis. Contribution of Working Group I to the Fifth Assessment Report of the Intergovernmental Panel on Climate Change*; Stocker, T.F., Qin, D., Plattner, G.K., Tignor, M., Allen, S.K., Boschung, J., Nauels, A., Xia, Y., Bex, V., Midgley, P.M., Eds.; Cambridge University Press: Cambridge, UK; New York, NY, USA, 2013.

8. Björnsson, H.; Pálsson, F.; Guðmundsson, S.; Magnússon, E.; Aðalgeirsdõttir, G.; Jõhannesson, T.; Berthier, E.; Sigurdsson, O.; Thorsteinsson, T. Contribution of Icelandic ice caps to sea level rise: Trends and variability since the Little Ice Age. *Geophys. Res. Lett.* **2013**, *40*, 1546–1550. [CrossRef]
9. Björnsson, H.; Pálsson, F. Icelandic glaciers. *Jökull* **2008**, *58*, 365–386.
10. Schmidt, L.S.; Aðalgeirsdóttir, G.; Guðmundsson, S.; Langen, P.L.; Pálsson, F.; Mottram, R.; Gascoin, S.; Björnsson, H. The importance of accurate glacier albedo for estimates of surface mass balance on Vatnajökull: Evaluating the surface energy budget in a regional climate model with automatic weather station observations. *Cryosphere* **2017**, *11*, 1665–1684. [CrossRef]
11. Gascoin, S.; Guðmundsson, S.; Aðalgeirsdóttir, G.; Pálsson, F.; Schmidt, L.; Berthier, E.; Björnsson, H. Evaluation of MODIS Albedo Product over Ice Caps in Iceland and Impact of Volcanic Eruptions on Their Albedo. *Remote Sens.* **2017**, *9*, 399. [CrossRef]
12. Nawri, N.; Björnsson, H. *Surface Air Temperature and Precipitation Trends for Iceland in the 21st Century*; Technical Report; Veðurstofa Íslands: Reykjavik, Iceland, 2010.
13. Greuell, W.; Genthon, C. Modelling land-ice surface mass balance. In *Mass Balance of the Cryosphere*; Bamber, J.L., Payne, A.J., Eds.; Cambridge University Press: Cambridge, UK, 2004; pp. 117–168.
14. Meijgaard, E.V.; Ulft, L.H.V.; Bosveld, F.C.; Lenderink, G.; Siebesma, A.P. *The KNMI Regional Atmospheric Climate Model RACMO Version 2.1*; Technical Report, TR-302; Koninklijk Nederlands Meteorologisch Instituut: De Bilt, The Netherlands, 2008; p. 43.
15. Skamarock, W.C.; Skamarock, W.C.; Klemp, J.B.; Dudhia, J.; Gill, D.O.; Barker, D.M.; Wang, W.; Powers, J.G. *A Description of the Advanced Research WRF Version 3*; NCAR Technical Note-475+STR; Scientific Research: Wuhan, China, 2008.
16. Gallée, H.; Schayes, G. Development of a Three-Dimensional Meso-γ Primitive Equation Model: Katabatic Winds Simulation in the Area of Terra Nova Bay, Antarctica. *Mon. Weather Rev.* **1994**, *122*, 671–685. [CrossRef]
17. Christensen, O.B.; Drews, M.; Christensen, J.H.; Dethloff, K.; Ketelsen, K.; Hebestadt, I.; Rinke, A. *The HIRHAM Regional Climate Model Version 5*; Technical Report; Danish Meteorological Institute: Copenhagen, Denmark, 2006.
18. Box, J.E.; Rinke, A. Evaluation of Greenland Ice Sheet Surface Climate in the HIRHAM Regional Climate Model Using Automatic Weather Station Data. *J. Clim.* **2003**, *16*, 1302–1319. [CrossRef]
19. Langen, P.L.; Fausto, R.S.; Vandecrux, B.; Mottram, R.H.; Box, J.E. Liquid Water Flow and Retention on the Greenland Ice Sheet in the Regional Climate Model HIRHAM5: Local and Large-Scale Impacts. *Front. Earth Sci.* **2017**, *4*. [CrossRef]
20. Lenaerts, J.T.M.; Van Den Broeke, M.R. Modeling drifting snow in Antarctica with a regional climate model: 2. Results. *J. Geophys. Res. Atmos.* **2012**, *117*. [CrossRef]
21. Agosta, C.; Fettweis, X.; Datta, R. Evaluation of the CMIP5 models in the aim of regional modelling of the Antarctic surface mass balance. *Cryosphere* **2015**, *9*, 2311–2321. [CrossRef]
22. Giorgi, F.; Jones, C.; Asrar, G.R. Addressing climate information needs at the regional level: The CORDEX framework. *World Meteorol. Organ. Bull.* **2009**, *58*, 175.
23. Nawri, N.; Pálmason, B.; Petersen, N.G.; Björnsson, H.; Þorsteinsson, S. *The ICRA Atmospheric Reanalysis Project for Iceland*; Technical Report; Veðurstofa Íslands: Reykjavik, Iceland, 2017.
24. Christensen, J.H.; Boberg, F.; Christensen, O.B.; Lucas-Picher, P. On the need for bias correction of regional climate change projections of temperature and precipitation. *Geophys. Rese. Lett.* **2008**, *35*, L20709. [CrossRef]
25. Hagemann, S.; Chen, C.; Haerter, J.O.; Heinke, J.; Gerten, D.; Piani, C.; Hagemann, S.; Chen, C.; Haerter, J.O.; Heinke, J.; et al. Impact of a Statistical Bias Correction on the Projected Hydrological Changes Obtained from Three GCMs and Two Hydrology Models. *J. Hydrometeorol.* **2011**, *12*, 556–578. [CrossRef]
26. Muerth, M.J.; Gauvin St-Denis, B.; Ricard, S.; Velázquez, J.A.; Schmid, J.; Minville, M.; Caya, D.; Chaumont, D.; Ludwig, R.; Turcotte, R. On the need for bias correction in regional climate scenarios to assess climate change impacts on river runoff. *Hydrol. Earth Syst. Sci.* **2013**, *17*, 1189–1204. [CrossRef]
27. Gudmundsson, L.; Bremnes, J.B.; Haugen, J.E.; Engen-Skaugen, T. Technical Note: Downscaling RCM precipitation to the station scale using statistical transformations—A comparison of methods. *Hydrol. Earth Syst. Sci.* **2012**, *16*, 3383–3390. [CrossRef]
28. Switanek, M.B.; Troch, P.A.; Castro, C.L.; Leuprecht, A.; Chang, H.I.; Mukherjee, R.; Demaria, E.M.C. Scaled distribution mapping: A bias correction method that preserves raw climate model projected changes. *Earth Syst. Sci.* **2017**, *215194*, 2649–2666. [CrossRef]

29. Bengtsson, L.; Andrae, U.; Aspelien, T.; Batrak, Y.; Calvo, J.; de Rooy, W.; Gleeson, E.; Hansen-Sass, B.; Homleid, M.; Hortal, M.; et al. The HARMONIE–AROME Model Configuration in the ALADIN–HIRLAM NWP System. *Mon. Weather Rev.* **2017**, *145*, 1919–1935. [CrossRef]
30. Xu, M.; Yan, M.; Kang, J.; Ren, J. Comparative studies of glacier mass balance and their climatic implications in Svalbard, Northern Scandinavia, and Southern Norway. *Environ. Earth Sci.* **2012**, *67*, 1407–1414. [CrossRef]
31. Engelhardt, M.; Schuler, T.V.; Andreassen, L.M. Sensitivities of glacier mass balance and runoff to climate perturbations in Norway. *Ann. Glaciol.* **2015**, *56*, 79–88. [CrossRef]
32. De Woul, M.; Hock, R. Static mass-balance sensitivity of Arctic glaciers and ice caps using a degree-day approach. *Ann. Glaciol.* **2005**, *42*, 217–224. [CrossRef]
33. Gudmundsson, M.T.; Thordarson, T.; Höskuldsson, Á; Larsen, G.; Björnsson, H.; Prata, F.J.; Oddsson, B.; Magnússon, E.; Högnadóttir, T.; Petersen, G.N.; et al. Ash generation and distribution from the April–May 2010 eruption of Eyjafjallajökull, Iceland. *Sci. Rep.* **2012**, *2*, 572. [CrossRef] [PubMed]
34. Oerlemans, J.; Björnsson, H.; Kuhn, M.; Obleitner, F.; Palsson, F.; Smeets, C.; Vugts, H.F.; Wolde, J.D. Glacio-Meteorological Investigations On Vatnajökull, Iceland, Summer 1996: An Overview. *Bound.-Layer Meteorol.* **1999**, *92*, 3–24. [CrossRef]
35. Guðmundsson, S.; Björnsson, H.; Pálsson, F.; Haraldsson, H.H. Energy balance of Brúarjökull and circumstances leading to the August 2004 floods in the river Jökla, N-Vatnajökull. *Jökull* **2006**, *55*, 121–138.
36. Björnsson, H.; Palsson, F.; Guðmundsson, M.T. *Afkoma, Hreyfing og Afrennsli á Vestan-og Norðanverðum Vatnajokli Jökulárin 1992–1993 og 1993 (Mass Balance, Movement and Runoff on Western and Northern Vatnajökull Hydrological Years 1992–1993 and 1993–1994)*; Technical Report; University of Iceland: Reykjavik, Iceland, 1995.
37. Landsvirkjun. *Wiski Database 28.11.2017—M00328*; WISKI: Roseville, CA, USA, 2017.
38. Snorrason, A.; Gunnarsson, A.; Jónsson, P.; Einarsson, K.; Sigurðsson, O. *Summary of Available Hydrological Information in the Jökulsá á Deal and Jökulsá í Fljótsdal Basins, Iceland*; Technical Report; Orkustofnun: Reykjavik, Iceland, 1998.
39. Icelandic Meteorological Office Database. *Discharge Data 1986–2016*; Icelandic Meteorological Office Database: Reykjavik, Iceland, 2017.
40. Hardarðóttir, J.; Snorrason, A. Sediment monitoring of glacial rivers in Iceland: New data on bed load transport. *Hydrol. Sci. J.* **2003**, *283*, 154–163.
41. Schulla, J. *Model Description WaSiM (Water Balance Simulation Model)*; Technical Report; Hydrology Software Consulting J. Schulla: Zurich, Switzerland, 2017.
42. Jónsdóttir, J.F. A runoff map based on numerically simulated precipitation and a projection of future runoff in Iceland / Une carte d'écoulement basée sur la précipitation numériquement simulée et un scénario du futur écoulement en Islande. *Hydrol. Sci. J.* **2008**, *53*, 100–111. [CrossRef]
43. Einarsson, B. *Improving Groundwater Representation and the Parameterization of Glacial Melting and Evapotranspiration in Applications of the WaSiM Hydrological Model within Iceland Improving Groundwater Representation and the Parameterization of Glacial Melting and Eva*; Technical Report; Icelandic Meteorological Office: Reykjavi, Iceland, 2010.
44. Björnsson, H. The cause of jökulhlaups in the Skaftá-river, Vatnajökull. *Jökull* **1977**, *27*, 71–78.
45. Björnsson, H. *Hydrology of Ice Caps in Volcanic Regions*; Societas Scientarium Islandica, University of Iceland: Reykjavik, Iceland, 1988; p. 139.
46. Eerola, K. About the performance of HIRLAM version 7.0. *HIRLAM Newsl.* **2006**, *51*, 93–102.
47. Roeckner, E.; Bäuml, G.; Bonaventura, L.; Brokopf, R.; Esch, M.; Giorgetta, M.; Hagemann, S.; Kirchner, I.; Kornblueh, L.; Manzini, E.; et al. *The Atmospheric General Circulation Model ECHAM 5 PART I: Model Description*; Technical Report 349; MPI für Meteorologie: Hamburg, Germany, 2003.
48. Dee, D.P.; Uppala, S.M.; Simmons, A.J.; Berrisford, P.; Poli, P.; Kobayashi, S.; Andrae, U.; Balmaseda, M.A.; Balsamo, G.; Bauer, P.; et al. The ERA-Interim reanalysis: Configuration and performance of the data assimilation system. *Q. J. R. Meteorol. Soc.* **2011**, *137*, 553–597. [CrossRef]
49. Stendel, M.; Christensen, J.H.; Petersen, D. High-Arctic Ecosystem Dynamics in a Changing Climate. In *Advances in Ecological Research*; Elsevier: Amsterdam, The Netherlands, 2008; Volume 40, pp. 13–43. [CrossRef]
50. Lucas-Picher, P.; Wulff-Nielsen, M.; Christensen, J.H.; Aðalgeirsdóttir, G.; Mottram, R.H.; Simonsen, S.B. Very high resolution regional climate model simulations over Greenland: Identifying added value. *J. Geophys. Res.* **2012**, *117*, 2108. [CrossRef]

51. Langen, P.L.; Mottram, R.H.; Christensen, J.H.; Boberg, F.; Rodehacke, C.B.; Stendel, M.; van As, D.; Ahlstrøm, A.P.; Mortensen, J.; Rysgaard, S.; et al. Quantifying energy and mass fluxes controlling godthåbsfjord freshwater input in a 5-km simulation (1991–2012). *J. Clim.* **2015**, *28*, 3694–3713. [CrossRef]
52. Rae, J.G.L.; Aðalgeirsdóttir, G.; Edwards, T.L.; Fettweis, X.; Gregory, J.M.; Hewitt, H.T.; Lowe, J.A.; Lucas-Picher, B.; Mottram, R.H.; Payne, A.J.; et al. Greenland ice sheet surface mass balance: Evaluating simulations and making projections with regional climate models. *Cryosphere* **2012**, *6*, 1275–1294. [CrossRef]
53. Seity, Y.; Brousseau, P.; Malardel, S.; Hello, G.; Bénard, P.; Bouttier, F.; Lac, C.; Masson, V.; Seity, Y.; Brousseau, P.; et al. The AROME-France Convective-Scale Operational Model. *Mon. Weather Rev.* **2011**, *139*, 976–991. [CrossRef]
54. Schaaf, C.; Wang, Z. MCD43A3 MODIS/Terra+Aqua BRDF/Albedo Daily L3 Global—500 m V006. *NASA EOSDIS Land Process. DAAC* **2015**. [CrossRef]
55. Guðmundsson, M.T. Mass balance and precipitation on the summit plateau of Öræfajökull, SE-Iceland. *Jökull* **2000**, *48*, 49–54.
56. Belart, J.M.; Magnússon, E.; Berthier, E.; Gunnarsson, A.Þ.; Pálsson, F.; Aðalgeirsdóttir, G.; Björnsson, H. Spatially distributed mass balance of Icelandic glaciers and ice caps, 1945–present. Trends and link with climate. *Earth Syst. Sci. Data* **2018**, in press.
57. Guðmundsson, S.; Björnsson, H.; Pálsson, F.; Haraldsson, H.H. Comparison of energy balance and degree-day models of summer ablation on the Langjökull ice cap, SW-Iceland. *Jökull* **2009**, *59*, 1–18.
58. Bellaire, S.; Jamieson, B. Forecasting the formation of critical snow layers using a coupled snow cover and weather model. *Cold Reg. Sci. Technol.* **2013**, *94*, 37–44. [CrossRef]
59. Vionnet, V.; Dombrowski-Etchevers, I.; Lafaysse, M.; Quéno, L.; Seity, Y.; Bazile, E.; Vionnet, V.; Dombrowski-Etchevers, I.; Lafaysse, M.; Quéno, L.; et al. Numerical Weather Forecasts at Kilometer Scale in the French Alps: Evaluation and Application for Snowpack Modeling. *J. Hydrometeorol.* **2016**, *17*, 2591–2614. [CrossRef]
60. Larsen, K.M.H.; Gonzalez-Pola, C.; Fratantoni, P.; Beszczynska-Möller, A.; Hughes, S.L. ICES Report on Ocean Climate 2015. *ICES Coop. Res. Rep.* **2016**, *331*, 79.
61. Jones, P.D.; Lister, D.H.; Osborn, T.J.; Harpham, C.; Salmon, M.; Morice, C.P. Hemispheric and large-scale land-surface air temperature variations: An extensive revision and an update to 2010. *J. Geophys. Res. Atmos.* **2012**, *117*. [CrossRef]
62. Dragosics, M.; Meinander, O.; Jónsdóttír, T.; Dürig, T.; De Leeuw, G.; Pálsson, F.; Dagsson-Waldhauserová, P.; Thorsteinsson, T. Insulation effects of Icelandic dust and volcanic ash on snow and ice. *Arab. J. Geosci.* **2016**, *9*, 126. [CrossRef]
63. Wittmann, M.; Groot Zwaaftink, C.D.; Steffensen Schmidt, L.; Guðmundsson, S.; Pálsson, F.; Arnalds, O.; Björnsson, H.; Thorsteinsson, T.; Stohl, A. Impact of dust deposition on the albedo of Vatnajökull ice cap, Iceland. *Cryosphere* **2017**, *11*, 741–754. [CrossRef]
64. Fountain, A.G. Effect of snow and firn hydrology on the physical and chemical characteristics of glacier runoff. *Hydrol. Process.* **1996**, *10*, 509–521. [CrossRef]
65. Nienow, P.; Hubbard, B. Surface and Englacial Drainage of Glaciers and Ice Sheets. In *Encyclopedia of Hydrological Sciences*; John Wiley & Sons, Ltd.: Chichester, UK, 2005. [CrossRef]
66. Banwell, A.; Hewitt, I.; Willis, I.; Arnold, N. Moulin density controls drainage development beneath the Greenland ice sheet. *J. Geophys. Res. Earth Surf.* **2016**, *121*, 2248–2269. [CrossRef]
67. Flowers, G.E.; Björnsson, H.; Pálsson, F. New insights into the subglacial and periglacial hydrology of Vatnajökull, Iceland, from a distributed physical model. *J. Glaciol.* **2003**, *49*, 257–270. [CrossRef]

Sample Availability: The ICRA HARMONIE-AROME runs over Iceland, as well as the Skaftá runoff time series and WaSiM model results, can be acquired by contacting the Icelandic Meteorological office. The runoff measurements from Hálslón and Hjarðarhagi can be acquired by contacting the Icelandic power company Landsvirkjun. Measurements from automatic weather stations and from in situ mass balance surveys are partially owned by the National Power Company of Iceland and are therefore not publicly available at this time.

Paper III

Dynamic simulations of Vatnajökull ice cap from 1980-2300

Louise Steffensen Schmidt, Guðfinna Aðalgeirsdóttir, Sverrir Guðmundsson, Peter L. Langen, Finnur Pálsson, and Helgi Björnsson

In preparation for The Cryosphere

Dynamic simulations of Vatnajökull ice cap from 1980-2300

Louise Steffensen Schmidt[1], Guðfinna Aðalgeirsóttir[1], Finnur Pálsson[1], Peter L. Langen[2], Sverrir Guðmundsson[1,3], and Helgi Björnsson[1]

[1]Institute of Earth Science, University of Iceland, 101 Reykjavik, Iceland
[2]Danish Meteorological Office, 2100 Copenhagen, Denmark
[3]Veitur Utilities, 110 Reykjavik, Iceland

Correspondence: L.S. Schmidt (lss7@hi.is)

Abstract. Like most ice caps and glaciers worldwide, Icelandic glaciers are losing mass and retreating in a warming climate. Here, the evolution of Vatnajökull ice cap, Iceland, from 1980-2300 is simulated by one-way coupling of Regional Climate Models with the Parallel Ice Sheet Model (PISM). For climate simulations of the recent past, we use simulations derived from the numerical weather prediction model HARMONIE-AROME forced by ERA-Interim global reanalysis dataset, which have previously been evaluated over Vatnajökull. For future climate conditions we use simulations from HIRHAM5 forced by the GCM EC-EARTH. While PISM has been used for ice sheets on both Greenland and Antarctica, it has not previously been used for Vatnajökull. The model is therefore first evaluated against surface velocity measurements from 1992-2016, in order to determine the most appropriate glacier softness and sliding parameters. A model spin-up using the simulated 1980-1999 climate is performed in order for the modeled ice flow to be in equilibrium with the simulated climate forcing. The modeled spin up ice cap is reasonably close to the observed Vatnajökull geometry during this period, with a volume and area that are within 3.5% and -2.5% of the present day values. Considering that most of the outlets of Vatnajökull are surge type glaciers, these discrepancies are considered acceptable.

The glacier evolution is modeled using the representative concentration pathway (RCP) 4.5 scenario (assumes radiative forcing stabilizes at 4.5 W/m^2 by 2100) and the RCP 8.5 scenarios (assumes radiative forcing reaches 8.5 W/m^2 by 2100 but the forcing does not stabilize) until 2100. To extend the time series, the 2081-2100 climate forcing is repeated until 2300. Forced by simulations under the RCP 4.5 scenario the ice cap loses 44% of its volume and 23% of its area by 2300, whereas when forced by simulations under the RCP 8.5 scenario it loses 85% of its volume and 65% of its area. These simulations are one-way coupled, and therefore do not include any elevation feedback on the mass balance. In an attempt to estimate the likely effect of the feedback on precipitation and the energy balance, precipitation and temperature lapse rates are included in some of the simulations. By 2300, the lapse rate runs has a 9-14% smaller volume and a 9-20% smaller area than the runs without a lapse rate correction.

The model simulations were also conducted using available simulations from the Coordinated Regional Downscaling Experiment (CORDEX) over Iceland at a 12 km resolution for the same RCP scenarios. When using CORDEX simulations to force the ice flow model, a large span of area and volume changes is simulated due to differences in atmospheric physics between the CORDEX models. The RCP 4.5 scenario leads to volume losses between 31 and 64% by 2300 and area losses between 13 and 37%. For RCP 8.5 scenario, the volume decrease is between 51 and 94% by 2300 and the area decrease is between 24 and 80%.

1 Introduction

As a response to a globally changing climate, glaciers and ice caps worldwide have been retreating with increasing speed (e.g. IPCC, 2013; Barletta et al., 2013; Huss and Hock, 2018). Future climate change will likely have a significant impact on the dimensions of existing glaciers, which will affect the sea level and climate throughout the world. On regional scales, glacier retreat can affect hydropower production, freshwater availability, infrastructure, and wildlife (e.g. Xu et al., 2012; Kaser et al., 2010; Boberg et al., 2018). It is therefore important to investigate the effect of climate change on the cryosphere both on global and regional scales.

In order to asses the large-scale effects of a changing climate, state-of-the-art Global Climate Models (GCMs) are used internationally to make past and future projections. The Coupled Model Intercomparison Project (CMIP) was initiated in 1995 to provide a framework for GCM validation and provide publicly available simulations from a large collection of models. Simulations from phase 5 of the project (Taylor et al., 2012) have provided simulations spanning until at least 2100, and simulations for the next phase of the project (Eyring et al., 2016) are currently in progress.

However, due to the high computational cost of GCMs, they run with a coarse (100-200 km) resolution which neither resolves smaller glaciers nor accounts for all significant surface processes. Dynamically downscaling climate projections from GCMs using Regional Climate Models (RCMs) is therefore a useful method to better resolve specific areas or investigate surface processes not resolved in GCMs. RCMs have been used and evaluated in several studies of the surface mass balance of glaciers in e.g. Greenland (e.g. Box and Rinke, 2003; Rae et al., 2012; Langen et al., 2017; Fettweis et al., 2017), Antarctica (e.g. Lenaerts and Van Den Broeke, 2012; Agosta et al., 2015), and Iceland (e.g. Schmidt et al., 2017, 2018). To advance and evaluate models used for regional downscaling through international cooperation, the Coordinated Regional Downscaling Experiment (CORDEX) was started in 2009 (Giorgi et al., 2009). Through this project, a collection of historical and future simulations with different RCMs, driving GCMs, domains, and initialization were made publicly available. The RCMs included in the CORDEX project are forced by selected GCM simulations from CMIP Phase 5 at the vertical boundaries. Different RCMs and GCMs can project a highly variable evolution of the cryosphere even when the same initial conditions and greenhouse gas concentration scenarios are used. In order to have confidence in climate projections, it is therefore important to consider the output from several different models.

Most RCMs have a fixed topography, and therefore do not account for feedback caused by surface elevation changes nor for glacier retreat/advance. Coupling to a flow model is therefore needed in order to simulate a dynamically evolving glacier surface. One way coupling of RCMs to ice flow models have been attempted in a number of studies (e.g. Aðalgeirsdóttir et al., 2011; Gong et al., 2014; Aðalgeirsdóttir et al., 2014), which allows for a dynamically changing ice cap but does not include feedbacks on precipitation, temperature, wind speed etc. due to changes in surface elevation. Studies have shown that neglecting these feedbacks can lead to a significant underestimation in sea level projections (Edwards et al., 2014; Schäfer et al., 2015). However, as a two-way coupling of climate models with ice flow models present substantial computational challenges, fully coupled simulations are rarely performed. Some studies have attempted to solve this issue by adding an elevation dependent correction to the simulated mass balance in order to estimate the effect of the feedback (e.g. Edwards et al., 2014; Schäfer et al., 2015).

Like most glaciers worldwide, Icelandic glaciers have been loosing mass since the late 1990s. Glaciers currently cover about 10% of Iceland (Björnsson, 2017). Vatnajökull ice cap, the largest ice cap in Iceland and the focus of this study, experienced slightly positive mass balance in the 1980s, but mass balance shifted towards negative after the mid-1990s following a sud-

den increase in sea-surface temperatures at the SE-coast (Björnsson et al., 2013). From the 1995-96 glaciological year until 2013-14, the ice cap had a negative mass balance of approximately -0.8 m water equivalent (w.eq.) pr year. In the 2014-15 glaciological year, the mass balance was positive, while in the 2016-17 and 2017-18 glaciological years the mass balance was close to zero (e.g. Pálsson et al., 2015, 2017).

For Vatnajökull, the RCM HIRHAM5 has been used for studies of the ice cap climate by Schmidt et al. (2017, 2018). Only reanalysis driven runs were used for these studies, and therefore only the reconstruction of the past climate was evaluated. The simulations had a high correlation with observed specific mass balance observations back to 1992, but with an overestimation of the precipitation in areas with high orographic forcing. Several other studies by e.g. Aðalgeirsdóttir et al. (2006, 2011) have used RCM output for studies of the past and present climate of the ice cap, but these studies only use the precipitation and temperature fields from the RCMs to simulate the ablation using a positive degree day model.

In this study, the RCM HIRHAM5 forced by EC-EARTH at a 5.5 km resolution is evaluated and used to simulate the climate of Vatnajökull ice cap until 2100, thus expanding on the work of Schmidt et al. (2017). Two greenhouse gas concentration scenarios are considered, Representative Concentration Pathways (RCP) 4.5 and 8.5. In the RCP 4.5 scenario (Thomson et al., 2011), greenhouse gas concentration steadily increase until the radiative forcing stabilizes at 4.5 Wm^{-2} in 2100. At the end of the century, the average worldwide temperature increase is approximately 2.4 °C. The RCP 8.5 scenario (Riahi et al., 2011) is the RCP scenario with the highest projected greenhouse gas concentration, as the concentration increases significantly during the second half of the 21st century until the radiative forcing reaches 8.5 Wm^{-2} in 2100. The radiative forcing does not stabilize in this scenario, and it leads to an average worldwide temperature increase of 4.7 °C. In order to investigate the range in values for different simulations, available CORDEX simulations over Iceland at a 12 km resolution are used to get a range of projections. The HIRHAM5-ECEARTH simulations are also included within the CORDEX framework but at a lower spatial resolution. The same two RCP scenarios are considered from the CORDEX simulations.

The RCM simulations are used to force the Parallel Ice Flow Model (PISM) (Bueler and Brown, 2009) in order to simulate the changes in glacier volume and area. The optimal settings and flow parameters for simulations of Vatnajökull are investigated by comparing the simulated surface velocities with available observations. PISM is one-way coupled to the RCMs, which means that important elevation feedback on the mass balance is neglected. In order to estimate the sensitivity of the ice cap to elevation changes, precipitation and temperature lapse rates are added to some of the simulations.

This is the first study using PISM and distributed surface mass balances from several RCMs to model the evolution of all of Vatnajökull. However, modelling of the evolution of the whole ice cap or selected glacier outlets using flow models has been done in studies by e.g. Björnsson et al. (2000), Aðalgeirsdóttir (2003); Aðalgeirsdóttir et al. (2005, 2006, 2011), Flowers et al. (2003, 2005) and Marshall et al. (2005). Aðalgeirsdóttir (2003) used a flow model with the shallow ice approximation (SIA), a prescribed sliding, and a mass balance depending on the equilibrium line altitude (ELA) to try to model the present state of the entire ice cap. They found that Vatnajökull is not close to a stable steady state at the present time, with simulated steady states either smaller or much larger than the current ice cap. Flowers et al. (2003) modeled the whole ice cap with a glaciohydraulic model, which was later coupled to an ice sheet model in Flowers et al. (2005) and Marshall et al. (2005). The coupled model included hydrological feedback on the basal sliding and was driven by climate change scenarios with an increased warming of 0-4°C. The mass balance was calculated using a positive degree day model. The authors were able to simulate a present day, steady state ice cap that was within 3-4% of the observed volume and area. In addition, the simulations showed that Vatnajökull is sensitive to modest warming, with a 2°C warming leading to a 18-25% decrease in volume by 2100, and that it can react rapidly to sustained changes in climate. Marshall et al. (2005) similarly found that an equilibrium state could be found for Vatnajökull which resembled the present day volume. However, the equilibrium configuration was very dependant on

temperature, with even small changes in temperature leading to a much larger or much smaller ice cap. The authors concluded that Vatnajökull is very sensitive to small, sustained shifts in temperature. The results of these studies will be discussed in the context of the simulations presented in this paper.

2 Study area and Observations

2.1 Study Area

Vatnajökull ice cap, currently $\sim$7800 km^2, is the largest temperate ice cap in Europe. It has a surface elevation in the range 0–2110 m above sea level (a.s.l.) and is located close to the southeastern coast of Iceland (Figure 1). Annual average temperatures on the ice cap are close to or below freezing. The summer balance has in recent years been negative for the entire ice cap, but the central area occasionally turns slightly positive during repeated cold spells. At the highest areas of the glacier, there are only 10-20 days a year with melting, while at lower elevation the ablation season generally lasts 3-4 months (Björnsson and Pálsson, 2008).

Vatnajökull lies partly within the active volcanic zone, and covers several of Iceland's largest volcanoes where eruptions are frequent (e.g. Björnsson and Einarsson, 1990; Gudmundsson et al., 2012). Western Vatnajökull mainly lies on porous lava beds, while eastern Vatnajökull lies on impermeable unconsolidated till (e.g. Björnsson, 1988). Tephra layers in the glacier ice dominate its spectral properties, and volcanic ash therefore has a large effect on the melt in the ablation zone (e.g. Larsen et al., 2016; Gascoin et al., 2017; Schmidt et al., 2017, 2018). Frequent dust storms also occur over the ice cap, darkening the surface and increasing melt (e.g. Dragosics et al., 2016). In addition to surface melting, geothermal activity below the glacier provides a small contribution to the total melt on average (Björnsson and Pálsson, 2008).

All the major outlets of Vatnajökull are surge-type glaciers, and about 75% of the ice cap area can be affected by surges (Björnsson et al., 2003). Recorded surge histories suggest that some outlets surge at regular intervals, with e.g. north-facing Brúarjökull surging at 80-100 years intervals, while others surge at varying intervals, with e.g. south-east facing Breiðamerkurjökull surging at between 6 and 38 year intervals. In the 1990s, approximately 25% of the ice surplus in the accumulation area of Vatnajökull was transported to the ablation area by surges (Björnsson et al., 2003).

2.2 Available observations

Automatic Weather Stations (AWSs) have been operated on Vatnajökull since 1994, with 1-13 stations measuring on the ice cap during the summer months (e.g. Oerlemans et al., 1999; de Ruyter de Wildt et al., 2003; Guðmundsson et al., 2006; Björnsson et al., 2006). Radiation balance components have been measured since 1996, while the 2 m temperature, 2 m relative humidity, 4 m wind speed, and the 4 m wind direction have been measured for the entire period. Observations from five AWSs, three on Brúarjökull and two on Tungnaárjökull (Figure 1), which have been operated at approximately the same locations since 2001, are used to evaluate the simulated temperatures in the HIRHAM5-EC-EARTH simulations. ERA-Interim forced simulations from HIRHAM5 have previously been evaluated by Schmidt et al. (2017).

In situ mass balance and surface velocity measurements have been carried out twice a year every glaciological year since 1991-92 (Björnsson et al., 1998), with an average of 60 measured locations every year (Figure 1). The ablation has been observed using stake measurements, and the location of the stakes has been measured by Global Position System (GPS) in order to estimate the average seasonal velocity. The uncertainty in the mass balance measurements has been estimated to be $\pm$0.3 m water equivalent (w.eq.) (Björnsson et al., 1995, 2013). The observations are used to evaluate the mass balance in the HIRHAM5-EC-EARTH runs and to determine the flow and sliding parameters used in the PISM simulations.

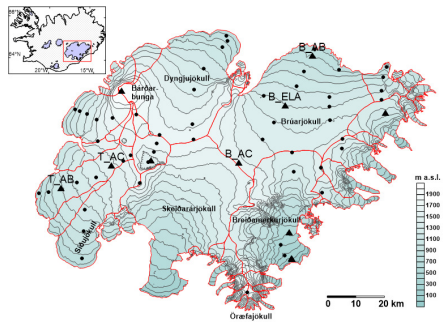

Figure 1. Vatnajökull ice cap. Shown are the locations of AWS stations (black triangles) and surface mass balance/surface velocity sites (black dots) used in this study. The red lines show the outlines of the ice divides.

The surface and bedrock topographies are needed as boundary conditions for PISM. For the surface topography, a surface elevation map of the ice cap from 2010 is used. The map is based on images from the Spot5 satellite (Berthier and Toutin, 2008) from June and September 2010. The uncertainty on the acquisition day is approximately 1-2 m. However, due to differences between acquisition days in the surface elevation due to glacier melt, the uncertainty may be higher at ∼5 m in some areas.

The bedrock topography maps are based on radio echo profiles from surveys since 1980 (Björnsson, 1986). Each pulse from the radio transmitter illuminates an approximate disc with a radius of ∼100-200 m, thus the received echo is composed of energy from that area. An attempt to trace the energy to point sources at the bed is made using migration along the profile; a detailed description can be found in e.g. Magnússon et al. (2016). The sounding lines were typically conducted 1 km apart and then interpolated to create a map using manual interpolation. The uncertainty along each sounding line is estimated to be approximately ±15 m (Björnsson, 2000), but due to uncertainty in the interpolation between the survey lines, the uncertainty of the bedrock topography map is estimated to be 20-50 m.

3 Model description

3.1 Regional Climate Models

In this study, we mainly use the RCM HIRHAM5 for simulations of the mass balance. HIRHAM5 was developed by the Danish Meteorological Institute, and is a hydrostatic RCM which combines the dynamical core of the HIRLAM7 numerical forecasting model (Eerola, 2006) and physics schemes from the ECHAM5 general circulation model (Roeckner et al., 2003). A detailed description of the model configuration can be found in Christensen et al. (2006). In this study it is run over a domain containing Greenland and Iceland, with a horizontal resolution of 0.05° x 0.05° on a rotated-pole grid. This corresponds to ∼ 5.5 km resolution. The atmospheric model has 31 vertical levels, from the surface to 10 hPa. The model time step is 90 s. HIRHAM5 model simulations have been successfully validated over Greenland (e.g. Box and Rinke, 2003; Stendel et al., 2008; Lucas-Picher et al., 2012; Langen et al., 2015; Rae et al., 2012; Langen et al., 2017) and Iceland (Schmidt et al., 2017) using AWS and ice core data.

However, when the model is forced by ERA-Interim reanalysis data (Dee et al., 2011), which is a global atmospheric reanalysis by ECMWF spanning back to 1979, Schmidt et al. (2017) found that there is an overestimation in the winter accumulation over parts of Vatnajökull which e.g. affect the simulation of the albedo. Schmidt et al. (2018) found that by

using the well-evaluated snow pack scheme from HIRHAM5, but forcing it with incoming mass and energy-fluxes from the numerical weather projection model (NWP) HARMONIE-AROME, a better agreement with mass balance observations could be achieved.

HARMONIE-AROME is a non-hydrostatic, convection-permitting model (Bengtsson et al., 2017), which is based on the AROME-France model (e.g. Seity et al., 2011), but now differs from the original model in various aspects (Bengtsson et al., 2017). Details on the model configuration are described in Bengtsson et al. (2017). In autumn 2015, the Icelandic Meteorological Office started a reanalysis project for Iceland (ICRA) using the HARMONIE-AROME model (details on the model setup can be found in Nawri et al. (2017)). ICRA currently spans from September 1st, 1979, until December 31st, 2017. It is run over a domain containing only Iceland at a horizontal resolution of 0.025° x 0.025°, corresponding to $\sim$ 2.5 km. HARMONIE-AROME is forced by ERA-Interim reanalysis data at the lateral boundaries at 6 hour intervals. Since HARMONIE-AROME is non-hydrostatic and calculates precipitation diagnostically, it provides a better representation of the accumulation in areas with high orographic forcing than HIRHAM5 (Schmidt et al., 2018).

Due to the better agreement between mass balance observations and simulations when the snow pack scheme from HIRHAM5 is forced by HARMONIE-AROME meteorological forcing, the mass balance from these runs are used for simulations in the reanalysis period (1980-present). In order to get a more accurate mass balance, the precipitation correction used by Schmidt et al. (2018) is also used in this study. The method is described in detail in Schmidt et al. (2018), and the details on the snow pack scheme are described in Langen et al. (2017) and Schmidt et al. (2017).

For future simulations, we rely on HIRHAM5 forced by EC-EARTH (Hazeleger et al., 2012) at the lateral boundaries. EC-EARTH is based on the operational seasonal forecast system of the European Centre for Medium-Range Weather Forecasts (ECMWF). It has a 2°C cold bias over the Arctic (Koenigk et al., 2013), which leads to an overestimation of the sea ice extent, but it performs well when simulating dynamic variables, which comparison with other coupled models of similar complexity confirms (Hazeleger et al., 2012). HIRHAM5 was run at a 5.5 km resolution, with a domain containing Greenland and Iceland. Two greenhouse gas concentration scenarios are considered, RCP 4.5 and 8.5. Due to the high computational cost of these simulations, they are only available in three 20 year time slices: a historical period from 1991-2010 and two future periods from 2031-2050 and 2081-2100. The output from these runs was evaluated over Greenland by Boberg et al. (2018).

In order to present a larger number of projections, this study also considers available simulations within the CORDEX project (Giorgi et al., 2009). Iceland is represented both in the Europe and Arctic domains, but the highest resolution simulation (12 km) can be found in the Europe domain. For the RCP 8.5 scenario, a total of 30 simulations are available at a 12 km resolution, but only 15 simulations provided the output parameters needed for this study and included an appropriate snow/ice mask over Vatnajökull. Altogether, five different RCMs, eight GCMs, and three ensembles are represented by these simulations.

Fewer simulations are available for the RCP 4.5 scenario, as only 19 simulations are available at a 12 km resolution. Of these, 11 simulations provide the output parameters needed for this study. In total, four different RCMs, six GCMs, and three ensembles are represented by these simulations. A list of the simulations used in this study is shown in Table 1.

3.2 The Parallel Ice Sheet Model

The Parallel Ice Sheet Model (PISM) (Bueler and Brown, 2009) is an open-source, 3-D, thermo-mechanically coupled ice-sheet model which has been applied in various studies of the Antarctic and Greenland ice sheet (e.g. Winkelmann et al., 2011; Aschwanden et al., 2013, 2016; Aðalgeirsdóttir et al., 2014). PISM numerically solves the shallow ice and shallow shelf

RCM	GCM	Ensemble	RCP 4.5	RCP 8.5	Reference
HIRHAM5	ICHEC-EC-EARTH	r3i1p1	x	x	Christensen et al. (2006)
	MOHC-HadGEM2-ES	r1i1p1		x	
	NCC-NorESM1-M	r1i1p1	x	x	
CCLM4-8-1	CCCma-CanESM2	r1i1p1		x	Rockel et al. (2008)
	MIROC-MIROC5	r1i1p1		x	
RACMO22E	ICHEC-EC-EARTH	r12i1p1	x	x	Van Meijgaard et al. (2008)
	ICHEC-EC-EARTH	r1i1p1	x	x	
	MOHC-HadGEM2-ES	r1i1p1	x	x	
RCA4	ICHEC-EC-EARTH	r12i1p1	x	x	Samuelsson et al. (2011)
	CNRM-CERFACS-CNRM-CM5	r1i1p1	x	x	
	IPSL-IPSL-CM5A-MR	r1i1p1	x	x	
	MOHC-HadGEM2-ES	r1i1p1	x	x	
	MPI-M-MPI-ESM-LR	r1i1p1	x	x	
	NCC-NorESM1-M	r1i1p1		x	
WRF331F	IPSL-IPSL-CM5A-MR	r1i1p1	x	x	Hines et al. (2008)

Table 1. CORDEX simulations used in this study.

approximations (SIA and SSA) in parallel. The SIA is solved with a non-sliding base, and the SSA can be used as a sliding law (Bueler and Brown, 2009). In this study, both the SIA and the combined SIA+SSA schemes are investigated for Vatnajökull.

Basal sliding can be estimated in PISM using a fully plastic or pseudo-plastic law. In the case of a pseudo-plastic power law, it relates bed-parallel shear stress, $\boldsymbol{\tau_b}$, to the basal velocity $\boldsymbol{u}_b$

$$\boldsymbol{\tau_b} = -\tau_c \frac{\boldsymbol{u}_b}{u_{threshold}^q |\boldsymbol{u}_b|^{1-q}} \tag{1}$$

where τ_c is the yield stress, which represents the strength of the glacier till, $\boldsymbol{u}_{threshold}$ is a threshold speed, and q is the pseudo-plastic exponent. Setting $q = 0$ gives the fully plastic case. Sliding is likely to occur if the driving stress is larger than the yield stress. The yield stress can either be considered constant or calculated dynamically by relating the till material properties, i.e. the till friction angle ϕ, and the effective pressure on the till, N_{till}, using the Mohr-Coulomb criterion:

$$\tau_c = c_0 + tan\phi \cdot N_{till} \tag{2}$$

where c_0 is called the till cohesion and is generally set to zero. The effective pressure on the till is determined by

$$N_{till} = min\left\{ P_o, N_0 \left(\frac{\delta P_o}{N_0} \right)^{W_{till}/W_{till}^{max}} 10^{(e_0/C_c)(1-W_{till}/W_{till}^{max})} \right\} \tag{3}$$

where P_o is the ice overburden pressure, determined entirely by the ice thickness, density and the gravitational acceleration, and W_{till} is the effective thickness of water in the till computed in the model. The remaining variables are constants which describe the till mechanics: $N_0 = 1000$ Pa is the reference effective pressure of the till, δ is the effective fraction overburden, $e_0 = 0.69$ is the reference void ratio, $C_c = 0.12$ is the compressibility coefficient, and $W_{till}^{max} = 2$ m is the maximum water thickness allowed in the till (Tulaczyk et al., 2000; Bueler and van Pelt, 2015).

While till deformation plays a major role in the ice flow of parts of Greenland and Antarctica, till deformation may not be the main reason for basal sliding beneath Vatnajökull. We are therefore not claiming that the sliding model in PISM describe the physics of basal sliding beneath Vatnajökull, but by tuning the parameters of the till model, basal sliding which are in accord

with observed total velocities may be simulated. On the other hand, the sliding model is forced by melt water, ice thickness, and slope, which are realistic drivers of basal sliding of Vatnajökull.

Within the framework of PISM, there is a hierarchy of flow laws with different complexities. In this study, tests are conducted using the isothermal Glen's flow law, wherein the ice softness is fixed but can be determined manually, and the enthalpy-based Glen-Paterson-Budd-Lliboutry-Duval law (gpbld) (Lliboutry and Duval, 1985), which is the PISM default and the ice softness depends on both temperature and liquid water fraction. Aðalgeirsdóttir et al. (2005) found a good correlation between an isothermal flow law with a softness of A=$2 \cdot 10^{-24}$ Pa s^{-1} and velocity measurements from Vatnajökull when additional sliding is allowed. However, an enthalpy based scheme should perform better when simulating temperate ice as the latent heat of liquid water within the ice is taken into account (Aschwanden et al., 2012), and energy conservation is therefore better simulated. Both the enthalpy and isothermal schemes are tested in this study.

PISM includes several calving parameterisations. In this study, the physically-based 2D eigen calving method (Levermann et al., 2012) is used with a thickness threshold of 150 m. This parameterisation assumes that the average calving rates are proportional to the product of principal strain rates, which are derived from SSA-velocities (Levermann et al., 2012).

The model parameters within PISM are highly customizable, and previous studies have determined what the optimal parameters are for the ice sheets on Greenland (e.g. Aschwanden et al., 2013) and Antactica (e.g. Winkelmann et al., 2011). A similar determination of parameters is conducted for Vatnajökull before the model is used for coupled simulations.

3.3 Model setup

3.3.1 RCM climatic mass balance

In this study, the snow pack scheme from HIRHAM5, which is run offline from the atmospheric component, is used to simulate the mass balance. The scheme has 25 subsurface layers, and includes a dynamic surface scheme that explicitly calculates the surface mass budget, accounts for the melting of snow and bare ice, and resolves the retention and refreezing of liquid water in the snow pack (Langen et al., 2015, 2017). This scheme only runs for designated glacier gridpoints, and it is run offline forced by 6-hour surface energy (incoming shortwave (SW↓) and longwave (LW↓) radiation and turbulent fluxes) and mass fluxes (snow, rain, evaporation, and sublimation) from a previous HIRHAM5 simulation. While a fully coupled, high-resolution HIRHAM5 run is computationally very expensive, this offline model offers a quicker alternative to test new model implementations.

This snow pack scheme has previously been evaluated for Vatnajökull by Schmidt et al. (2017). The authors used an updated snow albedo scheme, which was tuned to better fit with observations from AWSs operated on Vatnajökull. In addition, the albedo of the ice that emerges as the snow melts away in the ablation zone, was improved by using a background map based on MODIS observations (Gascoin et al., 2017; Schmidt et al., 2017). This version of the model is used in this study.

The offline model can be forced by incoming energy and mass components from another climate model, although then additional missing feedbacks have to be taken into considerations. Schmidt et al. (2018) used the model forced with energy and mass fluxes from the NWP HARMONIE-AROME, and achieved improved simulations of the mass balance compared to using HIRHAM5 forcing. A similar approach will be used in this study, as the CORDEX simulations will all be used to force the snow pack scheme. This is done in order to get the most similar conditions for the climate runs, and the differences in mass balance are not due to e.g. different complexities of the albedo parameterisation. The way the output from RCMs can be used to force the HIRHAM5 snow pack scheme is described in detail in Schmidt et al. (2018).

The calculated monthly mass balance fields are used to force the ice flow model PISM, in order to get an estimate of the future volume and area change of the ice cap. Since this is a one way coupling, the elevation-mass balance feedback is not taken into account. As a way to test how much of an effect the elevation change has on the mass balance, a set of model runs where a lapse-rate correction is added to the precipitation and temperature are also conducted. A lapse rate of $\delta P/\delta h_s = 0.00176$ a^{-1} is used following Flowers et al. (2005), where P is the precipitation and h_s is the surface elevation in metres, and a temperature lapse rate of $\delta T/\delta h_s = 0.006$ K/m following Guðmundsson et al. (2006) is used to correct the incoming longwave radiation and the sensible heat flux, as these fluxes can both be parameterised as a function of the air temperature. A schematic of how the models are coupled for these runs is shown in Figure 2.

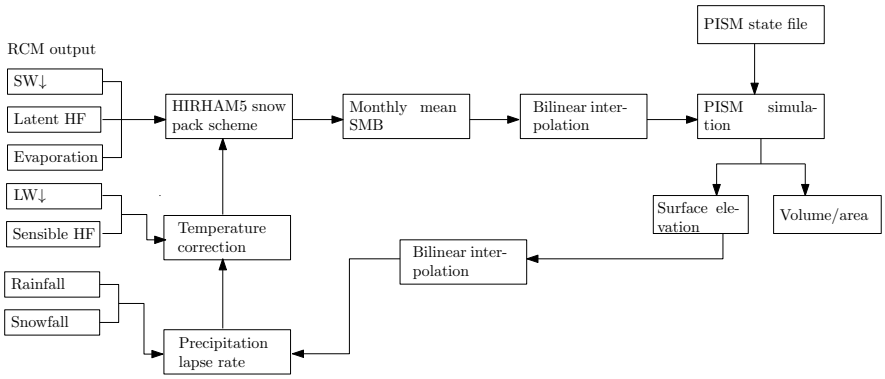

Figure 2. The setup of the model coupling. The precipitation and temperature lapse rate corrections are only added for the elevation feedback experiments.

3.3.2 PISM initialization

To simulate the ice flow with PISM, the model needs the following boundary conditions; the bedrock elevation, an initial ice thickness estimate, a geothermal heat flux map, the monthly mean climatic mass balance, and the monthly mean ice surface temperatures. The bed elevation and initial ice thickness fields are based on observations, and both maps have a resolution of 500x500 m.

An important source of meltwater beneath Vatnajökull is due to geothermal heat-flux melting the ice from below. The basal water computed in PISM is important e.g. for determining the saturation of the till. A NW-SE heat-flux gradient surrounds Vatnajökull, with maximum heat fluxes of 0.25 W m^{-2} above the active rift zone (Flóvenz and Saemundsson, 1993). Some central volcanoes have much higher localized values of up to 50 W m^{-2}. In the absence of a map of geothermal heat-fluxes, the method used by Flowers et al. (2003) is used to estimate the background fluxes. The eastern sector of Vatnajökull is assigned a value of 0.18 W m^{-2}, while the western sector is assigned no heat-flux since the subsurface hydrothermal circulation is assumed to be sufficiently strong to prevent heat from reaching the ice. Active geothermal areas beneath Vatnajökull are assigned values following the suggestions of Björnsson (1988); 50 W m^{-2} at Grímsvötn and the Skaftá cauldrons.

When using a climatic mass balance to force PISM, the ice temperature, i.e. the temperature below snow and firn processes, is required as input for the model. Icelandic glaciers are temperate (Björnsson and Pálsson, 2008), and while a winter cold wave is

observed in the glacier snow, it generally does not reach deep into the underlying ice. Using the HARMONIE-HIRHAM5 simulated ice temperatures and conduction a constant geometry spin up run for 1000 years with the the enthalpy based model, an ice cap that is approximately 80% temperate ice is achieved, with e.g. the ablation zones of Brúarjökull and Dyngjujökull being frozen to the bed in the simulation. Based on field observations, this is not a realistic result. In this study, the ice temperature is instead forced to be 0°C for the entire domain, in order to simulate a completely temperate ice cap.

Several simulated climatic mass balance fields are used in this study, as described in Section 3.1. If the flow model is run at the resolution of the RCMs, i.e. with a grid size of 2.5 km x 2.5 km, high velocity areas occur in some grid points due to the large topographic gradients between grid points at this resolution. The climatic mass balance fields are therefore interpolated onto the 500 m grid of the bedrock and surface maps using bi-linear interpolation, which results in a more accurate representation of the surface velocities.

3.3.3 Spin-up techniques

Before projections of the future evolution of Vatnajökull can be conducted, the coupled RCM-ice flow model needs to be initialized to represent the present state of the glacier, as the initial model state strongly influences the initial trajectory of projections (e.g. Aðalgeirsdóttir et al., 2014).

A common initialization method is to do a 'constant climate spin-up'. Here, the initial state of the surface is obtained by continuously using the present day climate forcing until the ice cap reaches an equilibrium. Using a forcing period where the glacier has approximately a zero mass balance is preferable in order to obtain the most realistic geometry.

Another common procedure for Greenland and Antarctica is to do a 'paleo spin-up'; running the model for a full glacial cycle by parameterizing changes in the climate forcing using climate records from ice cores (e.g. Aðalgeirsdóttir et al., 2005; Nielsen et al., 2018). This method is expected to give a more accurate representation of the ice temperature and basal conditions, but often produces an ice sheet that differs in size and shape from present day (e.g. Aðalgeirsdóttir et al., 2014).

Since Icelandic glaciers are temperate (Björnsson and Pálsson, 2008), a model spin-up is expected to be less important than for e.g. Greenland. However, a spin-up is still needed for the model to be in balance with the reference climate forcing, to make certain that the initial response of the ice cap is due to a changing climate and not a result of model adjustment to the reference forcing. In addition, uncertainties in the bedrock topography will affect the shape of the ice cap, and conducting a spin-up will remove any model drift as a result of these uncertainties. Since the constant climate spin-up is expected to produce a more accurate glacier geometry, this initialization method is chosen for this study. Vatnajökull was approximately in balance from 1980-1999, so this period is used for the spin up. After the spin-up, the model is forced until 2010 for comparisons with the observed geometry of that year.

It is important to note that Vatnajökull is most likely not in a steady state; previous studies have shown that the current shape can be best represented by an ice cap that is not in equilibrium with the current climate (e.g. Aðalgeirsdóttir et al., 2005; Marshall et al., 2005). One of the explanations for a non-equilibrium ice cap is that most of the outlet glaciers of Vatnajökull are surge-type. Surges have a major effect on the shape and mass balance of Icelandic glaciers, with about 25% of the surplus in the accumulation area of Vatnajökull being transported down-glacier by surges in the 1990s (Björnsson et al., 2003). Performing a spin-up without surges is therefore expected to produce an ice cap with a too large volume and too small area. Since PISM physics is not complex enough to capture surge dynamics, it is not possible to have dynamically occurring surges in the model.

4 Results

4.1 Determining optimal flow law and sliding parameters in PISM

In order to determine the optimal parameters and flow laws to model the ice flow of Vatnajökull, a series of model runs are performed to assess the different model options. First, a 1000 year fixed geometry spin-up is performed until both the glacier ice and the glacier till are in equilibrium. Then, the model is run for 1 year while allowing the surface to change in order to slightly smooth the surface but still retain the present day geometry. This method has e.g. previously been used by Aðalgeirsdóttir et al. (2005). The one year ice surface velocities are then compared to available observations.

Firstly, tests are conducted to investigate if the ice velocities can be simulated with only SIA and therefore no sliding. The results using both the gpbld enthalpy based flow model and the isothermal Glen's flow model using three different values of the softness A are shown in Table 2.

Flow law	A [$s^{-1}Pa^{-3}$]	rmse [m/yr]							
		W Brúar	E Brúar	Köldukvíslar	Tungnaár	Síðu	Dyngju	Breiðamerkur	Eyjabakka
gpbld	variable	11.9	26.4	82.9	28.4	11.1	69.9	231.2	42.1
Isothermal Glen's	$2.4{\cdot}10^{-24}$	20.1	13.2	8.6	29.8	29.3	17.7	82.8	6.1
	$3.6{\cdot}10^{-24}$	18.1	10.6	10.3	28.2	26.0	16.1	70.5	3.7
	$6.0{\cdot}10^{-24}$	11.4	8.4	32.3	24.7	13.8	29.6	67.4	13.4

Table 2. Average root mean square error (rmse) between the simulations and the mean of the velocity observations. Gpbld is the enthalphy based flow law. Surge velocities have been removed from the observation time series for the comparison.

The gpbld flow law produces the softest ice, and while the resulting simulated surface velocities provide a good fit compared to observations for e.g. Tungnaárjökull and Síðujökull, for most of the outlets the modeled surface velocities are much higher than observed. For this study, the isothermal Glen's flow model will therefore be used. While the measured velocities can be simulated well using a SIA model with no sliding, different ice viscosities are needed for each outlet. A better model choice would therefore be to choose a softness that models the lowest measured velocities well and add sliding to the simulations. This is similar to the conclusions drawn by Aðalgeirsdóttir et al. (2005). We therefore chose to use the isothermal Glen's flow law with A equal to $2.4 \cdot 10^{-24}$ $s^{-1}Pa^{-3}$, as it fits well with lowest observed velocities (Figure 3). In addition, it is the ice viscosity suggested for temperate ice by Cuffey and Paterson (2011).

In PISM, the sliding law can be chosen to be purely plastic or pseudo-plastic. Both options were investigated for this study, and the pseudo plastic exponent q and the till friction angle ϕ were varied in order to obtain the best fit. We find that the best fit with observations is obtained when a pseudo-plastic flow law with $q = 0.5$ and a till friction angle that varies linearly with bed elevation is used. However, a velocity mismatch arises for points near the outlet terminus. These points generally have a low observed velocity and can for several of the outlets be modeled without sliding. After the end of the constant geometry spin-up, the glacier till is completely filled with water under the entire ice cap. The thin, low elevation outlet terminus of e.g. Brúarjökull will therefore start sliding resulting in a velocity much higher than observed, unless the till friction angle is made sufficiently high. When this occurs, almost no sliding is allowed in the model in the higher elevation glacier points. A way to counter this effect is to add a large till cohesion (see Equation 2). Using a till cohesion of 125 KPa in combination with a till friction angle that is varied between 10° and 65° for bed elevations between 700 and 1000 m a.s.l. gives the best correlation with the observations. The changes from the default PISM settings are summarized in Table 3.

Parameter	value
Flow law	isothermal Glen's
Sliding law	pseudo-plastic
A	2.4E-24
q	0.5
c_0	125 kPa
$\mathbf{b}_{min}$	700 m a.s.l.
$\mathbf{b}_{max}$	1000 m a.s.l.
ϕ_{min}	10°
ϕ_{max}	65°
δ	0.05

Table 3. Model choices changed from the PISM default settings.

The simulated velocities when adding a SSA sliding with the parameter choices given in Table 3 are shown along eight flow lines in Figure 3. The modeled velocities of Brúarjökull and Köldukvíslarjökull have the best fit with the average observations. Breiðamerkurjökull has the largest deviation, but the simulated velocities are still mostly within the range of the observations. Eyjabakkajökull is the only outlet which significantly deviates from the observations, which suggest that generally very little sliding occurs along this outlet. Brúarjökull, Síðujökull, Breiðamerkurjökull, and part of Dyngjujökull, are most affected by sliding.

Since Breiðamerkurjökull and Skeiðarárjökull both will be affected by calving at some point during the future simulations, due to an over-deepening of the bedrock beneath the glaciers, a calving parameterisation is added to the simulations. The eigen-calving scheme (Levermann et al., 2012) and a thickness threshold of 150 m was used to simulate calving when proglacial lakes are formed.

4.2 Model spin-up using 1980-1999 climate

The results of the constant climate spin-up are shown in Figure 4. As expected, the equilibrium state has a smaller area (by 2.5%) and a larger volume (by 3.5%) compared to the present day reference geometry. This can partly be attributed to the lack of surges in the model. Dyngjujökull has the largest thickness deviation from the observed, which could be due to the short surge cycle of this outlet. The mass balance in the upper part of the outlet is much higher than that needed to sustain the current thickness, which causes the outlet to surges approximately every 20 years. For Brúarjökull, on the other hand, there is only a small difference between the mass balance needed to sustain the current thickness and the actual mass balance, and it therefore has a long surge cycle of 80 years. The simulated outlet is still thicker than observed and is shorter than the current extent, but the thickness of most of the outlet is overestimated by less than 50 m, whereas Dyngjujökull is overestimated by between 50 and 150 m. The thickness of the south-facing outlets is underestimated in the ablation zone and overestimated in the accumulation zone, which could once again be attributed to the fact that there are no surges in the model to bring excess mass from the accumulation zone down to the ablation zone.

As previously mentioned, another important factor is that the present day ice cap is most likely not in equilibrium with the current climate, so an equilibrium ice cap will not capture the present day geometry even if surge dynamics were included. A non-equilibrium present day geometry e.g. explains the thin ice at the terminus of several outlets which disappear during the constant climate spin-up. Errors in the reanalysis forcing and uncertainties in the bedrock topography also affect the spin-up geometry.

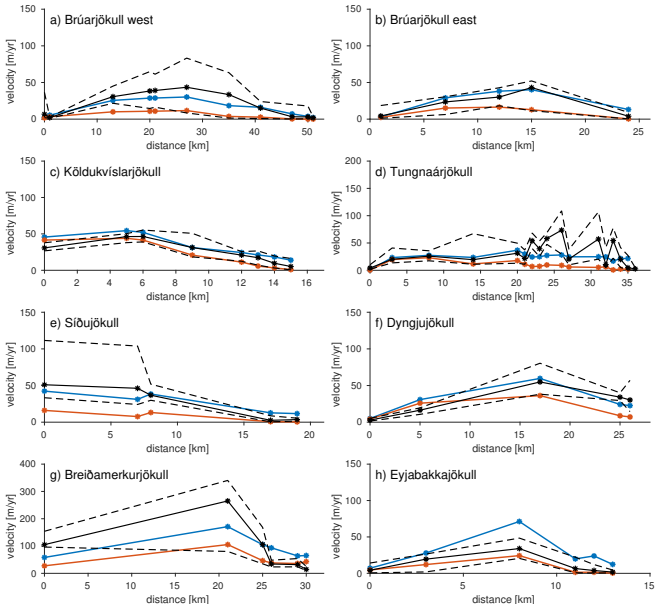

Figure 3. Comparison of flow velocities after one year with measured velocities at the mass balance stakes (Figure 1) for a) western Brúarjökull, b) eastern Brúarjökull, c) Köldukvíslarjökull, d) Síðujökull, e) Tungnaárjökull, f) Dyngjujökull, g) Breiðamerkurjökull, and h) Eyjabakkajökull. The horizontal axis is the distance from the ice divide. The red line shows the simulated velocities using only SIA with A=2.4·10^{-24} $s^{-1}Pa^{-3}$, and the blue lines shows SSA+SIA velocities when the options in Table 3 are used. Solid black line shows the average over the observation period, while stippled black lines show the maximum and minimum observation.

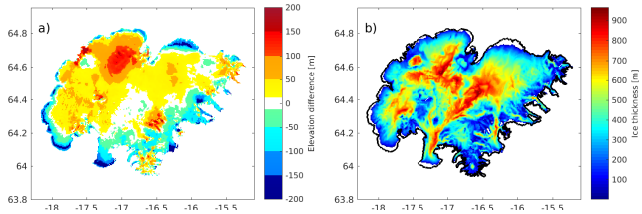

Figure 4. a) The elevation difference between the reference ice surface and the model after the constant climate spin-up. b) The ice thickness and extent after the constant climate spin-up. The black line shows the current extent of the ice cap.

Figure 5 shows the profiles of six outlet glaciers along a flowline both for the observed 2010 geometry and for the simulated geometry. As previously mentioned, Brúarjökull and Dyngjujökull are the outlets with the largest differences between the spin up geometry and the observed geometry. After the spin-up, Brúarjökull is shorter by ∼7.5 km in the simulation. Therefore it is the outlet whose extent is the furthest from the observed. The simulated Dyngjujökull is shorter by 2 km, while the simulated Skeiðarárjökull and Tungnaárjökull are shorter by approximately 3 km. Hoffellsjökull and Breiðamerkurjökull have the same extent in the simulations as observed.

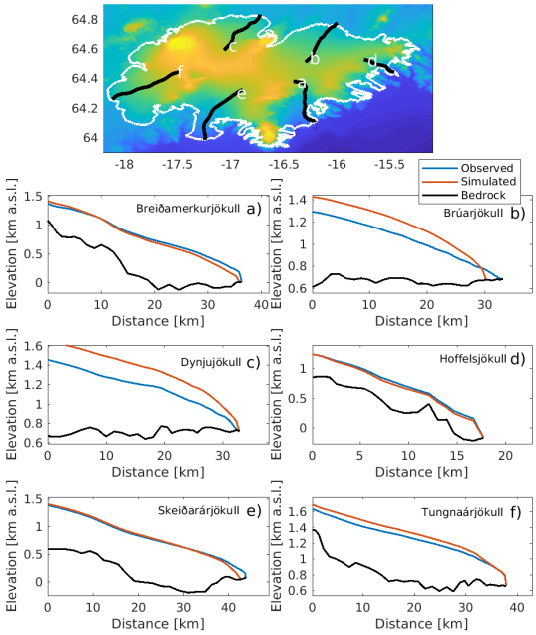

Figure 5. The spin-up profiles compared to observed 2010 profiles from six outlet glaciers. Profiles are shown in black in the top figure.

Due to these changes in area and thickness, the simulated velocities for this geometry do not fit as well with the observations as in the one year geometry run. The root mean square error (rmse) of the difference between observed and simulated surface velocities at the end of the spin-up are given in Table 4. The main reason for the bigger errors is that the edges of the ice cap have become thicker and steeper compared to the one year run, hence the velocities become much higher near the outlet terminus. Especially Dyngjujökull, which has the highest deviation in thickness in the steady state simulations, reaches velocities much higher than those simulated with the current geometry.

	Bru_w	Bru_e	Kol	Tun	Siðu	Dyng	Bre	Eyja
1 yr [m/yr]	7.7	6.2	7.9	21.2	9.6	8.8	55.0	19.0
CC spin-up [m/yr]	9.0	18.3	25.9	19.8	30.0	44.5	78.9	52.9

Table 4. The mean rmse between average surface velocity observations and the simulated surface velocities for all sites. The 1 year velocities are modeled using the same shape of the outlet glaciers as observed, while CC spin-up velocities are taken at the end of a constant climate spin-up.

4.3 Reanalysis simulations from 1980-2016

The simulated changes in mass balance, volume, and area of Vatnajökull during the period 1980-2016 are shown in Figure 6. The measured change in volume from the 1991-92 glaciological year until 2014-15 is approximately 3%. In the model

simulations, the volume loss is approximately half of the observed: 1.7% since 1991-92. This is due to an overestimation of the net balance from 1995 to 2000 (see Figure 6a), as well as the effect of volcanic eruptions on the albedo and thus the surface ablation. The glacier surface was affected by tephra from eruptions occurring in 1996, 1998, 2004, 2010, and 2011. The facts that parts of the ablation zone melted away during spin-up, and that surges occurred in 1991, 1994, and 2000 in western and north-western outlet glaciers, which transported additional mass down to the ablation zone, also contribute to the difference in volume loss.

The simulated change in area is also shown in Figure 6c. Only very small changes are simulated during the reference period: 1.2% from 1991-92 to 2014-15. This small change is because the spin-up state is in balance with the 1980 to 1999 climate, and that the thinnest parts of the ablation zone melted away during the model spin-up.

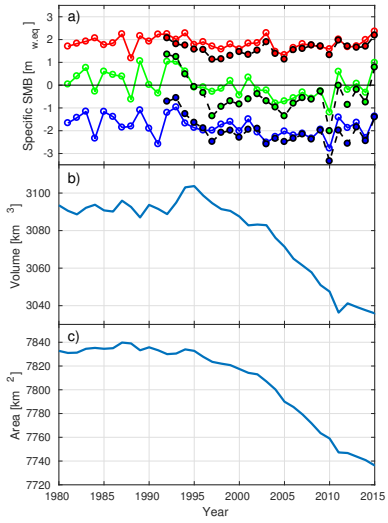

Figure 6. a) HARMONIE-HIRHAM5 reconstructed summer (red), winter (blue), and net (green) mass balance compared with observations (black). b) volume and c) area change in simulation from 1980-2015.

Since the ice cap is temperate both in reality and in the simulations, the spin-up of the ice cap should not be as important as for example for Greenland. If only a constant geometry spin-up had been conducted before using the reanalysis, so the ice cap started from the 2010 shape, then the results would be significantly different. In that case, only a slightly higher volume loss of 2.1% is simulated since 1991-92, but a significantly higher area loss of 3.0% is simulated for the same period. This is closer to the observed values, but since the ice cap is not in balance with the reference forcing, some of this signal could be due to the ice cap adjusting to the reference forcing. As mentioned in the previous section, the spin-up is important to adjust the ice cap shape to the forcing, which does have some significant biases (Schmidt et al., 2018), as well as smoothing any drift that results from uncertainties in the bedrock topography. However, as can be seen from the reanalysis results, this leads to a slower than observed outlet retreat in the beginning of the run.

4.4 HIRHAM5-EC-Earth 5.5 km simulations

4.4.1 Evaluation

The output from HIRHAM5 with the same setup as the simulations used in this study was previously evaluated by Schmidt et al. (2017), but in that study ERA-Interim reanalysis was used to force the model at the lateral boundaries and not a GCM. The biases in the simulations used in this study are therefore larger. The climate of EC-EARTH has (as any freely running GCM) a variability that is out of phase with reality, and comparison with observations is therefore best done using a statistical method. Boberg et al. (2018) analyzed the HIRHAM5-EC-EARTH simulations over Greenland in a similar way, and found that the temperature was simulated equally well with HIRHAM5 forced by ERA-Interim and EC-EARTH, but the ablation and runoff was underestimated by the EC-EARTH forced simulations.

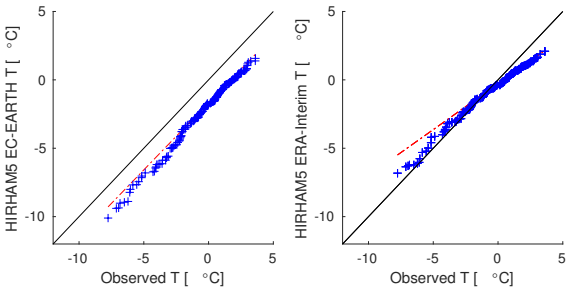

Figure 7. Quantile-Quantile plots of the monthly mean temperatures from five AWSs compared to a) EC-EARTH forced simulations and b) ERA-Interim forced simulations. Red line shows the straight line the quantiles follow and the black line shows a one-to-one line

Figure 7 shows quantile-quantile plots of the modeled and observed monthly mean temperatures. Both the EC-EARTH and ERA-Interim forced simulations are compared to the temperatures measured at five AWSs from 2001-2010. The figures show that statistically the EC-EARTH and ERA-Interim forced simulations are from a similar distribution as the observations, as all the results lie on an approximately straight line (shown in red) except at low temperatures. However, there is a clear temperature bias in the EC-EARTH runs, which is apparent when comparing the quantile-quantile plots to the one-to-one line. EC-EARTH has a 1.9 °C cold bias over Vatnajökull, which is consistent with the general 2 °C cold bias found over the Arctic in EC-EARTH (Koenigk et al., 2013), whereas the ERA-Interim forced simulations only have a cold bias of 0.4 °C over Vatnajökull (Schmidt et al., 2017).

A comparison of the simulated and observed specific summer, winter, and net mass balance for the period 1991-2010 is shown in Figure 8. The simulations have a clear overestimation in both the summer, winter, and net balance, simulating a net mass balance that is positive for the whole historical period, whereas the observations show that the mass balance has been negative since the mid-1990s. Over the entire period, the average overestimation of the winter mass balance is 1.0 m w.eq., the overestimation of the summer balance is 0.9 m w.eq., and the overestimation of the total balance is therefore 1.9 m w.eq. For the ERA-Interim forced runs, the winter balance was overestimated by 0.5 m w.eq., the summer balance by only 0.06 m w.eq., and the net balance was therefore overestimated by ∼0.6 m w.eq. The biases in the EC-EARTH forced simulation are therefore much larger than in the ERA-Interim forced simulation, in part due to the larger temperature bias.

Figure 8 shows the evolution of the mass balance until 2100 for the two RCP scenarios used in this study. Both runs have approximately the same temperature increase until 2050 (1.5°C increase relative to the 1991-2010 average for RCP 4.5 and

1.4°C increase for RCP 8.5), and the mass balance change is therefore almost equal in the first time slice. However, as can be seen from the plots, the net mass balance does not reach negative values until after 2030. For the last time slice the net mass balance is mostly negative in both scenarios, and in this period there is a significant acceleration of the warming over Iceland in the RCP 8.5 scenario, as temperatures have increased with 4.7°C relative to the 1991-2010 average. The temperature has increased with 3°C in the RCP 4.5 scenario.

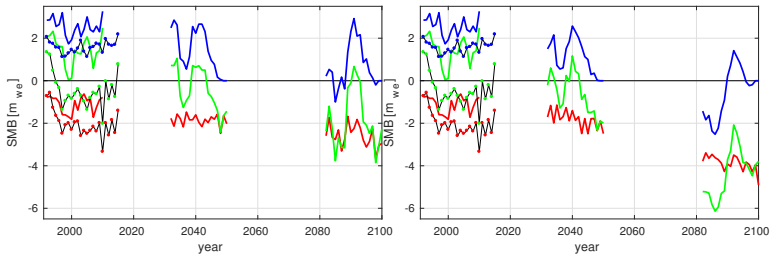

Figure 8. The simulated summer (red), winter (blue), and annual (green) mass balance by HIRHAM5-EC-EARTH using the a) RCP 4.5 scenario and b) RCP 8.5 scenario. Black lines with coloured dots show the observations.

If the mass balance fields from these simulations are used directly to force the flow model, significant mass balance biases would be introduced into the projections. Instead of using the absolute values computed by the offline model, the flow model is therefore forced with mass balance anomaly fields. These are computed by subtracting the projections for each year from the mean of the historical period. The anomaly is then added to the average HARMONIE-HIRHAM5 simulated mass balance from 1991-2010.

4.4.2 Step-wise climate response

To estimate the response of the ice cap to a sudden climate change, the flow model is first forced with the climate forcing for each of the time slices. Starting from the spin-up state, the model is run for 2000 years recycling the anomaly of the forcing from 2031-2050 and 2081-2100 for the RCP 4.5 scenario, and 2081-2100 for the RCP 8.5 scenario. This corresponds to a sudden temperature change of 1.5°C, 3.0°C, and 4.7°C. The resulting changes in area and volume are shown in Figure 9**a-c**.

For the 2031-2050 RCP 4.5 scenario (1.5°C warming) the ice cap stabilizes at a volume and area that are 30% and 16% smaller than the starting value, respectively. For the 2081-2100 RCP 4.5 scenario (3.0°C warming) the ice cap takes longer to reach a steady state than the other two scenarios, but the volume and area eventually stabilize at a 66% smaller volume and a 40% smaller area. For the last scenario, 2081-2100 RCP 8.5 with 4.7°C warming, only the highest points of the ice cap (for example Öræfajökull and Bárðarbunga) stay glacierized. Here, 97% of the volume and 92% of the area has disappeared. The current glaciation limit for southern Iceland is 1100 m (Björnsson and Pálsson, 2008), so if the ice cap disappears, it may not grow back during the current climatic conditions. However, because there is no elevation feedback in these runs, the ice cap will rebuild until it reaches the spin-up state if the climate is returned to that of 1980-1999 in these simulations.

When adding precipitation and temperature lapse rates to the forcing, to estimate the effect of elevation feedback on the mass balance, the response of the ice cap is slightly faster (Figures 9**d-f**). After 200 years, the lapse rate runs have volumes and areas that are 5-11% and 3-18% smaller than the runs without a lapse rate correction, respectively. Initially, the RCP 8.5 run has the largest sensitivity to the lapse rate correction, as the ice cap melts the fastest during this run. However, since the ice cap almost completely disappears even in the run without the lapse rate correction, there is not a large difference between the

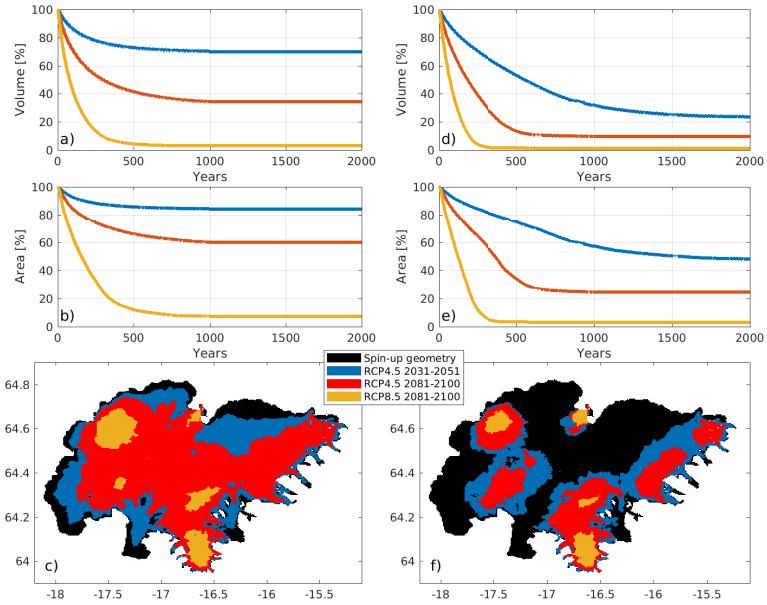

Figure 9. Changes in ice cap volume and area with step-wise climate forcing. Figures (a)-(c) do not take elevation feedback into account, while Figures (d)-(e) use a lapse rate correction. Figures (a) and (d) show the volume change relative to the reference ice cap, (b) and (e) show the area change relative to the reference ice cap, and (c) and (f) show the steady-state area, with the different colors showing the different scenarios at the end of the simulations.

simulations at the end of the run. Once the ice cap reaches a steady state, the lapse rate simulation project a volume and area that are only 2% and 4% smaller than the simulations without the correction.

The two more moderate warming scenarios (1.5°C and 3.0°C warming) are more sensitive to the elevation-dependent feedback. After ∼300 years, the volume and area drop below those found without the lapse rate correction and keep decreasing for the rest of the run. At the end of the 2000 year run, the simulation with a 1.5°C temperature increase has a volume and area that is 46% and 36% smaller than the no feedback simulations, while the 3°C temperature increase has a volume and area that is 24% and 35% smaller than the no feedback simulations.

4.4.3 Continous climate response

For these simulations, the ERA-Interim forced HARMONIE-HIRHAM5 output is used for the period 1980-2016, after which the mass balance anomalies between the future and reference period in the EC-EARTH forced HIRHAM5 simulations are used. In between the time slices, the mass balance is simulated by adding a linear trend between the time slices with the variability from the previous period added to the trend. After 2100, the climate from 2081-2100 is repeated for another 200 years.

The results from these simulations are shown in Figure 10. The volume loss happens more rapidly than the area loss in both scenarios. Without any precipitation and temperature lapse rate, the ice cap volume decreases by 17% for RCP 4.5 and 34% for

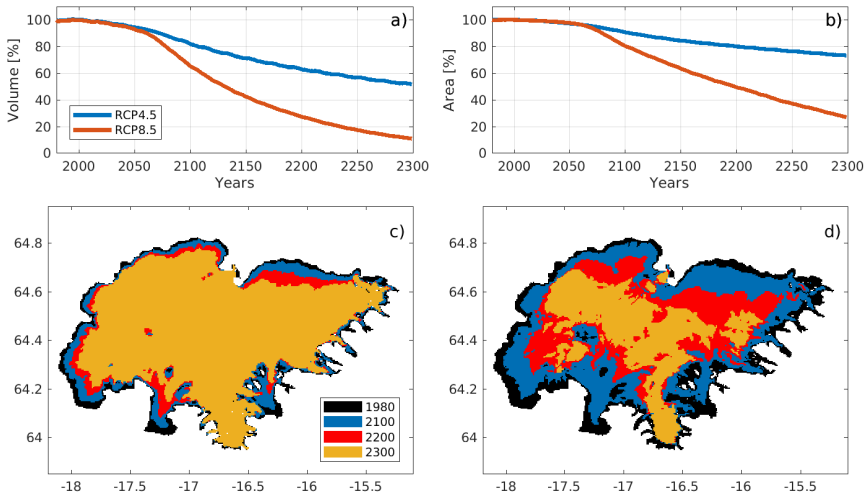

Figure 10. (a-b) Changes in ice cap volume and area, compared with the reference ice cap, with varying forcing from 1980-2100 for RCP 4.5 and RCP 8.5 scenarios, and continued until 2300 using repeated 2081-2100 forcing. (c-d) The areal extent of the ice cap at 100 year time intervals for (c) RCP 4.5 and (d) RCP 8.5 scenarios.

RCP 8.5 by 2100, while the area decreases with 9% for RCP 4.5 and 19% for RCP 8.5 by 2100. By 2300, the volume decreases with 44% for RCP 4.5 and 85% for RCP 8.5, while the area decreases with 23% for RCP 4.5 and 65% for RCP 8.5.

Figure 10 also shows the response of the glacier outlets to the different climate scenarios. The low elevation southern outlets Skeiðarárjökull and Breiðamerkurjökull are the most sensitive to an increase in warming. To estimate the effect of climate warming on specific outlets, the elevation change along flow lines is investigated for six outlets: south-facing, low elevation Breiðamerkurjökull and Skeiðarárjökull, south-west facing Tungnaárjökull, the north-facing Brúarjökull and Dyngjujökull, and the south-east facing, small and steep Hoffellsjökull. Figure 11 shows the retreat for the RCP 8.5 scenario, while Table 5 gives the retreat along the flowlines for both scenarios.

Breiðamerkurjökull, Skeiðarárjökull, and Hoffellsjökull are the most sensitive to even the lower emission scenario, retreating with 2.5-4.5 km by 2100. Dyngjujökull has the smallest retreat in both scenarios for all investigated periods. The retreat of most of the outlets significantly speeds up between 2100-2200, which is due to the increased ablation imposed in this period by repeating the high forcing from 2081-2100. In the RCP 4.5 scenario, most of the outlet retreat begins slowing down after 2200, in some cases reaching an almost steady state (e.g. Hoffellsjökull). In the RCP 8.5 scenario, outlet retreat continues rapidly except in cases where the outlet has almost disappeared by 2200 (Hoffellsjökull). Especially Tungnaárjökull has a rapid increase in outlet retreat between 2200 and 2300.

The retreat shown in Table 5 are relative to the spin-up geometry, which is significantly different from the current geometry (Figure 4). The retreat of both Brúarjökull and Dyngjujökull may therefore be underestimated in these simulations, as the spin-up areas of these outlets are smaller than present day (especially Brúarjökull, which retreated with 7.5 km during spin-up) while the simulated ice thickness is larger (especially for Dyngjujökull).

One of the reasons for the differences between the spin-up geometry and the present day geometry is that surges are not

Outlet		Scenario	0-100 years	0-200 years	0-300 years
Brúarjökull		RCP 4.5	1.5 km / 5%	5.0 km / 20%	8.5 km / 30%
		RCP 8.5	3.0 km / 10%	14.0 km / 50%	24.0 km / 90%
Dyngjujökull		RCP 4.5	1.0 km / 5%	3.0 km / 10%	3.5 km / 15%
		RCP 8.5	2.0 km / 5%	6.5 km / 20%	12.0 km / 40%
Tungnaárjökull		RCP 4.5	2.0 km / 5%	4.5 km / 10%	5.0 km / 15%
		RCP 8.5	3.5 km / 10%	10.5 km / 30%	35.5 km / 100%
Skeiðarárjökull		RCP 4.5	3.5 km / 10%	8.0 km / 20%	13.5 km / 35%
		RCP 8.5	4.0 km / 10%	23.0 km / 55%	31.0 km / 75%
	no calving	RCP 4.5	3.5 km / 10%	5.0 km / 10%	12.0 km / 30%
		RCP 8.5	4.0 km / 10%	23.0 km / 55%	31.0 km / 75%
Breiðamerkurjökull		RCP 4.5	4.5 km / 10%	11.0 km / 30%	13.0 km / 35%
		RCP 8.5	6.5 km / 20%	24.0 km / 65%	36.0 km / 100%
	no calving	RCP 4.5	3.5 km / 10%	9.0 km / 25%	11.0 km / 30%
		RCP 8.5	5.5 km / 15%	24.0 km / 65%	36.0 km / 100%
Hoffelsjökull		RCP 4.5	2.5 km / 15%	5.5 km / 30%	5.5 km / 30%
		RCP 8.5	5.5 km / 30%	16.0 km / 90%	17.5 km / 100%

Table 5. The amount of retreat of select outlet glaciers in km / percentage along the flowlines shown in Figure 5 in scenarios conducted with EC-EARTH forced climate. Distances have been rounded to the nearest 0.5 km and the nearest 5%. The retreat under the RCP 8.5 scenario is also shown in Figure 11.

taken into account in the flow model. Surges make it difficult to relate the simulated retreat with the actual retreat of the outlet front, since they speed up volume response but slow down initial areal response. The spin-up geometry was created using the flow law parameters which simulated velocities that fit the best with velocity observations, but the fact that the spin-up volume and area are fairly close to the current geometry even without surges suggests that there may be an overestimation in the velocities. This is partly due to the thickening of the outlet during spin-up. The simulated outlet retreat is therefore probably too slow during normal flow periods and too fast during surges.

Effect of calving

Another important factor for the ice cap retreat is calving of outlets that terminate into proglacial lakes. The two outlets that are affected most by this are south-flowing Skeiðarárjökull and Breiðamerkurjökull, which both terminate into a proglacial lake for parts of the runs due to an over-deepening of the bedrock. However, only Breiðamerkurjökull is calving at the start of the run, which is known to have a big effect on its mass loss: currently, about 1/3 of the mass loss from this outlet is due to calving. To investigate how much calving contributes to the retreat of Skeiðarárjökull and Breiðamerkurjökull, simulations without calving are conducted and compared to the previous simulations where calving is included.

For the RCP 4.5 scenario, the simulation without calving has the same amount of retreat for Skeiðarárjökull as the one with calving in 2100, but the calving simulation speeds up the retreat after 2100 due to the creation of a proglacial lake. By 2200, the outlet has retreated 5.0 km without calving and 8.0 km with calving compared to the simulated 1980 extent. Calving therefore is responsible for more than 50% of the simulated retreat from 2100-2200. By 2300, the difference between the runs has decreased as the outlet has moved above the proglacial lake, and the simulation without calving has retreated 12 km (13.5 km with calving). For Breiðamerkurjökull, the simulation without calving retreated 3.5 km by 2100, so 1 km less than in the

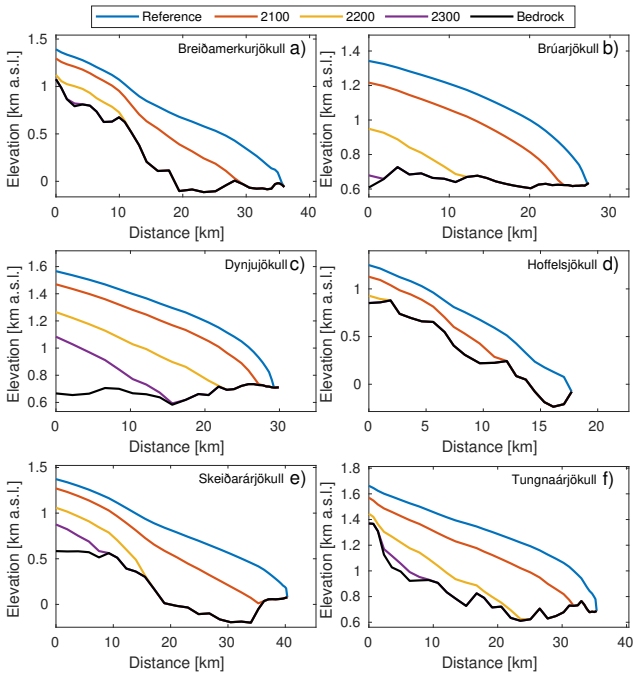

Figure 11. Profiles of six outlets showing the thickness and extent for the RCP 8.5 scenario in 1980, 2100, 2200, and 2300. Locations of the flowlines are shown in Figure 5

calving simulation, and thus calving contributed ∼20% to the retreat. By 2200, the difference between the simulations is 1.5 km, and by 2300 the difference is 2 km.

For the RCP 8.5 scenario, there is no difference in the retreat of Skeiðarárjökull, most likely because the strong forcing causes the outlet to retreat quickly even without calving. For Breiðamerkurjökull, the outlet retreat starts accelerating in 2030, and in 2080 the outlet has retreated 3.5 km with calving and 2.5 km without. Calving has therefore contributed ∼ 30% to the retreat in the first 100 years of the run. From 2080-2100 the difference between the two runs becomes smaller, and there continues to be a 1 km difference between the simulation with and without calving. In 2100, the simulation without calving has retreated 5.5 km, and calving has therefore contributed 15% to the retreat since 1980 compared to the spin-up geometry. By 2200, both simulations have the same amount of retreat, as the outlet has moved above the proglacial lake. Calving therefore has the most effect during moderate warming in these simulations.

Effects of lapse rate correction

When adding precipitation and temperature lapse rates, in the same manner as was done in the step-wise climate simulations, the response of the ice cap is faster. By 2300, the volume is 9-14% smaller than in the runs with no feedback, while the area is 9-20% smaller. Especially the retreat of Brúarjökull and Dyngjujökull are affected by the precipitation changes. In the RCP 4.5 scenario, Dyngjujökull has retreated 7.5 km by 2300, and has therefore retreated by twice the distance of the no feedback

simulation. Brúarjökull has retreated 15.0 km by 2300, approximately 75% further than in the no feedback simulation. In the RCP 8.5 simulation, a similar trend is observed, with Brúarjökull completely disappearing by 2300 and Dyngjujökull retreating by 27 km, equivalent to a 125% increase compared to the runs with no elevation feedback, by 2300.

Looking at the changes in mass balance due to the elevation feedback, we found that for the RCP 4.5 scenario, the mass balance decreased by an additional 9% in 2100 and by 15% in 2200 and 2300 compared to the simulation without feedback. Edwards et al. (2014) investigated the elevation feedback of the Greenland ice sheet under the A1B scenario, which has a similar amount of warming as RCP 4.5, and found that elevation feedback from the Greenland ice sheet contributed an extra 4.3% to the runoff by 2100, and an extra 9.6% by 2200. The simulated elevation feedback for Vatnajökull is therefore stronger than for the Greenland ice sheet. The RCP 8.5 is more sensitive to the elevation feedback, as the mass balance decreased by an additional 9% in 2100, by 21% in 2200, and by 28% in 2300 compared to the simulation without feedback.

Peak runoff

An important estimation from future simulations is when peak runoff (Huss and Hock, 2018) is reached for Vatnajökull and its outlets. For both investigated RCP scenarios, the ice cap does not reach peak runoff by 2100. The two scenarios are equal until 2060, but from 2081-2100 the RCP 8.5 has a larger increase in runoff due to the accelerated temperature increase during the second half of the century. Since the forcing is kept constant for the remaining 200 years but the area steadily decreases, the runoff amount decreases from 2100-2300 in these simulations. The runoff is approximately constant from 2100-2200 in the RCP 4.5 scenario, and for the last 100 years it decreases slightly. The RCP 8.5 simulation has a faster area retreat and therefore the runoff steadily decreases after 2100. If the climate had continued to warm, the runoff peak may have occurred later in both scenarios, and we therefore cannot give an estimate of the peak runoff.

4.4.4 Effect of glacier flow

In order to estimate how much of the volume change is due to ice flow and how much is due to changes in surface mass balance, the rate of mass loss due to flow is investigated for the two 1980-2300 runs. Figure 12 shows the rate of mass loss due to glacier flow in Gt/month for the RCP 4.5 and RCP 8.5 runs from 1980-2300. The ice flow contributes the largest mass loss when the ice cap has the largest accumulation area, and the ice flow aids melting by transporting ice into low elevation areas. As temperature rises and the size of the accumulation area decreases, so does the rate of mass loss due to ice flow. For the RCP 4.5 scenario, mass loss due to ice flow steadily decreases until 2100 as the temperature rises, and then remains approximately constant for the rest of the run. For the RCP 8.5 scenario, there is a fast drop in mass loss after 2050, which is when the scenario has the highest increase in temperature. After 2150, the mass loss is constant for the rest of the run, but at a much lower value than for the RCP 4.5 scenario. These figures clearly show that the importance of ice flow steadily decrease as the temperature rises, as the accumulation zone becomes smaller and the mass loss due to ice transport from the accumulation area to the ablation area thus becomes smaller. It does not seem to be much affected by volume and area changes, as even when the two scenarios have the same area they do not have similar mass loss rates due to ice flow.

4.4.5 Ice cap regeneration

During the current climate, the glaciation limit for the southern part of Iceland is 1100 m (Björnsson and Pálsson, 2008). Only 20% of the bedrock of Vatnajökull is above this limit. Here, a test is conducted to investigate if the ice cap could be rebuilt if the climate is returned to the simulated climate from 1980-1999 after the ice cap has disappeared. The precipitation and temperature lapse rates are used in these runs, and the model is run for 2000 years. At the end of the run, the ice cap has stabilized at a volume and area approximately 55% and 80% of the spin-up values. Figure 13 shows the rebuilding of the ice

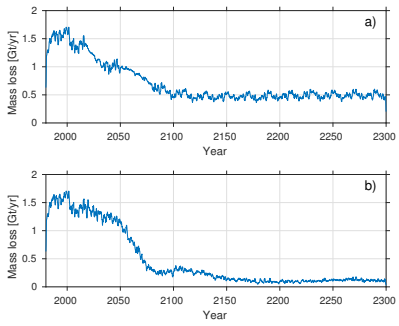

Figure 12. Mass loss due to ice flow from 1980-2300 for a) RCP 4.5 scenario, and b) RCP 8.5 scenario.

cap at different time intervals. The ice cap first builds up in areas with high elevation and high orographic precipitation. As the ice starts to flow downslope, it increases the surface elevation and as a result the precipitation increases and the temperature decreses. Almost the entire area of the ice cap is rebuilt, except for the low-elevation Breiðamerkurjökull and Skeiðarárjökull and the north-facing Brúarjökull and Dyngjujökull.

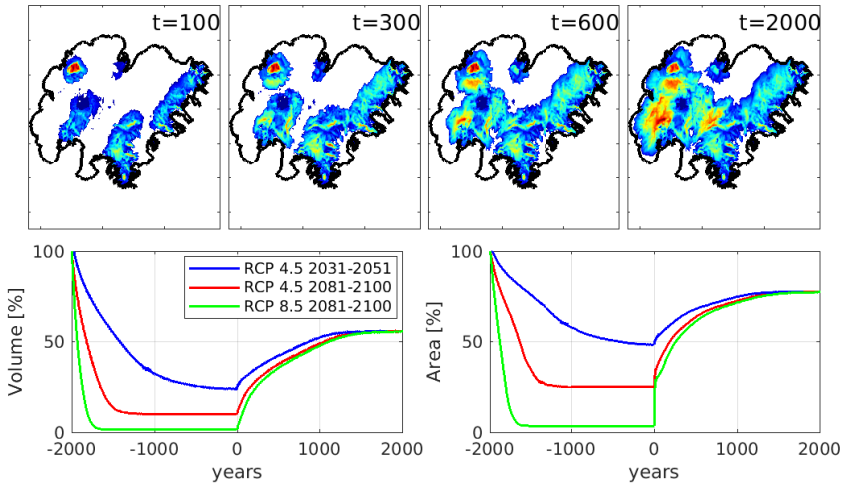

Figure 13. (top) Ice cap regeneration using elevation-corrected 1980-2000 forcing. (bottom) response of ice cap area and volume to sudden shifts in climate. Before year zero in the Figure show the time slice runs from Figure 9, and afterwards the ice cap is rebuilt using simulated, elevation corrected 1980-1999 climate.

The response time, i.e. the time it takes the ice cap to adjust all but 1/e from one steady state to another steady state, of the ice cap to the 1980-1999 forcing is generally longer than for the warming scenarios. Figure 13 shows the results of the step-wise climate runs with the precipitation and temperature lapse rates presented above (see Section 4.4.5) and how long it

would take to reach a new steady state if the climate is returned to the simulated, elevation corrected 1980-1999 climate. The response time of the reference steady state ice cap to the 4.7°C climate forcing is 150 years, whereas the response time of the steady state ice cap under the 4.7°C forcing to the 1980-1999 climate is 520 years. The response times for the 3.0°C climate forcing is 340 years (warming) and 540 years (rebuilding), while for the 1.5°C climate forcing the response time is 690 years (warming) and 500 years (rebuilding).

4.5 CORDEX simulations

Until now, we have only focused on simulations forced by the output from one RCM (HIRHAM5) forced by one GCM (EC-EARTH). In order to get a wider range of possible climate scenarios, the flow model is also forced with output from available CORDEX simulations over Iceland.

Figures 14**a-d** show the changes in temperature and precipitation over Iceland for the CORDEX models used in this study (see Table 1). The average temperature change by 2100 compared to a 1991-2010 reference period is 2.4°C for the RCP 4.5 scenario and 3.5°C for the RCP 8.5 scenario. The minimum change in temperature for the RCP 4.5 and RCP 8.5 CORDEX simulations is 1.3°C and 2.7°C, respectively, while the maximum change is 3.5°C and 5.1°C. The HIRHAM5-EC-EARTH simulations are therefore some of the simulations with the highest temperature increase in this sample.

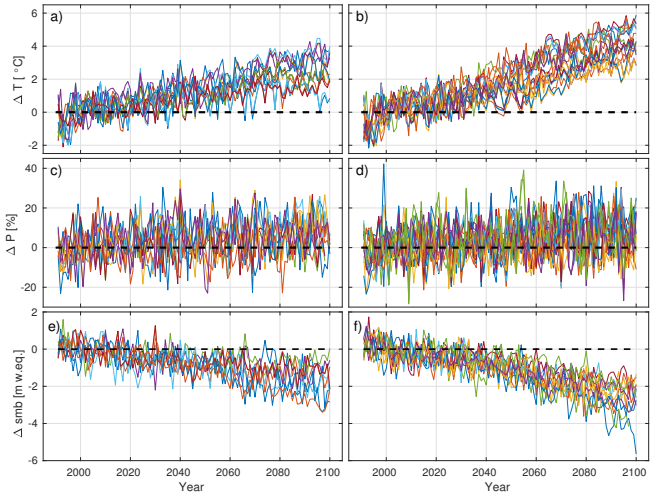

Figure 14. The change in (a-b) temperature, (c-d) precipitation, and (e-f) SMB compared to 1991-2010 average in the CORDEX simulations. RCP 4.5 scenario is shown in left panels and RCP 8.5 scenario is shown in right panels.

The models do not show a consistent trend in the change of precipitation; some models project a decrease, although most simulations project an increase. In the RCP 4.5 simulations, the precipitation change by the end of the century is 0.5-14.5%, with an average of 6.8%. For the RCP 8.5 simulations, the precipitation change is -2.5-16.8%, with an average of 6.4%. In the HIRHAM5-EC-EARTH simulations, precipitation increases by 8.3% in the RCP 4.5 scenario and by 12.8% in the RCP 8.5 scenario. The HIRHAM5-EC-EARTH runs therefore also project one of the highest increases in precipitation. A comparison of the average CORDEX temperature and precipitation with those in the HIRHAM5-EC-EARTH simulation is shown in Table

6.

Scenario	period	ΔT HIRHAM5 [K]	mean ΔT CORDEX [K]	ΔP HIRHAM5 [%]	mean ΔP CORDEX [%]
RCP 4.5	2031-2050	1.5	1.0	6.0	3.9
	2081-2100	3.0	2.3	8.3	6.8
RCP 8.5	2031-2050	1.4	1.4	1.0	2.6
	2081-2100	4.7	3.5	12.8	6.4

Table 6. The change in temperature and precipitation between the reference period (1991-2010) and the future time slices in the 5.5 km HIRHAM5 simulations, and the mean temperature and precipitation increase of the CORDEX runs for the same periods.

The meteorological parameters from the CORDEX runs (daily values of incoming radiation, turbulent fluxes, and incoming mass fluxes) are used to force the HIRHAM5 subsurface scheme. The CORDEX simulations provide continuous forcing for the period 1991-2100. The changes in simulated surface mass balance (SMB) between the reference period and 2081-2100 are very variable for each of the models (Figure 14**e-f**). The change in SMB in the RCP 4.5 scenario simulations compared to the reference period ranges from -0.5 to -2.7 m w.eq. with a median decrease in SMB of -1.5 m w.eq.. The RCM RACMO forced by EC-EARTH gives the largest changes in SMB while the RCM RCA4 forced by CNRM-CM5 gives the smallest change.

For the RCP 8.5 scenario, the maximum change in SMB is simulated by the RCM HIRHAM5 forced by EC-EARTH (ΔSMB=-3.8 m w.eq.) while the minimum change is simulated using the RCM RCA4 forced by CNRM-CERFACS-CNRM-CM5 (ΔSMB=-1.5 m w.eq.). The median decrease in SMB is -2.2 m w.eq..

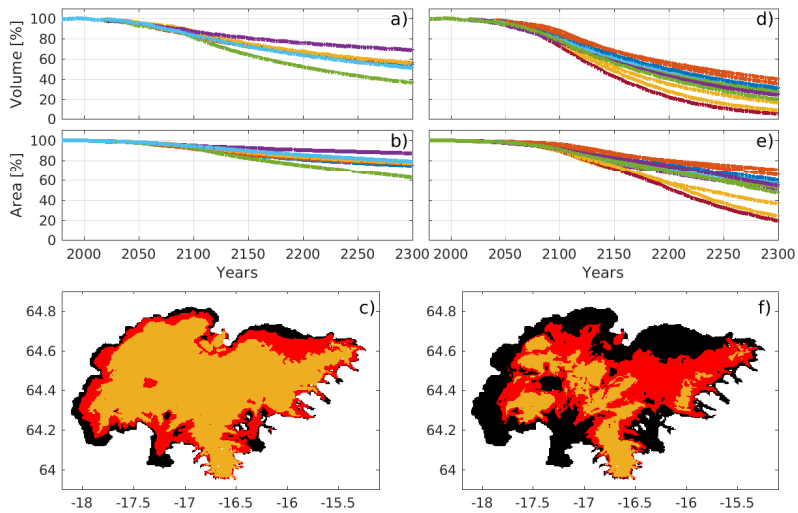

Figure 15. Results of CORDEX forced PISM runs for RCP 4.5 (a-c) and RCP 8.5 (d-f). a+d) volume change, b+e) area change, and c+f) the reference area (black), the largest simulated 2300 area (red) and the smallest simulated 2300 area (yellow).

The simulated SMB fields are subsequently used to force PISM in the same way as the 5.5 km resolution runs, and a wide range of future volumes and areas are found (Figure 15). The largest change in area and volume by 2300 for the RCP 4.5 scenario is simulated using RACMO22E-EC-EARTH-r12, where the area decreases by 37% and the volume decreased by 64%. The smallest change in area and volume is simulated using RCA4-CNRM-CERFACS-CNRM-CM5, where the area decreases by 13% and the volume by 31%. The mean reduction in area for all the runs is 24%, while the mean reduction in volume is 46%.

For the RCP 8.5 scenario, the largest change in area and volume by 2300 is found using RACMO22E-MOHC-HadGEM2-ES, where the area decreases by 80% and the volume by 94%. The smallest change in area and volume is found using CCLM4-8-1-CCCma-CanESM2, where the area decreases by 24% and the volume by 51%. The mean change in area for all the runs is 49%, while the mean change in volume is 74%.

Using HIRHAM5-EC-EARTH at a 5.5 km resolution for RCP 8.5, 65% and 85% area and volume changes were simulated, respectively (Figure 10). When comparing to the retreat using HIRHAM5-EC-EARTH at a 12 km resolution, very similar results are found: 64% area and 83% volume reduction. The bilinearly interpolated 12 km forcing provides as accurate simulations as the 5.5 km runs, at least when no elevation feedback is taken into account. Only two of the CORDEX models project a faster retreat than HIRHAM5-EC-EARTH.

5 Discussion

5.1 Simulation of the glacier till

As previously mentioned, till deformation may not be the main reason for basal sliding below Vatnajökull. In the beginning of the ablation season, the water pressure increases at the base of the glaciers as surface melt water reaches the glacier bed. This is expected to lead to lifting of part of the glacier thus causing a basal sliding event. These events are repeated over the ablation season, and most of the outlets of Vatnajökull therefore do not experience steady continuous sliding. The till deformation model used in this study is adapted from PISM to induce basal flow, but we do not expect the model to describe the physical properties of sliding below Vatnajökull. For example, in these simulations a low till friction angle of 10° is used for Breiðamerkurjökull. However, Breiðamerkurjökull has been observed to have much higher till friction angles of 27-48° (Derbyshire et al., 1981; Cuffey and Paterson, 2011). The used till friction angle therefore does not reflect the actual properties of the till, but is determined in order to provide the best fit with available velocity measurements.

In this study, the till friction angle used in the sliding law (Equation 1) depends on the elevation of the bedrock topography. This is an heuristic approach, but it has been proven to be an effective way to simulate sliding for Greenland (Aschwanden et al., 2013), Antarctica (Winkelmann et al., 2011), and now Vatnajökull. For Greenland and Antarctica, the reasoning behind using this elevation dependence is that bedrock with a marine history is expected to be weak. The reason why this assumption of a elevation dependent till friction angle works is also because of the hydrological properties of the bedrock, but not because of till deformation. The bedrock with low elevation and low till friction angle in the simulations coincide well with areas with older, impermeable bedrock where water is more likely to pool beneath the glacier, causing it to slide more readily. The bedrock under e.g. Brúarjökull, Skeiðarárjökull, and Breiðamerkurjökull is impermeable, and hydrological modelling of Vatnajökull by Flowers et al. (2003) showed that the ice cap is most likely to slide in these areas. The high-elevation bedrock areas which are assigned high till friction angles in the simulations coincide well with younger, permeable bedrock areas on which the ice cap is less likely to slide.

5.2 Elevation feedback

Previous studies of the flow of Vatnajökull have shown that there is a strong coupling between the mass balance and the ice elevation. Aðalgeirsdóttir et al. (2005) used an empirical parameterisation to model the present mass balance distribution; it had a piece wise linear elevation dependant mass balance with a variable ELA. The authors found that the ice cap does not reach an equilibrium similar in size as the present day ice cap with the used mass balance parameterization. Instead it either was considerable smaller or expanded well beyond the current margins of Vatnajökull due to a strong feedback between elevation and mass balance. Similar results were found by Hubbard (2006).

As previously mentioned, PISM has not been two-way coupled with HIRHAM5 in this study. In order to estimate the effect of elevation changes on the ice cap response time, precipitation and temperature lapse rates were added to some of the simulations. This model is up to eight times more computationally expensive than the ones without feedback, as the meteorological parameters have to be corrected and created every year, and therefore not all experiments have been conducted using this method. This is a simple way to estimate the effect of elevation feedback, but the simulations demonstrate the importance of including the feedback.

North-facing Brúarjökull and Dyngjujökull are especially sensitive to the lapse rate correction. This is in agreement with the findings by Schmidt et al. (2018), who found that the mass balance of these two outlets is especially sensitive to variations in snow thickness. In addition, Brúarjökull often experiences snowfall during the summer, which raises the albedo and therefore decreases the melt. A decrease in the amount of summer snow as the surface elevation decreases therefore also contributes to this sensitivity.

The lapse rate correction applied here only gives an estimate of the possible precipitation and temperature elevation feedback, and in order to more accurately investigate the effects of the elevation changes, a fully coupled simulation is needed. The lapse rate may change during the run or not be applicable for the entire ice cap. In addition, the increase in temperature when the ice disappears in a grid cell, as there is no melting surface to dampen the temperature, is e.g. not taken into account by the lapse rate correction. Including this effect could decrease the amount of snowfall and increase the amount of rain.

As the precipitation is overestimated by the EC-EARTH simulations, some of the albedo feedback due to a decrease in precipitation may also not have been captured in these simulations. This would most likely remain an issue even in coupled simulations.

5.3 Comparison to previous studies

One important distinction between this study and previous studies of Vatnajökull is that an realistic present day spin-up of the ice cap is achieved using the climatic conditions from the end of the 20th century. Using simulations of the present day climatic mass balance, Aðalgeirsdóttir et al. (2005) found that the ice cap either reached a size that was either smaller or grew much beyond the reference ice cap, while Marshall et al. (2005) and Flowers et al. (2005) found that the ice cap almost completely disappeared within 1500 years when forced by the climate of 1961–1990, and Hubbard (2006) simulated an ice cap with a significantly underestimated extent of the ablation area. Unlike this study, all these previous studies used an empirical model to estimate the mass balance. The mass balance in Aðalgeirsdóttir et al. (2005) is simulated as a piece wise linear elevation dependent mass balance, and in the other two studies a positive degree day model was used. The reason a steady-state ice cap similar to the present day state is simulated in this study could therefore be because a distributed surface mass balance is used based on physical simulations of the atmosphere and the cryosphere. On the other hand, steady state ice caps for neighbouring

Hofsjökull and Langjökull have been simulated using a positive degree day model for the 1981-1999 climate (Guðmundsson et al., 2009). The steady state configurations were close to the present day observed geometries, except for outlets with complex dynamic properties like the surging outlets of southern Langjökull. The steady state configuration could therefore also indicate that the PISM ice flow model is more capable of capturing the complex dynamic properties of Vatnajökull than the models used in previous studies.

The computed steady state configuration could also be due to an overestimation in the mass balance in the HARMONIE simulations. However, the mass balance is well validated over Vatnajökull, both spatially and temporally (Schmidt et al., 2018), and precipitation and temperature corrections were added to achieve the most accurate representation of the present climate, which gives confidence in the presented results. However, the most important contributing factor to the steady-state ice cap is that no elevation feedback is included in the spin-up, which would affect the steady state geometry. Both Marshall et al. (2005) and Hubbard (2006) also did not include the feedback between elevation and precipitation, and a steady state ice cap was still not reached in these studies, but they both had a strong temperature-elevation feedback.

Marshall et al. (2005) and Flowers et al. (2005) managed to achieve a steady state ice cap which was close to the current geometry by lowering the 1961-1990 temperature by 1.5°C. The geometry is comparable to the one found in this study, with an areal extent approximately $\pm 3\%$ smaller than observed and a volume approximately 3% larger. However, the deviations in ice thickness compared to observed are spatially different from this study. Dyngjujökull has the most overestimated ice thickness and the thickness in the ablation zones of Skeiðarárjökull and Breiðarmerkurjökull are underestimated (Figure 5a), whereas Flowers et al. (2005) simulated a steady state ice cap which has the most accurate ice thickness across Dyngjujökull and is overestimated for the low-elevation southern outlets. These differences are most likely a result of the different mass balance schemes used in the models. Flowers et al. (2005) also found that the ice cap geometry could be better simulated by a non-steady state ice cap, which is consistent with the results in this study.

Future projections of the ice cap geometry have previously been done by Flowers et al. (2005), who simulated a faster response of the ice cap to climate change than those found in this study. For a temperature increase of 3°C per century, which is similar to the RCP 4.5 scenario, the authors found that the ice cap would lose approximately 30% of its volume and 20% of its area after 100 years. For the RCP 4.5 scenario in our study, the ice cap looses 17% of its area and 9% of its volume. The closest temperature increase to the RCP 8.5 scenario in that study is a 4°C per century warming, and for this scenario the ice cap would loose approximately 45% of its volume and 25% of its area after 100 years. In our study, the volume decreases by 34% and the area decrease by 17% for a 4.7°C warming. Several factors probably contribute to this difference, most importantly the different approaches in calculating the mass balance. Differences in the rate of change of temperature and precipitation, the chosen flow parameters, and the model spin-up all contribute to the differences. When adding the temperature and precipitation lapse rate to the simulations, the decrease in volume and area is only 1-3% by 2100, and therefore neglected temperature feedbacks do not appear to be the source of the difference.

The response of Hoffellsjökull, a southeastern flowing outlet glacier, to an approximately 2°C warming by 2100 was investigated by (Aðalgeirsdóttir et al., 2011) using the temperature and precipitation from several RCMs. The authors found that the outlet would almost completely disappear by 2100, and therefore it retreats much quicker than in our results. One reason for this could be that the outlet is not very well resolved by the 2.5 km and 5.5 km resolution, and the mass balance for this outlet is therefore overestimated.

6 Conclusions

By one-way coupling an ice flow model with several regional climate models, projections for the future evolution of Vatnajökull ice cap are simulated. The flow model is tuned by comparing simulated surface velocities for the current ice cap geometry to available velocity observations, and the optimal flow parameters are determined for simulations of the flow of Vatnajökull. To force the model, we use 2.5 km resolution climatic mass balance simulated by HARMONIE-HIRHAM5 forced by ERA-Interim reanalysis (described in Schmidt et al. (2018)) from 1980-2016, and for the future climate projections we use 5.5 km resolution simulations by HIRHAM5 forced by EC-EARTH at the model boundaries. These future projections are compared to 12 km resolution CORDEX projections for the same period and RCP scenarios.

To initialize the coupled simulations, a steady state ice cap in balance with the reference forcing is achieved by repeating the model climate from 1980-1999 for 1000 years. The deviation between the spin-up state and the current geometry is approximately 3% for both area and volume. Previous studies by e.g. Aðalgeirsdóttir et al. (2005) and Marshall et al. (2005) could not simulate a realistic steady state ice cap using the present climate. The reason it is successful in this study may be that no elevation feedbacks were included in the spin-up.

The future evolution of the ice cap geometry is simulated under the RCP 4.5 and RCP 8.5 scenarios by forcing PISM with the output from HIRHAM5 simulations. The time series was expanded by continuing the run until 2300 by recycling the 2081-2100 forcing for 200 years. By 2300, the ice cap loses 44% of its volume and 23% of its area under the RCP 4.5 scenario, equivalent to a $\sim$3.0°C warming over Iceland. In the RCP 8.5 scenario, equivalent to an approximately 4.7°C warming over Iceland, the ice cap loses 85% of its volume and 65% of its area by 2300.

These simulations are performed with a one way coupling of HIRHAM5 with PISM, and therefore do not include elevation feedback on the climatic mass balance. To determine the effect of elevation changes on the mass balance, precipitation and temperature lapse rates are included in some of the simulations. By 2300, the area is 9-20% smaller than in the runs with no feedback, and the volume is 9-14% smaller. Brúarjökull and Dyngjujökull on the north side of Vatnajökull are found to be especially sensitive to changes in precipitation, in agreement with the findings of Schmidt et al. (2018). An experiment is conducted to determine if the ice cap will be able to rebuild if the climate is brought back to that of 1980-1999, and it is found that $\sim$80% of the ice cap area and $\sim$55% of the ice cap volume would grow back (except low-elevation Skeiðarárjökull and Breiðamerkurjökull and north-facing Brúarjökull and Dyngjujökull) but it would take about 1500 years to reach a steady state for the present climate. The reason that Skeiðarárjökull and Breiðamerkurjökull do not grow back could be that they currently lie in valleys with bedrock over deepening. During the growth of the glaciers during the little ice age, these valleys were sediment filled, and the outlets were therefore lying on higher-elevation bedrock.

Using a lapse rate correction is the only available solution for testing the elevation feedback within the scope of this study, but it would be interesting to test alternative methods. While a two-way coupling would of course be preferable, determining a SMB lapse rate by running HIRHAM5 online for a limited period with different elevations, similar to the method used for Greenland and the RCM MAR by Edwards et al. (2014), may provide a better estimate of the elevation feedback. Adding the lapse rate to the SMB field instead of the precipitation and energy balance components would also significantly reduce the simulation time, as new mass balance fields do not have to be created.

Finally, available CORDEX simulations over Iceland at a 12 km resolution are used to estimate the change in SMB until 2100. For the RCP 4.5 scenario, 11 simulations are used and for the RCP 8.5 scenario 15 simulations are used. A wide range of temperature increases and possible future ice cap geometries are found. A temperature increase of 1.3-3.5°C by 2100 compared to the 1991-2010 average is found for the RCP 4.5 scenario and an increase of 2.7-5.1°C is found for the RCP 8.5 scenario. This translates into volume losses between 31 and 64 % and area losses between 13 and 37% for the RCP 4.5 scenario in 2300. For the RCP 8.5 scenario, volume losses between 51% and 94% and area losses between 24% and 80% are simulated

by 2300. The large span in model results shows the importance of investigating several different models and initialization for future projections.

Code and data availability. HIRHAM5 output is freely accessible from http: //prudence.dmi.dk/data/temp/RUM/HIRHAM/GL2/. Measurements from automatic weather stations and from in situ mass balance surveys are partially owned by the National Power Company of Iceland and are therefore not publicly available at this time. PISM code is available at http://www.pism-docs.org.

Competing interests. The authors declare that they have no conflict of interest

Acknowledgements. This work is supported by project SAMAR (Short and long term ablation modelling based on Automatic Weather Station data and Regional Climate Models), funded by the Icelandic Research Fund (RANNIS, Grant no. 140920-051), as well as the National Power Company of Iceland (Landsvirkjun) and Eimskip University fund. The simulations were performed on resources provided by the Icelandic High Performance Computing Centre at the University of Iceland. We acknowledge the World Climate Research Programme's Working Group on Regional Climate, and the Working Group on Coupled Modelling, former coordinating body of CORDEX and responsible panel for CMIP5. We also thank the climate modelling groups (listed in Table 1) for producing and making available their model output. We also acknowledge the Earth System Grid Federation infrastructure an international effort led by the U.S. Department of Energy's Program for Climate Model Diagnosis and Intercomparison, the European Network for Earth System Modelling and other partners in the Global Organisation for Earth System Science Portals (GO-ESSP).

References

Agosta, C., Fettweis, X., and Datta, R.: Evaluation of the CMIP5 models in the aim of regional modelling of the Antarctic surface mass balance, The Cryosphere, 9, 2311–2321, https://doi.org/10.5194/tc-9-2311-2015, http://www.the-cryosphere.net/9/2311/2015/, 2015.

Aschwanden, A., Bueler, E., Khroulev, C., and Blatter, H.: An enthalpy formulation for glaciers and ice sheets, Journal of Glaciology, 58, 441–457, https://doi.org/10.3189/2012JoG11J088, https://www.cambridge.org/core/product/identifier/S0022143000210216/type/journal_article, 2012.

Aschwanden, A., Aðalgeirsdóttir, G., and Khroulev, C.: Hindcasting to measure ice sheet model sensitivity to initial states, The Cryosphere, 7, 1083–1093, https://doi.org/10.5194/tc-7-1083-2013, http://www.the-cryosphere.net/7/1083/2013/, 2013.

Aschwanden, A., Fahnestock, M. A., and Truffer, M.: Complex Greenland outlet glacier flow captured, Nature Communications, 7, 10 524, https://doi.org/10.1038/ncomms10524, http://www.nature.com/articles/ncomms10524, 2016.

Aðalgeirsdóttir, G.: Flow dynamics of Vatnajökull ice cap, Iceland, Ph.D. thesis, ETH Zürich, https://doi.org/10.3929/ETHZ-A-004489563, https://www.research-collection.ethz.ch/handle/20.500.11850/147229, 2003.

Aðalgeirsdóttir, G., Gudmundsson, G. H., and Björnsson, H.: Volume sensitivity of Vatnajökull Ice Cap, Iceland, to perturbations in equilibrium line altitude, Journal of Geophysical Research: Earth Surface, 110, n/a–n/a, https://doi.org/10.1029/2005JF000289, http://doi.wiley.com/10.1029/2005JF000289, 2005.

Aðalgeirsdóttir, G., Jóhannesson, T., Björnsson, H., Pálsson, F., and Sigurðsson, O.: Response of Hofsjökull and southern Vatnajökull, Iceland, to climate change, Journal of Geophysical Research: Earth Surface, 111, 2006.

Aðalgeirsdóttir, G., Guðmundsson, S., Björnsson, H., Pálsson, F., Jóhannesson, T., Hannesdóttir, H., Sigurðsson, S. T., and Berthier, E.: Modelling the 20th and 21st century evolution of Hoffellsjökull glacier, SE-Vatnajökull, Iceland, The Cryosphere, 5, 961–975, https://doi.org/10.5194/tc-5-961-2011, https://www.the-cryosphere.net/5/961/2011/, 2011.

Aðalgeirsdóttir, G., Aschwanden, A., Khroulev, C., Boberg, F., Mottram, R., Lucas-Picher, P., and Christensen, J.: Role of model initialization for projections of 21st-century Greenland ice sheet mass loss, Journal of Glaciology, 60, 782–794, https://doi.org/10.3189/2014JoG13J202, https://www.cambridge.org/core/product/identifier/S0022143000203134/type/journal_article, 2014.

Barletta, V. R., Sørensen, L. S., and Forsberg, R.: Scatter of mass changes estimates at basin scale for Greenland and Antarctica, The Cryosphere, 7, 1411–1432, https://doi.org/10.5194/tc-7-1411-2013, https://www.the-cryosphere.net/7/1411/2013/, 2013.

Bengtsson, L., Andrae, U., Aspelien, T., Batrak, Y., Calvo, J., de Rooy, W., Gleeson, E., Hansen-Sass, B., Homleid, M., Hortal, M., Ivarsson, K.-I., Lenderink, G., Niemelä, S., Nielsen, K. P., Onvlee, J., Rontu, L., Samuelsson, P., Muñoz, D. S., Subias, A., Tijm, S., Toll, V., Yang, X., and Køltzow, M. Ø.: The HARMONIE–AROME Model Configuration in the ALADIN–HIRLAM NWP System, Monthly Weather Review, 145, 1919–1935, https://doi.org/10.1175/MWR-D-16-0417.1, http://journals.ametsoc.org/doi/10.1175/MWR-D-16-0417.1, 2017.

Berthier, E. and Toutin, T.: SPOT5-HRS digital elevation models and the monitoring of glacier elevation changes in North-West Canada and South-East Alaska, Remote Sensing of Environment, 112, 2443–2454, https://doi.org/10.1016/j.rse.2007.11.004, http://linkinghub.elsevier.com/retrieve/pii/S0034425707004713, 2008.

Björnsson, H.: Surface and Bedrock Topography of Ice Caps in Iceland, Mapped by Radio Echo-Sounding, Annals of Glaciology, 8, 11–18, https://doi.org/10.3189/S026030550000104X, https://www.cambridge.org/core/product/identifier/S026030550000104X/type/journal_article, 1986.

Björnsson, H.: Hydrology of Ice Caps in Volcanic Regions, Visindafelag Íslendiga, rit 45, 139 s, 21 maps. Reykjavik, 1988.

Björnsson, H.: Surface and bedrock topography of the Mýrdalsjökull ice cap Iceland: The Katla caldera, eruption sites and routes of jökulhlaups, Jökull, 49, 29–46, http://www.academia.edu/2826077/Surface_and_bedrock_topography_of_the_Mýrdalsjökull_ice_cap, 2000.

Björnsson, H.: The glaciers of Iceland : a historical, cultural and scientific overview, Advances in Quarternary Science. Atlantis Press. ISBN: 978-94-6239-206-9, 2017.

Björnsson, H. and Einarsson, P.: Volcanoes beneath Vatnajökull, Iceland: Evidence from radio echo-sounding, earthquakes and jökulhlaups, Jökull, 40, 147–168, 1990.

Björnsson, H. and Pálsson, F.: Icelandic glaciers, Jökull, 58, 365–386, 2008.

Björnsson, H., Pálsson, F., and Guðmundsson, M. T.: Afkoma, hreyfing og afrennsli á vestan- og norðanverðum Vatnajokli jökulárin 1992–1993 og 1993 (Mass balance, movement and runoff on western and northern Vatnajökull hydrological years 1992–1993 and 1993–1994), Tech. rep., University of Iceland, Reykjavik, 1995.

Björnsson, H., Pálsson, F., Guðmundsson, M. T., and Haraldsson, H. H.: Mass balance of western and northern Vatnajökull, Iceland, 1991-1995, Jökull, 45, 35–58, 1998.

Björnsson, H., Pálsson, F., and Gudmundsson, S.: Jökulsárlón at Breidamerkursandur, Vatnajökull, Iceland: 20th century changes and future outlook, Jökull, 50, 1–18, 2000.

Björnsson, H., Pálsson, F., Sigurðsson, O., and Flowers, G. E.: Surges of glaciers in Iceland, Annals of Glaciology, 36, 82–90, https://doi.org/10.3189/172756403781816365, https://www.cambridge.org/core/product/identifier/S0260305500259260/type/journal_article, 2003.

Björnsson, H., Guðmundsson, S., and Pálsson, F.: Glacier winds on Vatnajökull ice cap, Iceland, and their relation to temperatures of its lowland environs, Annals of Glaciology, 42, 291–296, 2006.

Björnsson, H., Pálsson, F., Guðmundsson, S., Magnússon, E., Aðalgeirsdõttir, G., Jóhannesson, T., Berthier, E., Sigurdsson, O., and Thorsteinsson, T.: Contribution of Icelandic ice caps to sea level rise: Trends and variability since the Little Ice Age, Geophysical Research Letters, 40, 1546–1550, https://doi.org/10.1002/grl.50278, 2013.

Boberg, F., Langen, P. L., Mottram, R. H., Christensen, J. H., and Olesen, M.: 21st-century climate change around Kangerlussuaq, west Greenland: From the ice sheet to the shores of Davis Strait, Arctic, Antarctic, and Alpine Research, 50, S100 006, https://doi.org/10.1080/15230430.2017.1420862, https://www.tandfonline.com/doi/full/10.1080/15230430.2017.1420862, 2018.

Box, J. E. and Rinke, A.: Evaluation of Greenland Ice Sheet Surface Climate in the HIRHAM Regional Climate Model Using Automatic Weather Station Data., Journal of Climate, 16, 1302–1319, https://doi.org/10.1175/1520-0442-16.9.1302, 2003.

Bueler, E. and Brown, J.: Shallow shelf approximation as a "sliding law" in a thermomechanically coupled ice sheet model, Journal of Geophysical Research: Solid Earth, 114, https://doi.org/10.1029/2008JF001179, 2009.

Bueler, E. and van Pelt, W.: Mass-conserving subglacial hydrology in the Parallel Ice Sheet Model version 0.6, Geoscientific Model Development, 8, 1613–1635, https://doi.org/10.5194/gmd-8-1613-2015, https://www.geosci-model-dev.net/8/1613/2015/, 2015.

Christensen, O. B., Drews, M., Christensen, J. H., Dethloff, K., Ketelsen, K., Hebestadt, I., and Rinke, A.: The HIRHAM Regional Climate model Version 5., Tech. rep., Danish Meteorological institute, 2006.

Cuffey, K. M. and Paterson, W. S. B.: The Physics of Glaciers, Elsevier, 2011.

de Ruyter de Wildt, M. S., Klok, E. J., and Oerlemans, J.: Reconstruction of the mean specific mass balance of vatnajökull (iceland) with a seasonal sensitivity characteristic, Geografiska Annaler: Series A, Physical Geography, 85, 57–72, https://doi.org/10.1111/1468-0459.00189, https://www.tandfonline.com/doi/full/10.1111/1468-0459.00189, 2003.

Dee, D. P., Uppala, S. M., Simmons, A. J., Berrisford, P., Poli, P., Kobayashi, S., Andrae, U., Balmaseda, M. A., Balsamo, G., Bauer, P., Bechtold, P., Beljaars, A. C. M., Bidlot, J., Bormann, N., Delsol, C., Dragani, R., Fuentes, M., Geer, A. J., Isaksen, L., Haimberger, L., Healy, S. B., Hersbach, H., Matricardi, M., Mcnally, A. P., Peubey, C., Rosnay, P. D., Tavolato, C., and Vitart, F.: The ERA-Interim reanalysis: configuration and performance of the data assimilation system, Quarterly Journal of the Royal Meteorological Society, 137, 553–597, https://doi.org/10.1002/qj.828, 2011.

Derbyshire, E. D., Gregory, K. J. K. J., and Hails, J. R.: Geomorphological processes, Butterworths, 1981.

Dragosics, M., Meinander, O., Jónsdóttír, T., Dürig, T., De Leeuw, G., Pálsson, F., Dagsson-Waldhauserová, P., and Thorsteinsson, T.: Insulation effects of Icelandic dust and volcanic ash on snow and ice, Arabian Journal of Geosciences, 9, 126, https://doi.org/10.1007/s12517-015-2224-6, http://link.springer.com/10.1007/s12517-015-2224-6, 2016.

Edwards, T. L., Fettweis, X., Gagliardini, O., Gillet-Chaulet, F., Goelzer, H., Gregory, J. M., Hoffman, M., Huybrechts, P., Payne, A. J., Perego, M., Price, S., Quiquet, A., and Ritz, C.: Effect of uncertainty in surface mass balance–elevation feedback on projections of the future sea level contribution of the Greenland ice sheet, The Cryosphere, 8, 195–208, https://doi.org/10.5194/tc-8-195-2014, https://www.the-cryosphere.net/8/195/2014/, 2014.

Eerola, K.: About the performance of HIRLAM version 7.0, HIRLAM Newsletter, 51, 93–102, 2006.

Eyring, V., Bony, S., Meehl, G. A., Senior, C. A., Stevens, B., Stouffer, R. J., and Taylor, K. E.: Overview of the Coupled Model Intercomparison Project Phase 6 (CMIP6) experimental design and organization, Geoscientific Model Development, 9, 1937–1958, https://doi.org/10.5194/gmd-9-1937-2016, https://www.geosci-model-dev.net/9/1937/2016/, 2016.

Fettweis, X., Box, J. E., Agosta, C., Amory, C., Kittel, C., Lang, C., van As, D., Machguth, H., and Gallée, H.: Reconstructions of the 1900–2015 Greenland ice sheet surface mass balance using the regional climate MAR model, The Cryosphere, 11, 1015–1033, https://doi.org/10.5194/tc-11-1015-2017, https://www.the-cryosphere.net/11/1015/2017/, 2017.

Flóvenz, G. and Saemundsson, K.: Heat flow and geothermal processes in Iceland, Tectonophysics, 225, 123–138, https://doi.org/10.1016/0040-1951(93)90253-G, https://www.sciencedirect.com/science/article/pii/004019519390253G, 1993.

Flowers, G. E., Björnsson, H., and Pálsson, F.: New insights into the subglacial and periglacial hydrology of Vatnajökull, Iceland, from a distributed physical model, Journal of Glaciology, 49, 257–270, https://doi.org/10.3189/172756503781830827, https://www.cambridge.org/core/product/identifier/S0022143000210460/type/journal_article, 2003.

Flowers, G. E., Marshall, S. J., Björnsson, H., and Clarke, G. K. C.: Sensitivity of Vatnajökull ice cap hydrology and dynamics to climate warming over the next 2 centuries, Journal of Geophysical Research, 110, F02 011, https://doi.org/10.1029/2004JF000200, http://doi.wiley.com/10.1029/2004JF000200, 2005.

Gascoin, S., Guðmundsson, S., Aðalgeirsdóttir, G., Pálsson, F., Schmidt, L., Berthier, E., and Björnsson, H.: Evaluation of MODIS Albedo Product over Ice Caps in Iceland and Impact of Volcanic Eruptions on Their Albedo, Remote Sensing, 9, 399, https://doi.org/10.3390/rs9050399, http://www.mdpi.com/2072-4292/9/5/399, 2017.

Giorgi, F., Jones, C., and Asrar, G. R.: Addressing climate information needs at the regional level: The CORDEX framework, World Meteorological Organization Bulletin, 2009.

Gong, Y., Cornford, S. L., and Payne, A. J.: Modelling the response of the Lambert Glacier–Amery Ice Shelf system, East Antarctica, to uncertain climate forcing over the 21st and 22nd centuries, The Cryosphere, 8, 1057–1068, https://doi.org/10.5194/tc-8-1057-2014, https://www.the-cryosphere.net/8/1057/2014/, 2014.

Gudmundsson, M. T., Thordarson, T., Höskuldsson, , Larsen, G., Björnsson, H., Prata, F. J., Oddsson, B., Magnússon, E., Högnadóttir, T., Petersen, G. N., Hayward, C. L., Stevenson, J. a., and Jónsdóttir, I.: Ash generation and distribution from the April-May 2010 eruption of Eyjafjallajökull, Iceland, Scientific Reports, 2, 1–12, https://doi.org/10.1038/srep00572, http://www.nature.com/articles/srep00572, 2012.

Guðmundsson, S., Björnsson, H., Pálsson, F., and Haraldsson, H. H.: Energy balance of Brúarjökull and circumstances leading to the August 2004 floods in the river Jökla, N-Vatnajökull, Jökull, 55, 121–138, 2006.

Guðmundsson, S., Björnsson, H., Jóhannesson, T., Aðalgeirsdóttir, G., Pálsson, F., and Sigurðsson, O.: Similarities and differences in the response to climate warming of two ice caps in Iceland, Hydrology Research, 40, 495–502, https://doi.org/10.2166/nh.2009.210, https://iwaponline.com/hr/article/40/5/495/30993/Similarities-and-differences-in-the-response-to, 2009.

Hazeleger, W., Wang, X., Severijns, C., Ştefănescu, S., Bintanja, R., Sterl, A., Wyser, K., Semmler, T., Yang, S., van den Hurk, B., van Noije, T., van der Linden, E., and van der Wiel, K.: EC-Earth V2.2: description and validation of a new seamless earth system prediction model, Climate Dynamics, 39, 2611–2629, https://doi.org/10.1007/s00382-011-1228-5, http://link.springer.com/10.1007/s00382-011-1228-5, 2012.

Hines, K. M., Bromwich, D. H., Hines, K. M., and Bromwich, D. H.: Development and Testing of Polar Weather Research and Forecasting (WRF) Model. Part I: Greenland Ice Sheet Meteorology*, Monthly Weather Review, 136, 1971–1989, https://doi.org/10.1175/2007MWR2112.1, http://journals.ametsoc.org/doi/abs/10.1175/2007MWR2112.1, 2008.

Hubbard, A.: The validation and sensitivity of a model of the Icelandic ice sheet, Quaternary Science Reviews, 25, 2297–2313, https://doi.org/10.1016/J.QUASCIREV.2006.04.005, https://www.sciencedirect.com/science/article/pii/S0277379106001491, 2006.

Huss, M. and Hock, R.: Global-scale hydrological response to future glacier mass loss, Nature Climate Change, 8, 135–140, https://doi.org/10.1038/s41558-017-0049-x, http://www.nature.com/articles/s41558-017-0049-x, 2018.

IPCC: IPCC Fifth Assessment Report (AR5), IPCC, 2013.

Kaser, G., Grosshauser, M., and Marzeion, B.: Contribution potential of glaciers to water availability in different climate regimes., Proceedings of the National Academy of Sciences of the United States of America, 107, 20 223–7, https://doi.org/10.1073/pnas.1008162107, http://www.ncbi.nlm.nih.gov/pubmed/21059938http://www.pubmedcentral.nih.gov/articlerender.fcgi?artid=PMC2996705, 2010.

Koenigk, T., Brodeau, L., Graversen, R. G., Karlsson, J., Svensson, G., Tjernström, M., Willén, U., and Wyser, K.: Arctic climate change in 21st century CMIP5 simulations with EC-Earth, Climate Dynamics, 40, 2719–2743, https://doi.org/10.1007/s00382-012-1505-y, http://link.springer.com/10.1007/s00382-012-1505-y, 2013.

Langen, P. L., Mottram, R. H., Christensen, J. H., Boberg, F., Rodehacke, C. B., Stendel, M., van As, D., Ahlstrøm, A. P., Mortensen, J., Rysgaard, S., Petersen, D., Svendsen, K. H., Aðalgeirsdóttir, G., and Cappelen, J.: Quantifying energy and mass fluxes controlling godthåbsfjord freshwater input in a 5-km simulation (1991-2012), J. Climate, 28, 3694–3713, https://doi.org/10.1175/JCLI-D-14-00271.1, 2015.

Langen, P. L., Fausto, R. S., Vandecrux, B., Mottram, R. H., and Box, J. E.: Liquid Water Flow and Retention on the Greenland Ice Sheet in the Regional Climate Model HIRHAM5: Local and Large-Scale Impacts, Frontiers in Earth Science, 4, https://doi.org/10.3389/feart.2016.00110, http://journal.frontiersin.org/article/10.3389/feart.2016.00110/full, 2017.

Larsen, K. M. H., Gonzalez-Pola, C., Fratantoni, P., Beszczynska-Möller, A., and Hughes, S. L.: ICES Report On Ocean Climate 2015, ICES Cooperative Research Report, 331, 79, 2016.

Lenaerts, J. T. M. and Van Den Broeke, M. R.: Modeling drifting snow in Antarctica with a regional climate model: 2. Results, Journal of Geophysical Research Atmospheres, 117, https://doi.org/10.1029/2010JD015419, 2012.

Levermann, A., Albrecht, T., Winkelmann, R., Martin, M. A., Haseloff, M., and Joughin, I.: Kinematic first-order calving law implies potential for abrupt ice-shelf retreat, The Cryosphere, 6, 273–286, https://doi.org/10.5194/tc-6-273-2012, https://www.the-cryosphere.net/6/273/2012/, 2012.

Lliboutry, L. and Duval, P.: Various isotropic and anisotropic ices found in glaciers and polar ice caps and their corresponding rheologies, Annales Geophysicae, 3, 207–224, http://www.scopus.com/inward/record.url?eid=2-s2.0-0022251164&partnerID=40&md5=e157815704c7b2031acf31e73b241a4f, 1985.

Lucas-Picher, P., Wulff-Nielsen, M., Christensen, J. H., Aðalgeirsdóttir, G., Mottram, R. H., and Simonsen, S. B.: Very high resolution regional climate model simulations over Greenland: Identifying added value, Journal of Geophysical Research, 117, 2108, https://doi.org/10.1029/2011JD016267, 2012.

Magnússon, E., Muñoz-Cobo Belart, J., Pálsson, F., S. Anderson, L., Th. Gunnlaugsson, A., Berthier, E., Agustsson, H., and Geirsdóttir, : The subglacial topography of Drangajokull ice cap, NW-Iceland, deduced from dense RES-profiling, Jokull, 66, 1–26, 2016.

Marshall, S. J., Björnsson, H., Flowers, G. E., and Clarke, G. K. C.: Simulation of Vatnajökull ice cap dynamics, Journal of Geophysical Research, 110, F03 009, https://doi.org/10.1029/2004JF000262, http://doi.wiley.com/10.1029/2004JF000262, 2005.

Nawri, N., Pálmason, B., Petersen, N. G., Björnsson, H., and Þorsteinsson, S.: The ICRA atmospheric reanalysis project for Iceland, Tech. rep., http://www.vedur.is/media/vedurstofan-utgafa-2017/VI_2017_005_rs.pdf, 2017.

Nielsen, L. T., Aðalgeirsdóttir, G., Gkinis, V., Nuterman, R., and Hvidberg, C. S.: The effect of a Holocene climatic optimum on the evolution of the Greenland ice sheet during the last 10 kyr, Journal of Glaciology, 64, 477–488, https://doi.org/10.1017/jog.2018.40, https://www.cambridge.org/core/product/identifier/S0022143018000400/type/journal_article, 2018.

Oerlemans, J., Björnsson, H., Kuhn, M., Obleitner, F., Palsson, F., Smeets, C., Vugts, H. F., and Wolde, J. D.: Glacio-Meteorological Investigations On Vatnajökull, Iceland, Summer 1996: An Overview, Boundary-Layer Meteorology, 92, 3–24, https://doi.org/10.1023/A:1001856114941, http://link.springer.com/10.1023/A:1001856114941, 1999.

Pálsson, F., Gunnarsson, A., Jónsson, Þ., Steinþórsson, S., and Pálsson, H. S.: Vatnajökull: Mass balance, meltwater drainage and surface velocity of the glacial year 2014_15, Tech. rep., Institute of Earth Sciences, University of Iceland and National Power Company, RH-06-2015, 2015.

Pálsson, F., Gunnarsson, A., Gunnlaugsson, , Jónsson, G., Pálsson, H. S., Steinþórsson, S., and Jónsson, : VATNAJÖKULL: Mass balance, meltwater drainage and surface velocity of the glacial year 2016_17, Tech. rep., Institute of Earth Sciences University of Iceland and National Power Company, RH-07-2017, 2017.

Rae, J. G. L., Aðalgeirsdóttir, G., Edwards, T. L., Fettweis, X., Gregory, J. M., Hewitt, H. T., Lowe, J. A., Lucas-Picher, b., Mottram, R. H., Payne, A. J., Ridley, J. K., Shannon, S. R., van de Berg, W. J., van de Wal, R. S. W., and van den Broeke, M. R.: Greenland ice sheet surface mass balance: evaluating simulations and making projections with regional climate models, The Cryosphere, 6, 1275–1294, https://doi.org/10.5194/tc-6-1275-2012, 2012.

Riahi, K., Rao, S., Krey, V., Cho, C., Chirkov, V., Fischer, G., Kindermann, G., Nakicenovic, N., and Rafaj, P.: RCP 8.5-A scenario of comparatively high greenhouse gas emissions, Climatic Change, 109, 33–57, https://doi.org/10.1007/s10584-011-0149-y, 2011.

Rockel, B., Will, A., and Hense, A.: The Regional Climate Model COSMO-CLM (CCLM), Meteorologische Zeitschrift, 17, 347–348, https://doi.org/10.1127/0941-2948/2008/0309, http://www.schweizerbart.de/papers/metz/detail/17/56726/The_Regional_Climate_Model_COSMO_CLM_CCLM?af=crossref, 2008.

Roeckner, E., Bäuml, G., Bonaventura, L., Brokopf, R., Esch, M., Giorgetta, M., Hagemann, S., Kirchner, I., Kornblueh, L., Manzini, E., Rhodin, A., Schlese, U., Schulzweida, U., and Tompkins, A.: The atmospheric general circulation model ECHAM 5 PART I: Model description, Tech. Rep. 349, Report / MPI für Meteorologie, 2003.

Samuelsson, P., Jones, C. G., Will´En, U., Ullerstig, A., Gollvik, S., Hansson, U., Jansson, E., Kjellstro¨M, C., Nikulin, G., and Wyser, K.: The Rossby Centre Regional Climate model RCA3: model description and performance, Tellus A: Dynamic Meteorology and Oceanography, 63, 4–23, https://doi.org/10.1111/j.1600-0870.2010.00478.x, https://www.tandfonline.com/doi/full/10.1111/j.1600-0870.2010.00478.x, 2011.

Schäfer, M., Möller, M., Zwinger, T., and Moore, J.: Dynamic modelling of future glacier changes: mass-balance/elevation feedback in projections for the Vestfonna ice cap, Nordaustlandet, Svalbard, Journal of Glaciology, 61, 1121–1136, https://doi.org/10.3189/2015JoG14J184, https://www.cambridge.org/core/product/identifier/S0022143000200300/type/journal_article, 2015.

Schmidt, L., Langen, P., Aðalgeirsdóttir, G., Pálsson, F., Guðmundsson, S., Gunnarsson, A., Schmidt, L. S., Langen, P. L., Aðalgeirsdóttir, G., Pálsson, F., Guðmundsson, S., and Gunnarsson, A.: Sensitivity of Glacier Runoff to Winter Snow Thickness Investigated for Vatnajökull Ice Cap, Iceland, Using Numerical Models and Observations, Atmosphere 2018, Vol. 9, Page 450, 9, 450, https://doi.org/10.3390/ATMOS9110450, https://www.mdpi.com/2073-4433/9/11/450/htm, 2018.

Schmidt, L. S., Aðalgeirsdóttir, G., Guðmundsson, S., Langen, P. L., Pálsson, F., Mottram, R., Gascoin, S., and Björnsson, H.: The importance of accurate glacier albedo for estimates of surface mass balance on Vatnajökull: evaluating the surface energy budget in a regional climate model with automatic weather station observations, The Cryosphere, 11, 1665–1684, https://doi.org/10.5194/tc-11-1665-2017, https://www.the-cryosphere.net/11/1665/2017/, 2017.

Seity, Y., Brousseau, P., Malardel, S., Hello, G., Bénard, P., Bouttier, F., Lac, C., Masson, V., Seity, Y., Brousseau, P., Malardel, S., Hello, G., Bénard, P., Bouttier, F., Lac, C., and Masson, V.: The AROME-France Convective-Scale Operational Model, Monthly Weather Review, 139, 976–991, https://doi.org/10.1175/2010MWR3425.1, http://journals.ametsoc.org/doi/abs/10.1175/2010MWR3425.1, 2011.

Stendel, M., Christensen, J. H., and Petersen, D.: High-Arctic Ecosystem Dynamics in a Changing Climate, vol. 40 of *Advances in Ecological Research*, Elsevier, https://doi.org/10.1016/S0065-2504(07)00002-5, http://www.sciencedirect.com/science/article/pii/S0065250407000025, 2008.

Taylor, K. E., Stouffer, R. J., and Meehl, G. A.: An overview of CMIP5 and the experiment design, Bulletin of the American Meteorological Society, 93, 485–498, https://doi.org/10.1175/BAMS-D-11-00094.1, 2012.

Thomson, A. M., Calvin, K. V., Smith, S. J., Kyle, G. P., Volke, A., Patel, P., Delgado-Arias, S., Bond-Lamberty, B., Wise, M. A., Clarke, L. E., and Edmonds, J. A.: RCP4.5: A pathway for stabilization of radiative forcing by 2100, Climatic Change, 109, 77–94, https://doi.org/10.1007/s10584-011-0151-4, 2011.

Tulaczyk, S., Kamb, W. B., and Engelhardt, H. F.: Basal mechanics of Ice Stream B, west Antarctica: 1. Till mechanics, Journal of Geophysical Research: Solid Earth, 105, 463–481, https://doi.org/10.1029/1999JB900329, http://doi.wiley.com/10.1029/1999JB900329, 2000.

Van Meijgaard, E., Van Ulft, L. H., de Berg, W. J., Bosveld, F. C., den Hurk, B., Lenderink, G., and Siebesma, A. P.: The KNMI regional atmospheric climate model RACMO version 2.1, Koninklijk Nederlands Meteorologisch Instituut, 43, 2008.

Winkelmann, R., Martin, M. A., Haseloff, M., Albrecht, T., Bueler, E., Khroulev, C., and Levermann, A.: The Potsdam Parallel Ice Sheet Model (PISM-PIK) – Part 1: Model description, The Cryosphere, 5, 715–726, https://doi.org/10.5194/tc-5-715-2011, http://www.the-cryosphere.net/5/715/2011/, 2011.

Xu, M., Yan, M., Kang, J., and Ren, J.: Comparative studies of glacier mass balance and their climatic implications in Svalbard, Northern Scandinavia, and Southern Norway, Environmental Earth Sciences, 67, 1407–1414, https://doi.org/10.1007/s12665-012-1585-3, http://link.springer.com/10.1007/s12665-012-1585-3, 2012.